

24 February 2016

To:

Dr Olaf Morgenstern, Editor GMD, olaf.morgenstern@niwa.co.nz

Re: Manuscript GMD-2016-169

Dear Olaf, dear Copernicus editorial team,

Please accept my apologies for this long delay in coming back to you with a revised paper version. The high number of figures made the overall processing time to accommodate the reviewer's suggestions a rather lengthy one. My apologies.

I do however feel that this dataset of historical greenhouse gas concentration fields is to become a rich resource for multiple future studies – as well as of course the set of CMIP6 climate models.

I am furthermore indebted to all the co-authors. Many of them have painstakingly sifted through code, incorrect English and large sets of rather inhomogeneous datasets.

As our detailed replies to reviewers have already been submitted last November, and given that we have not heard any feedback on those yet, I do not attach them again here.

Sincerely,



A/Prof. Malte Meinshausen

Director of the Australian-German Climate & Energy College

Historical greenhouse gas concentrations for climate modelling (CMIP6)

Malte Meinshausen^{1,2,3}, Elisabeth Vogel^{1,2}, Alexander Nauels^{1,2}, Katja Lorbacher^{1,2}, Nicolai Meinshausen⁴, David Etheridge⁵, Paul Fraser⁵, Stephen A. Montzka⁶, Peter Rayner², Cathy Trudinger⁵, Paul Krummel⁵, Urs Beyerle⁷, Josep G. Canadell⁸, John S. Daniel⁹, Ian Enting¹⁰, Rachel M. Law⁵, [Chris R. Lunder¹¹](#), [Simon O'Doherty¹¹](#), [O'Doherty¹²](#), Ron G. [Prinn¹²](#), [Prinn¹³](#), Stefan [Reimann¹²](#), [Reimann¹⁴](#), Mauro Rubino^{5,15}, Guus J.M. [Velders¹⁵](#), [Velders¹⁶](#), Martin K. [Vollmer¹²](#), [Vollmer¹⁴](#), Ray [Weiss¹⁶](#), [H.J. Wang¹⁷](#), [Ray Weiss¹⁸](#)

¹Australian-German Climate & Energy College, The University of Melbourne, Parkville, Victoria, Australia

²Department of Earth Sciences, The University of Melbourne, Parkville, Victoria, Australia

³Potsdam Institute for Climate Impact Research, Potsdam, Germany

⁴Seminar for Statistics, Swiss Federal Institute of Technology (ETH Zurich), Zurich, Switzerland.

⁵CSIRO, Oceans and Atmosphere, Aspendale, Victoria, Australia

⁶NOAA, Earth System Research Laboratory, Global Monitoring Division, Boulder, Colorado, USA

⁷Institute for Atmospheric and Climate Science, Swiss Federal Institute of Technology, ~~Zurich~~ (ETH Zurich), [Zurich](#), Switzerland

⁸Global Carbon Project, CSIRO Oceans and Atmosphere, Canberra, ACT, Australia

⁹NOAA, Earth System Research Laboratory, Chemical Sciences Division, Boulder, Colorado, USA

¹⁰The University of Melbourne, Victoria, Australia (retired)

¹¹[University¹¹ Norwegian Institute for Air Research, Kjeller, Norway](#)

¹²[University of Bristol, Bristol, United Kingdom](#)

¹³[MIT¹³ MIT, Cambridge, MA, United States USA](#)

¹⁴[Empa¹⁴ Empa, Swiss Federal Laboratories for Materials Science and Technology, Laboratory for Air Pollution and Environmental Technology, Switzerland](#)

¹⁵[Dipartimento¹⁵ Dipartimento di matematica e fisica, Seconda Università degli studi di Napoli, ~~81100~~ Caserta, Italy](#)

¹⁶[National¹⁶ National Institute for Public Health and the Environment \(RIVM\), Bilthoven, Netherlands](#)

¹⁷[Scripps¹⁷ School of Earth and Atmospheric Sciences, Georgia Institute of Technology, Atlanta, Georgia, USA](#)

¹⁸[Scripps Institution of Oceanography, La Jolla, CA, United States USA](#)

30 Correspondence to: M. Meinshausen (malte.meinshausen@unimelb.edu.au)

Abstract. Atmospheric greenhouse gas (GHG) concentrations are at unprecedented, record-high levels compared to pre-industrial reconstructions over the last 800,000 years. Those elevated greenhouse gas GHG concentrations warm the planet and together with partially offset by net cooling effects by aerosols, they are largely responsible for the reason of observed climate change warming over the past 150 years. An accurate representation of those GHG concentrations is hence important to understand and model recent and future climate change. So far, community efforts to create composite datasets of GHG concentrations with seasonal and latitudinal information have focused on marine boundary layer conditions and recent trends since the 1980s. Here, we provide consolidated data sets of historical atmospheric (volume) mixing ratios concentrations (mole fractions) of 43 greenhouse gases specifically for the purpose of climate model runs: GHGs to be used in the Climate Model

Intercomparison Project – Phase 6 (CMIP6) experiments. The presented datasets are based on AGAGE and NOAA networks, firm and ice core data, and archived air data, and a large set of literature published studies. –In contrast to previous intercomparisons, the new datasets are latitudinally resolved and include seasonality over. We focus on the period between year 0–1850 to 2014. We assimilate data for historical CMIP6 runs, but data are also provided for the last 2000 years. We

5 provide consolidated datasets in various spatiotemporal resolutions for carbon dioxide (CO₂), methane (CH₄) and nitrous oxide (N₂O), 5-chlorofluorocarbons (CFCs), 3-hydrochlorofluorocarbons (HCFCs), 16 as well as 40 other GHGs, namely 17 ozone depleting substances, 11 hydrofluorocarbons (HFCs), 3 halons, methyl bromide (CH₃Br), 39 perfluorocarbons (PFCs), sulfur hexafluoride (SF₆), nitrogen trifluoride (NF₃) and sulfur hexafluoride (SO₂F₂). We In addition, we provide three equivalence-species that aggregate concentrations of GHGs other than CO₂, CH₄ and N₂O, weighted by their radiative forcing

10 efficiencies. For the year 1850 that is used for pre-industrial control runs, we estimate 1850 annual and global mean surface mixing-ratio-concentrations of CO₂ at 284.3 ppmv ppm, CH₄ at 808.2 ppbv ppb and N₂O at 273.0 ppbv and quantify the seasonal ppb. The data are available at <https://pcmdi.llnl.gov/search/input4mips/> and hemispheric gradients of surface mixing ratios. Compared www.climatecollege.unimelb.edu.au/cmip6. While the minimum CMIP6 recommendation is to earlier intercomparisons, the stronger implied use the global and annual mean time series, modelling groups can also choose our

15 monthly and latitudinally resolved concentrations that imply a stronger radiative forcing in the northern hemisphere winter (due to the latitudinal gradient and seasonality) may help to improve the skill of climate models to reproduce past climate and thereby reduce uncertainty in future projections.

).

1 Introduction

The ~~Emissions from the~~ burning of fossil fuels, ~~emissions-related-to~~ deforestation and, agricultural activities and ~~the production of synthetic greenhouse gas emissions:~~GHGs are the ~~primary~~ reasons for the observed increases in ~~greenhouse gas:~~GHG concentrations. ~~Those, defined as mole fractions in dry air. The elevated greenhouse gas mixing ratios:~~GHG concentrations induce a radiative forcing that in turn ~~would~~ cause more than the observed recent ~~climate change as some of the global~~ warming if it were not for the cooling effect ~~is dampened~~ by aerosols (Fig. TS.10 in IPCC WG1 AR4 (IPCC)). An accurate quantification of anthropogenic and natural climate drivers is crucial for general circulation and Earth System models. Simulations by these models for the historical time periods, e.g. since 1850, can only be meaningfully compared to observations (e.g. surface temperature, ocean heat uptake) to the degree that input forcings are an accurate representation of the past. The difficulty with many anthropogenic ~~climate~~ drivers is that their global-mean magnitude, their latitudinal gradient and seasonal cycle are uncertain further back in time, even for the main ~~greenhouse gases:~~GHGs carbon dioxide (CO₂), methane (CH₄) and nitrous oxide (N₂O). Systematic observational efforts started in 1957-1958, measuring CO₂ at the South Pole and Mauna Loa observatories ~~Measurements of archived air, and~~ (Keeling et al., 2001). ~~Measurements of archived air,~~ firn air and ice cores from both polar regions provide records for the pre-observational time. To date, ~~there have been few attempts to reconstruct long-term reconstructions of millennial~~ global-mean ~~timeseries:~~time series based on ice and firn data ~~have been performed,~~ e.g. for CO₂ over the last millennia (Ahn et al., 2012; MacFarling Meure et al., 2006; Ahn et al., 2012; Rubino et al., 2013) ~~or to provide.~~ For the more recent past, several studies investigated firn and ice data to constrain halocarbons (Buizert et al., 2012; Martinerie et al., 2009; Mühle et al., 2010; Sturrock et al., 2002; Trudinger et al., 2016), some of them with hemispheric resolution. In terms of latitudinally-resolved, monthly ~~background mixing ratios of data,~~ there have only been a few synthesis products, namely for CO₂, CH₄ and N₂O over the instrumental record over the past 20 to 40 years (Cooperative Global Atmospheric Data Integration Project; NOAA, 2013; NOAA ESRL GMD, 2014a, NOAA ESRL GMD 2014b, NOAA ESRL GMD 2014c, c). For this recent past, the World Data Centre for Greenhouse Gases (WDCGG) (ds.data.jma.go.jp/gmd/wdcgg/) also provides a synthesis with global and hemispheric means for CO₂, CH₄ and N₂O (Tsutsumi et al., 2009). In light of the observational gaps further back in time, some studies, such as Keeling et al. (2011), used linear regressions between fossil fuel use and latitudinal CO₂ concentration trends to separate natural from anthropogenically-induced effects, which allows ~~us~~ to infer latitudinal gradients back in time.

In previous climate model inter-comparison projects (Meehl et al., 2005) (Meehl et al., 2005), global-mean concentrations have been prescribed (Meinshausen et al., 2011a) (Meinshausen et al., 2011), with some models constraining internally generated fields of ~~greenhouse gas mixing ratios:~~GHG concentrations to match those global-mean values. Here, we update those global-mean and annual-mean ~~greenhouse gas:~~GHG concentration time-series for the historical period over years 0 to 2014, with

‘historical’ simulations in the CMIP6 model intercomparison (Eyring et al., 2016) (Eyring et al., 2016) focussed on the most recent period 1850 to 2014. In addition, we provide hemispheric and latitudinal monthly-resolved fields for 43 greenhouse gases (GHGs) in total. In the past, the large latitudinal and seasonal gradient of greenhouse gas (GHG) radiative forcing has not been consistently applied to model radiative forcing and climate change. Our new dataset provides datasets provide a more consistent starting point for climate model experiments. The monthly and latitudinal resolution of this new greenhouse gas (GHG) dataset is in-line with designed to have a similar resolution as the monthly solar forcing (Matthes et al., 2016) (Matthes et al., 2016) and monthly and latitudinally resolved ozone and aerosol abundances. Many greenhouse gases (GHGs) also have significant longitudinal (land/ocean) and diurnal variations but we do not attempt to resolve these them. Neither do we provide vertical gradients of the greenhouse gases mixing ratios (GHGs concentrations) and only discuss possible vertical extension methods (section 4.1) ‘The vertical dimension’) in case that models do not have their own methods to derive vertical gradients. In this study, we compile one possible reconstruction of latitudinally and monthly resolved fields, as well as global annual means of surface greenhouse gas mixing ratios (GHG concentrations) for 43 gases from Year year 0 to 2014, as input for the forthcoming model inter-comparison experiments that are part of the Phase-6 Coupled Model Inter-comparison project (CMIP6) (Eyring et al., 2016), specifically (Eyring et al., 2016). Specifically, we provide the pre-industrial control runs at 1850 forcing levels (picontrol), the experiment with abruptly quadrupled CO₂ concentrations (abrupt4x), and the standard experiment of a 1% annual CO₂ concentration increase (1pct2co2) as well as, and the historical runs that are driven with best-guess estimates of historical forcings since 1850. Species that are radiatively less important than CO₂, CH₄ and N₂O (‘importance’ here being measured as radiative forcing exerted in year 2014 compared to 1750) are provided individually as well in aggregate as HFC-134a and CFC-12 equivalent mixing ratios as aggregated as HFC-134a and CFC-12 equivalent concentrations. The description of the datasets geared towards CMIP6 modelling groups is provided in section 4, including a description of available data formats and CMIP6 minimum recommendations.

The design principle for this long-term dataset is to provide a plausible reconstruction of past greenhouse gas mixing ratios (GHG concentrations) to be used in climate models. Using various gap-filling procedures, reconstruction and extensions, this dataset aims to reflect observational evidence of both recent flask and *in situ* observations from the worldwide network of NOAA ESRL and AGAGE stations, as well as the Law Dome Antarctic and Greenland ice core and firm data over the last two thousand years, where available. Furthermore, many detailed literature studies (Mühle et al., 2010b; Arnold et al., 2013; Velders et al., 2014; Vollmer et al., 2016) for radiatively less important species are taken into account and (Arnold et al., 2013; Arnold et al., 2014; Aydin et al., 2010; Butler et al., 1999; Ivy et al., 2012; Martinerie et al., 2009; Montzka et al., 2015; Mühle et al., 2010; Oram et al., 2012; Sturrock et al., 2002; Trudinger et al., 2004; Trudinger et al., 2016; Velders and Daniel, 2014; Vollmer et al., 2016; Worton et al., 2006) for radiatively less important species are compared with our data product in the factsheet figures for the specific gases (Table 12 and Appendix A with Fig. 20 to Fig. 59) or synthesised where direct observational records from the above networks were not available.

The predominant climate effect of ~~greenhouse-gas~~GHG increases is captured by the global- and annual mean ~~mixing ratio:concentrations~~ throughout the atmosphere. The surface global and annual mean ~~mixing-ratio:concentrations~~ provided here, in combination with the models' approximations for the vertical concentration profile, are the minimum standard for CMIP6 models. Assimilating a latitudinally and seasonally resolved data product serves two purposes. ~~On the one hand,~~
5 ~~deriving~~Firstly, to derive the global and annual means from sparse observations rests on knowledge or assumptions about spatial and seasonal distributions. Secondly, ~~a more-resolved-dataset-will~~to open the opportunity for some modelling groups to go beyond the prescription of global and annual mean ~~mixing-ratio:concentrations~~.

Undoubtedly, some of the assumptions stretch into unknown territory, such as the seasonality of the CO₂ ~~mixing ratio:concentrations~~ in pre-observational times or the time-variability of latitudinal gradients, let alone the higher frequency
10 fluctuations of global-mean ~~mixing-ratio:concentrations~~ during the time; when only ice core data are available. Errors in the historical forcing do propagate and can hinder the comparison between observations and models. This study therefore had to find a workable compromise between providing a complete dataset that covers the whole time and space domain and being as close as possible to ~~sometimes~~ sparse observations. Hence, the remaining uncertainties in concentration gradients should be kept in mind, although they might not be of primary concern in regard to the inter-comparison aspect of the multi-model
15 ensemble runs. Thus, while our CMIP6 community dataset will improve on the global- and annual-mean time-series prescribed for the last set of CMIP5 experiments on a number of key aspects, many research questions remain open.

The underlying ~~reason~~reasons for meridional gradients of annual-mean ~~mixing-ratio:is~~concentrations are manifold (Keeling et al. ~~1989a~~; Keeling et al. ~~1989b~~; Tans et al. ~~1989~~). For one, the sources of anthropogenic ~~greenhouse-gase:~~GHGs from fossil fuel burning and cement production or industrial activities are not evenly distributed with latitude, but concentrated in
20 the mid-northern land masses. In the case of CO₂, emissions from deforestation are not uniformly distributed with latitude either. The pattern of land ~~use~~-related emissions is even less stationary, with CO₂ uptakes and sources predominantly focussed in the mid-northern latitudes up until earlier in the 20th century, shifting more towards lower latitudes in recent decades (~~Hurt~~
~~et al. 2011~~)(Hurt et al., 2011). This study uses an approach based on simple regressions that implicitly rest on the assumption of a fixed pattern approximation (~~such as Keeling et al. 2011~~)(such as Keeling et al., 2011). One complication to retrieve the
25 latitudinal pre-industrial CO₂ concentration profile is that CO₂ fertilization and temperature effects on the carbon cycle ~~are~~
~~changing both~~, both over ocean and land, change both the magnitude and spatial patterns of natural CO₂ fluxes. Lastly, both the diurnal and seasonal cycle of photosynthesis and its covariance with vertical atmospheric mixing can have a pronounced effect on measured surface ~~mixing-ratio:concentrations~~ (the so-called 'rectifier' effect), increasing ~~annual mean~~ northern
hemispheric CO₂ ~~mixing-ratio:surface~~ concentrations by up to 2.5 ~~ppmv~~ppm (Denning et al. ~~1999~~).

~~In order to~~To dissect and analyse the different causes for temporal and spatial heterogeneity in surface ~~mixing ratio:concentrations~~, a rich body of literature analyses observed latitudinal and seasonal gradients with various inversion
30 techniques. Recent research provides a clearer picture in regard to the ~~root~~causes of the change in seasonality of CO₂ ~~mixing ratio:concentrations~~ (Forkel et al. ~~2016~~)(Forkel et al., 2016), a topic researched already in 1989 (Kohlmaier et al.

Field Code Changed

~~1989~~(Kohlmaier et al., 1989) based on the CO₂ fertilization effect on northern hemispheric terrestrial biota. Generally, the research into meridional and seasonal variations employs various atmospheric inversion techniques (Enting and Mansbridge ~~1989, Enting and Mansbridge, 1991, 1989~~; Enting et al., 1995; Enting, 1998; Rayner et al., 1999) to match observed ~~mixing ratio~~ concentrations with source and sink pattern estimates (~~Keeling et al., 1989a, Keeling et al., 1989b, Tans et al., 1990a, Enting et al., 1995, Rayner et al., 1999, Gurney et al., 2002, Gurney et al., 2003, Gurney et al., 2004, Baker et al., 2006, Peylin et al., 2013~~)(Baker et al., 2006; Enting et al., 1995; Gurney et al., 2002; Gurney et al., 2003; Gurney et al., 2004; Keeling et al., 1989a; Keeling et al., 1989b; Peylin et al., 2013; Rayner et al., 1999; Tans et al., 1989; Tans et al., 1990a). Similarly to CO₂, the spatial variation in CH₄ ~~mixing ratio~~ concentrations is used for model ~~synthesis~~ inversions (~~Fung et al., 1991~~) to infer sources and sinks (Fung et al., 1991; Kirschke et al., 2013).

10 There is a substantial lack of observational evidence of both seasonality and latitudinal CO₂ gradients in pre-industrial times. Given that atmospheric CO₂ is not well preserved in the ~~Greenland ice (Anklin et al., 1995, Barnola et al., 1995), the pre-observational north-south gradient cannot be calculated~~(Anklin et al., 1995; Barnola et al., 1995), ~~the pre-observational north-south gradient cannot be inferred or derived~~ from the Greenland and Antarctic ice core records. Alternatively, understanding biospheric sink and source dynamics could provide vital evidence to infer pre-industrial surface concentration patterns. In this

15 study, we do not employ any such inversion models or results, and only note that our pre-industrial meridional and seasonal variations should be regarded as highly uncertain. However, some plausibility of the CO₂ gradients is gained by comparison with some model studies (~~Discussion~~)section 5 'Discussion'. High-latitude records of CH₄ and N₂O are available from both hemispheres (~~Fluekeiger, MacFarling Meure et al., 2002, Schilt, 2006, Mitchell et al., 2010b, 2013, Rhodes et al., 2013~~) allowing us to estimate pre-industrial large-scale CH₄ concentration gradients.

20

2 Methods

In order to pursue To achieve the primary purpose goals of this study, namely the provision of a consistent set of historical surface greenhouse gas mixing ratios, a number of several analytical steps were taken to assimilate the observational data. Although global Global-mean and annual mean mixing ratios concentrations are of primary interest, but the discussion also covers latitudinal and seasonal variations in part because the. The assimilation procedure for sparse observational data does require requires accounting for this spatio-temporal heterogeneity in order to derive global and annual means.

We consider a total of 43 greenhouse gases in this study, namely GHGs: CO₂, CH₄, N₂O, a group of 17 ozone depleting substances, namely made up of five CFCs (CFC-12, CFC-11, CFC-113, CFC-114, CFC-115), three HCFCs (HCFC-22, HCFC-141b, HCFC-142b, CH₂CCl₂, CCl₄, CH₂Cl₂, CH₂Cl₂, CHCl₃, CH₃Br), three halons (Halon-1211, Halon-1301, Halon-2402), methyl chloroform (CH₃CCl₃), carbon tetrachloride (CCl₄), methyl chloride (CH₃Cl), methylene chloride (CH₂Cl₂), chloroform (CHCl₃), and methyl bromide (CH₃Br), and 23 other fluorinated compounds, namely made up of 11 HFCs (HFC-134a, HFC-23, HFC-32, HFC-125, HFC-143a, HFC-152a, HFC-227ea, HFC-236fa, HFC-245fa, HFC-365mfc, HFC-43-10mee), NF₃, SF₆, SO₂F₂, and 9 PFCs (CF₄, C₂F₆, C₃F₈, C₄F₁₀, C₅F₁₂, C₆F₁₄, C₇F₁₆, C₈F₁₈, and c-C₄F₈), NF₃, SF₆, and SO₂F₂.

All concentrations given here are dry air mole fractions and we use ‘mole fractions’, (mole) ‘mixing ratios’ and ‘concentrations’ interchangeably. For simplicity, we denote the dry air mole fractions ‘ $\mu\text{mol mol}^{-1}$ ’, ‘ nmol mol^{-1} ’ and ‘ pmol/mol^{-1} ’ as parts per million (ppm), parts per billion (ppb) and parts per trillion (ppt), respectively. Note that dry air mole fractions are independent of temperature and pressure, while volume mixing ratios (e.g. ppmv) for real non-ideal gases are not and at standard conditions can differ significantly from their corresponding mole ratios.

2.1 Summary of assimilation approach.

We perform three consecutive steps to synthesize the global mixing ratio mole fraction fields over the full time horizon from year 0 to year 2014. First, we aggregate the available observational data over the recent instrumental period. Second, we estimate three components of the global surface mixing ratio concentration fields from these data, namely global mean mixing ratios mole fractions, latitudinal gradients and seasonality. Thirdly Third, we extend those components back in time with inter alia – ice-core or firn data. The full historical GHG concentration field can then be generated by the time-varying components.

Under this basic assimilation model, the concentration $\hat{C}(l, t)$ at any point in time t and in a latitudinal band l can be written as:

$$\hat{C}(l, t) = \overline{C_{global}}(t) + \hat{S}_{l,m}(y) + \hat{L}_l(y) \quad (1)$$

Where $\overline{C_{global}}(t)$ is the global-mean mixing ratio dry air mole fraction at time t , and $\hat{S}_{l,m}$ is the seasonality in each latitude l and month m , and $\hat{L}_l(y)$ is the latitudinal annual-mean deviation in year y at latitude l . With this assimilation model, and the optimal low rank approximations of seasonality and latitudinal gradients, a regularisation of the data is performed by a principal components analysis, which creates a certain degree of robustness against data gaps or outliers. Other methods, like a harmonic

representation of station data, have, in principle, a similar smoothing and regularisation effect (Masarie and Tans 1995); although quantitative differences exist (section (Masarie and Tans, 1995), although quantitative differences exist (section 5.4): “Comparison”).

A detailed data flow diagram of how the historical greenhouse gas mixing ratios GHG mole fractions are derived in this study is provided in Figure 22-Fig. 1. The subsequent section will describe the method step-by-step, as indicated by the green circles in Figure 22-Fig. 1 and also tabulated for the three main GHGs in Table 1.

2.1.1 Step 1: Aggregating raw station data.

Atmospheric measurements are taken in remote environments or locations that are closer to pollution sources, in continental or marine areas, at different times of the day or night, at different altitudes, and different seasons of the year, often using different calibration scales. This poses challenges for any synthesis of observational data.

The observational station data over the recent decades used in this study are predominantly sourced from the networks operated by NOAA (Earth System Research Laboratories: ESRL), and AGAGE. In general, we use monthly station data provided by the respective networks as a starting point. In the case of the AGAGE network, monthly averages are provided with and without pollution events: (http://agage.eas.gatech.edu/data_archive/agage/ and http://cdiac.ornl.gov/ftp/ale_gage_Agage/AGAGE/).

We chose the monthly averages that include pollution events (file-endings ‘.mop’, with the exception of CH₂Cl₂, in which case data issues warranted the use of monthly station averages without pollution events). The approach that we do not restrict our source data to background conditions is consistent with our approach elsewhere – and the NOAA network monthly station averages - which do not screen out pollution events (although the dominant number of NOAA flask measurements might will likely be slightly biased towards background conditions rather than pollution events) - owing to their location and sampling

protocols at most sites focussed on collecting background air). In total, CO₂ data from 81 stations from the NOAA flask network, and 3 stations from the NOAA *in situ* data stations are used (Table 2). For CH₄, 87 sampling stations from the NOAA flask network and 5 stations from the AGAGE *in situ* network are compiled (Table 3). For N₂O, data from flask and *in situ* measurements at 13 stations of the NOAA HATS global network are combined with data from 5 stations from the AGAGE network (Table 4). For other gases, the AGAGE and NOAA coverage and timeframes vary, with individual station’s codes provided in panels f of the individual gases’ factsheets (Appendix A with Fig. 20 to Fig. 59). The complete AGAGE network is further described in Prinn et al. (2000a), with specific information for CFC-11 and CFC-12 provided in Cunnold et al. (1997), CH₂CCl₂ in Prinn et al. (2001, 2005) and Reimann et al. (2005), CCl₄ in Simmonds et al. (1998), CFC-113 in Fraser et al. (1996), CHCl₃ in O’Doherty et al. (2001), CH₃Br and CH₃Cl in Simmonds et al. (2004) and Cox et al. (2003), and HFC-134a, HCFC-141b, HCFC-142b and HCFC-22 in O’Doherty (2004) and Miller et al. (1998). We provide references to the used NOAA and AGAGE data in Table 12.

Calibration scales, i.e. the standardized gas mixtures that allow us to calibrate the instrumentation used for *in-situ* or flask measurements, are different between the NOAA and AGAGE networks. Gas measurements on different measurement scales, and even when using the same scales by different laboratories, are subject to uncertainties (Hall et al., 2014). For halocarbons,

the difference in calibration scales has been estimated as small, but not negligible, i.e. within 2.5%, often within 1% (Rhoderick et al., 2015).

While we use the station data that ~~has~~ have already been converted to the latest scales of the respective networks, some older comparison data products use previous scales (~~as~~ like the one published in the latest ozone assessment report (~~WMO 2014~~); (WMO, 2014)). Thus, where necessary, we convert those older data to the newer scales. For 7 gases, we use scale conversion factors to convert to the SIO14 scale, specifically 1.0826 for HFC-125 (from University of Bristol scale: UB98), 1.1226 for HFC-227ea (from Empa-2005), 1.1970 for HFC-236fa (from Empa-2009-p), and 1.1909 for HFC-245fa (from Empa-2005), 1.1079 for HFC-365-mfc (from Empa-2003), 1.0485 for HFC-43-10-mee (from SIO-10-p), and 0.9903 for CH₂Cl₂ (from UB98), with all conversion factors taken from the Appendix in WMO (2012).

Apart from those scale conversions to the latest NOAA and SIO scales mentioned above, we only make sure that the three main gases each are on a unified scaled. ~~As~~ In the case of CO₂, we source all our CO₂ station data from the NOAA network, ~~there is~~ which means no scale conversion ~~is~~ is necessary. In the case of CH₄, we account for different calibration scales by converting AGAGE CH₄ data (Tohuko University scale) to the NOAA scale (NOAA04) (multiplication by 1.0003). ~~Both~~ In the case of N₂O, both the AGAGE (SIO1998) and NOAA network calibration scales (NOAA-2006) ~~for N₂O~~ are compatible without the need for a conversion factor (~~WMO 2012~~); (WMO, 2012). The Law Dome data used here (MacFarling Meure et al., 2006; Rubino et al., 2013) have been updated for minor dating changes and upgrades to NOAA scales (http://www.esrl.noaa.gov/gmd/ccl/index.html).

Apart from those three main gases, we do not apply further scale conversions. Thus, given that our results are based on a mixture of the AGAGE and NOAA networks, they are de facto a weighted average between the respective two standard scales (SIO and NOAA) for each gas. The effective weight in this “weighted mean” depends on the station numbers and each ~~networks~~ network’s station distribution given that our assimilation method implicitly ~~weight~~ gives less weight to stations ~~less~~ that are geographically close, i.e. in the same latitude-longitude box. This mixture of scales is different from previous studies that either applied empirical scale conversions (so that global-mean or station averages are identical) or used both scales in parallel to estimate a measurement uncertainty ~~error~~ (~~WMO 2014~~), ~~for example when estimating emission with inverse techniques. Mathematically, our approach is similar to an approach~~ (~~WMO, 2014~~), ~~for example when estimating emissions with inverse techniques. Mathematically, our approach is similar to an approach~~ where a station-by-station scale conversion would be applied towards an intermediate scale between NOAA and AGAGE. However, for some applications, this approach is clearly a limitation as it hides the uncertainty and would for example warrant a new data assimilation if one network updates its scales (section 6); ‘Limitations’. The reason this “weighted mean” approach is chosen in the context of this study is that we intend to reconstruct a single ~~mixing-ratio~~ concentration history making use of the station data from both major measurement networks without giving preference to ~~the~~ one or the other measurement scale. Given that ~~scale~~ different scales between the two major networks result in differences ~~amount to~~ that are generally ~~below~~ less than 2% ~~differences~~; ~~and are~~ often for radiatively less important substances. this “middle of the road” approach seems justified given the other uncertainties in

climate ~~models~~ model forcings (vertical distributions, radiative forcing routines, other radiative forcings such as aerosols). Any conversion to a single scale would ease comparisons, but would not be able to address the inherent measurement uncertainty, and might even face a stronger bias (~~assuming that~~ if the two scales SIO and NOAA are equally plausible representations of the “truth”) (~~see limitations~~ section 6 ‘Limitations’).

5 ~~In~~ However, in regard to the time of the day, month or year, we do ~~however~~ not apply interpolation or adjustment techniques other than a simple monthly binning of all available data (see 2.1.2). The spatial and temporal coverages of the raw data used in this study are depicted in ~~Figure 17, Figure 18, Fig. 2, Fig. 3, and Figure 19~~ Fig. 4 for CO₂, CH₄ and N₂O data, respectively.

2.1.2 Step 2-4: Binning and spatial interpolation

10 We employ a simple monthly mean binning of all available data, separately averaged for each station. Stations with more than one measurement program, e.g. with flask and in-situ programs, are treated as distinct stations. Thus, the monthly average of an in-situ data series with 1000 measurement points gets the same weight as the monthly average from a flask measurement program with few observations. In each latitudinal / longitudinal box, all available monthly mean station data are averaged, with the mean being assigned to the grid box centre before employing a 2-dimensional spatial interpolation to extend available data points to longitudinal and latitudinal grid points that do not have observed data for any particular month. Our method provides equal weight to each station within a longitude-latitude box, no matter whether the station reports a few flask measurement samples or sub-hourly *in situ* instrument readings in each month. The chosen assimilation grid has 72 boxes with 12 equal-latitude bands of 15 degrees and 6 longitudinal bands of 30 degree. Following the temporal monthly binning and subsequent spatial linear interpolation, we average all data across the longitudes to obtain 12 latitudinally resolved monthly time series of surface mixing-ratios concentrations.

20 2.1.3 Step 5: Global mean mixing-ratios mole fractions

The annual-global mean concentration $\overline{C}_{global}(y)$ is ~~simply~~ derived as the area-weighted arithmetic mean of the binned latitudinal data (grey small “5” in ~~Figure 22~~ Fig. 1). In addition to the annual global mean, a time series of monthly values is derived as a smooth spline interpolation between the annual data points, with the constraint of being mean-preserving, i.e. that the average of the 12 monthly values is again the global annual average value initially-derived. Thus, the trend in the mixing-ratio mole fraction data is reflected in the global-mean time series from month to month.

25 2.1.4 Step 6: Latitudinal Gradient

The annual-mean latitudinal gradients are derived as first and second EOFs empirical orthogonal fields (EOFs) from the annual-average residuals per latitude after subtracting the global annual mean (step 6 in ~~Figure 22~~ Fig. 1). Let \mathbf{G} be the $n \times m$ matrix of n years with observations, and m latitudinal boxes, then \mathbf{G} can be decomposed into its EOFs and scores by calculating the singular value decomposition of $\mathbf{G} = \mathbf{U}\mathbf{D}\mathbf{V}^T$, where \mathbf{U} and \mathbf{V} are orthogonal matrices in $\mathbb{R}^n \times \mathbb{R}_n$ and $\mathbb{R}^m \times \mathbb{R}_m$, respectively, and \mathbf{D} is the $n \times m \times n \times m$ matrix with non-zero elements only on the diagonal. EOF _{i} is the i^{th} column of \mathbf{V} , and the score $S_i(y)$ of EOF _{i} in year y is given as the (y, i) entry of the \mathbf{UD} matrix. In other words, the EOFs are the eigenvectors of the gram matrix $1/m \times (\mathbf{G}^T \mathbf{G})$ and the scores are the projections of the observations \mathbf{G} onto the EOFs.

Those EOF scores are regressed with suitable predictors or extended constantly as constants. Thus, the term $\hat{L}(y)$ is the optimal low rank approximation of the latitudinal deviations from the global mean over-time-in-year y . The It is composed of the leading EOFs of latitudinal annual-mean variation multiplied with the observed or regressed score S of that year y .

$$\hat{L}(y) = \sum_{i=1}^{imax} EOF_i + S_i S(y) \quad (2)$$

5 with $imax$ being 1 or 2 if only the leading or the two leading EOFs are taken into account, respectively.

2.1.5 Step 7-10: Seasonality

The seasonality fulfils the condition that the sum of seasonal variations at each latitude is zero over the year, i.e.

$$\sum_{m=1}^{12} \hat{\delta}_{l,m} = 0 \quad (3)$$

10 This seasonality $\hat{\delta}_{l,m}(t)$ at time t is calculated for most gases as the relative seasonality $\frac{d\delta_{l,m}}{dc_{l,m}} \frac{dc_{l,m}}{dc_{global}}$, i.e. the seasonal/monthly deviation in mole fraction divided by the global-mean mole fraction, multiplied by the global-mean mixing-ratio/mole fraction at time t (step 7 and 10 in Figure-22 Fig. 1).

An exception is the case of CO_2 (step 8 and 9 in Figure-22 Fig. 1). In this case, the seasonality pattern over the observational period is held fixed as absolute mole fractions, i.e. not relative to the global mean. However, the residuals between this fixed seasonality and the seasonality, which is derived from the observations by subtracting the latitudinal averages, is-are used for a singular value decomposition. Let $R_{l,m}(t)$ be the residuals at latitude l and month m at time t , the optimal lower rank representation of this seasonal change is then given by the first EOF of the gram matrix $1/n \times \mathbf{R}^T \mathbf{R}$ with n being the number of observational data points. The derived score, i.e. the projection of the residuals onto the first EOF, is regressed against a time series P , a composite of global-mean CO_2 concentration and historical observed global-mean surface air temperatures.

25 This simplified choice is taken asbecause previous studies identified warmer temperatures and elevated CO_2 mixing-ratio/mole fractions as dominant reason/reasons for increased seasonality (Graven et al., 2013; Forkel et al., 2016; Graven et al., 2013; Welp et al., 2016), although anthropogenically induced cropland productivity increases are also suggested to play also some role (Gray et al., 2014) (Gray et al., 2014). Specifically, P is assumed as a composite of the product and the sum of normed global-mean surface air temperature and normed CO_2 mixing-ratio/mole fraction deviations from pre-industrial levels. The temperature and mixing-ratio/mole fraction deviations are normalized such that the 2000-2010 deviation from the 1850-1880

base period is set to one. Thus, the regressor P can be described as:

$$P(t) = \frac{\Delta T(t) + \Delta C(t)}{2} + \frac{\Delta T(t) + \Delta C(t)}{2} \quad (4)$$

With ΔT being the normed temperature deviation from the 1850-1880 period, specifically

$$\Delta T(t) = \frac{(T(t) - \sum_{i=1850}^{1880} T(i))}{\sum_{i=2000}^{2010} (T(t) - \sum_{i=1850}^{1880} T(i))} \quad (5)$$

30 And ΔC being synonymously the normed mixing-ratio-deviation. Note that this regressor P is one of multiple options that were tested and could be regarded as a plausible regressor for seasonality changes. However, given that seasonality changes in the case of CO_2 depend on a complex interaction of CO_2 fertilization of temperate, seasonal gross primary productivity, as well as

the influence of temperature, precipitation on biomass growth and respiration, this extension of the observed seasonality changes beyond the observational period is just that: a plausible extrapolation that needs to be refined by further research to replace this study's *ad hoc* assumption. Note that this regressor P is one of multiple options that were tested and could be regarded as a plausible regressor for seasonality changes. Specifically, we tested global-mean CO₂ concentrations, global-mean annual average surface air temperatures and lagged averages of surface air temperatures as regressors (see Fig. 5). The R-squared values of the regressions over the 1984-2014 period are relatively similar across all regressors, around 0.8. The marked difference is that the regression with only CO₂ concentrations would result in a stronger reduction of seasonality around 1940-1960 and before 1900. By 1850, the reduction of summertime CO₂ concentrations in the zonal band around 52.5°N would be around 8.6 ppm compared to 2014 (multiply the differences of the seasonality scaling difference between 1850 and 2014, about 21, with the 0.41 ppm maximum of the EOF pattern, shown in Fig. 9 a.2). In contrast, the other regression options would limit the maximal seasonality change to about 5.7ppm, closer to the maximal seasonality change detected within the period 1984-2014, of 4.5ppm (cf. Fig. 5e). Given the uncertainty in regard to pre-1960 seasonality, we opted for the more conservative extrapolation method that implies a less significant change outside the observational period and chose the regressor with the least variability, namely our composite regressor combining temperature and CO₂ concentrations.

Despite the differences in the regressors, it should be noted that early CO₂ observations are too sparse to come to a definite conclusion in regard to which regressor is best suited – given the induced differences around 1960s and 1970s are fairly small compared to the noise in the observations (see panel f and g of Fig. 5). Furthermore, seasonality changes in the case of CO₂ depend on a number of factors, inter alia: complex interaction of CO₂ fertilization of temperate, seasonal gross primary productivity, the influence of temperature, precipitation on biomass growth and respiration, as well as directly human-induced changes in land use areas and their productivity. Therefore, this extension of the observed seasonality changes beyond the observational period based on a regression with temperatures and CO₂ concentrations is just that: a plausible extrapolation that needs to be refined by further research to replace this study's *ad hoc* assumption.

The empirical measured seasonality of CH₄ and N₂O over the observational time period is found to be closely approximated by our default assumption of a seasonality that is proportional to global mean mixing ratios/mole fractions. For a number of several other substances, however, seasonality has been assumed to be zero – either because the diagnosed seasonality was very small or due to a lack of observational data.

2.1.6 Step 11-13: Extension of latitudinal gradients and global means with ice core and firn data

Historical GHG records from ice and firn provide high-latitude estimates of atmospheric greenhouse gas mixing ratios/GHG mole fractions before the instrumental record from air sampling stations. We rely mainly on the Law Dome (Etheridge et al., 1998b, 1998a; Etheridge et al., 1996; MacFarling Meure et al., 2006; Rubino et al., 2013) and, for northern hemisphere CH₄, Greenland NEEM ice core data (Rhodes et al., 2013) (Rhodes et al., 2013). Although we did not directly use their data, we acknowledge multiple other efforts, including, but not limited to Mitchell et al. (2013), and Bauska et al. (2015), Schilt et

al. (2010b), Flueckiger et al. (2002), and Sowers et al. (2003) (Fig. 6). Law Dome atmospheric composition records have the advantage of a very narrow air age spread that provides measurements with high temporal resolution and mean air ages up to the 1970s, where they overlap with the beginning of atmospheric observations for many gases. ~~The Law Dome data used here have been updated for minor dating changes and upgrades to NOAA scales (Rubino et al., 2013; <http://www.esrl.noaa.gov/gmd/ccel/index.html>).~~

Having obtained estimates of the latitudinal gradients over the observational period and having derived approximations back in time by regressing latitudinal gradients EOF scores with emissions (step 11 in Figure 22), ~~this allows estimating Fig. 1, Table 4), we can estimate~~ global mean ~~mixing ratios/mole fractions~~ based on the Law Dome data ~~in the case of~~ for both CO₂ and N₂O (step 12 in Figure 22) ~~Fig. 1~~. In the case of CH₄, the advantage is that there are northern hemispheric data ~~points~~ available from NEEM (Greenland) ~~(Rhodes et al., 2013) that complement the Law Dome record over the past 2000 years (Rhodes et al., 2013) over the past 2000 years.~~ This NEEM record hence allows an optimisation of both the EOF scores and global means at past time points to match both the Law Dome and NEEM records (step 13 in Figure 22) ~~Fig. 1~~. Some data ~~periods with gaps~~ in the NEEM record are filled by linearly interpolating the optimised EOF scores of the latitudinal gradient. With an interpolated EOF score, the global-mean ~~mixing ratio/mole fraction~~ can then be directly inferred from the Law Dome record.

All optimisations are performed by minimising area-weighted squared residuals.

The Law Dome ice core data are smoothed with a piecewise local 3rd degree polynomial median regression, using ad hoc expert judgement assumptions of errors and smoothing window widths specific to each gas in order to approximately reflect their long-term median evolution. In the case of CO₂, a random error of 2 ~~ppmv/ppm~~ was assumed, a percentage age error ~~(reaching a maximum of 60 years at age 2000 years before present)~~ with a bagging of 250 ensembles, a kernel width of 120 years, minimal number of data points of 7 and maximum of 25 (panel a in Fig. 8). Likewise, CH₄ Law Dome data ice core data are smoothed with a 3rd degree polynomial median regression with a maximum kernel width of 100 years, 4 minimal data points (a constraint that overwrites the maximum kernel width, if necessary) and 10 maximal data points. ~~Like As~~ for CO₂, 250 ensembles were averaged, after adding noise of 3ppb, and an age uncertainty of 50 years ~~for per~~ 2000 years. For N₂O, a kernel width of 300 years was chosen with a minimum number of 7 and maximum number of 15 data points to be included in the piecewise 3rd degree polynomial regression. As for CO₂ and CH₄, 250 ensembles were used for bagging after injecting a random noise of 3 ~~ppbv and an age-dependent x-axis uncertainty of 90 years per 2000 years: ppb and an age-dependent x-axis uncertainty of 90 years per 2000 years. The higher age uncertainty for N₂O in comparison to CO₂ and CH₄ was chosen to account for the larger age gaps in the N₂O Law Dome data that required a stronger horizontal smoothing for the median regression to converge. For CO₂, the slightly higher age uncertainty in comparison to CH₄ was chosen so that the smoothed record displays a comparable time evolution to the WAIS CO₂ record (Fig. 6).~~

The Greenland NEEM ice core CH₄ data ~~(Rhodes et al., 2013) exhibits some outliers in the recent period (Rhodes et al., 2013) exhibits some outliers in the recent period (Fig. 6d)~~ due to incursion of modern air into still-open pores of shallow ice. Spikes in deeper ice are likely due to impurities. Hence, we use the 5-year smoothed data provided by Rhodes et al. (2013) as a proxy

for atmospheric background mixing ratios. We dated the NEEM firn air samples (Buizert et al. 2012) using the effective age procedure as in Trudinger et al. (2002) with the ages published in Gosh et al. [Greenland atmospheric background mole fractions \(open red circles in Fig. 6b and d\)](#). We used the NEEM CH₄ firn measurements from Buizert et al. (2012) (2008 campaign), with effective ages from Ghosh et al. (2015) with a small correction to the NOAA-2006 scale data applied for gravity effects (as applied in other ice and firn data), using here only firn samples from the 2008 campaign, based on the iterative dating method of Trudinger et al. (2002b), corrected for the effect of gravity (as applied in other firn data) and put onto the NOAA 2006 primary calibration scale.

2.1.7 Step 14: Extension of latitudinal gradients and global means with literature data

For several gases, including ozone depleting substances, halons and PFCs, the available AGAGE and NOAA station data is sparse spatially. Before the start of systematic instrumental measurements, we use literature studies which make use of various data sources, such as air sample archives or firn records (step 14 in [Figure 22-Fig. 1](#)). Specifically, if a global mean is provided, we use that global mean in conjunction with our derived and regressed latitudinal gradients. In the case of hemispheric data-points, we adapt the latitudinal gradient to match the literature studies, as in the case of C₄F₁₀, C₅F₁₂, C₆F₁₄, C₇F₁₆ or C₈F₁₈, where we based both the global mean and latitudinal gradients on the data of Ivy et al. (2012),(2012). Other key studies used were Velders et al. (2014) and Daniel (2014), the data underlying the WMO Ozone Assessment Report (2014), Arnold et al. (2013; 2014), Trudinger et al. (2004), Mühle et al. (2010; 2009-2010a), Montzka et al. (2011), updated time series by Montzka et al. (1999) (updated at: ftp://ftp.cmdl.noaa.gov/hats/Total_Cl_Br/), the recent Halon study by Vollmer et al. (2016) in regard to Halons and PFC study by Trudinger et al (2016) as indicated in the gas-specific factsheet figures (Figure 23 to Figure 62) in regard to PFCs, and others (Arnold et al., 2013; Arnold et al., 2014; Butler et al., 1999; Ivy et al., 2012; Montzka et al., 2015; Mühle et al., 2010; Oram et al., 2012; Trudinger et al., 2016; Velders and Daniel, 2014; Vollmer et al., 2016; Worton et al., 2007), as indicated in the gas-specific factsheet figures (Appendix A Fig. 20 to Fig. 59 with references provided in Table 12). In the case of N₂O and CH₂Cl₂ we assumed a constant latitudinal gradient back in time before ongoing measurement records are available (Fig. 12, and Appendix A Fig. 26, respectively).

2.1.8 Step 15: Extrapolation

For some limited data segments, an extrapolation has been used. Either a piecewise smoothing spline to converge mixing ratio-concentrations back to zero or pre-industrial background mixing ratios-concentrations, e.g. before the WMO (2014) or Velders et al. (2014) data started. Furthermore, a linear extrapolation was applied, when there were not sufficient 2014 data available, or Velders and Daniel (2014) data started in 1978 or 1951, respectively. The three radiatively most important fluorinated species CFC-12, CFC-11 and HCFC-22 (Table 5) follow the global mean concentrations provided by Velders and Daniel (2014), in conjunction with separately derived latitudinal gradients and seasonality. Furthermore, a linear extrapolation was applied when there were not sufficient 2014 data available.

2.1.9 Step 16-19: Creating the composite surface ~~mixing-ratio~~concentration field

Following equation (1), the surface ~~mixing-ratio~~mole fraction fields over the full -time span are now synthesized from the lower rank representations of seasonality, latitudinal gradient and the smooth monthly representation of global mean ~~mixing ratios~~mole fractions. As per the original station data aggregation, the latitudinal resolution is 15 degrees and ~~the~~ time resolution is monthly. In order to assist ~~the~~with application in climate models with finer grids, we ~~also~~ produced ~~also~~ a finer grid interpolation to 0.5 degree latitudinal resolution using a mean-preserving smoothing. This finer grid interpolation should not be mistaken as ~~mixing-ratio~~a mole fraction field containing actual information at 0.5 -degree level. The purpose is simply to offer a smooth interpolation that avoids errors that will arise from, e.g., a linear interpolation between the provided 15 degree latitude points, as the mean across those (linearly) interpolated values, would not match the original field. The mean-preserving smoothing code is available from the authors on request. Finally, the 15 degree fields are aggregated ~~towards~~into global, northern and southern hemisphere monthly and annual means.

2.1.10 Step 20: Aggregating equivalent ~~mixing-ratios~~mole fractions

It is computationally inefficient to model the radiative effect of 43 individual ~~greenhouse-gases~~GHGs in today's Earth system models or general circulation models. Climate models use different pathways to approximate the radiative effects of the full set of ~~greenhouse-gases~~GHGs. As one strategy, only the radiatively-major ~~greenhouse-gases~~GHGs are explicitly modelled, such as CO₂, CH₄, N₂O, CFC-12, CFC-11, which together cause 94.5% of GHG warming effect (measured in radiative forcing) in 2014 ~~rel-relative to~~ 1750 and 98% of the total radiative effect compared to the full set of 43 GHGs (Table 5). Alternatively, radiatively-minor GHGs can be approximated by equivalent ~~greenhouse-gas~~GHG concentrations of a marker gas. In this way, the radiative effect of the group of gases is expressed by a single gas ~~mixing-ratio~~mole fraction. One definitional issue is whether the radiative forcing since 1750, i.e. only the changes since pre-industrial levels, are expressed by the marker gas (here called 'marginal equivalence' $C_{eq,i}$). In this case, the marker gas' concentrations $C_{eq,i}$ are sought that would exert the same aggregate radiative forcing since 1750 as the group of summarized gases. Thus, let $C_j(t)$ be the concentration (~~volumetric-or~~ mole ~~mixing-ratio~~fraction in dry air) of a ~~greenhouse-gas~~GHG and $C_{0,j}$ the pre-industrial level, i.e. in year 1750 that is routinely used as base year for radiative forcing (IPCC 2013). ~~A marker equivalence mixing-ratio-by-gas~~ $C_{eq,i}$ (IPCC, 2013). ~~A marker equivalence mole fraction by gas~~ $C_{eq,i}$ for group C_j with $j = 1, \dots, n$ is then given by:

$$C_{eq,i} C_{eq,i}(t) = R_i^{-1} \left(R_i(C_{0,i}) + \sum_{j=1}^n \left(R_j(C_j(t)) - R_j(C_{0,j}) \right) \right) \quad (6)$$

With $R_j(C)$ being the radiative forcing function relating ~~mixing-ratios~~concentrations $C(t)$ at time t to radiative forcing for gas j , in the linear case $R_j(C) = C * E_j$ with E_j being the radiative efficiency. $R_i^{-1}(F)$ is the inverse of this radiative forcing function, so that the ~~mixing-ratio~~concentration C that corresponds to a forcing F is given by $C = R_i^{-1}(F)$.

In contrast, equivalent ~~mixing-ratio~~concentrations can express the radiative effects of the summarized ~~greenhouse-gases~~GHGs including their natural background levels (here called 'full equivalence' $C'_{eq,i}$).

$$C'_{eq,i}(t) = R_i^{-1} \left(\sum_{j=1}^n R_j(C_j(t)) \right) \quad (7)$$

While the former definition ‘marginal equivalence’ is often used to express the total ~~greenhouse-gas~~GHG forcing in CO₂ equivalence ~~mixing-ratios~~concentrations, the latter ‘full equivalence’ is the more appropriate quantity to drive climate models, given that natural background ~~mixing-ratios~~concentrations of not-explicitly considered gases should nevertheless exert a radiative effect even in a pre-industrial control, even though that radiative effect does not count under a radiative forcing definition that looks at changes from 1750.

In the linear case, in which case radiative forcing is proportional to the gas’ ~~mixing-ratios~~concentrations, equation (7) can be written as:

$$C'_{eq,i} C_{eq,i}(t) = \frac{\sum_{j=1}^n \frac{\tau_j^{eff} C_j(t)}{\tau_j^{eff}}}{\tau_i^{eff}} \sum_{j=1}^n \tau_j^{eff} C_j(t) \quad (8)$$

With τ_i^{eff} being the radiative efficiency of the gas i in W/m² per ppbvppb.

Thus, climate models have the option to reduce the complexity of 43 GHGs and the associated computational burden by reducing the number of GHGs that are taken into account. With the top 5 GHGs, CO₂, CH₄, N₂O, CFC-11 and CFC-12, climate models would capture 98% of the total radiative effect in year 2014 and 94.5% of the radiative forcing since 1750, i.e. the change of the radiative effect between 1750 and 2014 (see [Table 5](#)). As an alternative, there is the option to use equivalent ~~mixing-ratios~~concentrations. For two such equivalence options, this study provides input data sets. Modelling groups should indicate the combination of files they employed:

- a) **Option 1:** Climate models implement a subset of 43 ~~greenhouse-gases~~GHGs.
- b) **Option 2:** Climate models implement the four most important GHGs with their actual ~~mixing-ratios~~mole fractions explicitly, namely CO₂, CH₄, N₂O and CFC-12 and summarize the effect of all other 39 gases in an equivalence ~~mixing-ratio~~concentration of CFC-11. For this purpose, we provide CFC-11-eq ~~mixing-ratios~~concentrations (‘full equivalence’).
- c) **Option 3:** Like option 2, but with a different split up of gases other than CO₂, CH₄ and N₂O. Climate models implement the three most important GHGs with their actual ~~mixing-ratios~~mole fractions explicitly, namely CO₂, CH₄, and N₂O and summarize the radiative effect of the ozone depleting substances in a CFC-12-eq ~~mixing-ratio~~concentration and the radiative effect of all other fluorinated gases as a HFC-134a-eq ~~mixing-ratio~~concentration. For this purpose, we provide CFC-12-eq and HFC-134a-eq ~~mixing-ratios~~concentrations (‘full equivalence’).

2.2 Data analysis for ~~comparisons~~comparison with CMIP5 ESMs

We compare our results to ~~a number of comparison products, namely the~~various other datasets (see [section 5](#)), *inter alia* to CO₂ fields from CMIP5 Earth System Models (ESMs) ([section 5.3](#)). Here, we briefly describe the analytical steps that we performed for retrieving the CMIP5 ESM data.

Analyzed are We analyse ten CMIP5 ESMs models that have an interactive carbon cycle model and provided the mole fraction of carbon dioxide in the air as function of different pressure surfaces for the *esmhistorical* experiment. We diagnosed those *esmhistorical* experiments in terms of the simulated CO₂ mixing ratio mole fraction at surface pressure (1bar = 100000 Pa) for 10 CMIP5 ESM model: ESMs, for which data were available: (1) BNU-ESM (BNU, China), (2) CanESM2 (CCCMA, Canada),
5 (3) CESM1-BGC (NSF-DOE-NCAR, USA), (4) FIO-ESM (FIO, China), (5) GFDL-ESM2G (NOAA GFDL, USA), (6) GFDL-ESM2M (NOAA GFDL), (7) MIROC-ESM (MIROC, Japan), (8) MPI-ESM-LR (MPI, Germany), (9) MRI-ESM1 (MRI, Japan), (10) NorESM1-ME (NCC, Norway). For the models CanESM2, MIROC-ESM and MPI-ESM-LR more than one realization is available. We calculated an ensemble mean based on the all available ensemble members. The climatological seasonal cycle (Figure-13 Fig. 62, Figure-14 Fig. 63) is calculated relative to the linear trend of the corresponding 30-year
10 periods.

3 Results

Here, we describe the historical mixing-ratios/concentrations of the main greenhouse-gases/GHGs and provide a fact sheet for all 43 individual gases.

3.1 Carbon Dioxide

The 800-thousand-year EPICA composite ice-core record (Lüthi et al., 2008) indicates that CO₂ mixing-ratios have fluctuated between 170 and 270 ppmv. The 800,000 years EPICA composite ice-core record (Ahn and Brook, 2014; Bereiter et al., 2015; Bereiter et al., 2012; Lüthi et al., 2008; MacFarling Meure et al., 2006; Marcott et al., 2014; Monnin et al., 2004; Petit et al., 1999; Schneider et al., 2013; Siegenthaler et al., 2005) (available at <ftp://ftp.ncdc.noaa.gov/pub/data/paleo/icecore/antarctica/antarctica2015co2.xls>) indicates that CO₂ concentrations have fluctuated between 170 and 270 ppm (Fig. 6a) in conjunction with glacial- and inter-glacial temperature variations. From the year 0 to 1000, our piecewise fit of the 3rd degree polynomial of Law Dome ice core data allows a derivation of global mean mixing-ratios/concentrations of around 278.6 ppmv/ppm (min-max range of 277.0 to 280.2 ppmv/ppm).

Our smoothed Law Dome results do not reflect the higher frequency variations suggested by the individual data points (Etheridge et al., 1996; MacFarling Meure et al., 2006; Rubino et al., 2013) and are comparable to the frequency spectrum that would result from a smoothed median estimate of WAIS data by Bauska et al. (2015) and Ahn et al. (2012). The WAIS record is generally 3-6 ppmv/ppm higher than the Law Dome record and is also higher than South Pole and EPICA DML ice cores (Ahn et al., 2012). The cause for this difference is not yet known (Figure 1b). In terms of the various possible frequency spectra (Ahn et al., 2012) and the Dronning Maud Land ice (Rubino et al., 2016). The cause for this difference is not yet known (Fig. 6b). The differences between the WAIS and the Law Dome record persist in 1850 to 1890 with subsequent data points being more aligned with each other (Fig. 6c). CMIP6 modelling groups might want to test an alternative data set that captures those higher frequency characteristic characteristics of the Law Dome record (data can be generated by the authors on request). In that higher frequency data set, the minimum of global mean CO₂ mixing-ratios/concentrations is close to 270 ppmv/ppm around the year 1615/1610. The smoother version now provided for CMIP6 has its minimum in year 1666 at 276.27 ppmv/ppm (Fig. 6b). The reason for the 1610 dip in the Law Dome record and why this does not show in the WAIS record is not yet fully understood. The current understanding of how the age kernel (to estimate the distribution of age of air at the time of bubble trapping) is different for the two sites cannot yet explain this difference in mixing-ratios/concentrations around 1610.

In regard to the latitudinal gradient, we explored various options. If we regress the scores of the first EOF of the latitudinal gradient (Fig. 9d) against global fossil CO₂ emissions, the pre-industrial latitudinal minimum of surface CO₂ mixing ratios/concentrations would be estimated in the mid-northern latitudes (approximately 1.8 ppmv/ppm below the global-mean), where the maximum was observed in recent decades (e.g. 4.8 ppmv/ppm above the global-mean in 2010). Previously a similar regression approach between mixing-ratios/concentrations and CO₂ emissions was used by Keeling et al. (2011) to separate the anthropogenic from the natural component in the mixing-ratio/concentration difference between Mauna Loa and the South Pole. While this This approach is not perfect due to the covariance of regional fossil fuel emissions with natural sinks over the same

period, different patterns of anthropogenic land-use emissions, and a latitudinal gradient component that merely results from seasonal CO₂ exchange (e.g. Denning et al. 1995), it can nevertheless (e.g. Denning et al., 1995). However, it can provide a first indication of the influence of anthropogenic emissions on the latitudinal gradient. Furthermore, this approach would have resulted in an approximately 0.4 ppmv higher pre-industrial Antarctic CO₂ concentration compared to the global mean, coinciding with the assumption taken by Rubino et al. (2013).

However, given the evidence by CMIP5 ESM models of a slight tropical local maximum (Fig. 9b) and large uncertainties with regard to pre-industrial sinks and source distributions and hence the latitudinal gradients of CO₂, we assumed a zero pre-industrial latitudinal gradient. Thus we performed a zero-intercept regression of the scores of the latitudinal gradient EOF1 with global fossil CO₂ emissions and converging the score of the second EOF towards zero, resulting in a flat latitudinal gradient in pre-industrial times.

The second EOF of the latitudinal gradient of CO₂ does not exhibit the same linearity over time as the first EOF, and the reasons are currently unknown. Potential candidates for this pronounced spike of mid-northern latitude mixing ratios in the case of CO₂ are a shift in station sampling locations with more 'polluted' land station coming on line after 1995, the 'rectifier' effect due to an enhanced seasonal cycle (Denning et al. 1995), and the rise of Chinese emissions (albeit the onset of the recent surge in Chinese CO₂ emissions is often demarked to start slightly later, only by 2003 (Francey et al. 2013)). One suggested explanation for this 2010 change in north-south gradients are changes in interhemispheric transport (Francey and Frederiksen 2016). Recently, i.e. after 2010, this spike in mid-latitude northern mixing ratios seemed to somewhat subside again according to our analysis (see scores for EOF1 and EOF2 in Figure 2d). Future research could further investigate Potential candidates for this pronounced spike (Fig. 9c) of mid-northern latitude concentrations in the case of CO₂ are a shift in station sampling locations with more 'polluted' land station coming on line after 1995, the 'rectifier' effect due to an enhanced seasonal cycle (Denning et al., 1995), and the rise of Chinese emissions (the onset around year 2003 of the recent surge in Chinese CO₂ emissions is approximately coinciding with the respective EOF score becoming strongly positive (Fig. 9d) (Francey et al., 2013)). One suggested explanation for this 2010 change in north-south gradients are changes in interhemispheric transport (Francey and Frederiksen, 2016). Recently, i.e. after 2010, this spike in mid-latitude northern concentrations seemed to somewhat subside again according to our analysis (see scores for EOF1 and EOF2 in Fig. 9d). Future research could address the underlying reasons of this change in latitudinal patterns and a physical explanation will allow a more appropriate backward extension in time.

The diagnosed average seasonality of atmospheric CO₂ concentrations over the observational period reflects the standard carbon cycle pattern of strong CO₂ uptake in spring and release in autumn due to photosynthesis and heterotrophic respiration in the northern hemispheres ecosystems. Our EOF analysis of the residuals then shows (Fig. 9a.2 and Fig. 9a.3) that the seasonality has increased over recent decades in line with previous studies, which explore the link to increased ecosystem productivity (Graven et al. 2013; Forkel et al., 2016; Graven et al., 2013; Welp et al., 2016) and increased cropland productivity (Gray et al. 2014) (Gray et al., 2014). Specifically, our analysis shows a slight shift of the seasonality to earlier

months in the year, i.e. the negative and positive deviations of the EOF pattern are shifted by a month compared to the average seasonality (cf. Fig. 9a.1 and Fig. 9a.2). The strongest change in CO₂ seasonality is derived for the latitudinal bins centered around 37.5 to 67.5 degree north bins with a maximum strengthening of negative deviations in the 52.5 degree north latitudinal band in July by around 4 ppmv over 1984 to 2013 (4 ppmv results from multiplying the EOF pattern value in July in the 52.5-degree bin with the EOF score difference of around 10, see Fig. 9a.2 and a.3). Although the maximum strengthening of the seasonal cycle happens in July in the 52.5-degree latitudinal band, however the maximum seasonal cycle deviation is still observed slightly later in August and extends also slightly more towards the northern latitudes (Fig. 9a.1).

In 1850, the start of the historical CMIP6 simulations, the estimated global-mean CO₂ concentration is 284.32 ppmv, rising to 295.67 ppmv in 1900, 312.82 ppmv in 1950, 369.12 ppmv in year 2000 up to 397.55 ppmv in 2014 (Table 6). Here and elsewhere (e.g. Table 6) we provide more significant figures than customary - not to claim a 5-digit precision of the data (which is not given), but to avoid unnecessary (even if small) step changes in mixing ratios between the pre-industrial run and the historical and other runs. Variations in Our methodology does not include a formal uncertainty analysis. As a minimum uncertainty for the increase of global 1850's pre-industrial values, we refer to the 1.2ppm variability stated by Etheridge et al. (1996), also used in Rubino et al. (2013) and Trudinger et al. (2002a) as minimum uncertainty for that period.

Global-mean surface CO₂ concentration growth slightly flattens off in the 1930s and then a stronger flattening occurs during the World War II until the 1950s (Bastos et al., 2016). The increase from 1970 onwards has a slightly positive curvature (accelerating trend) with small deviations around 1973, 1981 and the temporary flattening of CO₂ concentrations after the 1991 Pinatubo eruption (Jones and Cox, 2001; Peylin et al., 2005) (Fig. 9 and Fig. 10).

3.2 Methane

Over the 800 thousand years before Year 0, atmospheric CH₄ concentrations varied between 348.7 ppbv and 728.4 ppbv according to the EPICA ice core composite (Barbante et al., 2006, 2006b; Capron et al., 2010; Loulergue et al., 2008; Capron et al., 2010) (Fig. 6c and Fig. 11). The Law Dome record (Etheridge et al., 1998a; MacFarling Meure et al., 2006) indicates an onset of increasing mixing ratios around the year 1720 (Figure 1d, and). The Law Dome record (Etheridge et al., 1998a; MacFarling Meure et al., 2006) indicates an onset of increasing concentrations around the year 1720 (Fig. 6d, and Fig. 11). From Year 1850 with slightly higher than 800 ppbv mixing ratios, a slight rise is observed until the 1950s, when CH₄ concentrations markedly increase first in the latter half of the 1950s, then again from 1965 onwards. The Greenland firn and ice core data (Rhodes et al., 2013) (Rhodes et al., 2013) are more difficult to interpret because part of the record is affected by high frequency ice core CH₄ signals, possibly of non-atmospheric origin. CH₄ spikes are accompanied by elevated concentrations of black carbon, ammonium and nitrate, suggesting that biological *in situ* production may be responsible – particularly in the later years of the record since 1940. Taking here the 5-

yearly average measurement values with outliers removed (Rhodes et al., 2013) (Rhodes et al., 2013) that approximate the lower bounds of the raw data points until 1942, we can then infer global gradients back in time and derive an estimate of global-mean ~~mixing-ratios:concentrations~~. These global-mean ~~mixing-ratios:concentrations~~ are estimated to be around 30 ~~ppbv:ppb~~ higher than the Law Dome record by 1850, with the difference growing to 45 ~~ppbv:ppb~~ by 1940s, increasing further from there (Fig. 6d). This approximately matches the findings by Mitchell et al. (2013) of inter-polar differences between ~~about 35~~ and 45 ~~ppbv since 400ppb between 800 BC and 1700 AD~~.

Our analysis of CH₄ ~~mixing-ratios:concentrations~~ in the recent decades is based on a large number of stations (Table 3 and Fig. 11f). While the annual increase of global CH₄ ~~mixing-ratios:concentrations~~ slowed over the 1980s and markedly after 1992 towards stabilized ~~mixing-ratios:concentrations~~ between 1999 to 2005, CH₄ increased again after 2006 at about 5.4 ~~ppbv:ppb/yr~~ (Fig. 11f).

~~We retrieve a~~ (Nisbet et al., 2016; Nisbet et al., 2014).

~~We retrieve a recent~~ seasonal cycle of CH₄ that is similar in the spatial-temporal seasonality pattern as that of CO₂ (Fig. 11a). Each hemisphere exhibits its lowest CH₄ ~~mixing-ratios:concentrations~~ just after the summer solstice, up to 1.6% or 28 ~~ppbv:ppb~~ lower than the global mean in the case of the high-latitude northern summer (Fig. 11a). Quantifying the underlying reasons is beyond the scope of this study, although the seasonally varying atmospheric ~~sinks:sink~~ by OH oxidation ~~are:is~~ likely the main contributor to that ~~seasonal~~ pattern – in combination with seasonally varying natural and anthropogenic sources.

The latitudinal annual-mean gradient of CH₄ ~~mixing-ratios:concentrations~~ is separated into its first two EOFs, with the first EOF being a continuous north-to-south gradient of about 90 ~~ppbv:ppb~~ in the recent observational period (combination of EOF and its score, see Fig. 11c and d). The second EOF is a distinct mid-northern latitude local maximum with a high-latitude low, showing a slight but marked rise in 2008 within the 1985 to 2014 observational data window. Quantifying the reasons for this hump are again beyond the scope of this study, with the possibility of a shift in locations of sampling stations or coal-seam gas-fracking related fugitive emissions being possible contributors. While we optimize the first EOF, the general north-south gradient to match the Greenland data and Antarctic Law Dome data in the past, we keep the second EOF of the latitudinal gradient constant at its 1985 value.

As a result of the constant extrapolation of the second EOF, and the optimization of the first EOF's score (Fig. 11d), we yield a total annual-mean meridional gradient for the last decades that features around 80 ~~ppbv:ppb~~ higher surface CH₄ ~~mixing-ratios:concentrations~~ in mid-to-high northern latitudes compared to the global mean and around 60 ~~ppbv:ppb~~ lower CH₄ ~~mixing-ratios:concentrations~~ at the high southern latitudes (Fig. 11b). In pre-industrial times, our approach of regressing the score of EOF1 with global emissions (Gütschow et al., 2016) suggests this gradient to be smaller, with only approximately 20-30 ~~ppbv:ppb~~ higher northern and 20 ~~ppbv:ppb~~ lower southern latitude surface ~~mixing-ratios:concentrations~~ (Fig. 11b). These mean inter-polar differences and their variations have earlier been quantified by Etheridge (1998a) and Mitchell et al. (1998a) and Mitchell et al. (2013), yielding similar results (between 30 to 60 ~~ppbv:ppb~~) compared to our 40 to 50 ~~ppbv:ppb~~ estimate.

3.3 Nitrous Oxide

N₂O ~~mixing-ratios~~concentrations from ice cores dating back 800 ~~thousand,000~~ years (Fluckiger et al., 2002; Schilt et al., 2010b) ~~varied approximately between 200 ppbv and 300 ppbv, with most recent glacial mixing ratio minima of 180 ppbv around 23 thousand years ago (Sowers et al., 2003)~~ (varied approximately between 200 ppb and 300 ppb, with most recent glacial concentration minima of 180 ppb around 23 thousand years ago (Sowers et al., 2003) (Fig. 6a)). The ice core record over the last 2000 years indicates marked difference between the Law Dome and GISPII record (Sowers et al., 2003) (Sowers et al., 2003), with the latter being up to 10 ppbv/ppb lower. Here, as with CH₄, we use again a median quantile piecewise polynomial regression on the Law Dome record, assuming constant N₂O ~~mixing-ratios~~concentrations between year 0 and the first Law Dome data point in Year year 154. In contrast to CH₄, there is not a monotonic increase of ~~mixing-ratios~~concentrations, but rather an initial slight decrease until year 630 down to a minimum ~~mixing-ratio~~concentration of 265 ppbv/ppb in our smoothed ~~timeseries~~time series with a subsequent slow increase until the 9th century AD, then a slight decrease until 1650 in the smoothed global-mean ~~mixing-ratios~~mole fraction. A temporary local maximum indicated by individual Law Dome data in the 15th century is not resolved by our smoothing, and a similar spike in the 17th century is only just reflected (Fig. 6f). Several data points indicate a small decrease after a 1750 maximum with a minimum in 1850 of around 273.02 ppb. This maximum around 1750 and subsequent minimum around 1800-1850 is also apparent in the H15 ice core record by Machida (1995) (we scale-corrected the Machida data downwards by 1 ppb as in Battle et al. (1996)) (Fig. 6b). After 1850, N₂O concentrations increased markedly, reaching 1900, 1950, 2000 and 2014 values of 279.5, 289.7, 315.8 and 327.0 ppb, respectively (Table 6). Comparing the different firn and ice records, the 1920 – 1940 period seems particularly uncertain with some high measurements close to and beyond 290 ppb from both Law Dome and H15, while some of the Law Dome data is still at levels around 285 ppb or even 280 ppb in the case of H15 (Fig. 6e). The South Pole firn data (Battle et al., 1996) suggest lower N₂O concentrations in the 1920s and around 1960 – compared to both the smoothed Law Dome data (thin dashed line in Fig. 6e) and consequently our even higher global-mean estimate. Although the Ishijima estimate (Ishijima et al., 2007) (their Figure 6a) around 1952 is almost identical to our global-mean, their modelling study suggests slightly lower values around 1960 before being closely matching again from 1970 onwards. The Law Dome firn record (Park et al., 2012) suggests slightly higher N₂O concentrations for the high southern latitudes compared to our global-mean Fig. 6e).

The variability of our derived N₂O global-mean concentrations, in particular the steps in 1920s and 1940s, reflect the smoothing algorithm choices to noisy data (section 2.1.6), but should not be over-interpreted. Our algorithm does for example not include information on the lifetime of N₂O that would guard against inferring too rapid declines of N₂O mole fractions and mole fraction growth rates. The fit of the smoothing algorithm was chosen to balance the resolution of smaller scale features with the uncertainty present in the input data sources for the full-time horizon from year 0 to year 2014. Given overall uncertainties (Fig. 6e), a smoother representation between 1900 and 1980 seems equally justified.

~~Compared to CH₄ and CO₂, the seasonality and latitudinal gradient of N₂O are relatively small. Several data points indicate a small decrease after a 1750 maximum, with a minimum in 1850 of around 273.02 ppbv. After that, N₂O mixing ratios~~

increased markedly, reaching 1900, 1950, 2000 and 2014 values of 279.45, 289.74, 315.76 and ~~326.00~~ ppbv, respectively (Table 7).

Compared to CH₄ and CO₂, the seasonality and latitudinal gradient of N₂O are relatively small. The N₂O seasonality is only 0.1% of global ~~mixing ratios~~ mole fractions and is almost symmetric and seasonally time-synchronized between the northern and southern hemispheres with minima in the southern hemisphere late autumn and northern hemisphere summer/autumn (Fig. 12a). The seasonality is currently of the same size as the underlying trend, leading to global mean N₂O ~~mixing ratios~~ mole fractions increasing in the latter months of any year with a subsequent flattening in the first half of any calendar year (e.g. Fig. 12h). ~~Given a counter-intuitive slight decrease of the north-south gradient with increasing global N₂O emissions in recent years.~~ ~~h). Given a counter-intuitive slight decrease of the north-south gradient with flat or slightly increasing global N₂O emissions (Gütschow et al., 2016) in recent years (Fig. 12d),~~ we assumed constant scores for the latitudinal gradient EOFs for times before 1996 (Fig. 12d). Due to measurement fluctuations in the first years when systematic measurements started in 1978 that are larger compared to the recent period, we chose to interpolate N₂O global-mean ~~mixing ratios~~ mole fractions over 1966 to 1987. For the period between 1978 and 1987, this interpolation is closely aligned with ~~and can be seen as a~~ smooth representation of the atmospheric measurements (Fig. 12f, cf. ALE/GAGE/AGAGE data as shown at http://agage.eas.gatech.edu/data_archive/data_figures/gcmd_month/n2o_monS5.pdf).

3.4 Ozone Depleting Substances and other chlorinated substances

Ozone depleting substances (ODSs), i.e. the substances destroying ozone and being controlled under the Montreal Protocol, ~~also~~ have a large warming effect. (Velders et al., 2007; Velders et al., 2009). In particular CFC-12 and CFC-11 are important ~~greenhouse-gases~~ GHGs, as well as the replacement substance HCFC-22, which, unlike CFCs, continues to increase in the atmosphere, albeit at a declining rate. The radiative forcing of CFC-12 alone since 1750 is equivalent to that of N₂O, which is usually considered the third most important ~~greenhouse-gas~~ GHG after CO₂ and CH₄ (Table 5). The impact of ODSs on climate is somewhat complicated by their destruction of stratospheric ozone, which ~~leads to~~ has a cooling ~~effect on~~ the global climate. The latest estimates suggest that this cooling might offset roughly two-thirds of the warming of the entire class of ODSs (Shindell et al., 2013) (Shindell et al., 2013). Note that we consider here also methylene chloride and methyl chloride, although these chlorinated substances are not controlled by the Montreal Protocol and hence often not termed ozone depleting substances (WMO, 2014).

The most abundant ozone depleting substances in the atmosphere (in 2014) ~~are~~ were CFC-12 (520.6 pptv ~~ppt~~), CFC-11 (233.1 pptv ~~ppt~~) and HCFC-22 (229.5 pptv ~~ppt~~), with their mole fractions being about six orders of magnitude lower than currently measured for CO₂ (Table 7). In addition, methyl chloride CH₃Cl has a high mole fraction (539.54 pptv ~~ppt~~), although is not considered an ODS here as it is not controlled by the Montreal Protocol. Out of the 17 considered chlorinated and ozone depleting substances, only 6 have currently increasing ~~mixing ratios~~ concentrations. Those are the three HCFCs, of which the increase in HCFC-22 alone has offset the reducing radiative forcing of all other ~~ozone-depleting substances (ODS)~~ ODSs over the past decade (Fig. 8m). The other three substances that are still increasing are Halon-1301, methylene chloride (CH₂Cl₂)

Field Code Changed

and chloroform (CHCl₃). Chloroform had been decreasing in the 1990s and stabilized in the 2000s, but again recently showed an increase (Fig. 30).

Four of the considered chlorinated and ozone depleting substances are assumed to have natural emissions and hence ~~non-zero pre-industrial mixing ratios~~. Specifically, methyl chloride (CH₃Cl) is assumed to have pre-industrial global-mean mixing ratios of 457 pptv, carbon tetrachloride (CCl₄) of 0.025 pptv, and methyl bromide (CH₃Br) of 5.3 pptv. Chloroform (CHCl₃) is assumed to have a pre-industrial mixing ratio of about 6 pptv, approximately in line with findings by Worton et al. ~~above-zero pre-industrial concentrations~~. We estimate those pre-industrial natural background concentration by a simple budget equation under the assumption of a constant lifetime (IPCC, 2013) of 1 year for CH₃Cl and 0.8 years for CH₃Br – minimizing the error term when taking into account anthropogenic emission and atmospheric concentration estimates over 1950 to 1990 by Velders and Daniel (2014). Specifically, methyl chloride (CH₃Cl) is assumed to have pre-industrial global-mean concentrations of 457 ppt, and methyl bromide (CH₃Br) of 5.3 ppt. Chloroform (CHCl₃) is assumed to have a pre-industrial concentration of about 6 ppt, approximately in line with findings by Worton et al. (2006) and the estimation by Aucott et al. (1999) that in 1990 CHCl₃ was at about 8 pptv, ~~ppt, with 80% are of emissions assumed to be~~ of natural origin. Lastly, ~~in the absence of other information (a good understanding of the natural vs anthropogenic source fraction or historical industrial production records) the available firm measurements (e.g., Trudinger et al., 2004) supplying information about~~ methylene chloride (CH₂Cl₂) ~~is estimated to have~~ mole fractions in the early 20th century are used to suggest a 6.9 pptv ppt pre-industrial ~~mixing ratio~~ mean concentration with a strong latitudinal gradient that results in northern (southern) hemisphere average ~~mixing ratios~~ concentrations of 12.8 (1.0) pptv, ~~even though this isn't well described by observational data~~ ppt. The transition of ~~mixing ratios~~ concentrations of some species between the observational station data and pre-industrial levels are also uncertain. For CH₂Cl₂, our derivation is in line with the smooth trajectory of Trudinger et al. (2004), indicating an almost monotonic transition between 1997 values and pre-industrial ~~mixing ratio~~ concentrations (Fig. 26f-f). ~~Our assimilation approach (which is based on the Walker et al. data (2000)) causes our carbon tetrachloride (CCl₄) reconstruction to have a near-zero pre-industrial concentration of 0.025 ppt (0.025% of its peak value of 100ppt). We note that Walker et al. (2000) suggest zero pre-industrial concentrations before 1910, although the lowest empirical evidence from firm records suggest <5 ppt (Butler et al., 1999) or 3-4ppt as measured by S. Montzka for 1863 firm air and reported in Liang et al. (2016).~~

The seasonal cycle of ozone depleting substances and other synthetic GHGs can be influenced by seasonally varying stratospheric-tropospheric air exchanges, interhemispheric transport, tropopause heights, emissions and, for those substances with OH-related sinks, the seasonally varying OH ~~mixing ratios~~ concentrations. For 11 out of the 17 considered ozone depleting substances we find some indication of seasonal cycles based on the analyzed station data, namely for CCl₄, CFC-11, CFC-12, CFC-113, CH₂Cl₂, CH₃Br, CH₃CCl₃, CH₃Cl, CHCl₃, Halon-1211, and HCFC-112. Our analysis indicates that HCFC-141b also shows some signs of a seasonal cycle, although we here assumed a zero seasonal cycle due to data sparsity (see Fig. 35a). We find the strongest seasonal cycles in case of the short-lived species CH₃Cl, CHCl₃, CH₃Br and CH₂Cl₂ with absolute maximal seasonal deviations of -11%, -12%, ±9%, -32% compared to the annual mean, respectively. For the

radiatively important and longer-lived species CFC-12, CFC-11 and HCFC-22, the seasonal cycle is much smaller, with $\pm 0.2\%$, $\pm 0.4\%$, $\pm 0.8\%$, respectively.

Similar to the seasonality, the latitudinal gradient is found to be especially pronounced for the short-lived substances. Specifically, CH_2Cl_2 with a lifetime of 0.4 years, CH_3Br with a lifetime of 0.8 years, CH_3CCl_3 with a lifetime of 5 years and CH_3Cl with a lifetime of approximately 1 year and CHCl_3 with a lifetime of 0.4 years show substantial latitudinal gradients due to spatially heterogeneous sinks and sources (lifetimes following Table 8.A.1 in IPCC WG1 AR5 (2013)). While chemicals with predominantly anthropogenic sources normally the exhibit highest mole fractions at mid to high northern latitudes experience the highest mixing ratios for these compounds, the measurements, the observations for several substances suggest a pronounced high-latitude with substantial natural sources exhibit highest mole fractions in the tropics or lower northern hemisphere decline in annual average mixing ratios (see latitudes in the recent observational period (e.g. CH_3Cl in Fig. 29b and c).

3.5 Other fluorinated greenhouse gases fluorinated GHGs

The 23 other gases in this study are the hydrofluorocarbons (HFCs), which have recently been added to the substances controlled under the Montreal Protocol (Kigali amendment in October 2016), and those substances whose production and consumption is not controlled under the Montreal Protocol are the hydrofluorocarbons (HFCs), namely perfluorocarbons (PFCs) as well as Sulphur/sulfur hexafluoride (SF_6), nitrogen trifluoride (NF_3), and sulphuryl/sulfuryl fluoride (SO_2F_2). Except for the latter, the emissions of all these species are controlled under the Kyoto Protocol and covered by most “nationally determined contributions” (NDCs) under the Paris Agreement. In aggregate, However, currently the aggregated greenhouse effect of this group of synthetic GHGs however exerts an is still almost a factor of 10 smaller greenhouse gas effect to date compared to the ozone depleting substances (ep. ODSs (cf. Fig. 8g and m). In contrast to the gases controlled under the Montreal Protocol ODSs, nearly all of these other fluorinated gas mixing ratios concentrations are still rising however, with the exception of is HFC-152a, which has stopped growing since 2012 and may now be in decline, (Fig. 52f). Thus, a primary concern with these gases is the potential for substantial climate forcing in the future if uncontrolled growth continues.

The most abundant of these gases is the refrigerant HFC-134a with 2014 mixing ratios concentrations estimated to be 80.5 pptv ppt, followed by HFC-23 (26.9 pptv ppt), HFC-125 (15.4 pptv ppt) and HFC-143a (15.2 pptv ppt). At the other end of the mixing ratios concentration spectrum, we include results from Ivy et al. (2012) for some PFCs that exhibit low mixing ratios concentrations of 0.13 pptv ppt (C_5F_{12} and C_7F_{16}) or 0.09 pptv ppt (C_8F_{18}) (Table 7). The only fluorinated gas considered to have substantial natural sources and hence a pre-industrial background concentration is CF_4 with an assumed pre-industrial mixing ratio concentration of 34.05 pptv ppt (see Fig. 45) in line with findings by (Trudinger et al. 2016).), in line with findings by Trudinger et al. (2016) and Mühle et al. (2010).

For a number of substances, especially the PFCs with lower abundances, there were not sufficient data available to estimate the seasonality of atmospheric mixing ratios concentrations. We consider seasonality only for 3 of the 23 species. HFC-134a has a somewhat atypical pattern of lowest mixing ratios mole fractions in the spring northern hemisphere (-2.6% compared to

annual mean) as other gases normally show a summer or autumn low point of ~~mixing-ratios-concentrations~~. This spring minimum results from a seasonality of sources of this refrigerant (Fig. 50a), although seasonality in loss also likely plays a role (Xiang et al., 2014). ~~Secondly, the short-lived HFC-152a (lifetime 1.5 years) shows seasonal variations of up to~~ (Xiang et al., 2014). ~~Secondly, the short-lived HFC-152a (lifetime 1.5 years) shows seasonal variations of up to~~ $\pm 13\%$ while the very long lived SF₆ (lifetime of 3200 years) exhibits a much smaller seasonality of up to $\pm 0.5\%$.

For most of the considered substances, the latitudinal gradient is rather small. Exceptions are the shorter-lived species like HFC-32, whose ~~mixing-ratio-concentration~~ rose relatively quickly since 2000 due to rapidly increasing northern hemispheric sources (Fig. 47b), HFC-152a, and some other shorter lived HFCs. For the three heavier PFCs with very low abundances of well below 1 ~~ppb~~ ppt in 2014, namely C₆F₁₄, C₇F₁₆ and C₈F₁₈, we incorporated hemispheric data from Ivyy et al. (2012). (2012). Before about 1990, those three gases are suggested to have ~~reverse~~ reversed latitudinal gradients with higher southern hemispheric ~~mixing-ratios-concentrations~~. Due to the very low ~~mixing-ratios-mole fractions~~ near the limit of measurement, future studies may need to confirm whether those reverse gradients existed (and if so, why). Given the negligible radiative forcing from these gases to date, this uncertainty does not affect the overall results.

4 The CMIP6 recommendation and data format

We present the community CMIP6 data sets of historical GHG ~~mixing-ratios~~. ~~In conjunction with other data, these greenhouse gas surface mixing-ratio data sets are to be used in the concentration-driven runs for the climate model inter-comparison project phase 6 (CMIP6) (Eyring et al., 2015), specifically the historical run, and the idealized runs of abrupt4x, 1pctCO2 as well as the picontrl. The CMIP6 recommendation as decided by the CMIP Panel is: "In the CO₂-concentration-driven historical simulations, time-varying global annual mean mixing ratios for CO₂ and other long-lived greenhouse gases are prescribed. If a modelling center decides to represent additional spatial and seasonal variations in prescribed greenhouse gas forcings, this needs to be adequately documented."~~ (Eyring et al., 2016); ~~mole fractions~~. ~~In conjunction with other data, these GHG surface mole fraction data sets are to be used in the historical concentration-driven runs for the climate model inter-comparison project phase 6 (CMIP6) (Eyring et al., 2016). Depending on the specific CMIP6 experiment, different protocols and recommendations can apply. Modellers should hence also check the experiment specific descriptions (see special issue available at http://www.geosci-model-dev.net/special_issue590.html), including protocols regarding the important other forcing input datasets like aerosols, their emissions and optical properties, landuse patterns, but also short-lived GHGs like tropospheric and stratospheric ozone for models without interactive ozone chemistry.~~ ~~The historical GHG concentrations of this study are specifically designed to be useful for the historical run, and the idealized runs of abrupt4x, 1pctCO2 as well as the picontrl. Also, the PMIP4 related last millennium experiment will be based on the~~ GHG concentrations of this study (Jungclaus et al., in preparation; Kageyama et al., 2016).

Regarding the historical runs of the DECK simulations, the CMIP6 recommendation as decided by the CMIP Panel is: “In the CO₂-concentration-driven historical simulations, time-varying global annual mean mole fractions for CO₂ and other long-lived GHGs are prescribed. If a modelling center decides to represent additional spatial and seasonal variations in prescribed GHG forcings, this needs to be adequately documented.” (Eyring et al., 2016).

5 This study provides the data for both the simple global annual mean mixing-ratios mole fractions as well as the mixing-ratio mole fraction histories that take latitudinal and seasonal variations into account (see data description further below). CMIP6 modelling groups should indicate which time and space resolution of the data version they applied. All data are freely available via the PCMDI servers (<https://pcmdi.llnl.gov/search/input4mips/>) as netcdf files. In addition, summary-tables The data is also available via ftp servers, and multiple data formats (netcdf, csv, xls and MATLAB mat versions-of-the-data-files-are-provided) as described at climatecollege.unimelb.edu.au/cmip6.

10 In terms of the spatio-temporal resolution, four files for each of the 43 greenhouse-gases GHGs and the three equivalence species CFC-12-eq, HFC-134a-eq and CFC-11-eq (section 2.1.10) are provided as:

- I. latitudinal 15-degree bins with monthly resolution (filename-code: '_15degreelatXmonth'), with monthly means for each latitudinal band provided at the centre of the box, i.e. -82.5, -67.5, ... 67.5, 82.6.
- 15 II. interpolated latitudinal half degree bins with monthly resolution (filename-code: '_0p5degreelatXmonth'), with means for each latitudinal band provided at the center of the box, i.e. -89.75, -89.25, ... 89.25, 89.75. The area-weighted mean over 15-degree latitudinal bands is the same as the files under (1).
- III. Global and hemispheric means with monthly resolution (filename-code '_GMNHSHmeanXmonth').
- IV. Global and hemispheric means with annual resolution (filename-code '_GMNHSHmeanXyear')

20 Given that climate effects will vary depending on whether global, annual-mean or seasonally varying latitudinally-resolved surface mixing-ratios mole fractions are prescribed, modelling groups are asked to document which data set(s) they choose.

The CMIP6 recommendation for the **picontrl** experiment are to use the 1850 greenhouse-gas-mixing-ratios GHG mole fractions with annual means as provided in [Table 8](#) (CO₂ annual-mean mixing-ratios mole fractions of 284.32 ppmv ppm, CH₄ mixing-ratios mole fractions of 808.25 ppbv ppb and N₂O mixing-ratios mole fractions of 273.02 ppbv ppb). Other gases are covered, depending on the choice of the modelling group by either following Option 1, Option 2, or Option 3, described in Table 5, or an equivalently suited method that aggregates the radiative effect of the remaining 40 GHGs or a large fraction thereof.

30 The **abrupt4x** experiment should keep all greenhouse-gas-mixing-ratios GHG mole fractions unchanged from the picontrl run except for the CO₂ mixing-ratios mole fractions, which should be increased instantaneously in year 1 (=1850) of the experiment to four times the 1850 value, namely to 1137.27 ppmv ppm ([Table 10](#)).

The **1pctCO2** experiment should also keep all greenhouse-gas-mixing-ratios GHG mole fractions unchanged from the picontrl run except for CO₂ mixing-ratios mole fractions. Starting in year 1 of the experiment, CO₂ mixing-ratios mole

fractions should increase by 1% per annum, reaching slightly over doubled CO₂ mixing-ratio:mole fractions in year 70 (or 1920, if the startyear is set to 1850) with 570.56 ppmv:ppm and 1,264.76 ppmv:ppm in year 150 (or year 2000) (Table 9).

As with the abrupt4x and 1pctCO2 scenarios, the **historical** experiment should diverge from the picontrol run. Greenhouse gases:GHGs should then follow the historical observations as derived in this study, reaching e.g. CO₂ mixing-ratio:mole fractions of 397.55 ppmv:ppm in 2014, and CH₄ and N₂O mixing-ratio:mole fractions of 1831.47 ppbv:ppb and 326.99 ppbv:ppb, respectively. Modelling groups should document which spatial and temporal resolution (see above) of the provided data they use, as the climate effect will likely be different with different resolutions.

The future concentration pathways, the so-called ‘SSP-RCP’ scenarios, considered under ScenarioMIP (O’Neill et al. 2016) (O’Neill et al., 2016) are planned to provide the same data formats and spatio-temporal resolutions. The methodological approach to derive and adapt both seasonality and latitudinal gradients in this study was designed such that a future extrapolation will be possible.

4.1 The vertical dimension

The purpose of our reconstructions is to provide radiative forcing for climate models. This radiative forcing depends on the vertical as well as horizontal distribution of a gas:mixing-ratio:gases’ mole fraction. Our reconstructions describe only surface concentrations and modelers:modellers need some method for calculating the three-dimensional distribution. If the model is capable of calculating tracer transport, includes any sinks and sources in the free atmosphere and has an appropriate treatment of the boundary layer, we recommend using this study’s surface reconstruction as a mixing-ratio:mole fraction lower boundary condition for the-tracer-transport-a mass balance inversion. If this is not possible then, we propose a simple equation to reflect the relaxation of horizontal gradients with height and the upward propagation of mixing-ratio:mole fraction changes from the surface.

In case of CO₂, there are no sinks in the middle and upper troposphere or stratosphere and only slight sources due to the oxidization of CH₄ and carbon monoxide (CO). Evidence from Earth System Models (Fig. 13) indicates an almost well-mixed tropospheric column in the tropics and little or partly reversed vertical gradient in the southern troposphere, while the annual-mean gradient in the northern hemisphere is – depending on the season – variable. The annual average vertical gradient in the northern hemisphere is decreasing in all CMIP5 ESM models analysed here (Fig. 13).

In order to enable the implementation of surface mixing-ratio:mole fractions in models that do not have an inherent transport model to capture vertical gradients, we offer here simplified parameterizations as default options. While an assumption about a well-mixed atmospheric vertical column seem a justifiable simplification, these simple vertical extensions could increase the realism, vertical heating structure and overall climatic effect. Specifically, modelling teams could use the following approximation to extend surface mixing-ratio:concentration fields (at the 1000hPa:1000 hPa level) towards higher tropospheric and stratospheric levels. First, a bell-shaped mixing-ratio:concentration distribution is assumed at the 100hPa:100 hPa level for the higher latitude:latitude tropopause and tropical upper troposphere:

$$C(l, 100\text{hPa}, t) = \bar{C}(global, 1000\text{hPa}, t)(global, 1000\text{hPa}, t) \dots + (\bar{C}(global, 1000\text{hPa}, t - 5\text{yrs}) - \bar{C}(global, 1000\text{hPa}, t)) (C(global, 1000\text{hPa}, t - 5\text{yrs}) - C(global, 1000\text{hPa}, t)) * \frac{\sin(l)^2}{2} \quad (9)$$

With $\bar{C}(global, 1000\text{hPa}, t)(global, 1000\text{hPa}, t)$ indicating global-average, annual-average mixing ratio concentrations at the surface 1000hPa level at time t . Ideally, a smoothed mean-preserving monthly dataseriestime series of these annual-average global averages is used to prevent step changes from calendar month 12 to 1. Equivalently, $\bar{C}(global, 1000\text{hPa}, t - 5\text{yrs})(global, 1000\text{hPa}, t - 5\text{yrs})$ indicates the global-average, annual-average surface mixing ratio mole fraction 5 years earlier. The $\frac{\sin(l)^2}{2}$ factor depends on the latitude l and results in the bell-shaped mixing ratio concentration curve with concentrations at the tropical 100hPa 100 hPa level to be identical to the global average surface mixing ratio concentrations, while the polar mixing ratio mole fractions are effectively of a medium age (2.5 years in the case of linearly increasing concentration history). Having defined this 100hPa 100 hPa concentration level, the tropospheric mixing ratio mole fractions at latitude l and pressure level p (with $p > 100\text{hPa}$) can then be assumed as a simple linear interpolation between the surface mixing ratio mole fraction level at latitude l and the 100hPa 100 hPa level, so that:

$$C(l, p, t) = C(l, 100\text{hPa}, t)(l, 100\text{hPa}, t) + (C(l, 1000\text{hPa}, t) - C(l, 100\text{hPa}, t)) (C(l, 1000\text{hPa}, t) - C(l, 100\text{hPa}, t)) * \frac{(p - 100\text{hPa})}{(1000\text{hPa} - 100\text{hPa})} \frac{(p - 100\text{hPa})}{(1000\text{hPa} - 100\text{hPa})} \quad (10)$$

Above 100hPa 100 hPa - i.e. in the tropical upper troposphere and stratosphere, the mixing ratio mole fraction is a simple linear interpolation between the 100hPa 100 hPa level and the top-of-the atmosphere 1hPa 1 hPa level that is assumed to have a median age of air of 5 years, so that for $p < 100\text{hPa}$:

$$C(l, p, t) = \bar{C}(global, 1000\text{hPa}, t - 5\text{yrs}) \dots + (C(l, 100\text{hPa}, t) - \bar{C}(global, 1000\text{hPa}, t - 5\text{yrs})) \dots * \frac{(p - 1\text{hPa})}{(100\text{hPa} - 1\text{hPa})} (global, 1000\text{hPa}, t - 5\text{yrs}) \dots + (C(l, 100\text{hPa}, t) - \bar{C}(global, 1000\text{hPa}, t - 5\text{yrs})) \dots * \frac{(p - 1\text{hPa})}{(100\text{hPa} - 1\text{hPa})} \quad (11)$$

With $\bar{C}(global, 1000\text{hPa}, t - 5\text{yrs})(global, 1000\text{hPa}, t - 5\text{yrs})$ being again the global-mean surface mixing ratio concentration (1000hPa) five years ago and $C(l, 100\text{hPa}, t)(l, 100\text{hPa}, t)$ the latitudinally-dependent mixing ratio concentration at the 100hPa level.

This equation captures the general form of the vertical CO₂ mixing ratio mole fraction gradient observed in CMIP5 ESM models - with the 100hPa 100 hPa being an approximate division line of the vertical CO₂ gradient in all CMIP5 models (see bold red line in Fig. 13). The annual-average vertical gradient in the northern hemisphere will be somewhat reducing the effect of the strong surface latitudinal gradient. The idealized shaped of the above parameterization for an hypothetical flat surface mixing ratio mole fraction of 100 ppmv ppm is shown in Fig. 14b. Assuming linearly increasing surface mixing ratio mole fractions from a south pole minimum towards a 3 ppmv ppm higher north pole maximum will - under this simplified parameterization - result in an almost zero vertical tropospheric gradient in the southern hemisphere (Fig. 14a).

For non-CO₂ gases, we here suggest a scheme adapted from the CESM model current parameterization – in case that models do not have their own vertical extrapolation methods. These parameterisations assumed a simplified vertically well-mixed troposphere and define a tropopause height as:

$$p_{\text{tropopause}}(l) = 250 \text{ hPa} - 150 \text{ hPa} - 150 \text{ hPa} * \cos(l)^2 \quad (12)$$

5 With $p_{\text{tropopause}}(l)$ being the tropopause height in hPa, depending on the latitude l . Thus, below the tropopause, the zonal mean mixing-ratio-concentrations are assumed to be well-mixed vertically, so that:

$$C(l, p, t) = C(l, 1000 \text{ hPa}, t) \quad \text{for } p > p_{\text{tropopause}}$$

The stratospheric mixing-ratio-concentration can then be modelled for $p < p_{\text{tropopause}}$ as:

$$C(l, p, t) = \bar{C}(global, 1000 \text{ hPa}, \bar{t} - 1 \text{ yrs})(global, 1000 \text{ hPa}, \bar{t} - 1 \text{ yrs}) * \left(\frac{p}{p_{\text{tropopause}}(l)} \right)^s * \left(\frac{p}{p_{\text{tropopause}}(l)} \right)^s \quad (13)$$

10 with $\bar{C}(global, 1000 \text{ hPa}, \bar{t})(global, 1000 \text{ hPa}, \bar{t})$ being the global mean and annual-mean surface mixing-ratio-mole fraction of the previous year, $p/p_{\text{tropopause}}(l)$ being the ratio of the pressure at level p and the tropopause pressure at that latitude and s being a gas-dependent scaling factor (Table 11).

As mentioned above, this simple vertical extrapolation option of the provided surface data is only to be regarded as a simplified fall-back option in case that there are no model-intrinsic parameterizations-parameterisations available or active
 15 tracer transport part of the model. While this study provides the main step from global-mean and annual-mean mixing-ratio-concentration histories towards zonally and monthly resolved ones, future research will be needed to provide more robust 4-D fields of mixing-ratio-concentrations.

5 Discussion

We compare our results with a number of other data products. First, a comparison with the previous CMIP5 recommendation for historical GHG ~~mixing-ratios~~concentrations is provided (5.1). ~~Then~~Second, we analyse and compare our CMIP6 recommendations to what the Earth System Models from the previous CMIP5 intercomparison produced in terms of CO₂ ~~mixing-ratio~~concentration fields in the ~~emission~~emissions-driven runs (5.3). ~~Thirdly~~Third, we compare our data sets to the other global-mean, hemispheric and latitudinally-resolved data sets, namely the NOAA Marine Boundary Layer product and the WDCGG time series (5.4).

5.1 Comparison to CMIP5 input datasets.

For the CMIP5 inter-comparison, ~~greenhouse-gas~~mixing-ratiosGHG concentrations were specified for historical times until 2005, followed by RCPs and their extensions until 2300. The recommendations for GHG ~~mixing-ratios~~concentrations were global and annual mean time series (~~Meinshausen et al. 2011b~~)(Meinshausen et al., 2011), not including a seasonal cycle or latitudinal gradient. Those historical time series were composite products of existing ice core and instrumental data annual means (see references in Meinshausen et al. 2011). Global, annual-mean CO₂ ~~mixing-ratios~~concentrations over 1975 to 2005 were very close (<0.7 ~~ppmv~~ppm different) to our current recommendations for CMIP6. The CMIP5 time series did not show the slight maximum in CO₂ ~~mixing-ratios~~concentrations around 1973 (difference 1.2 ~~ppmv~~ppm), and was generally lower between 1940 and 1956 at about the time of the World War II, when CO₂ ~~mixing-ratios~~concentrations briefly plateaued (differences between 1.0 and 2.3 ~~ppmv~~ppm) (Fig. 15). While the CMIP5 historical ~~greenhouse-gases~~GHGs were an ad-hoc extension to the RCP pathways, our CMIP6 recommendation advanced the integration of historical data by accounting for latitudinal gradients (ice core data in CMIP5 has not been adjusted for the latitudinal gradients) and by taking into account a large array of additional data beyond a single network average for more recent times.

Recommended global-mean CH₄ ~~mixing-ratios~~concentrations for CMIP5 were generally lower than derived here, up to 50 ~~ppbv~~ppb around 1910 and between 25-30 ~~ppbv~~ppb more recently (2000-2005). The primary reason is that the CMIP5 data did not take into account the strong latitudinal gradient of CH₄ ~~mixing-ratios~~. In terms of N₂O ~~mixing-ratios~~concentrations. For N₂O concentrations, the CMIP5 historical timeseries did not capture some higher frequency variability, which caused the CMIP6 recommendation for the piconrol 1850 global-mean ~~mixing-ratio~~concentration being lower by around 2.5 ~~ppbv~~ppb, and N₂O ~~mixing-ratios~~concentrations in the 1910s being higher by up to 2.3 ~~ppbv~~ppb (Fig. 15).

Overall, CMIP5 and CMIP6 recommendations are relatively similar. The 1850 piconrol values at the time of CMIP5 were slightly higher for CO₂ and N₂O (0.14% or 0.4 ~~ppmv~~ppm and 0.87% or 2.4 ~~ppbv~~ppb, respectively), countered to some degree by slightly lower values for CH₄ (2.18% or 17.3 ~~ppbv~~ppb). This is equivalent to a small net change in base year radiative forcing of 0.0065 W/m², when applying linear radiative efficiencies of IPCC AR5 (Appendix 8.A in IPCC WG1 AR5).

5.2 Comparison to CO₂ station data between 1958 and 1984.

As our data synthesis used monthly station data only from 1984 onwards (except for Mauna Loa annual averages back to 1958), a comparison to available station data from before 1984 is useful to qualitatively validate the extension method applied

in this study. While latitudinal gradients (or rather: their first two EOFs) and seasonality changes are extended by regression (sections 2.1.4 to 2.1.7), the CO₂ fields' global-mean has been optimised to match both the annual average Mauna Loa record and the Law Dome ice record, specifically our smoothed version thereof (see Table 1 and Fig. 7k). Thus, it is informative to compare our data product to available station data from the period before 1984 both in terms of seasonality and the absolute amplitude (which is derived from the global-mean and the regressed latitudinal gradient) (see Fig. 7). We here use the Scripps CO₂ data series, available at http://scrippsc02.ucsd.edu/data/atmospheric_co2/sampling_stations.

In general, the comparison suggests that this study's data product matches rather closely earlier station data, thereby validating our chosen extension approach to some degree. There are two noteworthy issues arising from this comparison though. For high southern latitudes, both Law Dome as well as SPO in-situ and flask station data are available. It seems that our CMIP6 high latitude data in the southern hemisphere could be ~1ppm too low over the period 1959 to 1972 (Fig. 7l). Earlier, in 1958, and subsequently from 1973 onwards, the match is rather close between SPO station data at -90° and our latitudinal average for the -90° to -75° zonal mean. Given our data product matches the MLO record quite closely (somewhat by design, given the optimisation to match the annual-average MLO record over that time), this points to a slightly exaggerated latitudinal gradient between 1959 and 1972.

The second issue relates to a bump in the concentration series centred around 1974. In our data assimilation, this bump is a propagation of an anomaly in the MLO record over that time and seems to a lesser degree to also show up in other northern hemisphere records. However, the southern hemispheric SPO record does not (or only minimally) show this slight upwards aberration from 1972 to 1974 and subsequent slowing and stagnating growth from 1974 to 1976 (while the lower precision Law Dome data would be consistent with that MLO pattern, see Fig. 7k). To what extent this bump has been present in the southern hemisphere is unknown, although earlier studies (Bacastow, 1976) relate the increased atmospheric CO₂ concentrations to decreased oceanic uptake during the El Nino back then. Such a process explanation would suggest the atmospheric signal also to be present throughout large parts of the southern hemisphere, while a predominantly extra-tropical land-related respiration increase during El Nino could imply the signal to be predominantly present in the Northern hemisphere. In summary, our assimilation's hemispheric upwards anomaly around 1974 of around ~2ppm could largely be an artefact of our methodology which propagates the MLO anomaly globally under the assumption of exogenously emission-regressed latitudinal gradients.

5.2.5.3 Comparison to CMIP5 ESM CO₂ mixing-ratio concentration fields.

Several Earth System models during CMIP5 used prescribed CO₂ emissions instead of CO₂ mixing-ratio concentrations and derived CO₂ mixing-ratio concentration fields endogenously. For the year 1875, we see that models vary greatly, with some showing reverse latitudinal gradients with higher mixing-ratio concentrations in the south (e.g. CanESM2), almost no gradient (CESM1-BCC), a local maximum in the tropics with lower poleward mixing-ratio concentrations (MIROC-ESM) and very heterogeneous fields with high mixing-ratio concentrations over the tropical rainforests (NorESM1-ME) (see Figure 10; Fig. 60). Similarly, for 1990 (Figure 11; Fig. 61), the fields are dissimilar, with some models exhibiting very strong north-south

gradients (MPI-ESM-LR), while others show little gradients (CanESM2), although all models indicate an increase of northern hemispheric ~~mixing-ratios:concentrations~~ compared to the global mean between 1875 and 1990 (~~Figure-12~~Fig. 64).

Though not as strong as NorESM1-ME, most models show a slight tropical maximum in the latitudinal gradient (exceptions are CanESM2, MIROC-ESM) both during 1875 and 1990 (~~Figure-12~~Fig. 65 and Fig. 66). The high-latitude southern ~~mixing~~

5 ~~ratioconcentration~~ deviations from the global-mean in the 1875 time slices have different signs across the models, with some indicating clearly lower ~~mixing-ratios:concentrations~~ (BNU-ESM, MPI-ESM-LR, NorESM1-ME) and others suggesting slightly positive ~~mixing-ratios:concentrations~~ (CanESM2, MIROC-ESM in 1875). The average of three CMIP5 ESMs with full CO₂ data coverage at the surface 1000 hPa level and ~~approximately-correct~~ global mean CO₂ ~~mixing-ratio:mole fraction~~ values

10 ~~in line with observational records~~ (CanESM2, MPI-ESM-LR, and NorESM1-ESM) shows a latitudinal gradient for 1990 comparable to the observed one derived in this study (~~Fig. 9b~~). ~~In light of this evidence, we assumed constant mixing-ratios b~~.

~~Thus, given that the pre-industrial latitudinal gradient is almost flat for the models with the highest skill to replicate current observations, we assumed constant mole fractions~~ with latitude for pre-industrial times.

In general, all ESMs show climatological seasonal cycles of CO₂ ~~mixing-ratios:concentrations~~ similar to the seasonality derived in this study (~~Fig. 9a~~). The climatological 1861-1890 average ~~mixing-ratios:concentrations~~ across the models clearly exhibits

15 higher seasonality in the northern hemisphere, especially above 40°N. While the seasonality in some models is weaker, especially CESM1-BCC, others show variations of up to ± 10 ~~ppmvppm~~ (MPI-ESM-LR). In addition, the latter model exhibits

~~as a larger~~ southern hemisphere seasonality ~~larger~~ than other models and what we observe. As expected from our analysis of observational data, this seasonality strengthens up to 1990 across all models (~~Figure-14~~)(cf. Fig. 63 and Fig. 62). The latitudinal

20 spread of the northern hemisphere minimum extends southwards towards the equator in August, September and October as we observe (~~Fig. 9a~~), with the exception of the BNU-ESM model (~~Figure-14~~Fig. 63), which indicates a northward propagation of the minimum summer ~~mixing-ratioconcentration~~ values.

Overall, the basic features of the latitudinal gradient and seasonal cycle are represented in the ESMs as seen in the observational data. However, the variation across the models is substantial. This difference of several ~~ppmvppm~~ in the latitudinal gradient or seasonal cycles will lead to follow-on differences in the climate response observed in those models.

25 As common input for the CMIP5 concentration-driven experiments, all models were provided with the same historical global and annual mean CO₂ ~~mixing-ratios:concentrations~~. Some models had the capability to nudge internally-generated CO₂ ~~mixing~~

~~ratioconcentration~~ fields to match the prescribed annual and global mean CO₂ ~~mixing-ratios:concentrations~~. Nevertheless, the differences in those internally-generated fields can be substantial, as our analysis from CMIP5 shows, and different from the observations. ~~While the internally-generated CO₂-mixing-ratio-fields are a better match to observations compared to globally~~

30 ~~uniform annual mean values, the question arises as to how important those differences are for cross-model comparisons and detection and attribution studies. Differences between model output and observational diagnostics are influenced by the quality~~

~~of the prescribed input data, and input data have been prescribed in different ways across models.~~

For future model inter-comparisons, it seems preferable that any concentration-driven runs would use the same starting point. Of course, the longer-term aspiration has to be that emission-driven ESMS reliably reproduce observational **mixing ratio/concentration** patterns. For CMIP6, modelling groups are requested to document their choice of concentration input data, specifically in relation to the chosen temporal and spatial resolutions.

5.3.5.4 Comparison of global-means to NOAA marine boundary layer products and WDCGG

The primary observational data product with coverage across all latitudes **are** is the marine boundary layer (MBL) or GLOBALVIEW fields (**NOAA 2013, NOAA ESRL GMD 2014c**)(**NOAA, 2013; NOAA ESRL GMD, 2014c**) produced by NOAA based on the Cooperative Global Air Sampling Network (Conway et al., 1994; Dlugokencky et al., 1994b; Troler et al., 1996) for CO₂, CH₄ and N₂O (available at <http://www.esrl.noaa.gov/gmd/ccgg/mb/mb.html>, with N₂O data pers. comm. Pieter Tans). The aggregation method used to produce this data set is to first fit parametric functions to the weekly data of each station, thereby providing a gap-filling method. In a next step, the procedure fits smooth weekly latitudinal distributions to the various station data points (**Tans et al. 1989**)(**Tans et al., 1989**). These latitudinal distributions are then combined into a 2-D field of latitude versus time, comparable to this study's data product. The time period **for which of** these NOAA MBL data products is 1979 to 2014 for CO₂, 1983 to 2014 for CH₄ and 2001 to 2014 for N₂O.

The four main methodological differences between the NOAA MBL data product and ours are (1) the NOAA data product has a higher resolution in time (weekly instead of monthly) and latitudes, (2) the NOAA MBL data product includes only a subset of the NOAA network data (sites within the marine boundary layer), while this study mixes both NOAA and AGAGE network data in the case of CH₄ and N₂O, (3) this study characterizes the global fields by lower rank representations (EOFs) of annual mean latitudinal gradients and seasonality, while the NOAA product derives latitudinal gradients (and seasonality thereby only implicitly) directly from the observations at each time step. In other words, the main smoothing/regularization step in our study happens at a later level in the analysis, and (4) this study is extended by ice core and firm data, regressions and extra-/interpolation to span the full-time period between year 0 and 2014. **In other words: Thus**, this study seamlessly merges in situ observational, air archive, ice and firm data to generate a comprehensive data product.

For several applications, the NOAA data product has clear advantages. However, with the task to produce a continuous data product beyond the instrumental observations, this study had to choose a method that was readily extendable. Hence, this study chooses the characterization of global fields into global-means, latitudinal gradients and seasonality. This implies a high degree of regularizations by relying on EOFs and corresponding scores. By regression, these EOF scores for latitudinal gradients or seasonality changes can be easily extended to cover the full-time period of interest. Hence, our method allows an estimate of global-means even if there is **only** a single data point (such as a Law Dome ice core record for a specific year), under the assumption that latitudinal gradients and seasonality are captured by the derived EOFs and regressed EOF scores.

Global-average time series of monthly **greenhouse gas mixing ratios:GHG mole fractions** are also provided by the World Data Center for Greenhouse Gases (WDCGG) (**Tsutsumi 2009**)(**Tsutsumi, 2009**). The WDCGG product uses similar smoothing techniques as the NOAA product, but include, like this study, a broader set of measurement stations, both in terms of regional

coverage (including continental stations) and different networks that use different calibration scales, sampling, gas handling etc.

We compare the results of this study and NOAA MBL and WDCGG products ~~for the time periods covered by the latter.~~ Overall, our monthly hemispheric averages of CO₂ closely match the NOAA MBL product. The NOAA MBL product (which is not the same as NOAA network monthly averages) suggests a slightly faster increase of northern hemispheric mixing ratios/concentrations in the latter months of each calendar year (cf. thick and thin orange lines in Fig. 16a). Specifically, this difference results from the mid-latitude northern hemispheric bands from about 1995 onwards (with monthly-average differences of up to 4 ppmv/ppm) where our study is higher than the NOAA MBL product. This could be because this study does not screen out land stations closer to the pollution sources, as the NOAA MBL product does, hence named MBL for
5
10 “marine-boundary-layer product does.”

Likewise, the WDCGG includes a broader set of stations and matches very closely with our global-mean time series, with our study being very close to WDCGG or in between NOAA MBL and WDCGG (Fig. 16a). Given that the difference between the NOAA study and our study has a strong seasonality, the nature of those pollution sources and how they become mixed in the atmosphere, if these effects contribute to the differences, could be a combination of fossil fuel related and (more seasonally-
15 varying) biospheric sources (Fig. 17c). The southern hemispheric means of our study and NOAA MBL are very closely matched (cf. thick and thin blue lines in Fig. 16a). Consequently, the global-mean mixing ratios/concentrations from NOAA MBL and our study are closely matched, although again our data suggests NH autumn mixing ratios/concentrations rising slightly faster than the NOAA MBL product, reflecting the northern hemispheric difference (cf. thick and thin black lines in Fig. 16a).

20 For CH₄, the differences between this study and the NOAA MBL data are more systematic and stronger (~10 ppbv/ppb), with generally higher surface CH₄ mixing ratios/concentrations implied by this study (Fig. 16b). Again, this study’s global mean matches closely the WDCGG or sits in between the NOAA MBL and the WDCGG data products. There are some differences in the seasonality compared to the NOAA MBL product though. The seasonal variation is similarly shaped between our study and NOAA MBL for the southern hemisphere, although there seems to be a slight phase-shift of about a month with the NOAA
25 MBL product in the southern hemisphere assuming a slightly earlier increase and decrease and slightly higher amplitude (Fig. 16b). This phase-shift of the southern hemisphere together with sometimes lower peak northern hemispheric mixing ratios/concentrations in the NOAA MBL product suggests global-mean NOAA MBL CH₄ mixing ratio/concentration that show a double peak within any year, while our data assimilation and the WDCGG product suggests a smoother single-peak oscillation of global-mean CH₄ mixing ratios/concentrations (Fig. 16b). This peak results from the mid northern latitudes, where
30 in the summer months, our study suggests up to 40 or 50 ppbv/ppb higher mixing ratios/concentrations (Fig. 18c).

For N₂O, the WDCGG global-mean and our data match very closely, with our implicit smoothing due to our lower rank representation of seasonal cycles and latitudinal means resulting in a smoother global mean compared to WDCGG (Fig. 16c).

Similarly, the draft data product of the NOAA MBL indicates almost identical ~~mixing-ratios~~ mole fractions to our concentration fields over the available time period from 2001 to 2014, with maximal differences being 0.8 ~~ppb~~ ppb (Fig. 19).

In summary, our dataset closely matches the global-means of WDCGG in many years, but provides a complete 2-D field of ~~mixing-ratios~~ mole fractions. In comparison to the NOAA MBL products, there is one more systematic difference. Our CMIP6 GHG ~~mixing-ratio~~ concentration fields are meant to represent the mean monthly state of the latitudinally-averaged surface atmosphere, including land and polluted areas, i.e. not confined to areas with background ~~mixing-ratios~~ (see Section concentrations (section 6 ~~limitations~~: Limitations). This is a key difference to the NOAA Marine Boundary Layer product, which is a consistent background ~~mixing-ratio~~ concentration product, resulting in slightly lower global-mean ~~mixing-ratio~~ concentration estimates.

10 5.4.5.5 Comparison to mid-troposphere CO₂ ~~mixing-ratios~~ concentrations by NASA Aqua satellite

Since its launch in 2002, the Aqua satellite and its infrared sounder provides an additional independent data product to estimate tropospheric CO₂ ~~mixing-ratios~~ mole fractions. Rather than at ground level, this sensor provides an estimate of tropospheric ~~mixing-ratios~~ concentrations with a maximum sensitivity around 7km height, i.e. in the mid-troposphere. In the tropics and the parts of the southern hemisphere that are covered by the Aqua satellite product, the agreement between our data and the AIRS level 3 data (available at: ftp://acdisc.gsfc.nasa.gov/ftp/data/s4pa/Aqua_AIRS_Level3/AIRX3C2M.005/) is encouraging, although the overall gradient is lower in line with 3-D atmospheric transport model results (~~Olsen and Randerson 2004~~), (~~Olsen and Randerson, 2004~~). In the northern hemisphere, the difference in the phase and amplitude of the seasonal cycle is most apparent, with satellite data showing a later onset of the autumn ~~mixing-ratio~~ concentration increase by about 4 months while the drawdown of ~~mixing-ratios~~ concentrations seems closer in phase between mid-troposphere and surface ~~mixing-ratios~~ concentrations (Fig. 16a). Overall the amplitude is less than half of the surface hemispheric mean amplitude, leading to seasonally higher winter and lower summer ~~mixing-ratios~~ concentrations of our surface data product in the northern hemisphere by up to 10 ~~ppm~~ ppm (Fig. 17e).

This systematic difference between ground-level and mid-atmosphere ~~mixing-ratio~~ concentrations, supported by 3-D transport modelling studies (~~Olsen and Randerson 2004~~), ~~has ramifications for the implementation of vertical mixing ratio~~ (~~Olsen and Randerson, 2004~~), ~~has ramifications for the implementation of vertical concentration~~ profiles in climate models. Without taking into account the dampened seasonal cycle and latitudinal gradient in the mid and higher troposphere, the models could overestimate the variations in the radiative effects, if our latitudinally and monthly resolved surface ~~mixing-ratio~~ concentration fields are prescribed. On the other hand, if global- annual mean values are prescribed, the radiative forcing effect variations over latitudes and within a year will obviously be underestimated.

30 5.5.5.6 Comparison to other literature studies.

Our ~~greenhouse gas~~ GHG derivations over the recent instrumental periods are based on the AGAGE and NOAA station-by-station data and we extended our 2-D ~~mixing-ratio~~ concentration field results back in time by using e.g. global-mean estimates of previous studies' estimates (Methods). The AGAGE and NOAA networks themselves publish global-mean results, and

WMO as well as other literature studies produce composite long-term global-mean and/or hemispheric mixing ratio:concentration estimates. Thus, while often not entirely independent, as the studies use the same original data sources or we rely on some studies' previous derivations, we here provide a comparison to a selection of the literature. Specifically, in addition to the comparisons with NOAA marine boundary layer, WDCGG and NASA Aqua satellite data, we discuss some instances where our results show substantial differences compared to earlier studies that have derived hemispheric or global means from instrumental data (Montzka et al., 2014; Rigby et al., 2014)(Montzka et al., 2015; Rigby et al., 2014), from firm data (Butler et al., 1999; Trudinger et al., 2016) or are themselves composites of multiple data sources (Martinerie et al., 2009; Velders et al., 2014; WMO, 2014);(Martinerie et al., 2009; Velders and Daniel, 2014; WMO, 2014). The comparisons are shown in the panels f, g, and h of the factsheets for each gas (Fig. 9, Fig. 11, Fig. 12, and Fig. 20 to Fig. 59):

Martinerie et al. (2009) provided high latitude northern hemisphere data for atmospheric mixing ratios, used by (and made available mole fractions is reported in the supplement of) Buizert et al. (2012), provided by Vas Petrenko and Patricia Martinerie (Table 12). For CO₂, the MartineriePetrenko data set has, as expected for the high northern latitudes, a very strong seasonal cycle, stronger than consistent with our less pronounced northern hemispheric average cycle, as the data represents higher northern latitudes (Fig. 9f, g, and h). The long-term mixing ratio:concentration trend over time in the MartineriePetrenko CO₂ record seems similar to the global CMIP5 data set which in turn was based on previous Law Dome data, indicating a slight local maximum in 1890 and lower 1940s plateau (cf. Fig. 9g and Fig. 15).

For CH₄, the Martinerie et al. Petrenko record shows a comparable, yet again stronger, seasonality. The annual means are very comparable to our derivation (compare the high latitude red circles, indicating annual-mean station averages of our analysis and Martinerie et al. Petrenko data as shown in Fig. 11f), although there are some steps in annual means in the Martinerie et al. Petrenko data set around 1956 and 1975, which are not present in our dataset (Fig. 11f). For earlier times, i.e. between 1860 to and the 1920s, the MartineriePetrenko annual mean is closer to our global-mean, not the high-latitude estimates, as our study assumes a large latitudinal gradient based on the NEEM and Law Dome data differences (Methods) (Fig. 11g).

For CCl₄, the Martinerie data show a lower increase from 1955 to the late 1960s and strong increase around 1970. The firm data by Butler et al. (1999) suggests an earlier start of atmospheric mixing ratio:concentration increases around 1890, and then slightly lower levels over 1960 to 1990 compared to the WMO (2014), Velders et al. (2014) timeseries to which we nudge our 2-D fields, and Velders and Daniel (2014) timeseries which we use as optimisation target for our 2-D fields. The difference between the Butler and Velders datasets can probably be explained by the wider firm air age distribution in the study by Butler. The findings by Sturrock et al. (2002) suggest an onset of detectable atmospheric mixing ratios:concentrations around 1920 (Figure 5f therein). The NOAA global mean that is available from 1992 onwards (Montzka et al. (1999) updated at <http://www.esrl.noaa.gov/gmd/hats/combined/CCI4.html>) and indicates initially slightly higher global mean estimates than our derivation, which is for the instrumental period based on 6 AGAGE and 13 NOAA HATS stations (Fig. 20f, g, h).

For CFC-11 (Fig. 21g), the NOAA Montzka-ODS reconstruction of the global-mean is slightly higher (1 pptv) than ours, which is almost identical to the WMO (2014) and data by Velders et al. (2014) and Daniel (2014). Those differences presumably result from differences in station coverage, different calibration scales and air sampling and analysis techniques between the NOAA and AGAGE networks. The seasonalities show comparable amplitudes, as they do for CFC-12 (Fig. 22h).

5 With CFC-115, our study follows the historical shape of the WMO (2014) record, with Velders et al. (2014) being slightly lower (~0.5 pptv) (record, with Velders and Daniel (2014) being slightly lower (~0.5 ppt) (Fig. 25f).

For CH₂Cl₂, the in situ instrumental record we use only reaches back to 1994, although the Cape Grim air archive record goes back to 1978. From 1994 to 2003, the northern latitude measurements imply a mixing ratio reduction from 40 to 30 pptv, whereas the southern hemispheric measurements are almost flat during that time. Similarly, the southern hemispheric firm reconstructions (Trudinger et al., 2004) indicate an almost flat southern hemispheric evolution from 1997 onwards (mole fraction reduction from 40 to 30 ppt, whereas the southern hemispheric measurements are almost flat during that time (also shown in Trudinger et al. (2004)) (Fig. 26f). We note however that there are substantial uncertainties in the pre-1995 mixing ratios/concentrations, as e.g. Koppmann (1993) reported 18 pptv and 36 pptv average mixing ratios/concentrations for the southern hemispheric and northern hemispheric measurements from a 1989 Atlantic transect ship measurement campaign (not shown in the figure). This could imply a global average value of approximately 27 pptv in 1989, instead of the 20 pptv assumed in this study – although different calibration scales might contribute to this difference. Recent seasonality and increases of CH₂Cl₂ are closely matching other time series, such as the AGAGE monthly global means and NOAA results from the Medusa instruments GCMS measurements (Fig. 26f), although there is a slight offset in the absolute level, possibly caused by our study not sorting out data points from so-called pollution events in the case of CH₂Cl₂. AGAGE data for CH₂Cl₂, whereas NOAA results are from flasks collected only in baseline air conditions (Spivakovsky et al., 2000).

For CH₃Br, our CMIP6 recommendations match very closely the NOAA (Montzka et al. (2003) updated on ftp://ftp.cmdl.noaa.gov/hats/methylhalides/ch3br/flasks) and AGAGE global means (2014) after 1995. Before then, the Butler (1999) global-mean firm reconstruction coincides closely with our southern-hemispheric mean. The 2004 firm reconstruction by Trudinger (2004) is close to the southern hemispheric mean, but shows somewhat more variation than the smooth exponential increase assumed by this study, WMO (2014) and Velders et al. (2014) and Velders and Daniel (2014).

For CH₃CCl₃, the overall agreement between the different (although not independent) studies considered here is excellent, for example the high northern latitude data in Martinerie et al. (2009) in the south pole from Martinerie (Buizer et al., 2012; Martinerie et al., 2009) in the South Pole firm data reconstruction (Montzka et al., 2010) (Montzka et al., 2010), approximately in line also with the findings by Sturrock et al. (2002).

30 The atmospheric mixing ratios/concentrations of CH₃Cl show a strong seasonal cycle, as is to be expected from the short lifetime due to the OH-related sink. As in the case of methyl bromide (CH₃Br), the pre-instrumental period before 1995 implies a number of uncertainties in our CH₃Cl time series. Here, we follow again the WMO (2014) and (not independent) Velders et

al and Daniel (2014) (2014) reconstruction that are in-line with shape of the based on Butler et al. firm-reconstructions (1999) firm reconstructions. However, we note that the more recent Trudinger et al. (2004) CH₃Cl reconstruction indicates both a significantly lower mixing-ratio-concentration for southern latitudes in the 1970s and a smoother increase compared to the more sudden rise of mixing-ratio-concentrations around 1940 as implied in this study (Fig. 29g).

5 As briefly discussed in section 3.4, the CHCl₃ history in this study relies on the Worton et al. (2006). reconstruction, whose shape is similar to Trudinger et al. (2004), although the latter is indicates lower global mean mixing-ratios-concentrations and not the diminishing latitudinal gradient suggested by Worton et al. (2006). The As with other gases (e.g. CH₂Cl₂), the implied pre-industrial value of around 6 pptv-ppt should be investigated in the future (Fig. 30).

10 For Halon-1211, the recent study by Vollmer et al. (2016) and also the earlier study by Sturrock et al. (2002) (not shown) suggest slightly higher initial mixing-ratio-concentrations (around 1975 to 1988) compared to the initially-lower and then larger exponential increase we assumed by following Velders (2014). After 1990 the southern hemispheric reconstruction by the Bristol and CSIRO models and Daniel (2014). We follow the global-mean derivation in the CSIRO inversion from Vollmer et al. in case of Halon-1211. After 1990 the southern hemispheric reconstruction by the Bristol and CSIRO inversions (Vollmer et al. 2016) (Vollmer et al., 2016) are slightly lower and hence the latitudinal gradient slightly larger than what we derived from

15 the AGAGE and NOAA station data, but the differences are small (Fig. 31f). Similarly, the very early mixing-ratio-increases of the Halon-1301 between 1970 and 1978 are higher in the Vollmer f). The Cape Grim measurements analysed on the UEA volumetric scale (Newland et al., 2013) are also in good agreement with the small offset to our global mean consistent with the derived latitudinal gradient (Fig. 31f). Similarly to Halon-1211, the very early concentration increases of the Halon-1301 between 1970 and 1978 are higher in the Vollmer et al. (2016) study and again the more recent years from 2007 onwards

20 (Figure 35h) are higher in Vollmer, than in Velders and Daniel (2014), and again the more recent years from 2007 onwards (Fig. 32h) are higher in Vollmer. In those latter years, our aggregation of AGAGE and NOAA station data however suggests slightly lower mixing-ratios, although the absolute difference (0.05 pptv) is within the measurement uncertainty and the overall agreement is very good concentrations, although the absolute difference (0.05 ppt) is within the measurement uncertainty and the overall agreement is very good. The Newland et al. (Newland et al., 2013) study of southern hemispheric concentrations

25 at Cape Grim would suggest slightly lower concentrations, although part of the slight offset could be related to differences in scales. However, our Halon-1301 record suffers from a potentially inadequate scaling of the latitudinal gradient. A low gradient around 2000 to 2002 (Fig. 32d and f) results from our scaling with global emissions that are assumed to drop in that period (Velders and Daniel, 2014) although subsequent station data suggest again a slightly stronger gradient. Furthermore, a second issue with our Halon-1301 record is a slight drop of the monthly data in year 2014 (Fig. 33f), which is likely an artefact of our assimilation procedure to be corrected by assimilations that consider observational data beyond 2014.

30 Halon-2402 is likely the most obvious example. where a shifting measurement spatial coverage density can lead to small jumps in latitudinal gradients or global means (Fig. 33f and h). The overall mixing-ratios-mole fractions are very small and the early agreement between the WMO (2014) time series and the Vollmer et al. (2016) findings is very good. In 2009, when data

coverage increased, the latitudinal gradient is suggested to suddenly decrease, which is likely an artefact of the assimilation procedure that is only able to cope with time-varying data coverage to a certain degree (Methods). However, overall, the implied shifts of 0.02 pptv ppt are negligible in the larger picture, and certainly negligible for radiative forcing, as the shift in Southern hemispheric radiative forcing is equivalent to only about 0.000003 W/m² (Fig. 33b-h). Halon-2402 is also an illustration of how big differences in some measurement scales can potentially be. The Cape Grim data analysed by Newland

with a volumetric UEA scale indicates 10-15% lower concentrations (Fig. 33f) (Newland et al., 2013). For HCFC-142b our derived global-mean is in the middle of the AGAGE and NOAA network averages, despite our study including those data points that are subject to 'pollution' events in the case of HCFC-142b, with large positive outliers (Fig. 36f), similar as in the case of HFC-134a (Fig. 50f). Pollution events might however be contributing to the difference between our HFC-152a global-means and the two independently derived network global means for AGAGE and NOAA, which largely exclude pollution events by e.g. using statistical methods (O'Doherty et al., 2001) (see using statistical methods or conditional sampling (O'Doherty et al., 2001) (see Fig. 52f). Two more issues can be observed with HCFC-142b data. Firstly, our end of 2014 mixing-ratios concentrations are somewhat uncertain and in this case possibly wrongly decreasing, which results from the smooth annual mean representation and our assimilation procedure. The differences are again very small and negligible in radiative forcing terms, but a smooth connection will have to be designed for the adjacent datasets representing SSP-RCP scenarios. Secondly, since 2010, our estimates for the HCFCs, namely HCFC-22 (Fig. 34f), HCFC-141b (Figure 38f) and HCFC-142b (Figure 39f) indicate smaller increases than implied by Velders et al. (2016). As f), HCFC-141b (Fig. 35f) and HCFC-142b (Fig. 36f) indicate smaller increases than implied by the post-2010 non-observational scenario data represented by Velders and Daniel (2014). As in the early study by Sturrock et al. (2002), our study represents the slow onset of HCFC-142b mixing-ratios concentrations in between 1960 and 1990 as shown in WMO (2014) and Velders et al. and Daniel (2014).

For the three main PFCs, i.e. CF₄ (Fig. 45), C₂F₆ (Fig. 37), and C₃F₈ (Fig. 38), we find a similar and good agreement of the main studies. The Trudinger et al. (2016) time series are slightly below those suggested by Mühle et al. (2010b) (-0.5 pptv, -0.1 pptv, -0.01 pptv (2010) (-0.5 ppt, -0.1 ppt, -0.01 ppt, respectively), but the overall agreement again is very good. The outliers are the previously recommended CMIP5 mixing-ratios (Meinshausen et al., 2011b) for these gases, which were at the time not yet based on either the Trudinger et al. concentrations (Meinshausen et al., 2011) for these gases, which were at the time not yet based on either the Trudinger et al. (2016) or Mühle et al. (2010b) studies. As mentioned above, the mixing ratios of the lesser important PFCs, C₄F₁₀ (2010) studies. As mentioned above, the concentrations of the lesser important PFCs, C₄F₁₀ (Fig. 39), C₅F₁₂ (Fig. 40), C₆F₁₄ (Fig. 41), C₇F₁₆ (Fig. 42) and C₈F₁₈ (Fig. 43) are based on the Ivy et al. (2012) (2012) reconstructions, with reversing latitudinal gradients in the case of C₆F₁₄, C₇F₁₆, and C₈F₁₈, which are unexplained so far and require further confirmation. Our historical c-C₄F₈ mixing-ratios concentrations are based on the study by Oram et al. (2012) with assumed conversions of the Cape Grim measurements to northern hemispheric and global-averages.

For HFC-43-10mee, we based our trajectory on the NH and SH estimates of Arnold et al. (2014) with relatively small latitudinal gradient and hemispheric means being informed by the recently available observations since 2010 from the AGAGE

Field Code Changed

Medusa instruments (Fig. 48f). Note that ~~the difference~~ for HFC-365mfc data (Fig. 56~~), the difference~~ between the station data and those published in Montzka ~~(2014)~~(2015) reflects a difference that ~~is now vanished~~ is now much smaller after a calculation-related correction was applied to the NOAA calibration scale ~~since~~after the publication of ~~the~~ Montzka et al. ~~(2014) study~~(2015). All studies are now in relatively close alignment with the shown AGAGE network average, the Vollmer et al. (2011) study and our derivation (which is slightly lower, <0.1ppt). ~~The~~ In addition, the air archive and AGAGE network analysis by Vollmer et al. (2011) investigated ~~in addition~~ the HFCs HFCs-236fa, HFC-227ea, and HFC-245fa. Those results are closely aligned with the ones constructed here based on the ~~basis of the~~ WMO AGAGE network average estimates (Fig. 54, Fig. 53, Fig. 55).

~~Similar to~~ Like our study, there are also studies that assimilate a wide range of gases with latitudinal and seasonal variation. For example, the AGAGE network assimilation with a 12-box model and optimization approach to reconcile emissions and ~~mixing ratios~~ concentrations (Rigby et al., 2011; Rigby et al., 2013) produces 4 semi-hemispheric concentration timeseries with 3 vertical levels ~~(Rigby et al., 2014)~~(Rigby et al., 2014). Those studies based on AGAGE data are more comprehensive than this one, as both emissions and concentrations as well as lifetimes are optimized and reconciled. In our case, we only assimilate AGAGE and NOAA observations to derive atmospheric mole fractions in 15 degree latitudinal bands (methods).

6 Limitations

Even though the presented dataset of historical surface ~~greenhouse gas~~ GHG concentrations is – to our knowledge - more comprehensive than other composite datasets before, there are ~~a number of~~ several key limitations.

6.1 Specific use of dataset

~~First of all,~~ the dataset was assimilated from ~~a number of~~ several sources ~~in order~~ to provide a common starting point for global climate models ~~as part of the CMIP6 experiments~~. Thus, for example, the data was not designed ~~to perform~~ as a starting point for inversion studies, which estimate emissions, or studies of biogeochemical processes. Those studies tend to require pure observations, ~~rather than partly interpolated composite products or at least products with appropriate uncertainty information (including auto-correlations) attached to it, rather than partly interpolated composite products. As mentioned earlier, our assimilation does not incorporate early atmospheric CO₂ measurements from the South Pole, which might result in a systematic bias for that latitude for some years of ~1ppm (Fig. 7, panel I).~~ This warning in terms of our data use is especially important for the fine-grid interpolation we present. The 0.5-degree mean-preserving smooth interpolation should not be misinterpreted to ~~actually~~ portray measurement information at such a fine scale.

6.2 Secondly, the No vertical and longitudinal resolution

~~The~~ purpose of forcing climate models correctly would best be accomplished by vertically resolved latitudinal and longitudinal fields, which (in the case of CO₂) even include a diurnal cycle. Our latitudinally and monthly resolved dataset offers climate models ~~already~~ an option to capture some key variability compared to the global and annual mean CMIP5 concentration

recommendation (Meinshausen et al., 2011b) (Meinshausen et al., 2011). However, a correct implementation of this additional monthly and latitudinal variability is also dependent on an appropriate propagation of the surface signal throughout the troposphere and stratosphere. For example, some studies (Olsen and Randerson, 2004) (Olsen and Randerson, 2004) find that column CO₂ is found to only exhibit roughly half of the latitudinal gradient and seasonal variation compared to the surface mixing-ratio-concentrations. In the CESM1 model (Hurrell et al., 2013) with prescribed surface greenhouse gas concentrations, the vertical propagation of CO₂ mixing ratio is assumed to be constant. In the case of the other greenhouse gases (CH₄, N₂O and CFCs) a constant mixing ratio in the troposphere and a decrease of mixing ratio (Hurrell et al., 2013) with prescribed surface GHG concentrations, the vertical propagation of the CO₂ concentration is assumed to be constant. In the case of the other GHGs (CH₄, N₂O and CFCs) a constant concentration in the troposphere and a decrease of the concentration in the stratosphere is assumed in CESM1. In particular, the scale heights in the stratosphere of these trace gases depend on latitude, which produces a more realistic stratospheric distribution. We recommend vertical extensions to our surface mixing-ratio-concentration reconstructions only in the case that the model has no intrinsic transport model or extension parameterisation parameterisation. Furthermore, we do not include the longitudinal variation. Again, in-particular-specifically for CO₂, this longitudinal variation might be systematic given the land/ocean contrast. For example, the MPI-ESM-LR model indicates systematically higher surface CO₂ mixing-ratio-concentration over land, which in turn would have a radiative effect (cf. Figure 14 (Fig. 60 and Fig. 61)).

6.3 Thirdly, our Limited filtering of station measurements

Our assimilation procedure is a rather simple one and does not attempt to offset potential biases due to day and night-time sampling biases for CO₂ in the case of some flask measurements, or whether including pollution events would bias the latitudinal averages towards higher than current average values. In a world with continuing point sources, screening out pollution effects might cause proposed averages to lag slightly behind the true average mixing-ratio-concentration. The question is whether the correlation between sampling locations and source locations will inherently bias the average mixing-ratio-concentrations towards higher-than true average values in our assimilation for species, where we include pollution events. For most substances, we do not find any systematic difference between the network averages from AGAGE or NOAA, although there are some species (e.g. HFC-152a, see Fig. 52) for which our higher mixing-ratio-concentration reconstructions could in part be explained by this different method.

The opposite might also be the case, i.e. that despite including some pollution events, there could still be an inherent underestimation of true zonal means. That is because the NOAA and AGAGE sampling stations, which we are sourcing our raw data from, tend to be biased towards remote/clean-air/well mixed conditions and this will have implications for our latitudinal gradient and seasonal cycle. Where there are continental sites, they are often at altitude, and when flasks are sampled, they are generally for mid-afternoon when mixing is largest. Hence the fitted latitudinal gradient for CO₂ at least might be closer to the NOAA marine boundary layer product than to a true zonal mean. Also, the seasonal cycle will be more representative of marine conditions than continental ones (where a diurnal rectifier could potentially dampen or offset

seasonally low ~~mixing-ratios~~concentrations in summer in the case of CO₂). This bias towards remote measurements tends to increase the further back in time we go.

6.4 Calibration scales

Another limitation of our study is related to the different calibration scales of atmospheric gas measurements. In our data assimilation method with no scale conversion between the SIO and NOAA scales of the AGAGE and NOAA networks (Methods), a time-varying difference between the scales or time-varying coverage from one network to another can lead to spurious trends in the derived ~~mixing-ratios~~ concentrations. We argue that our “middle of the road” data assimilation method across the two networks is however one justifiable, yet not the only viable, assimilation method. The reasons for our chosen approach are a) uncertainties in absolute mole fractions estimates are small compared to other uncertainties that would affect the radiative forcing in climate models, b) alternative “pure” scale data assimilation could only deal with the trend uncertainty, not with the uncertainty arising for absolute mole fraction values (assuming that both the SIO and NOAA scales are equally sound), c) we intend to be “network”-neutral and d) a single “in-between” ~~mixing-ratio~~concentration estimate is likely the most appropriate for the primary application purpose (historical simulations of climate models) of the provided data. However, future researchers are encouraged to work directly with the principal investigators of the two networks to devise data assimilation methods that would be better suited for alternative applications, such as uncertainty estimates of inverse emissions etc. A clear limitation of our data ~~producee~~product is hence our implicit “in between” scale, with time-varying influences from measurements under the one or other network. Thus, differences to “pure” SIO or NOAA scale will partly arise from this “scale” issue.

6.5 No uncertainty estimates

Another important limitation of our study is that we do not provide uncertainty estimates. This is ~~primary~~primarily related to the fact that the purpose of this study was to provide a consolidated dataset for CMIP6 climate model experiments. Those models experiments can only be performed a limited number of times given today’s computational resources. The experimental protocol hence does not foresee an ability to vary ~~greenhouse-gas-mixing-ratios~~GHG mole fractions within its uncertainties, given that many aspects of climate models are affected by more substantial uncertainties, such as aerosols. The original AGAGE and NOAA (sometimes monthly averaged) sampling data points shown in the Factsheets (see panels f, g, and h) can however provide an indication of uncertainties and the spread in observations.

6.6 ~~Note that our~~Uncertain scaling of seasonality changes and latitudinal gradients back in time

~~Our~~ choice of predictor for the CO₂ seasonality change (namely the product of CO₂ ~~mixing-ratio~~concentration and global-mean temperature deviation since pre-industrial) is subjective and using only CO₂ ~~mixing-ratio~~concentration or temperature would have yielded ~~in~~ a larger seasonality difference between current and pre-industrial times. Further research will be necessary to obtain an optimal proxy for ~~presumed~~ pre-observational CO₂ seasonality changes.

Similarly, our common explanatory variable for regressions of latitudinal gradients, i.e. global emissions ([Boden et al., 2013](#)), is an approximation. Ideally, the time-changing latitudinal distribution of emissions would be ~~taken-into-account~~considered in

those backward extensions of the latitudinal gradient over time. More generally, further research into observational and modelling-derived constraints regarding pre-1950 latitudinal gradients of CO₂ could allow future studies to go beyond our simplified assumption of a zero pre-industrial gradient in the light of the uncertainty.

6.7 Broad, but not comprehensive data coverage

- 5 For the recent instrumental period, our study is predominantly based on the NOAA and the international AGAGE network data. Consistent quality control and consistent scales are advantages of that approach. Ideally however, our study should have started out from a yet more inclusive representation, e.g. including the multiple additional station datasets gathered and archived by the World Data Centre for Greenhouse Gases (WDCGG) that are neither part of AGAGE or NOAA networks. The WDCGG station raw data is available at: <http://ds.data.jma.go.jp/gmd/wdcgg/cgi-bin/wdcgg/catalogue.cgi> . While the
- 10 methodology of our study could be maintained or built upon, we hence recommend for any future updates, that those additional datasets are considered – with the appropriate quality control and scale conversion efforts.

7 Conclusion

Glacial and interglacial cycles are driven by Milankovich cycles. Ice core measurements over the past 800,000 years reveal how atmospheric greenhouse gas mixing ratios (GHG concentrations) of CO₂, CH₄ and N₂O varied in turn, indicating. These variations indicate various feedback mechanisms connected to the glacial and interglacial cycles driven by Milankovich cycles. With the arrival of homo sapiens, initially through activities such as deforestation and agriculture, and then the onset of the through fossil-fuel driven industrial activities from the start of the industrial revolution, the atmospheric composition changed. Unprecedented over this time the 800,000 years of the ice core record, CO₂, CH₄ and N₂O mixing ratios shot upwards concentrations suddenly rose to record levels, with global-mean CO₂ reaching a historical mark of 400 ppmv ppm in 2015. (Fig. 6). Recently, synthetic greenhouse gases (GHGs) arising from refrigerants, solvents, insulation appliances foam-blowing agents and even gas-cushioned shoe soles added to the warming effect, the radiative forcing. As the IPCC AR5 found, the most likely warming contribution from these greenhouse gases (GHGs) is now higher than the observed warming (Figure TS.10 in IPCC AR5 (IPCC-2013) (IPCC, 2013). That means that without the human activities that happen to cool the planet, namely the aerosols we emit, observed warming would have been even greater than what has already been experienced.

In this study, we compile a set of greenhouse gas (GHG) histories over the last 2000 years – based on numerous efforts by the scientific community to retrieve firm samples and ice cores in the most remote places on Earth, unlock their secrets by analyzing/analysing the enclosed air and by investing in a large network of in-situ and flask measurement stations across the planet. Our understanding of past climate change is vital to develop scenarios of the future and design humanities/humanity's response strategies in terms of mitigation and adaptation. Without the/The ongoing efforts to retrieve and monitor the composition of the planet's atmosphere, efforts are sometimes at risk/threatened (Lewis 2016), the future ahead of us remains shrouded in many uncertainties (Lewis, 2016). Without those efforts, the future ahead of us would remain shrouded in even greater uncertainty.

In this dataset, we attempted to provide a solid base for the next generation of climate and earth system models to further our understanding of past and future climate changes. Providing seasonal and latitudinal differences of the radiative forcing that drives the climate change across the globe, we can hope for an even more appropriate comparison between models and past land-ocean, regional land and oceanic temperature observations. Ignoring these seasonal and latitudinal differences can lead to different calculated climate impacts of GHG emissions. Thus, accurately including this variability is a necessary condition to accurately comparing/compare model calculations and observations and to understanding/understand the reasons for the differences. Those agreements and disagreements between what models and past observations tell us, will then allow us to calibrate our understanding of the earth system, its non-linearities and its many feedback cycles, the human influences and natural variabilities – in jargon called 'detection and attribution', called 'detection and attribution'. We have been engaging in a unique experiment with our climate. In order to achieve the limits we set forth in the Paris Agreement of how much further we push the planetary system out of the boundaries it has been in for thousands of years (up to 2°C and 1.5°C, respectively) and in order to cope with the climate change committed to already, the next generation of climate models will be vital. This

study into the main past driver of human-induced climate change intends to provide the basis for this further examination of a tremendous challenge we find ourselves in.

We have been engaging in a unique experiment with our climate. In order to stay below the warming limits, that were set forth in the Paris Agreement in 2015 (i.e. well below 2°C and 1.5°C relative to pre-industrial levels), the next generation of climate models and the examination of their response to climate drivers will be vital as an information basis for decision makers. This study into the main past driver of human-induced climate change will hence contribute to our collective examination of the tremendous challenge in which we find ourselves.

8 Code Availability

The ~~matlab~~[MATLAB](#) and R code that was used to assimilate the raw data is available from the authors on request.

9 Data Availability

A supplementary data table is available with global and annual mean mole fractions. The complete dataset with latitudinally and monthly resolved data in netcdf format is available via <https://pcmdi.llnl.gov/search/input4mips/>. Additional data formats, i.e. CSV, XLS, MATLAB .mat files of the same data are also available via www.climatecollege.unimelb.edu.au/cmip6. The respective raw data used in this study is available from the original referenced data providers on request. [or can be found at the web locations indicated in Table 12.](#)

10 Acknowledgements

10 The authors would first and foremost like to thank the large community of scientists, research assistants and measurement technicians that were involved [in](#) collecting the firm, ice core and atmospheric in-situ and flask measurements across the world. The primary networks AGAGE and the Cooperative Air Sampling Network managed by NOAA deserve the most credit, including all its individual researchers and the networks' policy to make the raw data available to the broader scientific community. ~~In~~[We thank in](#) particular, ~~we thank~~ the following researchers for invaluable efforts to collect, screen and make available NOAA network data: Ed Dlugokencky, Pieter Tans, David Nance, Bradley Hall, Geoff Dutton, James Elkins, Debra Mondeel, [Carolina Siso, Ben Miller](#). We [would](#) also like to thank the Editor O. Morgenstern for helpful suggestions [and Zebedee Nicholls for his comments.](#)

15 Furthermore, we thank the ESM CMIP5 modelling groups who contributed to the 5th Climate Model Intercomparison project and whose data we [analyzed analysed. Also, the reviewer comments from one anonymous reviewer and Piers Forster were](#)
20 [most helpful in improving the quality of the manuscript.](#)

Attributions: MM designed the study. EV wrote most of the data analysis and read-in routines together with MM. KL analysed the CMIP5 ESM models and produced related figures. Other figures and the factsheets were produced by MM. AN provided an initial literature overview. All authors wrote, commented on and/or discussed the manuscript based on a first draft by MM. NM designed the mean-preserving interpolation routines. Multiple authors provided vital data.

5

MM thankfully acknowledges the support by the Australian Research Council Future Fellowship grant FT130100809. This work was undertaken in close collaboration with partners in the European Union's Horizon 2020 research and innovation programme CRESCENDO (grant No 641816), of which the University of Melbourne is an unfunded partner. CSIRO's contribution was supported in part by the Australian Climate Change Science Program (ACCSP).

10

11 Tables

Gas	Time period	Main data source	Global and annual-mean \bar{c}_{global}	Seasonality $S_{l,m}$	Seasonality Change $\Delta S_{l,m}$	Latitudinal gradient \hat{L}
						industry emissions (Gütschow et al., 2016). Score for EOF2 kept constant before in situ instrumental period.
N ₂ O	1990 to 2013/2014	AGAGE monthly station means, incl. pollution events (Prinn et al., 1990) & Combined Nitrous Oxide data (monthly station averages) from the NOAA/ESRL Global Monitoring Division. AGAGE monthly station means, incl. pollution events (Prinn et al., 1990) & Combined Nitrous Oxide data (monthly station averages) from the NOAA/ESRL Global Monitoring Division.	Calculated based on observational data source (section 2.1.3).	Mean over 1990-2013 period. Applied as relative seasonality	Assumed zero	Two leadings EOF and their scores derived from residuals from observations. (2014: optimized to match observational data).
	Before 1990	Law Dome (MacFarling-Meure et al., 2006) Law Dome (MacFarling Meure et al., 2006) until 1968	Optimized to match smoothed Law Dome record until 1968. Interpolation until 1986 with optimization to sparse observational data until 1990.			The score for EOF1 is regressed against global annual fossil-fuel & industry emissions (Gütschow et al. 2016). Score for EOF2 kept constant before in situ instrumental period. Score for EOF1 and 2 kept constant before in situ instrumental period.

Table 2- Raw data used for CO₂ surface [mixing ratio](#) [concentration](#) field derivation

Dataset	Reference / URL	Stations / Location	Used for	Description / Filtering

NOAA ESRL GMD Surface Flask data.	(Conway et al., 1988; Conway et al., 1994; Komhyr et al., 1983, 1985; Komhyr et al., 1985; Thoning et al., 1987; Conway et al., 1988, 1983; Tans et al., 1989, 1989; Tans et al., 1990a; Tans et al., 1990b; Thoning et al., 1995; Thoning et al., 1989; Tans et al., 1990a, 1990b; Conway et al., 1990b; Conway et al., 1994, 1987; Thoning et al., 1995, 1989; Zhao and Tans, 2006)	81 stations of the surface flask network ^a : ABP, ALT, AMS, AOC, ASC, ASK, AVI, AZR, BAL, BHD, BKT, BME, BMW, BRW, BSC, CBA, CGO, CHR, CIB, CMO, CPT, CRZ, DRP, DSI, EIC, GMI, GOZ, HBA, HPB, HSU, HUN, ICE, IZO, KCO, KEY, KUM, KZD, KZM, LEF, LLB, LLN, LMP, MBC, MEX, MHD, MID, MKN, MLO, NAT, NMB, NWR, OPW, OXK, PAL, PAO, POC, PSA, PTA, RPB, SCS, SDZ, SEY, SGI, SGP, SHM, SMO, SPO, STC, STM, SUM, SYO, TAP, THD, TIK, USH, UTA, UUM, WIS, WLG, WPC, ZEP	Observational period estimation of global mean, latitudinal gradient seasonality and seasonality change over 1984-2013. Optimization of global mean and latitudinal gradient in 2014 and before 1984.	This study used monthly average data that uses all sample points which have an 'accepted' flag, i.e. initial two dots ('.*') in the three digit flag.
NOAA ESRL GMD Surface Flask data.	(NOAA ESRL GMD 2014c; NOAA ESRL GMD 2014b; NOAA ESRL GMD 2014a)	BRW, MLO, SMO		
Law Dome	(Etheridge et al., 1996, 1998b; Etheridge et al., 1998c, 1996; Rubino et al., 2013) (MacFarling Meure et al., 2006)	Law Dome ice core	Used as input for piecewise 3rd-degree polynomial smoothing over remainder of years 0 to 1966.	

^a See station descriptions here: http://www.esrl.noaa.gov/gmd/dv/site/site_table.html

Split Cells

Split Cells

Table 3 – Global-mean GHC- Raw data used for CH₄ surface mixing ratios for year 2011 and 2014, including a comparison to 2011 NOAA, AGAGE and UCI estimates – as provided in IPCC-AR5-WGI. Unit is pptv, unless otherwise stated. concentration field derivation

Dataset	Reference / URL	2014 Stations / Location	2011 Used for	2011 Description / Filtering	2011	2014
NOAA ESRL GMD Surface Flask data	(Dlugokencky et al., 2009; Dlugokencky et al., 1994a; Dlugokencky et al., 1998; Dlugokencky et al., 2005; Dlugokencky, 2015a; Dlugokencky et al., 1994c; Dlugokencky et al., 2001; Lang, 1990a, 1992, 1990b; Steele et al., 1992; Steele et al., 1987; Steele, 1991)	87 stations of the surface flask network ^a : ABP, ALT, AMS, AMT, AOC, ASC, ASK, AVI, AZR, BAL, BHD, BKT, BME, BMW, BRW, BSC, CBA, CGO, CHR, CIB, CMO, CPT, CRZ, DRP, DSI, EIC, GMI, GOZ, HBA, HPB, HSU, HUN, ICE, ITN, IZO, KCO, KEY, KPA, KUM, KZD, KZM, LEF, LLB, LLN, LMP, MBC, MCM, MEX, MHD, MID, MKN, MLO, NAT, NMB, NWR, NZL, OPW, OXK, PAL, PAO, POC, PSA, PTA, RPB, SCS, SDZ, SEY, SGI, SGP, SHM, SIO, SMO, SPO, STM, SUM, SYO, TAP, THD, TIK, USH, UTA, UUM, WIS, WKT, WLG, WPC, ZEP	Observational period estimation of global mean, latitudinal gradient, seasonality and seasonality change over 1984-2013. Optimization of global mean and latitudinal gradient in 2014 and before 1984. Rank of Abundance	This study used monthly station averages that include all sample points which have an 'accepted' flag, i.e. initial two dots (".*") in the three digit flag. <u>GMP6 (This Study)</u>	UCI	SIO NOAA b/AGAGE
AGAGE GC-MD	(Prinn et al., 2000b)	AGAGE GC-MD network ^b : CGO, MHD, RPB, SMO, THD		The monthly station averages that include pollution events ('.mop' file endings in case of AGAGE) were used.		
Law Dome	(Etheridge et al., 1998a; MacFarling Meure et al., 2006)	Law Dome ice core at -66.73-degree south.	Long-term high-latitude southern hemisphere reference point with piecewise 3rd-degree polynomial smoothing over years 154 to 1974.			
EPICA Dronning Maud Land Ice Core ^c	CO ₂ (ppmv)(Barbante et al., 2006b; Capron et al., 2010)	Dronning Maud Land Ice Core 307-55	Used as input for piecewise 3rd-degree polynomial smoothing over remainder of years 0 to 153. 390.48 ± 0.28	390.44 ± 0.46		
NEEM Greenland	N ₂ O (ppbv)(Dahl-Jensen et al., 2013; Rhodes et al., 2013)	NEEM ice core Greenland data 326.99	324.16	4798.1 ± 0.6	1893.1 ± 4.8	1893.2 ± 1.2
	CH ₄ (ppbv)	4834.47 4813.07				
				324.0 ± 0.1	Used for optimisation of global mean and latitudinal gradient score of EOF1 over timescale from year 0 to 1984, with linear	324.3 ± 0.1

- Deleted Cells
- Deleted Cells
- Deleted Cells
- Inserted Cells
- Inserted Cells
- Inserted Cells
- Merged Cells
- Deleted Cells

- Deleted Cells
- Deleted Cells

- Deleted Cells
- Deleted Cells

				interpolation of the score in between available 5-yearly NEM datapoints. (section 2.1.4)	
--	--	--	--	--	--

^aNOAA station descriptions here: http://www.esrl.noaa.gov/gmd/dv/site/site_table.html

^bAGAGE station descriptions here: <https://agage.mit.edu/global-network>

Table 4 - Raw data used for N₂O surface concentration field derivation

Dataset	Reference / URL	Stations / Location	Used for	Description / Filtering
NOAA ESRL GMD Surface Flask data.	Combined N ₂ O data from the NOAA/ESRL Global Monitoring Division. (ftp://ftp.cmdl.noaa.gov/hats/n2o/combined/HATS_global_N2O.txt , file date: Wed, Aug 19, 2015 2:40:55 PM)	13 stations of the NOAA HATS global ^a : alt, brw, cgo, kum, mhd, mlo, nwr, psa, smo, spo, sum, tdf, thd	Observational period estimation of global mean, latitudinal gradient, seasonality and seasonality change over 1990-2013. Optimization of global mean and latitudinal gradient in 2014.	This study uses station averages, which include all sample points which have an 'accepted' flag, i.e. initial two dots ('..*') in the three digit flag. ('.mop' file endings in case of AGAGE)
AGAGE GC-MD	(Prinn et al., 1990; Prinn et al., 2000b)	AGAGE GC-MD network ^b : CGO, MHD, RPB, SMO, THD		
Law Dome	(MacFarling Meure et al., 2006)	Law Dome ice core at -66.73 degree south.	Long-term high-latitude southern hemisphere reference point with piecewise 3rd-degree polynomial smoothing over years 155 to 1974.	
Gap			Sparse data availability in the period 1968 to 1986 suggested against optimisations of global-means with annual datapoints, which is why an interpolation between 1968 (starting from smoothed Law Dome record) to 1986 (ending with optimized global mean to fit observational data) was assumed.	

5 ^aNOAA station descriptions here: http://www.esrl.noaa.gov/gmd/dv/site/site_table.html

^bAGAGE station descriptions here: <https://agage.mit.edu/global-network>

Table 5- Options for reducing the number of GHGs to be taken into account in climate models to approximate full radiative forcing of all GHGs. The GHGs are ranked by their radiative forcing, with CO₂ having the highest radiative effect change between 1750 and 2014. The stated percentages in row X are cumulative, i.e. the radiative forcing of the GHG in row X plus the radiative forcing sum of all higher ranked GHGs. In Option 1, a climate model explicitly resolves actual GHG concentrations. With 8 and 15 species, 99.1% and 99.7% of the total radiative effect can be captured. In Option 2, only CFC-12 is modelled next to CO₂, CH₄, and N₂O; all other gases are summarized in a CFC-11-equivalence concentration. In Option 3, all ODS are summarized in a CFC-12-equivalence concentration, and all other fluorinated substances are summarized in HFC-134a-equivalence concentrations. Note that below shares are approximations, as linear radiative forcing efficiencies are assumed here for all gases, also for CO₂, N₂O and CH₄.

			<u>Option 1</u>	<u>Option 2</u>	<u>Option 3</u>	
4	CH ₂ Cl	539.54	534.17	=	=	
5	CFC-12	520.58	528.53	525.3 ± 0.8	529.5 ± 0.2	527.4 ± 0.4
6	CFC-11	233.08	238.25	237.0 ± 0.8	236.0 ± 0.4	238.5 ± 0.2
7	HCFC-22	229.54	244.56	209.0 ± 1.2	243.4 ± 0.8	243.2 ± 1.2
8	CCl ₄	83.07	86.06	87.8 ± 0.6	85.0 ± 0.4	86.5 ± 0.3
9	CF ₄	81.09	79.04		79.0 ± 0.4	
10	HFC-134a	80.52	62.85	63.4 ± 0.9	62.4 ± 0.3	63.0 ± 0.6
11	CFC-113	72.74	74.64	74.9 ± 0.6	74.29 ± 0.06	74.40 ± 0.04
12	CH ₂ Cl ₂	36.35	29.49	=	=	=
13	HFC-23	26.89	24.43		24.0 ± 0.3	
14	HCFC-141b	23.84	24.56	20.8 ± 0.5	24.38 ± 0.09	24.4 ± 0.2
15	HCFC-142b	22.08	24.35	24.0 ± 0.5	24.35 ± 0.06	24.0 ± 0.4
16	CFC-114	16.34	16.36	=	=	=
17	HFC-125	15.36	10.46		9.58 ± 0.04	
18	HFC-143a	15.25	11.92	=	12.04 ± 0.07	=
19	CHCl ₃	9.90	8.95			
20	CFC-115	8.43	8.39	=	=	=
21	HFC-32	8.34	5.47			
22	SF ₆	8.22	7.34	=	7.26 ± 0.02	7.31 ± 0.02
23	HFC-152a	7.73	7.99		6.4 ± 0.4	
24	CH ₂ Br	6.69	7.11	=	=	=
25	C ₂ F ₆	4.40	4.47		4.46 ± 0.02	
26	Halon-1211	3.75	4.05	=	=	=
27	CH ₃ CCl ₃	3.68	6.34	6.8 ± 0.6	6.3 ± 0.4	6.35 ± 0.07
28	Halon-1301	3.30	3.23	=	=	=
29	HFC-245fa	2.05	1.56			
30	SO ₂ F ₂	2.04	1.74	=	=	=
31	e-C ₂ F ₄	1.34	1.23			
32	NF ₃	1.24	0.93	=	=	=
33	HFC-227ea	1.04	0.74			
34	HFC-365mfe	0.77	0.56	=	=	=
35	C ₃ F ₈	0.60	0.56			
36	Halon-2402	0.43	0.45	=	=	=
37	C ₆ F ₁₄	0.28	0.27			
38	HFC-43-10mee	0.25	0.22	=	=	=
39	C ₄ F ₁₀	0.18	0.17			
40	HFC-236fa	0.13	0.10	=	=	=
41	C ₆ F ₁₂	0.13	0.12			
42	C ₂ F ₁₆	0.13	0.12	=	=	=
43	C ₆ F ₁₈	0.09	0.09			

Table 4—1petCO₂: Global-mean annual-mean surface CO₂ mixing ratios for idealized CMIP6 experiments 1petCO₂. All other gases, as in picontrol-run (see Table 5). The value 284.317 ppmv with 3-digit precision in year-1850 is increased by 1% per year.

YEAR	CO ₂ (PPMV)								
1850	284.32	1900	467.60	1950	769.02	2000	1264.76	2050	2080.07
1851	287.16	1901	472.27	1951	776.71	2001	1277.44	2051	2100.87
1852	290.03	1902	477.00	1952	784.48	2002	1290.18	2052	2121.88
1853	292.93	1903	481.77	1953	792.33	2003	1303.00	2053	2143.10
1854	295.86	1904	486.58	1954	800.25	2004	1316.12	2054	2164.63
1855	298.82	1905	491.45	1955	808.25	2005	1329.28	2055	2186.47
1856	301.81	1906	496.36	1956	816.34	2006	1342.57	2056	2208.03
1857	304.83	1907	501.33	1957	824.50	2007	1356.00	2057	2230.44
1858	307.87	1908	506.34	1958	832.74	2008	1369.56	2058	2252.42
1859	310.95	1909	511.40	1959	841.07	2009	1383.25	2059	2274.04
1860	314.06	1910	516.52	1960	849.48	2010	1397.08	2060	2297.69
1861	317.20	1911	521.68	1961	857.98	2011	1411.06	2061	2320.67
1862	320.38	1912	526.90	1962	866.56	2012	1426.17	2062	2343.87
1863	323.58	1913	532.17	1963	875.22	2013	1440.42	2063	2367.31
1864	326.82	1914	537.49	1964	883.97	2014	1453.81	2064	2390.98
1865	330.09	1915	542.87	1965	892.81	2015	1468.25	2065	2414.89
1866	333.38	1916	548.29	1966	901.74	2016	1483.03	2066	2439.04
1867	336.72	1917	553.78	1967	910.76	2017	1497.86	2067	2463.43
1868	340.09	1918	559.31	1968	919.87	2018	1512.84	2068	2488.07
1869	343.49	1919	564.91	1969	929.07	2019	1527.97	2069	2512.96
1870	346.92	1920	570.56	1970	938.36	2020	1543.26	2070	2538.08
1871	350.39	1921	576.26	1971	947.74	2021	1558.68	2071	2563.46
1872	353.89	1922	582.03	1972	957.22	2022	1574.27	2072	2589.09
1873	357.43	1923	587.85	1973	966.79	2023	1590.04	2073	2614.98
1874	361.01	1924	593.72	1974	976.46	2024	1605.91	2074	2641.13
1875	364.62	1925	599.66	1975	986.22	2025	1621.97	2075	2667.55
1876	368.26	1926	605.66	1976	996.08	2026	1638.19	2076	2694.22
1877	371.95	1927	611.71	1977	1006.04	2027	1654.67	2077	2721.16
1878	375.67	1928	617.83	1978	1016.11	2028	1671.42	2078	2748.38
1879	379.42	1929	624.01	1979	1026.27	2029	1688.33	2079	2776.86
1880	383.22	1930	630.25	1980	1036.53	2030	1704.71	2080	2803.62
1881	387.05	1931	636.55	1981	1046.89	2031	1721.76	2081	2831.65
1882	390.92	1932	642.92	1982	1057.36	2032	1738.97	2082	2859.97
1883	394.83	1933	649.35	1983	1067.94	2033	1756.36	2083	2888.57
1884	398.78	1934	655.84	1984	1078.62	2034	1773.93	2084	2917.46
1885	402.76	1935	662.40	1985	1089.40	2035	1791.67	2085	2946.63
1886	406.78	1936	669.02	1986	1100.30	2036	1809.58	2086	2976.10
1887	410.86	1937	675.71	1987	1111.30	2037	1827.68	2087	3006.86
1888	414.97	1938	682.47	1988	1122.41	2038	1845.96	2088	3036.92
1889	419.12	1939	689.29	1989	1133.64	2039	1864.41	2089	3066.28
1890	423.31	1940	696.19	1990	1144.97	2040	1883.06	2090	3096.04
1891	427.54	1941	703.15	1991	1156.42	2041	1901.89	2091	3127.01
1892	431.82	1942	710.18	1992	1167.99	2042	1920.91	2092	3159.19
1893	436.14	1943	717.28	1993	1179.67	2043	1940.12	2093	3190.78
1894	440.50	1944	724.46	1994	1191.46	2044	1959.52	2094	3222.69
1895	444.90	1945	731.70	1995	1203.38	2045	1979.11	2095	3254.91
1896	449.35	1946	739.02	1996	1215.44	2046	1998.90	2096	3287.46
1897	453.84	1947	746.41	1997	1227.57	2047	2018.89	2097	3320.34
1898	458.38	1948	753.87	1998	1239.84	2048	2039.08	2098	3353.54
1899	462.97	1949	761.41	1999	1252.24	2049	2059.47	2099	3387.08
								2100	3420.95

Table 5—piecontrol: Global and annual mean surface mixing ratios for the piecontrol-CMIP6 experiment. The hemispheric and latitudinally-resolved mixing ratios for 43 greenhouse gases and three aggregate equivalent mixing ratios are provided in the accompanying historical run dataset for the year 1850.

5 The complexity reduction options for capturing all GHGs with fewer species than 43 are indicated in the Table as Option 1, Option 2, and Option 3, with 'x' denoting relevant columns under each option.

Years	CO ₂	CH ₄	N ₂ O	CFC-12- eq	HFC- 134a- eq	CFC-11- eq	CFC-12	Other
Option-1	x	x	x				x	x
Option-2	x	x	x			x	x	
Option-3	x	x	x	x	x			
Units:	ppmv	ppbv	ppbv	pptv	pptv	pptv	pptv	
1850	284.317	808.25	273.02	16.54	19.15	32.11	0.00	All or a subset of other 30 individual gases, available in Supplementary

Rank	<u>The GHG contribution to climate change since 1750.</u>		<u>Using subset of actual concentrations, no equivalent gases</u>		<u>Summarizing all gases of lower importance than CFC-12 into CFC-11eq.</u>		<u>Summarizing all ODS into CFC-12- eq and all other fluorinated gases into HFC134a- eq</u>	
	<u>Shares of change of total warming effect since 1750: Approx. Radiative forcing contribution between 1750 and 2014 relative to that of all GHGs</u>		<u>Shares of total warming effect: Approx. Radiative effect compared to effect of all GHGs (absolute in 2014, not relative to 1850)</u>					
1	CO ₂	64.0%	CO ₂	72.9%	CO ₂	72.9%	CO ₂	72.9%
2	+CH ₄	79.5%	+N ₂ O	86.1%	+N ₂ O	86.1%	+N ₂ O	86.1%
3	+CFC12	86.0%	+CH ₄	95.0%	+CH ₄	95.0%	+CH ₄	95.0%
4	+N ₂ O	92.2%	+CFC12	97.2%	+CFC12	97.2%	+CFC12- eq	99.5%
5	+CFC11	94.5%	+CFC11	98.0%	+CFC11- eq	100.0%	+HFC134a- eq	100%
6	+HCFC22	96.4%	+HCFC22	98.6%				
7	+CFC113	97.2%	+CFC113	98.9%				
8	+CCl ₄	97.8%	+CCl ₄	99.1%				
9	+HFC134a	98.3%	+HFC134a	99.3%				
10	+CFC114	98.5%	+CF ₄	99.4%				
11	+HFC23	98.7%	+CH ₂ Cl	99.5%				
12	+SF ₆	98.8%	+CFC114	99.5%				
13	+CF ₄	99.0%	+HFC23	99.6%				
14	+HCFC142b	99.2%	+SF ₆	99.7%				
15	+HCFC141b	99.3%	+HCFC142b	99.7%				
...	+28 additional GHGs	100%	28 additional GHGs	100%				

Table 6 – abrupt4x-historical: Global- and annual-mean surface mixing-ratio-concentrations for the idealized-abrupt4x-CMIP6 experiment. The hemispheric and latitudinally resolved mixing ratios for 43 greenhouse gases and three aggregate equivalent mixing ratios are provided in the accompanying historical run dataset, with the 1850-CO₂ mixing ratio of 284.317 being multiplied by four. The complexity-reduction options for capturing all GHGs with fewer species than 43 are indicated in the Table as Option 1, Option 2, and Option 3, with 'x' denoting relevant columns under each option.

Years	CO ₂	CH ₄	N ₂ O	CFC-12- eq	HFC- 134a-eq	CFC-11- eq	CFC-12	Other
Option-1	x	x	x				x	x
Option-2	x	x	x			x	x	
Option-3	x	x	x	x	x			
Units:	ppmv	ppbv	ppbv	pptv	pptv	pptv	pptv	
0-450	1137.268	808.25	273.02	46.54	40.45	32.44	0.00	All or a subset of other 30 individual gases, available in Supplementary

Table 7—historical: Global- and annual-mean surface mixing ratios for the historical CMIP6 experiments. CMIP6 experiments. The year-to-year and monthly resolved global, hemispheric and latitudinally resolved mixing-ratio concentrations for 43 greenhouse gases GHGs and three aggregate global mixing-ratio concentrations are provided in the accompanying datasets over the time horizon year 0 (1 BC) to year 2014 A.C.A.D. The complexity reduction options for capturing all GHGs with fewer species than 43 are indicated in the Table as Option 1, Option 2, and Option 3, with ‘x’ denoting relevant columns under each option (see section 2.1.10).

Years	CO ₂	CH ₄	N ₂ O	CFC-12-eq	HFC-134a-eq	CFC-11-eq	CFC-12	Other
Option 1	x	x	x				x	x
Option 2	x	x	x			x	x	
Option 3	x	x	x	x	x			
Units:	ppm/ppm	ppbv/ppb	ppbv/ppb	ppt/ppt	ppt/ppt	ppt/ppt	ppt/ppt	
1750	277.15	731.41	273.87	16.51	19.15	32.11	0.00	All or a subset of other 39 individual gases, available online
1850	284.32	808.25	273.02	16.51	19.15	32.11	0.00	
1851	284.45	808.41	273.09	16.51	19.15	32.11	0.00	
1852	284.60	809.16	273.17	16.51	19.15	32.11	0.00	
1853	284.73	810.40	273.26	16.51	19.15	32.11	0.00	
1854	284.85	811.73	273.36	16.51	19.15	32.11	0.00	
1855	284.94	813.33	273.47	16.51	19.15	32.11	0.00	
1856	285.05	814.80	273.58	16.51	19.15	32.11	0.00	
1857	285.20	816.45	273.68	16.51	19.15	32.11	0.00	
1858	285.37	818.36	273.76	16.51	19.15	32.11	0.00	
1859	285.54	820.40	273.90	16.51	19.15	32.11	0.00	
1860	285.74	822.31	274.06	16.51	19.15	32.11	0.00	
1861	285.93	824.40	274.24	16.51	19.15	32.11	0.00	
1862	286.10	827.03	274.42	16.51	19.15	32.11	0.00	
1863	286.27	830.17	274.57	16.51	19.15	32.11	0.00	
1864	286.44	833.60	274.72	16.51	19.15	32.11	0.00	
1865	286.61	836.89	274.88	16.51	19.15	32.11	0.00	
1866	286.78	840.36	275.05	16.51	19.15	32.11	0.00	
1867	286.95	844.00	275.21	16.51	19.15	32.11	0.00	
1868	287.10	847.25	275.39	16.51	19.15	32.11	0.00	
1869	287.22	850.13	275.56	16.51	19.15	32.11	0.00	
1870	287.35	852.44	275.72	16.51	19.15	32.11	0.00	
1871	287.49	853.99	275.90	16.51	19.15	32.11	0.00	
1872	287.66	855.23	276.08	16.51	19.15	32.11	0.00	
1873	287.86	856.17	276.25	16.51	19.15	32.11	0.00	
1874	288.06	857.82	276.42	16.51	19.15	32.11	0.00	
1875	288.29	859.47	276.59	16.51	19.15	32.11	0.00	
1876	288.52	860.86	276.74	16.51	19.15	32.11	0.00	
1877	288.75	862.38	276.86	16.51	19.15	32.11	0.00	
1878	288.99	864.14	277.00	16.51	19.15	32.11	0.00	
1879	289.22	866.28	277.13	16.51	19.15	32.11	0.00	
1880	289.47	868.70	277.27	16.51	19.15	32.11	0.00	
1881	289.74	870.98	277.37	16.51	19.15	32.11	0.00	
1882	290.02	873.25	277.49	16.51	19.15	32.11	0.00	
1883	290.26	875.60	277.59	16.51	19.15	32.11	0.00	
1884	290.51	878.15	277.70	16.51	19.15	32.11	0.00	
1885	290.80	881.03	277.80	16.51	19.15	32.11	0.00	
1886	291.10	883.84	277.89	16.51	19.15	32.11	0.00	
1887	291.41	886.93	278.00	16.51	19.15	32.11	0.00	
1888	291.76	889.93	278.08	16.51	19.15	32.11	0.00	
1889	292.11	893.16	278.19	16.51	19.15	32.11	0.00	
1890	292.46	896.38	278.27	16.51	19.16	32.11	0.00	
1891	292.82	899.67	278.35	16.51	19.16	32.11	0.00	

Years	CO ₂	CH ₄	N ₂ O	CFC-12-eq	HFC-134a-eq	CFC-11-eq	CFC-12	Other
1892	293.17	903.53	278.44	16.51	19.16	32.11	0.00	
1893	293.48	907.27	278.55	16.51	19.16	32.11	0.00	
1894	293.79	910.48	278.69	16.51	19.16	32.11	0.00	
1895	294.08	913.23	278.83	16.51	19.16	32.11	0.00	
1896	294.36	914.77	278.94	16.51	19.16	32.11	0.00	
1897	294.65	916.27	279.05	16.51	19.16	32.11	0.00	
1898	294.95	919.02	279.16	16.51	19.16	32.11	0.00	
1899	295.30	922.28	279.31	16.51	19.16	32.11	0.00	
1900	295.67	925.55	279.45	16.51	19.16	32.11	0.00	
1901	296.01	928.80	279.61	16.51	19.16	32.11	0.00	
1902	296.32	932.73	279.86	16.51	19.16	32.11	0.00	
1903	296.65	936.78	280.16	16.51	19.16	32.11	0.00	
1904	296.95	942.11	280.43	16.51	19.16	32.12	0.00	
1905	297.29	947.44	280.71	16.51	19.16	32.12	0.00	
1906	297.66	953.09	280.98	16.51	19.17	32.12	0.00	
1907	298.10	959.16	281.28	16.51	19.17	32.12	0.00	
1908	298.52	964.09	281.61	16.51	19.18	32.13	0.00	
1909	298.94	969.40	281.95	16.51	19.18	32.13	0.00	
1910	299.38	974.79	282.31	16.51	19.19	32.13	0.00	
1911	299.83	979.47	282.72	16.54	19.20	32.18	0.00	
1912	300.35	983.61	283.02	16.55	19.21	32.20	0.00	
1913	300.91	986.24	283.36	16.56	19.23	32.22	0.00	
1914	301.42	988.61	283.72	16.60	19.24	32.28	0.00	
1915	301.94	991.46	284.05	16.67	19.26	32.37	0.00	
1916	302.48	998.45	284.31	16.78	19.28	32.51	0.00	
1917	303.01	1,003.57	284.62	16.90	19.31	32.68	0.00	
1918	303.45	1,010.13	284.81	16.99	19.34	32.81	0.00	
1919	303.81	1,017.63	284.85	17.08	19.37	32.94	0.00	
1920	304.25	1,025.07	284.93	17.12	19.40	33.01	0.00	
1921	304.60	1,032.20	285.04	17.16	19.43	33.08	0.00	
1922	304.94	1,039.10	285.17	17.24	19.44	33.18	0.00	
1923	305.27	1,045.13	285.47	17.37	19.46	33.36	0.00	
1924	305.63	1,049.45	285.61	17.50	19.49	33.53	0.00	
1925	305.81	1,052.16	285.65	17.65	19.54	33.74	0.00	
1926	305.95	1,053.60	285.69	17.84	19.58	34.00	0.00	
1927	306.18	1,055.77	285.74	17.97	19.62	34.19	0.00	
1928	306.33	1,060.64	285.83	18.15	19.67	34.45	0.00	
1929	306.49	1,066.66	285.89	18.42	19.73	34.82	0.00	
1930	306.62	1,072.64	285.94	18.72	19.80	35.22	0.00	
1931	306.82	1,077.49	286.12	19.08	19.85	35.71	0.00	
1932	307.09	1,081.96	286.22	19.46	19.89	36.19	0.00	
1933	307.40	1,086.54	286.37	19.85	19.92	36.69	0.00	
1934	307.78	1,091.77	286.47	20.30	19.95	37.26	0.00	
1935	308.23	1,097.08	286.59	20.86	19.98	37.97	0.00	
1936	309.01	1,101.83	286.75	21.57	20.04	38.88	0.00	
1937	309.76	1,106.32	286.95	22.34	20.11	39.87	0.00	
1938	310.29	1,110.63	287.19	23.09	20.21	40.86	0.00	
1939	310.85	1,116.91	287.39	23.89	20.32	41.90	0.00	
1940	311.36	1,120.12	287.62	24.80	20.45	43.11	0.00	
1941	311.81	1,123.24	287.86	25.89	20.59	44.53	0.00	
1942	312.17	1,128.19	288.14	27.25	20.77	46.32	0.00	
1943	312.39	1,132.66	288.78	28.89	21.00	48.48	0.00	
1944	312.41	1,136.27	289.00	30.85	21.31	51.06	0.02	
1945	312.38	1,139.32	289.23	32.67	21.53	52.94	0.42	
1946	312.39	1,143.66	289.43	35.15	21.59	54.53	1.64	

Years	CO ₂	CH ₄	N ₂ O	CFC-12-eq	HFC-134a-eq	CFC-11-eq	CFC-12	Other
1947	312.49	1,149.64	289.51	37.73	21.67	56.29	2.84	
1948	312.52	1,155.63	289.56	40.53	21.79	58.34	4.03	
1949	312.63	1,160.35	289.60	43.44	21.92	60.53	5.22	
1950	312.82	1,163.82	289.74	46.41	22.04	62.83	6.38	
1951	313.01	1,168.81	289.86	49.53	22.18	65.04	7.78	
1952	313.34	1,174.31	290.03	52.53	22.37	66.80	9.44	
1953	313.73	1,183.36	290.33	55.93	22.58	68.92	11.21	
1954	314.09	1,194.43	290.55	59.82	22.80	71.41	13.20	
1955	314.41	1,206.65	290.84	64.26	23.04	74.27	15.44	
1956	314.70	1,221.10	291.19	69.32	23.29	77.48	18.01	
1957	314.99	1,235.80	291.51	75.05	23.54	81.04	20.98	
1958	315.34	1,247.42	291.77	81.16	23.78	84.76	24.18	
1959	315.81	1,257.32	291.99	87.55	24.03	88.56	27.61	
1960	316.62	1,264.12	292.28	94.78	24.30	92.70	31.61	
1961	317.30	1,269.46	292.60	103.17	24.60	97.52	36.24	
1962	318.04	1,282.57	292.95	112.78	24.94	103.11	41.48	
1963	318.65	1,300.79	293.33	123.96	25.33	109.56	47.60	
1964	319.33	1,317.37	293.69	136.86	25.73	116.84	54.80	
1965	319.82	1,331.06	294.05	151.46	26.15	124.93	63.03	
1966	320.88	1,342.24	294.45	167.71	26.60	133.86	72.25	
1967	321.48	1,354.27	294.86	185.88	27.09	143.77	82.61	
1968	322.39	1,371.65	295.27	206.27	27.67	154.88	94.26	
1969	323.25	1,389.34	295.68	229.03	28.28	167.24	107.29	
1970	324.78	1,411.10	296.10	254.09	28.94	180.81	121.65	
1971	325.40	1,431.12	296.52	281.15	29.69	195.51	137.14	
1972	327.35	1,449.29	296.96	310.64	30.51	211.74	153.86	
1973	329.91	1,462.86	297.40	343.56	31.41	230.16	172.26	
1974	330.76	1,476.14	297.86	379.95	32.40	250.57	192.56	
1975	330.83	1,491.74	298.33	416.91	33.51	271.30	213.24	
1976	331.54	1,509.11	298.81	453.19	34.60	292.30	233.00	
1977	333.35	1,527.68	299.32	489.38	35.78	314.19	251.99	
1978	335.01	1,546.89	299.85	524.85	37.12	336.51	270.00	
1979	336.60	1,566.16	300.39	557.73	38.90	357.76	286.49	
1980	338.70	1,584.94	300.97	588.51	40.76	377.49	302.18	
1981	340.06	1,602.65	301.56	621.21	42.65	397.68	319.42	
1982	340.64	1,618.73	302.19	652.90	44.48	418.45	335.14	
1983	342.27	1,632.62	302.84	685.20	46.14	437.87	352.51	
1984	344.01	1,643.50	303.53	715.67	47.82	458.80	366.80	
1985	345.46	1,655.91	304.25	753.45	49.69	486.19	383.27	
1986	346.90	1,668.79	305.00	789.53	51.62	508.22	402.41	
1987	348.77	1,683.75	305.79	831.33	53.55	535.08	423.35	
1988	351.28	1,693.94	306.62	879.94	55.70	564.26	449.32	
1989	352.89	1,705.63	307.83	921.47	57.93	593.68	468.07	
1990	354.07	1,717.40	308.68	953.43	60.21	616.35	482.76	
1991	355.35	1,729.33	309.23	979.87	62.66	636.82	493.78	
1992	356.23	1,740.14	309.73	1,001.60	65.13	650.21	505.87	
1993	356.92	1,743.10	310.10	1,012.33	67.79	657.53	511.99	
1994	358.25	1,748.62	310.81	1,021.09	70.74	662.45	518.21	
1995	360.24	1,755.23	311.28	1,029.02	74.60	666.66	524.66	
1996	362.00	1,757.19	312.30	1,038.98	79.14	673.40	531.41	
1997	363.25	1,761.50	313.18	1,041.17	84.42	674.97	534.96	
1998	365.93	1,770.29	313.91	1,046.23	90.45	681.59	537.67	
1999	367.84	1,778.20	314.71	1,048.71	96.94	685.59	540.14	
2000	369.12	1,778.01	315.76	1,051.12	104.52	690.46	542.38	
2001	370.67	1,776.53	316.49	1,052.91	113.35	697.10	543.20	

Years	CO ₂	CH ₄	N ₂ O	CFC-12-eq	HFC-134a-eq	CFC-11-eq	CFC-12	Other
2002	372.83	1,778.96	317.10	1,053.74	121.44	702.52	543.66	
2003	375.41	1,783.59	317.73	1,053.52	129.89	707.84	543.35	
2004	376.99	1,784.23	318.36	1,053.30	139.31	713.98	542.85	
2005	378.91	1,783.36	319.13	1,053.46	150.43	721.88	542.15	
2006	381.01	1,783.42	319.93	1,053.71	160.64	730.31	540.65	
2007	382.60	1,788.95	320.65	1,053.94	171.15	739.81	538.43	
2008	384.74	1,798.42	321.57	1,054.80	181.99	750.11	536.33	
2009	386.28	1,802.10	322.28	1,054.17	191.13	758.10	533.78	
2010	388.72	1,807.85	323.14	1,054.37	203.07	768.76	531.28	
2011	390.94	1,813.07	324.16	1,053.45	216.23	779.12	528.53	
2012	393.02	1,815.26	325.00	1,051.97	227.84	787.77	525.83	
2013	395.72	1,822.58	325.92	1,051.74	244.88	801.30	523.11	
2014	397.55	1,831.47	326.99	1,049.51	257.06	809.19	520.58	

LEF,
 LLB,
 LLN,
 LMP,
 MBC,
 MCM,
 MEX,
 MHD,
 MHD,
 MKN,
 MLO,
 NAT,
 NMB,
 NWR,
 NZL,
 OPW,
 OXK,
 PAL,
 PAO,
 POC,
 PSA,
 PTA,
 RPB,
 SCS,
 SDZ,
 SEY,
 SGI,
 SGP,
 SHM,
 SHO,
 SMO,
 SPO,
 STM,
 SUM,
 SYO,
 TAP,
 THD,
 THK,
 USH,
 UTA,
 UUM,
 WIS,
 WKT,
 WLG,
 WPC,
 ZEP

AGAGE—GC-MD	(Prinn et al. 2000b)	AGAGE—GC-MD network: CGO, MHD, RPB, SMO, THD	The monthly station averages that include pollution events (.mop' file endings in
-------------	----------------------	--	---

				ease—of AGAGE) were used.
Law-Dome	(Etheridge—et—al— 1998a, MacFarling Meure—et—al—2006)	Law-Dome ice core at— 66.73-degree south.	Long-term—high-latitude—southern hemisphere—reference—point—with piecewise—3rd-degree—polynomial smoothing over years 155 to 1974.	

1	EPICA Dronning Maud Land-ice Core	(Barbante et al. 2006; Capron et al. 2010) CO ₂ (ppm)	397.55 Dronning Maud Land-ice Core	390.94	390.48 ± 0.28	Used as input for piecewise 3rd-degree polynomial smoothing over remainder of years 0 to 153.	390.44 ± 0.16	
2	NEEM Greenland	(Dahl- Jensen et al. 2013; Rhodes et al. 2013) CH ₄ (ppb)	1831.47 NEEM ice core Greenland data	1813.07	1798.1 ± 0.6	Used for optimisation of global mean and latitudinal gradient score of EOF1 over timescale from year 0 to 1984, with linear interpolation of score-1 in between available-NEEM datapoints. (section 2.1.4)	1803.1 ± 4.8	1803.2 ± 1.2
3		N ₂ O (ppb)	326.99	324.16			324.0 ± 0.1	324.3 ± 0.1
4		CH ₃ Cl	539.54	534.17				
5		CFC-12	520.58	528.53	525.3 ± 0.8		529.5 ± 0.2	527.4 ± 0.4
6		CFC-11	233.08	238.25	237.9 ± 0.8		236.9 ± 0.1	238.5 ± 0.2
7		HCFC-22	229.54	214.56	209.0 ± 1.2		213.4 ± 0.8	213.2 ± 1.2
8		CCl ₄	83.07	86.06	87.8 ± 0.6		85.0 ± 0.1	86.5 ± 0.3
9		CF ₄	81.09	79.04			79.0 ± 0.1	
10		HFC-134a	80.52	62.85	63.4 ± 0.9		62.4 ± 0.3	63.0 ± 0.6
11		CFC-113	72.71	74.64	74.9 ± 0.6		74.29 ± 0.06	74.40 ± 0.04
12		CH ₂ Cl ₂	36.35	29.49				
13		HFC-23	26.89	24.13			24.0 ± 0.3	
14		HCFC-141b	23.81	21.56	20.8 ± 0.5		21.38 ± 0.09	21.4 ± 0.2
15		HCFC-142b	22.08	21.35	21.0 ± 0.5		21.35 ± 0.06	21.0 ± 0.1
16		CFC-114	16.31	16.36				
17		HFC-125	15.36	10.46			9.58 ± 0.04	
18		HFC-143a	15.25	11.92			12.04 ± 0.07	
19		CHCl ₃	9.90	8.95				
20		CFC-115	8.43	8.39				
21		HFC-32	8.34	5.17				
22		SF ₆	8.22	7.31			7.26 ± 0.02	7.31 ± 0.02
23		HFC-152a	7.73	7.89			6.4 ± 0.1	
24		CH ₃ Br	6.69	7.11				
25		C ₂ F ₆	4.40	4.17			4.16 ± 0.02	
26		Halon-1211	3.75	4.05				
27		CH ₃ CCl ₃	3.68	6.31	6.8 ± 0.6		6.3 ± 0.1	6.35 ± 0.07
28		Halon-1301	3.30	3.23				
29		HFC-245fa	2.05	1.56				

Inserted Cells

Inserted Cells

Inserted Cells

<u>30</u>	<u>SO₂F₂</u>	<u>2.04</u>	<u>1.74</u>	=	=	=
<u>31</u>	<u>c-C₂F₆</u>	<u>1.34</u>	<u>1.23</u>	=	=	=
<u>32</u>	<u>NF₃</u>	<u>1.24</u>	<u>0.83</u>	=	=	=
<u>33</u>	<u>HFC-227ea</u>	<u>1.01</u>	<u>0.74</u>	=	=	=
<u>34</u>	<u>HFC-365mfc</u>	<u>0.77</u>	<u>0.56</u>	=	=	=
<u>35</u>	<u>C₃F₈</u>	<u>0.60</u>	<u>0.56</u>	=	=	=
<u>36</u>	<u>Halon-2402</u>	<u>0.43</u>	<u>0.45</u>	=	=	=
<u>37</u>	<u>C₆F₁₄</u>	<u>0.28</u>	<u>0.27</u>	=	=	=
<u>38</u>	<u>HFC-43- 10mee</u>	<u>0.25</u>	<u>0.22</u>	=	=	=
<u>39</u>	<u>C₄F₁₀</u>	<u>0.18</u>	<u>0.17</u>	=	=	=
<u>40</u>	<u>HFC-236fa</u>	<u>0.13</u>	<u>0.10</u>	=	=	=
<u>41</u>	<u>C₅F₁₂</u>	<u>0.13</u>	<u>0.12</u>	=	=	=
<u>42</u>	<u>C₇F₁₆</u>	<u>0.13</u>	<u>0.12</u>	=	=	=
<u>43</u>	<u>C₈F₁₈</u>	<u>0.09</u>	<u>0.09</u>	=	=	=

Table 8 – picontrol: Global- and annual-mean surface concentrations for the picontrol CMIP6 experiment. The hemispheric and latitudinally resolved concentrations for 43 GHGs and three aggregate equivalent concentrations are provided in the accompanying historical run dataset for the year 1850. The complexity reduction options for capturing all GHGs with fewer species than 43 are indicated in the Table as Option 1, Option 2, and Option 3, with ‘x’ denoting relevant columns under each option.

<u>Years</u>	<u>CO₂</u>	<u>CH₄</u>	<u>N₂O</u>	<u>CFC-12- eq</u>	<u>HFC- 134a-eq</u>	<u>CFC-11- eq</u>	<u>CFC-12</u>	<u>Other</u>
<u>Option 1</u>	<u>x</u>	<u>x</u>	<u>x</u>				<u>x</u>	<u>x</u>
<u>Option 2</u>	<u>x</u>	<u>x</u>	<u>x</u>			<u>x</u>	<u>x</u>	
<u>Option 3</u>	<u>x</u>	<u>x</u>	<u>x</u>	<u>x</u>	<u>x</u>			
<u>Units:</u>	<u>ppm</u>	<u>ppb</u>	<u>ppb</u>	<u>ppt</u>	<u>ppt</u>	<u>ppt</u>	<u>ppt</u>	
<u>1850</u>	<u>284.317</u>	<u>808.25</u>	<u>273.02</u>	<u>16.51</u>	<u>19.15</u>	<u>32.11</u>	<u>0.00</u>	<u>All or a subset of other 39 individual gases, available in Supplementary</u>

^aNOAA station descriptions here: http://www.esrl.noaa.gov/gmd/dv/site/site_table.html

^bAGAGE station descriptions here: <https://agage.mit.edu/global-network>

Table 9 – Raw data used for N₂O – 1pctCO₂: Global-mean annual-mean surface mixing-ratio field derivation

Dataset	Reference / URL	Stations / Location	Used for	Description / Filtering
NOAA ESRL GMD Surface Flask data.	Combined N ₂ O data from the NOAA/ESRL Global Monitoring Division. (http://fp.emdl.noaa.gov/hats/n2o/combined/HATS_global_N2O.txt ; file date: Wed, Aug 19, 2015 2:40:55 PM)	13 stations of the NOAA HATS global ^a : alt, brw, cgo, kum, mhd, mlo, nwr, psa, smo, spo, sum, tdf, thd	Observational period estimation of global mean, latitudinal gradient seasonality and seasonality change over 1990-2013. Optimization of global mean and latitudinal gradient in 2014.	This study uses station averages, which include all sample points, which have an 'accepted' flag, i.e. initial two dots ('..') in the three digit flag. ('-mop' file endings in case of AGAGE)
AGAGE GC-MD	(Prinn et al. 1990; Prinn et al. 2000b)	AGAGE GC-MD network ^b : CGO, MHD, RPB, SMO, THD		
Law Dome	(MacFarling-Meure et al. 2006)	Law Dome ice core at -66.73 degree south.	Long-term high-latitude southern hemisphere reference point with piecewise 3rd-degree polynomial smoothing over years 155 to 1974.	
NEEM Greenland	(Dahl-Jensen et al. 2013; Rhodes et al. 2013)	NEEM firn-Greenland data	Used for comparison only as latitudinal gradient estimated as very small and constant and assumed constant before observational period	
Gap			At this stage, sparse data availability in the period 1968 to 1986 suggests against optimisations of global means with annual datapoints, which is why an interpolation between 1968 (starting from smoothed Law Dome record) to 1986 (ending with optimized global mean to fit observational data) is assumed.	

^aNOAA station descriptions here: http://www.esrl.noaa.gov/gmd/dv/site/site_table.html

^bAGAGE station descriptions here: <https://agage.mit.edu/global-network>

Table 10—Options for reducing the number of GHGs to be taken into account to approximate full radiative forcing of all GHGs. In Option 1, a climate model explicitly resolves actual GHG mixing ratios. With 8 and 15 species, 99.1% and 99.7% of the total radiative effect can be captured. In Option 2, only CFC-12 is modelled next to CO₂, CH₄, and N₂O; all other gases are summarized in a CFC-11 equivalence mixing ratio. In Option 2, all ODS are summarized in a CFC-12 equivalence mixing ratio, and all CO₂ concentrations for idealized CMIP6 experiments 1pctCO₂. All other fluorinated substances are summarized in HFC-134a equivalence mixing ratios, as in piconrol run (see Table 8). The value 284.317 ppm with 3-digit precision in year 1850 is increased by 1% per year.

YEAR	CO ₂ (PPM)								
1850	284.32	1900	467.60	1950	769.02	2000	1264.76	2050	2080.07
1851	287.16	1901	472.27	1951	776.71	2001	1277.41	2051	2100.87
1852	290.03	1902	477.00	1952	784.48	2002	1290.18	2052	2121.88
1853	292.93	1903	481.77	1953	792.33	2003	1303.09	2053	2143.10
1854	295.86	1904	486.58	1954	800.25	2004	1316.12	2054	2164.53
1855	298.82	1905	491.45	1955	808.25	2005	1329.28	2055	2186.17
1856	301.81	1906	496.36	1956	816.34	2006	1342.57	2056	2208.03
1857	304.83	1907	501.33	1957	824.50	2007	1356.00	2057	2230.11
1858	307.87	1908	506.34	1958	832.74	2008	1369.56	2058	2252.42
1859	310.95	1909	511.40	1959	841.07	2009	1383.25	2059	2274.94
1860	314.06	1910	516.52	1960	849.48	2010	1397.08	2060	2297.69
1861	317.20	1911	521.68	1961	857.98	2011	1411.06	2061	2320.67
1862	320.38	1912	526.90	1962	866.56	2012	1425.17	2062	2343.87
1863	323.58	1913	532.17	1963	875.22	2013	1439.42	2063	2367.31
1864	326.82	1914	537.49	1964	883.97	2014	1453.81	2064	2390.98
1865	330.08	1915	542.87	1965	892.81	2015	1468.35	2065	2414.89
1866	333.38	1916	548.29	1966	901.74	2016	1483.03	2066	2439.04
1867	336.72	1917	553.78	1967	910.76	2017	1497.86	2067	2463.43
1868	340.09	1918	559.31	1968	919.87	2018	1512.84	2068	2488.07
1869	343.49	1919	564.91	1969	929.07	2019	1527.97	2069	2512.95
1870	346.92	1920	570.56	1970	938.36	2020	1543.25	2070	2538.08
1871	350.39	1921	576.26	1971	947.74	2021	1558.68	2071	2563.46
1872	353.89	1922	582.03	1972	957.22	2022	1574.27	2072	2589.09
1873	357.43	1923	587.85	1973	966.79	2023	1590.01	2073	2614.98
1874	361.01	1924	593.72	1974	976.46	2024	1605.91	2074	2641.13
1875	364.62	1925	599.66	1975	986.22	2025	1621.97	2075	2667.55
1876	368.26	1926	605.66	1976	996.08	2026	1638.19	2076	2694.22
1877	371.95	1927	611.71	1977	1006.04	2027	1654.57	2077	2721.16
1878	375.67	1928	617.83	1978	1016.11	2028	1671.12	2078	2748.38
1879	379.42	1929	624.01	1979	1026.27	2029	1687.83	2079	2775.86
1880	383.22	1930	630.25	1980	1036.53	2030	1704.71	2080	2803.62
1881	387.05	1931	636.55	1981	1046.89	2031	1721.76	2081	2831.65
1882	390.92	1932	642.92	1982	1057.36	2032	1738.97	2082	2859.97
1883	394.83	1933	649.35	1983	1067.94	2033	1756.36	2083	2888.57
1884	398.78	1934	655.84	1984	1078.62	2034	1773.93	2084	2917.46
1885	402.76	1935	662.40	1985	1089.40	2035	1791.67	2085	2946.63
1886	406.79	1936	669.02	1986	1100.30	2036	1809.58	2086	2976.10
1887	410.86	1937	675.71	1987	1111.31	2037	1827.68	2087	3005.86
1888	414.97	1938	682.47	1988	1122.41	2038	1845.95	2088	3035.92
1889	419.12	1939	689.29	1989	1133.64	2039	1864.41	2089	3066.28
1890	423.31	1940	696.19	1990	1144.97	2040	1883.06	2090	3096.94
1891	427.54	1941	703.15	1991	1156.42	2041	1901.89	2091	3127.91
1892	431.82	1942	710.18	1992	1167.99	2042	1920.91	2092	3159.19
1893	436.14	1943	717.28	1993	1179.67	2043	1940.12	2093	3190.78
1894	440.50	1944	724.46	1994	1191.46	2044	1959.52	2094	3222.69
1895	444.90	1945	731.70	1995	1203.38	2045	1979.11	2095	3254.91
1896	449.35	1946	739.02	1996	1215.41	2046	1998.90	2096	3287.46
1897	453.84	1947	746.41	1997	1227.57	2047	2018.89	2097	3320.34
1898	458.38	1948	753.87	1998	1239.84	2048	2039.08	2098	3353.54
1899	462.97	1949	761.41	1999	1252.24	2049	2059.47	2099	3387.08
								2100	3420.95

Table 10 – abrupt4x: Global- and annual-mean surface concentrations for the idealized abrupt4x CMIP6 experiment. The hemispheric and latitudinally resolved concentrations for 43 GHGs and three aggregate equivalent concentrations are provided in the accompanying historical run dataset, with the 1850 CO₂ concentration of 284.317 being multiplied by four. The complexity reduction options for capturing all GHGs with fewer species than 43 are indicated in the Table as Option 1, Option 2, and Option 3, with ‘x’ denoting relevant columns under each option.

Years	CO ₂	CH ₄	N ₂ O	CFC-12- eq	HFC- 134a-eq	CFC-11- eq	CFC-12	Other
Option 1	x	x	x				x	x
Option 2	x	x	x			x	x	
Option 3	x	x	x	x	x			
Units:	ppm	ppb	ppb	ppt	ppt	ppt	ppt	
0-150	1137.268	808.25	273.02	16.51	19.15	32.11	0.00	All or a subset of other 39 individual gases, available in Supplementary

first column indicates the importance of gases in terms of the radiative effect change between 1750 and 2014. Note that below shares are approximations, as linear radiative forcing efficiencies are assumed here for all gases, also for CO₂, N₂O and CH₄.

		Option-1	Option-2	Option-3
	<i>The GHG contribution to climate change since 1750.</i>	<i>Using subset of actual mixing ratios, no equivalent gases</i>	<i>Summarizing all gases of lower importance than CFC-12 into CFC-11eq.</i>	<i>Summarizing all ODS into CFC-12-eq and all other fluorinated gases into HFC134a-eq</i>
Rank	Shares of change of total warming effect since 1750: Approx. Radiative forcing contribution between 1750 and 2014 relative to that of all GHGs	Shares of total warming effect: Approx. Radiative effect compared to effect of all GHGs (absolute in 2014, not relative to 1850)		
1	CO ₂ 64.0%	CO ₂ 72.9%	CO ₂ 72.9%	CO ₂ 72.9%
2	CH ₄ 79.5%	N ₂ O 86.1%	N ₂ O 86.1%	N ₂ O 86.1%
3	CFC12 86.0%	CH ₄ 95.0%	CH ₄ 95.0%	CH ₄ 95.0%
4	N ₂ O 92.2%	CFC12 97.2%	CFC12 97.2%	CFC12-eq 99.5%
5	CFC11 94.5%	CFC11 98.0%	CFC11-eq 100.0%	HFC134a-eq 100%
6	HCFC22 96.4%	HCFC22 98.6%		
7	CFC113 97.2%	CFC113 98.9%		
8	CCl ₄ 97.8%	CCl ₄ 99.1%		
9	HFC134a 98.3%	HFC134a 99.3%		
10	CFC114 98.5%	CF ₄ 99.4%		
11	HFC23 98.7%	CH ₃ Cl 99.5%		
12	SF ₆ 98.8%	CFC114 99.5%		
13	CF ₄ 99.0%	HFC23 99.6%		
14	HCFC142b 99.2%	SF ₆ 99.7%		
15	HCFC141b 99.3%	HCFC142b 99.7%		
...	28 more GHGs 100%	28 more GHGs 100%		

5 Table 11 – Exponents ‘s’ to estimate vertical gradient of mixing-ratio:concentrations for gases with stratospheric sinks in the stratospheric column – depending on the latitude ‘lat’. See text. For HFC-134a and other species with stratospheric lifetimes shorter than 30 years, the CH₄ exponent parameterization can be used as approximation. This exponent scale parameterization is taken from the CESM model, implemented by J. Kiehl.

	TROPICS AND MID-LATITUDES ABS(LAT)<45°	MID TO HIGH LATITUDES, ABS(LAT)≥45°
CH ₄	0.2353	0.2353 + 0.0225489 \times (abs(lat) - 45);
N ₂ O	0.3478 + 0.00116 \times abs(lat)	0.40 + 0.013333 \times (abs(lat) - 45)
CFC-11	0.7273 + 0.00606 \times abs(lat)	1.00 + 0.013333 \times (abs(lat) - 45);
CFC-12	0.4000 + 0.00222 \times abs(lat)	0.50 + 0.024444 \times (abs(lat) - 45)

12—Figures

- 5 *Note: all mixing ratios (ppmv, ppbv, pptv) are mole mixing ratios and should be read as 9ppmv, ppbv and pptv, respectively).*

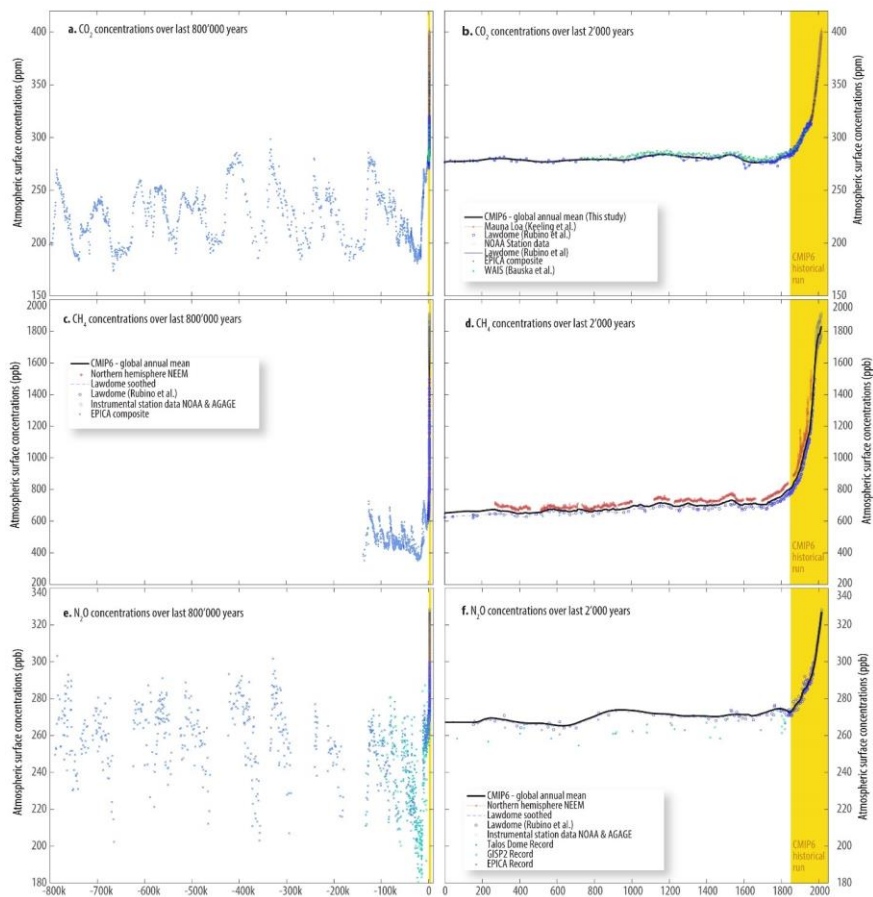


Figure 1—Atmospheric CO_2 , CH_4 and N_2O mixing ratios over different time-scales, from 800 thousand years ago until today (panel a, c, e), from Year 0 A.D. to today (panel b, d, f). The shown data is for CO_2 : Mauna Loa data by Keeling et al. (Keeling et al. 1976); the Law Dome ice record (Etheridge et al. 1998c, MacFarling Meure et al. 2006, Rubino et al. 2013); NOAA ESRL station data (NOAA 2013, NOAA ESRL GMD 2014c, NOAA ESRL GMD 2014b, NOAA ESRL GMD 2014a); the EPICA composite data (Lüthi et al. 2008, Bereiter et al. 2015) and the WAIS data (Bauska et al. 2015). For CH_4 , the shown data is the Law Dome data (Etheridge et al. 1998b, MacFarling Meure et al. 2006), the instrumental data from the NOAA and AGAGE networks (see Table S), NEM ice core measurements (Rhodes et al. 2013) and the EPICA composite (Barbante et al. 2006) — In case of N_2O , the shown data is the Law Dome record (MacFarling Meure et al. 2006), the Talos Dome record (Schilt et al. 2010b), the GISP2 record (Sowers et al. 2003) and the EPICA record (Flückiger et al. 2002, Spahni et al. 2005, Schilt et al. 2010a) [The figure will be updated to reflect references in legend and to include CH_4 data over the last 800,000 years based on data by Louergue (2008)].

CO2

Carbon dioxide (CO2) Lifetime: n/a, Approx. Rad. Efficiency: 1.37e-05(Wm2/ppb)

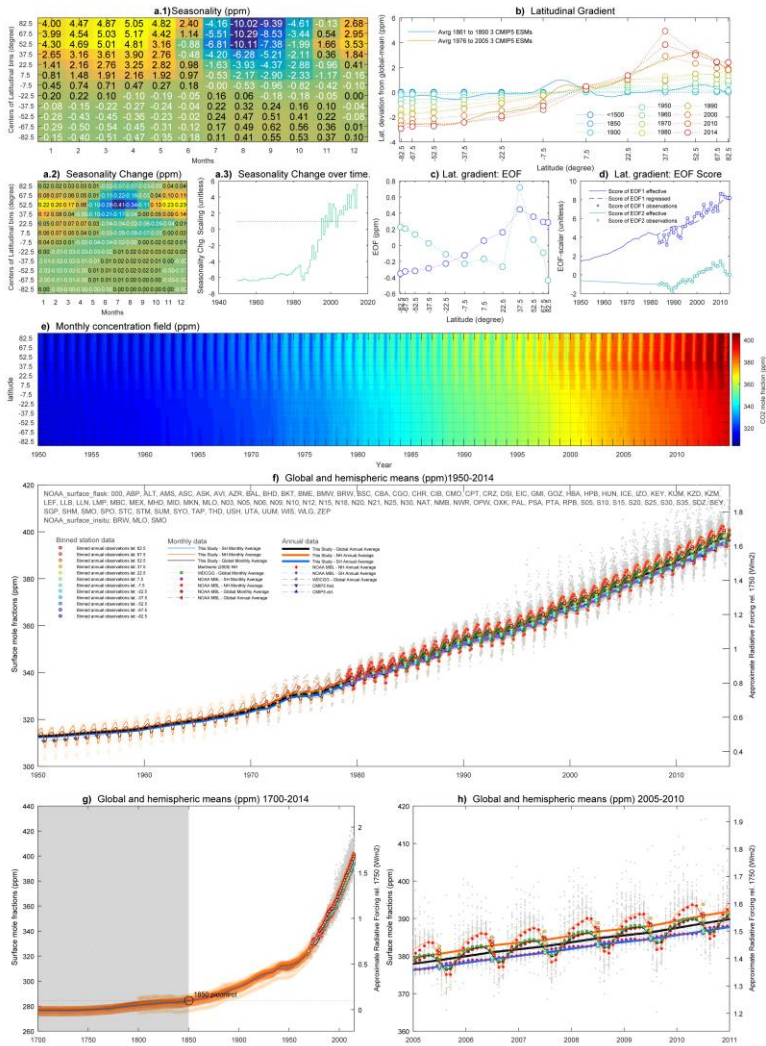


Figure 2 – Table 12 – Description of data labels shown in Factsheets, namely Fig. 9, Fig. 11, Fig. 12, and Appendix A with Fig. 20 to Fig. 59.

<u>Label</u>	<u>Gases</u>	<u>Description / Source</u>
<u>NOAA surface flask</u>	<u>CO₂</u>	<u>Atmospheric Carbon Dioxide Dry Air Mole Fractions from the NOAA ESRL Carbon Cycle Cooperative Global Air Sampling Network, 1968-2014. Version: 2015-08-03 Surface flask. available at data ftp://aftp.cmdl.noaa.gov/data/trace_gases/co2/flask/surface/ (Dlugokencky, 2015b)</u>
<u>NOAA surface insitu</u>	<u>CO₂</u>	<u>Atmospheric Carbon Dioxide Dry Air Mole Fractions from quasi-continuous measurements at Barrow, Alaska; Mauna Loa, Hawaii; American Samoa; and South Pole, 1973-2013; National Oceanic and Atmospheric Administration (NOAA); Earth System Research Laboratory (ESRL), Global Monitoring Division (GMD), Carbon Cycle Greenhouse Gases (CCGG); Version: 2014-11-10. available at: ftp://aftp.cmdl.noaa.gov/data/trace_gases/co2/in-situ/surface/ (NOAA ESRL GMD, 2014a, b, c, d)</u>
<u>NOAA surface flask</u>	<u>CH₄</u>	<u>Atmospheric Methane Dry Air Mole Fractions from the NOAA ESRL GMD Carbon Cycle Cooperative Global Air, Sampling Network, 1983-2014. File versions: 2015-08-03. available at: ftp://aftp.cmdl.noaa.gov/data/trace_gases/ch4/flask/ (Dlugokencky, 2015a)</u>
<u>HATS global combined</u>	<u>N₂O, CCl₄, CFC-11, CFC-113, CFC-12, SF₆</u>	<u>Combined data from the NOAA/ESRL Global Monitoring Division and two or more measurement programs: Wed, Aug 19, 2015 2:40:55 PM, available at: ftp://ftp.cmdl.noaa.gov/hats/n2o/combined/HATS_global_N2O.txt, ftp://ftp.cmdl.noaa.gov/hats/cfcs/cfc113/combined/HATS_global_F113.txt, ftp://ftp.cmdl.noaa.gov/hats/cfcs/cfc11/combined/HATS_global_F11.txt, ftp://ftp.cmdl.noaa.gov/hats/cfcs/cfc12/combined/HATS_global_F12.txt, ftp://ftp.cmdl.noaa.gov/hats/sf6/combined/HATS_global_SF6.txt, ftp://ftp.cmdl.noaa.gov/hats/solvents/CCl4/combined/HATS_global_CCl4.txt</u>
<u>Montzka NOAA GMD</u>	<u>CCl₄, CFC-11, CFC-113, CH₃CCl₃, CH₃Br, CH₃Cl, CH₂Cl₂, HCFC-22, HCFC-141b, HCFC-142b, HFC-134a, HFC-152a, HFC-32, HFC-125, HFC-</u>	<u>Flask data provided from the Global Monitoring Division of the National Oceanic and Atmospheric Administration's Earth System Research Laboratory (NOAA/ESRL/GMD) as a result of analysis on gas chromatography with mass spectrometry instrumentation. Principal investigators S. Montzka and James W. Elkins. Version 13 Nov. 2015. Data available at:</u>

<u>Label</u>	<u>Gases</u>	<u>Description / Source</u>
	143a, HFC-365mfc, HFC-227ea, Halon-1211, Halon-1301, Halon-2402	ftp://ftp.cmdl.noaa.gov/hats/cfcs/cfc113/flasks/GCMS/CFC113_GCMS_flask.txt ftp://ftp.cmdl.noaa.gov/hats/solvents/CH3CCl3/flasks/GCMS/CH3CCl3_GCMS_flask.txt ftp://ftp.cmdl.noaa.gov/hats/methylhalides/ch3br/flasks/CH3BR_GCMS_flask.txt ftp://ftp.cmdl.noaa.gov/hats/methylhalides/ch3cl/flasks/CH3Cl_GCMS_flask.txt ftp://ftp.cmdl.noaa.gov/hats/solvents/CH2Cl2/flasks/ch2cl2_GCMS_flask.txt ftp://ftp.cmdl.noaa.gov/hats/hcfc/hcfc22/flasks/HFC22_GCMS_flask.txt ftp://ftp.cmdl.noaa.gov/hats/hcfc/hcfc141b/HFC141B_GCMS_flask.txt ftp://ftp.cmdl.noaa.gov/hats/hcfc/hcfc142b/flasks/HFC142B_GCMS_flask.txt ftp://ftp.cmdl.noaa.gov/hats/hfcs/hfc134a_GCMS_flask.txt ftp://ftp.cmdl.noaa.gov/hats/hfcs/hf152a_GCMS_flask.txt ftp://ftp.cmdl.noaa.gov/hats/hfcs/HFC-32_M2_MS_flask.txt ftp://ftp.cmdl.noaa.gov/hats/hfcs/HFC-125_M2_MS_flask.txt ftp://ftp.cmdl.noaa.gov/hats/hfcs/HFC-143a_M2_MS_flask.txt ftp://ftp.cmdl.noaa.gov/hats/hfcs/HFC-365mfc_GCMS_flask.txt ftp://ftp.cmdl.noaa.gov/hats/hfcs/HFC-227ea_GCMS_flask.txt ftp://ftp.cmdl.noaa.gov/hats/halons/flasks/HAL1211_GCMS_flask.txt ftp://ftp.cmdl.noaa.gov/hats/halons/flasks/H-1301_M2_MS_flask.txt ftp://ftp.cmdl.noaa.gov/hats/halons/flasks/HAL2402_GCMS_flask.txt
<u>AGAGE gc-md monthly</u>	CFC-11, CFC-12, CH₂CCl₃, CCl₄, N₂O, CFC-113, CH₄, CHCl₃	Chemical species measured by AGAGE GC-ECD/FID/MRD system. Version 20 June 2015. Data available at: http://aqage.eas.gatech.edu/data_archive/aqage/gc-md/monthly/ (Cunnold et al., 2002; Cunnold et al., 1997; Fraser et al., 1996; O'Doherty et al., 2001; Prinn et al., 1990; Prinn et al., 2005; Prinn et al., 2001; Reimann et al., 2005; Simmonds et al., 1998)
<u>AGAGE gc-ms monthly</u>	HFC-134a, HCFC-22, HCFC-141b, HCFC-142b, CH₂Cl, CH₂Br, Halon-1211, Halon-1301, HFC-152a, CH₂Cl₂, CHClCCl₃, CCl₂CCl₂	Chemical compounds measured by AGAGE GC-MS (ADS) system. Version 20 June 2015. Data available at: http://aqage.eas.gatech.edu/data_archive/aqage/gc-ms/monthly/ (Cox et al., 2003; Miller et al., 1998; O'Doherty et al., 2004; Simmonds et al., 2004)
<u>AGAGE gc-ms-medusa monthly</u>	CFC-11, CFC-12, CFC-113, CFC-114, CFC-115, HCFC-22, HCFC-141b, HCFC-142b, HFC-125, HFC-134a, HFC-152a, HFC-365mfc, HFC-23, HFC-4310mee, Halon-1211, Halon-1301, Halon-2402, CH₂Cl, CH₂Cl₂, CHCl₃, CH₂Br, CH₂CCl₃, CCl₄, SF₆, SO₂F₂, NF₃, PFC-14, PFC-116	Chemical compounds measured by Medusa GCMS system. Version 20 June 2015. Data available at: http://aqage.eas.gatech.edu/data_archive/aqage/gc-ms-medusa/monthly/ (Prinn et al., 2000a)

<u>Label</u>	<u>Gases</u>	<u>Description / Source</u>
	<u>PFC-218, HFC-32, HFC-143a, HFC-227ea, HFC-236fa, HFC-245fa</u>	
<u>Montzka - NOAA ODS update 7/2015</u>	<u>HCFC-22, CFC-113, CFC-11, HCFC-141b, CCl₄, CFC-12, HCFC-142b, CH₃CCl₃, H-1211, H-1301, H2402, CH₃Br, HFC-134a, HFC-152a, HFC-143a, HFC-125, HFC-32, HFC-365mfc, HFC-227ea</u>	<u>Data from 7/2014 update of NOAA compilation of monthly global mean concentrations, made available on web as '2015 update total Cl Br & F July update.xls' by S. Montzka at: ftp://ftp.cmdl.noaa.gov/hats/Total_Cl_Br/. The substances HCFC-22, CFC-113, CFC-11, HCFC-141b, CCl₄, CFC-12, HCFC-142b, CH₃CCl₃, Halon-1211, Halon-1301, are Halon-2402, are updated from data displayed in Figure 1 in Montzka et al. (1999), with CH₃Br data published in Montzka et al. (2003) and with HFCs data published in Montzka et al. (2015).</u>
<u>Martinerie-2010</u>	<u>SF₆, CFC-11, CFC-12, CFC-113, CCl₄, CH₃CCl₃, HFC-134a</u>	<u>Monthly high-latitude NH data by Patricia Martinerie, made available as supplementary by Buizert et al. (2012) in files SCENARIO_NEEM08_XX.txt</u>
<u>Petrenko-2010</u>	<u>CO₂, CH₄</u>	<u>Monthly high-latitude NH data by Vas Patrenko, made available as supplementary by Buizert et al. (2012) in files SCENARIO_NEEM08_CO2.txt and SCENARIO_NEEM08_CH4.txt</u>
<u>WDCGG (2015)</u>	<u>CO₂, CH₄, N₂O</u>	<u>Data synthesis as available from the World Data Centre of Greenhouse Gas Emissions (Tsumumi, 2009), available at: http://ds.data.jma.go.jp/gmd/wdogg/. Version: co2_monthly_20151109.csv, ch4_monthly_20151109.csv and n2o_monthly_20151109.csv</u>
<u>NOAA MBL</u>	<u>CO₂, CH₄</u>	<u>NOAA Greenhouse Gas Marine Boundary Layer Reference, derived from atmospheric carbon dioxide, methane and nitrous oxide concentrations, from the NOAA ESRL Carbon Cycle Cooperative Global Air Sampling Network, available at http://www.esrl.noaa.gov/gmd/ccgg/mbll/ for CO₂ and CH₄. Zonal means for SH and NH, as well as global means. File creation dates: 2016-02-11</u>
<u>CMIP5 hist.</u>	<u>Many</u>	<u>The global-mean annual average concentrations that were used as default recommendation for concentration-driven runs in the CMIP5 experiment (Meinshausen et al., 2011)</u>
<u>CMIP5 ctrl.</u>	<u>Many</u>	<u>The global-mean annual average concentrations in 1850 that were recommended as piconcentrations in the CMIP5 experiment (Meinshausen et al., 2011).</u>
<u>Firn – Montzka-(2009)</u>	<u>CFC-12, HFC-134a, HCFC-22, and CH₃CCl₃</u>	<u>"Southern Hemisphere atmospheric trace-gas histories used in the analysis of firn air" data compiled by Montzka in 2009 (available at ftp://ftp.cmdl.noaa.gov/hats/firnair/ in file "SH Atmosphere Trace Gas Histories.xls"), based on several earlier studies (Butler et al., 1999; Elkins et al., 1993; Montzka et al., 1993; Montzka et al., 1996; Montzka et al., 2000; Prinn et al., 2005), and e.g. reported in Aydin et al. (2010) for CFC-12 and underlying (Montzka et al., 2010).</u>
<u>WMO (2014)</u>	<u>CFC-11, CFC-12, CFC-113, CFC-114, CFC-115, CCl₄, CH₃CCl₃, HCFC-22, HCFC-141b, HCFC-142b, Halon-1211,</u>	<u>Data from Table 5A2 in the 2014 Ozone Assessment (WMO, 2014), starting with 5-year intervals from 1955 to 1980 then annually. We</u>

<u>Label</u>	<u>Gases</u>	<u>Description / Source</u>
	<u>Halon-1202, Halon-1301, Halon-2402, CH₃Br, CH₃Cl</u>	<u>interpolated the data to annual values using a local polynomial regression between 1955-1980.</u>
<u>WMO2014/AGAGE 'late'/'early'</u>	<u>HFC125, HFC134a, HFC152a, HFC143a, HFC32, HFC245fa, HFC365mfc, HFC227ea, HFC236fa, CF₄, HFC23, C₂F₆, C₃F₈, SF₆, SO₂F₂, NF₃</u>	<u>The network average global-mean mole fractions from the AGAGE network as shown in the WMO (2014) Ozone Assessment Report. (WMO, 2014)</u>
<u>WMO2014/NOAA</u>	<u>HFC-134a, HFC-152a, SF₆</u>	<u>NOAA global-mean annual average time series as shown in WMO Ozone Assessment Report (WMO, 2014).</u>
<u>WMO2014/PFC</u>	<u>C₄F₁₀, C₅F₁₂, C₆F₁₄, C₇F₁₆, C₈F₁₈</u>	<u>PFC data compiled and shown in WMO Ozone Assessment Report (WMO, 2014)</u>
<u>AGAGE – Global Monthly Average</u>	<u>HFC-23, HFC-125, HFC-134a, HFC-152a, HFC-227ea, HFC-236fa, HFC-245fa, HFC-365mfc, HCFC-22, HCFC-141b, HCFC-142b, H-1211, H-1301, CH₃Br, CH₃Cl, CH₂Cl₂, CCl₂CCl₂, CHClCCl₂, SF₆, SO₂F₂, PFC-14, PFC-116, PFC-218, CFC-113, CFC-114, CFC-115, HFC-4310mee</u>	<u>Monthly global means of baseline data derived from AGAGE measurements based on AGAGE GC-MS/Medusa measurements (from 2004 to current) from file global_mean_ms.txt available at: http://agage.eas.gatech.edu/data_archive/global_mean/</u>
<u>Binned annual observations</u>	<u>All</u>	<u>These are the monthly averages for each 15-degree zonal mean derived from the analysed station data points (with three-digit station names provided in the top left corner of panel f of each factsheet). An "n/a" indication behind the latitude indicator means that not enough raw station data points were available to create zonal means for that latitude. The estimate of the latitudinal gradient is then based on the remainder available latitudinal bands.</u>
<u>OTHER LABELS, NAMELY: MONTZKA ET AL. (2015)</u> <u>VELDERS ET AL. (2014)</u> <u>MUEHLE ET AL. (2010)</u> <u>TRUDINGER ET AL. (2016)</u> <u>IVY ET AL. (2012)</u> <u>WORTON (2007)</u> <u>BUTLER ET AL. (1999)</u> <u>ARNOLD ET AL. (2013)</u>	<u>Various</u>	<u>See respective literature studies (Arnold et al., 2013; Arnold et al., 2014; Butler et al., 1999; Ivy et al., 2012; Montzka et al., 2015; Mühle et al., 2010; Newland et al., 2013; Oram et al., 2012; Trudinger et al., 2016; Velders and Daniel, 2014; Vollmer et al., 2016; Walker et al., 2000; Worton et al., 2007). Note, the CCl₄ data by Walker et al. is used as 1910 to 1950 amendment to the Velders and Daniel (2014) timeseries.</u>

<u>Label</u>	<u>Gases</u>	<u>Description / Source</u>
<u>ARNOLD ET AL. (2014)</u>		
<u>VOLLMER ET AL (2016)</u>		
<u>ORAM ET AL. (2012)</u>		
<u>WALKER ET AL. (2000)</u>		
<u>Newland et al. (2013)</u>		

12 Figure Captions

Fig. 1 - Data flow diagram of how historical GHG concentrations are derived in this study. See text.

Fig. 2 - Availability of instrumental carbon dioxide data from 1968 to 2015 from the NOAA ESRL network, shown as data samples per month, per latitudinal band (panels a to l) and per longitudinal bin within each latitudinal band.

5 Fig. 3 - Availability of instrumental CH₄ data from 1983 to 2015 from the AGAGE and NOAA ESRL networks, shown as data samples per month, per latitudinal band (panels a to l) and per longitudinal bin within each latitudinal band.

Fig. 4 - Availability of instrumental N₂O data from 1983 to 2015 from the AGAGE and NOAA ESRL networks, shown as data samples per month, per latitudinal band (panels a to l) and per longitudinal bin within each latitudinal band.

10 Fig. 5 - Comparison of various scaling options for the change of seasonality of CO₂ concentrations over time. The first EOF of the residual fields of observations minus the mean 1984-2014 CO₂ seasonality (Fig. 9 a.2) is scaled with an EOF score. Before 1984, this EOF score is regressed against a composite of global-mean CO₂ concentrations and global-mean surface air temperatures (see text and panel b). Alternative regressors include global-mean CO₂ concentrations (panel a), lagged averages of monthly global-mean surface air temperatures (panel c) and raw global-mean annual average surface air temperatures (HadCRUT4v) (Morice et al., 2012) (panel d). The regressed EOF score back in time is shown in panel e. A comparison to the first CO₂ measurements of higher northern latitudes at so-called Station P (STP) and Point Barrow in Alaska (PTB), where the seasonality change is most pronounced, is provided in panels f and g, respectively (see text for discussion).

20 Fig. 6 - Atmospheric CO₂, CH₄ and N₂O concentrations over different time-scales, from 800 thousand years ago until today (panel a), over the last 2000 years (panel b) and over 1850 to 2014 (panel c, d, e). The shown data is for CO₂: Mauna Loa data by Keeling et al. (Keeling et al., 1976); the Law Dome ice record (Etheridge et al., 1998b; MacFarling Meure et al., 2006; Rubino et al., 2013); NOAA ESRL station data (NOAA, 2013; NOAA ESRL GMD, 2014a, b, c); the EPICA composite data (Ahn and Brook, 2014; Bereiter et al., 2015; Bereiter et al., 2012; Lüthi et al., 2008; MacFarling Meure et al., 2006; Marcott et al., 2014; Monnin et al., 2004; Petit et al., 1999; Schneider et al., 2013; Siegenthaler et al., 2005) and the WAIS data (Bauska et al., 2015). For CH₄, the shown data is the Law Dome data (Etheridge et al., 1998a; MacFarling Meure et al., 2006), the instrumental data from the NOAA and AGAGE networks (see Table 3), NEEM ice core measurements (Rhodes et al., 2013) the EPICA composite (Barbante et al., 2006a; Barbante et al., 2006b) the long record by Loulergue et al. (2008) as well as the GISP2D, WDC05A and WDC06A records by Mitchell et al. (2013). In case of N₂O, the shown data is the Law Dome record (MacFarling Meure et al., 2006), the Talos Dome record (Schilt et al., 2010b), the GISP11 record (Sowers et al., 2003) and the EPICA record (Fluckiger et al., 2002; Schilt et al., 2010a; Spahni et al., 2005) in addition to the H15 ice core record from Antarctica (Machida et al., 1995), the South Pole firn record (Battle et al., 1996), the Law Dome firn record "Park" (Park et al., 2012) and a modelling synthesis by Ishijima (2007). For data sources behind "this study's" composite product, see Table 2, Table 3 and Table 4.

25 Fig. 7 - Comparison of 1950 to 1990 CO₂ concentrations with early Scripps station data (Keeling et al., 2001) for each 15°-degree latitudinal band. Also, the Law Dome ice record data is shown (panel k) with our 3rd degree polynomial smoothing. This study's monthly CO₂ zonal means were derived from station data from 1984 onwards. Before that, this study used Mauna Loa MLO annual average and smoothed Law Dome data (see Table 1 and section 2 "Methods"). The shown comparison with monthly Scripps station data before 1984 is a qualitative validation of the applied methodology to regress latitudinal gradient and seasonality changes to times before 1984. See text.

35 Fig. 8 - Historical GHG concentrations from 1750 to 2014 as global-mean (right panels), northern hemispheric (middle panels) and southern hemispheric averages (right panels). The top row comprises all GHGs, the middle row comprises HFCs, PFCs, SF₆, NF₃ and SO₂F₂. The lower row comprises all ozone depleting substances, expressed as equivalent CFC-12eq concentrations. In the narrow boxes, the last data year from 15 Jan 2014 to 15 Dec 2015 is shown, indicating the intra-annual trend (top row), increasing gradient (middle row) or relatively flat concentration levels (lower row).

45 Fig. 9 - Overview of historical CO₂ mixing-ratios concentrations. Panel a.1, the average seasonality of CO₂ over the observational period, a.2, the change of seasonality over time. a.3, the observationally derived and extended EOF score of the seasonality change. The first EOF1's score is almost linearly increasing over the time of instrumental data from 1984 to 2014. b, the latitudinal variation of mixing-ratios mole fractions (dashed lines), shown for example years from 1500 to 2014, including (for comparison) the average of three CMIP5 ESM models (solid lines). c, the first and second EOF of latitudinal variation. The second EOF exhibits a strong

signal around middle northern latitudes d, the EOF scores derived from the observational data (dots) and regression (dashed line) as well as the ultimately used EOF score (solid line). The second EOF's score indicates that the mid-latitude northern spike was only a recent phenomenon and the score is here assumed to linearly converge to zero. The first EOF's score is more linearly increasing, and regressed against global fossil emissions. e, the resulting latitudinal-monthly mixing-ratio:concentration field, here shown between 1950 and 2014. f, global and hemispheric means of the derived mixing-ratio:concentration field over the same time period 1950 to 2014 in comparison to monthly station data (grey dots), latitudinal average station data (colored:coloured circles), and various literature studies (see legend). g, same as panel f, except for time period 1750 to 2014. h, same as panel f but for time period 2005 to 2010.

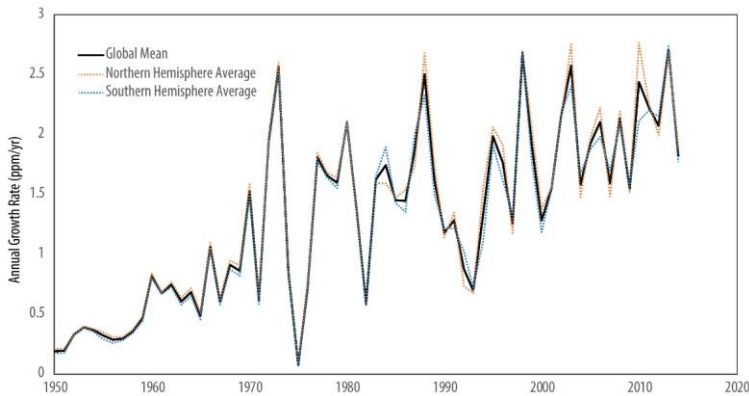


Figure Fig. 10 - Annual Growth Rate of CO₂ mixing-ratio:concentrations for global-mean, northern hemispheric average and southern hemispheric average mixing-ratio:concentrations. Before 1960, the smooth growth rate results from interpolated global mean values. After 1960, the growth rates are diagnosed from the surface station data, as shown in [Fig. 9f](#). Noticeable are fluctuations of the annual growth rate around 1973, 1981, and 1992.

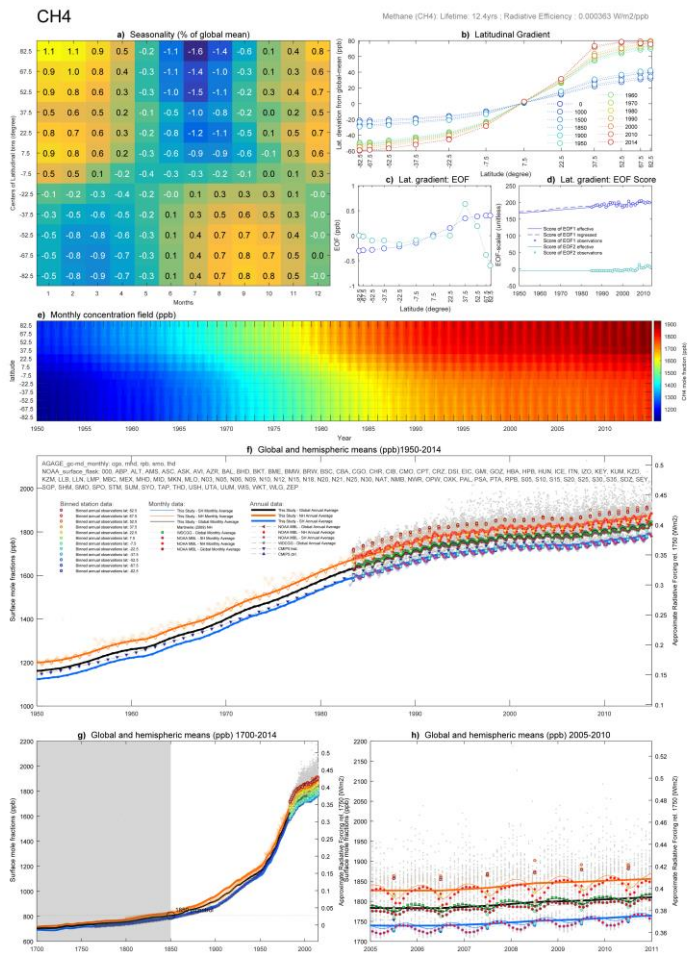


Figure 11 - Overview of historical CH₄ mixing-ratios, concentrations. Panel a.1, the relative seasonality of CH₄ over the observational period. b, the latitudinal variation of mixing-ratios concentrations (dashed lines), shown for example years. c, the first and second EOF of latitudinal variation. d, the EOF scores derived from the observational data (dots) and regression against global emissions (dashed line) as well as the ultimately used EOF score (solid line). e, the resulting latitudinal-monthly mixing

ratioconcentration field, here shown between 1950 and 2014. f, global and hemispheric means of the derived mixing ratioconcentration field over the same time period 1950 to 2014 in comparison to monthly station data (grey dots), latitudinal average station data (coloredcoloured circles), and various literature studies (see legend). g, same as panel f, except for time period 1750 to 2014. h, same as panel f but for time period 2005 to 2010.

N2O

Nitrous Oxide (N2O): Lifetime: 121yrs; Radiative Efficiency: 0.003 W/m2/ppb

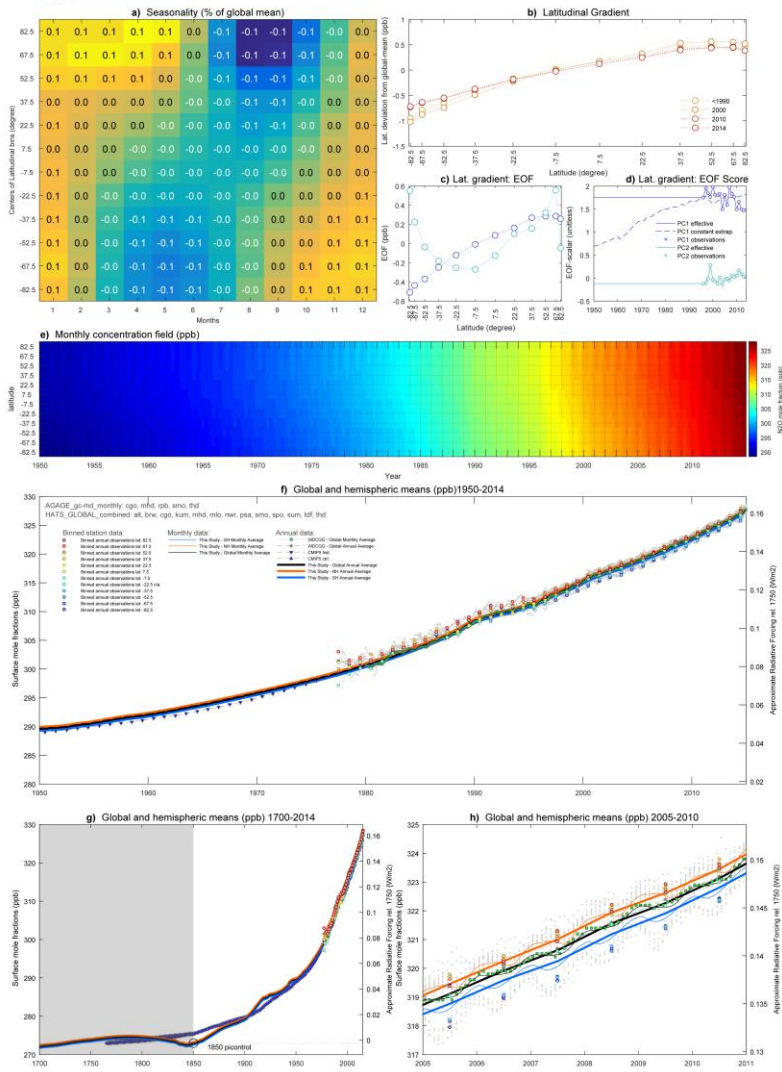


Figure Fig. 12 - Overview over historical N₂O mixing ratios concentrations. As Figure 4 Fig. 11, but for N₂O.

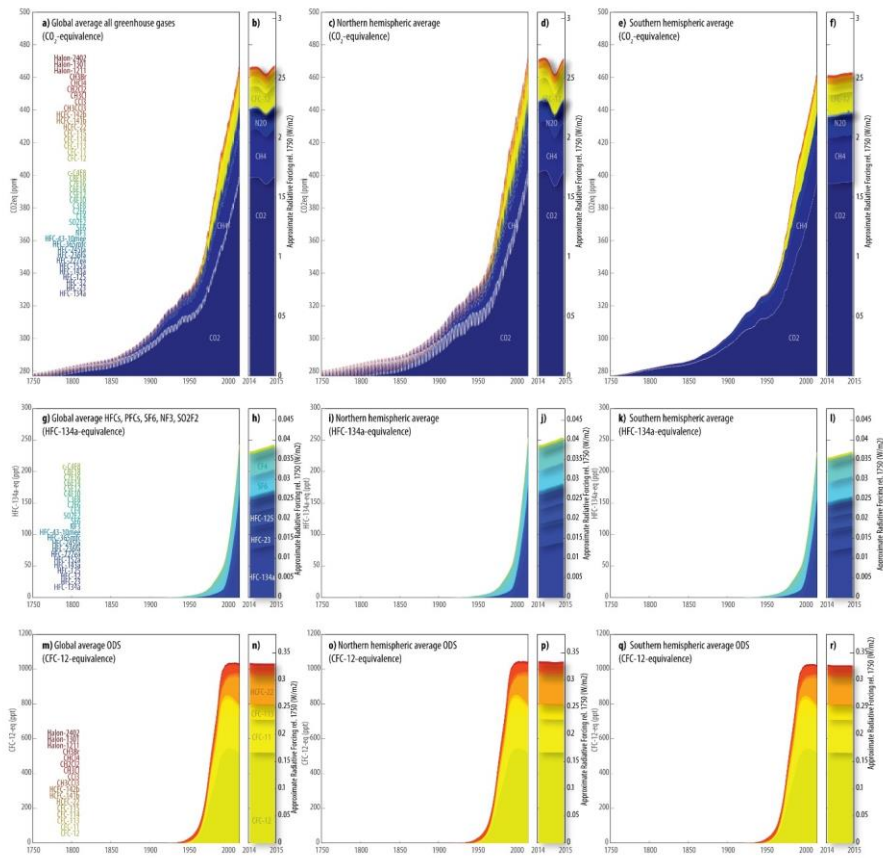


Figure Fig. 13—Historical GHG mixing ratios from 1750 to 2014 as global-mean-average (right panels)-northern-hemispheric average (middle panels) and-southern-hemispheric averages (right panels). The top row comprises all-greenhouse-gases, the middle row comprises HFCs, PFCs, SF₆, NF₃ and-SO₂F₂. The lower row comprises all-ozone-depleting substances, expressed-as equivalent CFC-12eq-mixing ratios. In the narrow boxes, the last data year from 15-Jan-2014 to 15-Dec-2015 is shown, indicating the intra-annual trend (top row), increasing gradient (middle row) or relatively flat-mixing ratio levels (lower row). [NOTE, the lower two rows of this figure need a slight update in regard to their left hand axes, as equivalent mixing ratios are positive due to some gases with natural background mixing ratios].

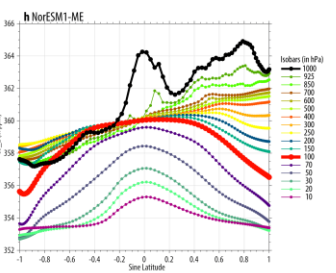
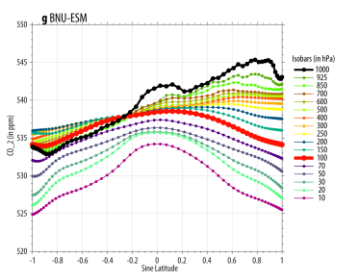
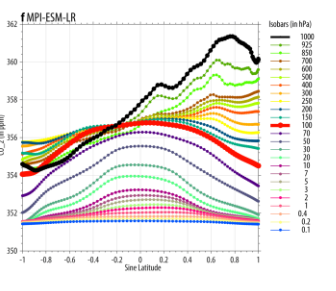
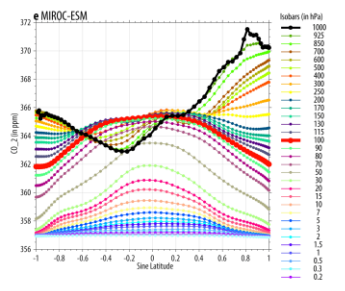
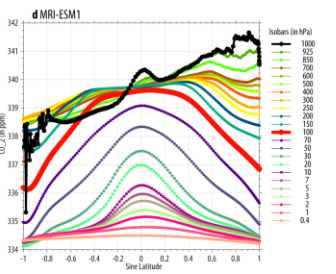
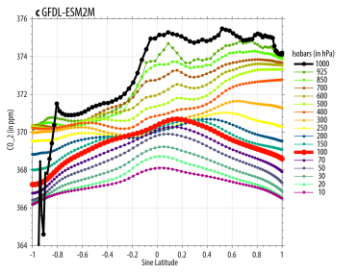
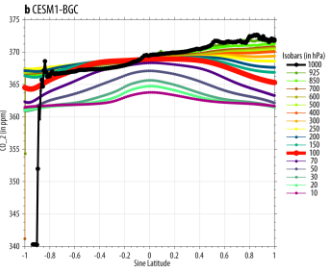
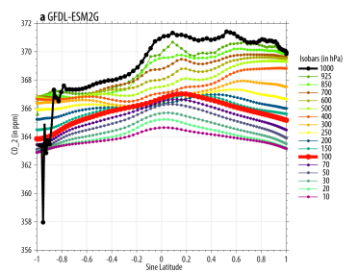


Figure 7 - CMIP5 ~~ESM model~~ **ESMs** vertical ~~mixing ratio~~ **mole fraction** averages at the provided pressure levels - as average **averaged** over the 30-year period 1976 to 2005. The black line indicates surface ~~mixing ratio~~ **mole fractions** at the 1000hPa pressure level. The red bold line indicates ~~mixing ratio~~ **mole fractions** at the 100hPa level (cf. Fig. 14a, and b).

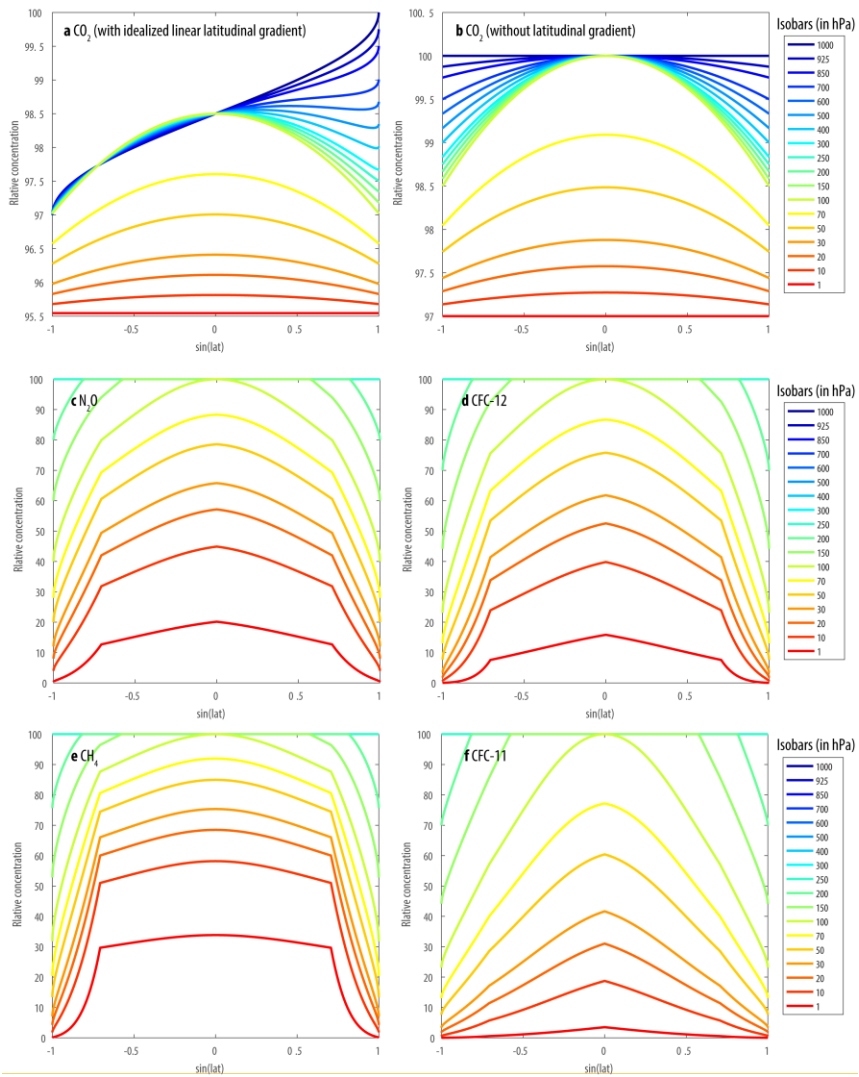


Figure Fig. 14 – Idealized vertical gradients recommended for implementation of surface mixing-ratio concentration fields. For parametric formulas, see text. Note that tropospheric columns of non-CO₂ gases are – for simplicity – assumed to be well-mixed. The assumed age of air at the 1haPa level for CO₂ is 5 years.

Fig. 15 - Comparison between the recommended annual global mean surface concentrations of CO₂, CH₄ and N₂O for CMIP5 and CMIP6 historical experiments. **Fig. 16** - Comparison of global-mean, and hemispheric monthly average concentrations of CO₂ (panel a), CH₄ (panel b) and N₂O (panel c) between the CMIP6 surface mole fractions (this study), the NOAA Marine Layer Boundary products, the World Data Centre of Greenhouse gases (WDCGG) products and the NASA AQUA satellite data of tropospheric CO₂ concentrations. For comparison, individual (monthly average) NOAA and AGAGE station data across all latitudes is shown in the background (grey dots).

Fig. 17 - Comparison of the CMIP6 historical CO₂ emissions (panel a) with the NOAA Marine Boundary Layer MBL product from 1979 to 2014 (panel b). Differences indicate that a seasonal higher CO₂ concentration is implied by the CMIP6 data of up to 5 ppm in mid-latitude northern bands, whereas some monthly tropical CO₂ mole fractions tend to be slightly lower in the CMIP6 product compared to NOAA MBL (panel c).

Fig. 18 - Comparison of the surface CH₄ monthly mean concentrations between CMIP6 (panel a), the NOAA Marine Boundary Layer product (panel b) and the difference (panel c). Since around 1992, there are seasonal differences in the mid northern latitudes with the CMIP6 data being up to 50ppb higher than the NOAA MBL product.

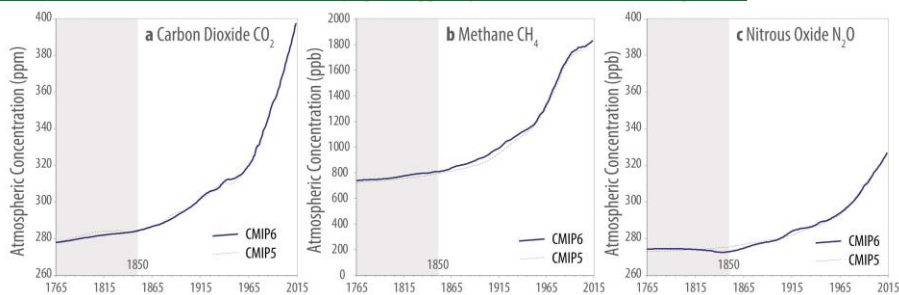
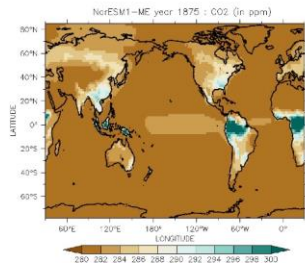
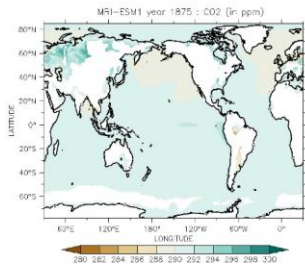
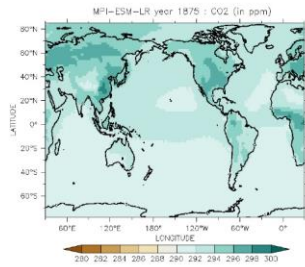
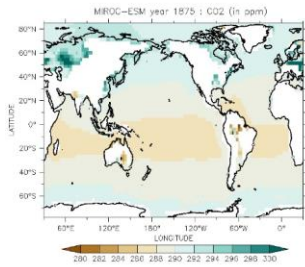
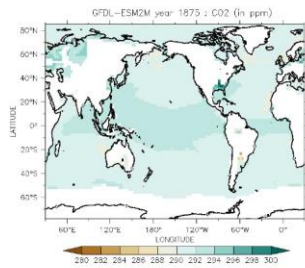
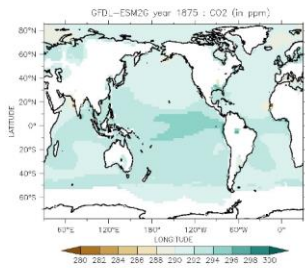
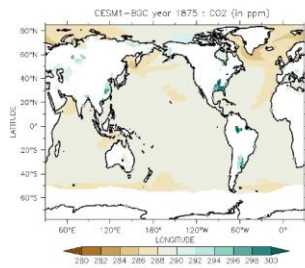
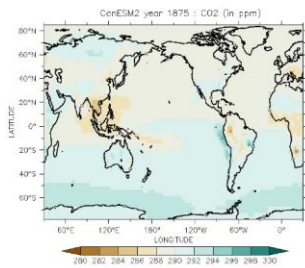


Figure Similarly, higher concentrations are apparent in the areas of tropical southern and lower latitude southern areas, presumably due to differences of data over land areas.

Fig. 19 - The comparison between latitudinal and monthly N₂O concentrations to the NOAA Marine Boundary Layer product (panel b). The differences (panel c) show that the CMIP6 historical GHG concentrations are slightly higher in the southern hemisphere (0.5ppb) and slightly lower in the tropics (0.5ppb), as the stronger latitudinal gradient from tropics to southern latitudes is not reproduced in CMIP6 data. **Note:** Data submitted by Pieter Tans, pers. Communication.

—Comparison between the recommendations for annual global-mean surface-mixing ratios of CO₂, CH₄ and N₂O between CMIP5 and CMIP6 for the historical experiment.



Figure

13 Appendix A: Factsheets of GHGs other than CO₂, CH₄ and N₂O

Fig. 20 - CCl₄ Factsheet

Fig. 21 - CFC-11 Factsheet

5 **Fig. 22 - CFC-12 Factsheet**

Fig. 23 - CFC-113 Factsheet

Fig. 24 - CFC-114 Factsheet

Fig. 25 - CFC-115 Factsheet

Fig. 26 - CH₂Cl₂ Factsheet

10 **Fig. 27 - CH₃Br Factsheet**

Fig. 28 - CH₃CCl₃ Factsheet

Fig. 29 - CH₃Cl Factsheet

Fig. 30 - CHCl₃ Factsheet

Fig. 31 - Halon-1211 Factsheet

15 **Fig. 32 - Halon-1301 Factsheet**

Fig. 33 - Halon-2402 Factsheet

Fig. 34 - HCFC-22 Factsheet

Fig. 35 - HCFC-141b Factsheet

Fig. 36 - HCFC-142b Factsheet

20 **Fig. 37 - C₂F₆ Factsheet**

Fig. 38 - C₃F₈ Factsheet

Fig. 39 - C₄F₁₀ Factsheet

Fig. 40 - C₅F₁₂ Factsheet

Fig. 41 - C₆F₁₄ Factsheet

25 **Fig. 42 - C₇F₁₆ Factsheet**

Fig. 43 - C₈F₁₈ Factsheet

Fig. 44 - c-C₄F₈ Factsheet

[Fig. 45 - CF₄ Factsheet](#)

[Fig. 46 - HFC-23 Factsheet](#)

[Fig. 47 - HFC-32 Factsheet](#)

[Fig. 48 - HFC-43-10-mee Factsheet](#)

5 [Fig. 49 - HFC-125 Factsheet](#)

[Fig. 50 - HFC-134a Factsheet](#)

[Fig. 51 - HFC-143a Factsheet](#)

[Fig. 52 - HFC-152a Factsheet](#)

[Fig. 53 - HFC-227ea Factsheet](#)

10 [Fig. 54 - HFC-236fa Factsheet](#)

[Fig. 55 - HFC-245fa Factsheet](#)

[Fig. 56 - HFC-365mfc Factsheet.](#)

[Fig. 57 - NF₃ Factsheet](#)

[Fig. 58 - SF₆ Factsheet](#)

15 [Fig. 59 - SO₂F₂ Factsheet](#)

14 Appendix B: CMIP5 Analysis of CO₂ concentration fields

Fig. 60 - Annual mean CO₂ ~~mixing-ratio~~ concentrations in 8 CMIP5 ESM models in the year 1875. The CMIP5 recommended value was 288.7 ppm+ppm for 1875. Two more models with higher average CO₂ ~~mixing-ratio~~ concentrations, namely BNU-ESM and FIO-ESM, are shown in ~~Figure 63~~ and Fig. 66.

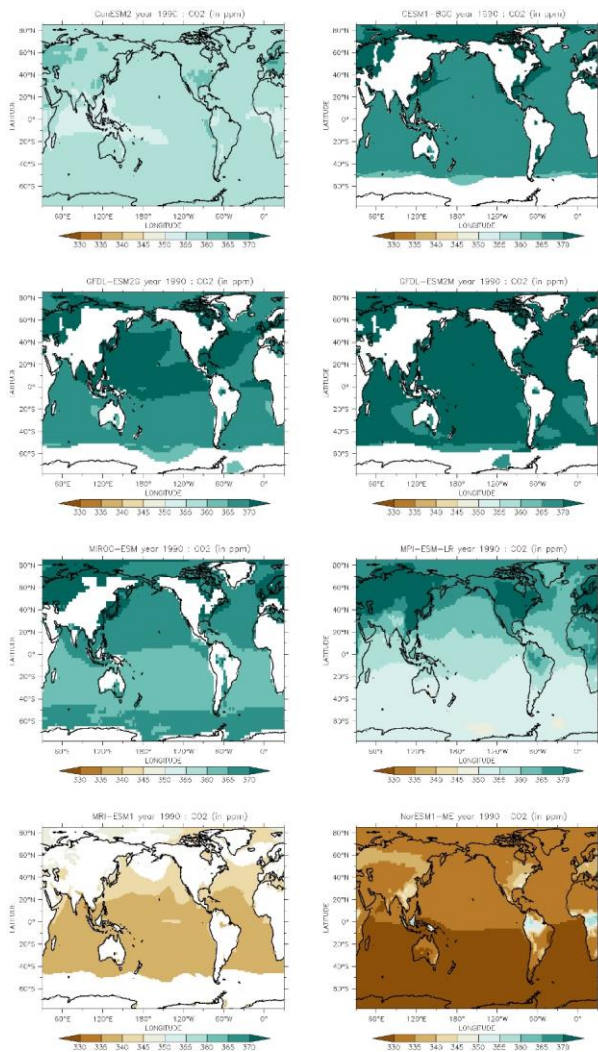


Figure Fig. 61 - Annual mean CO₂ mixing-ratios concentrations in 8 CMIP5 ESM models in the year 1990. The CMIP5 recommended value was 353.885 ppmvppm for 1990 in the historical experiment.

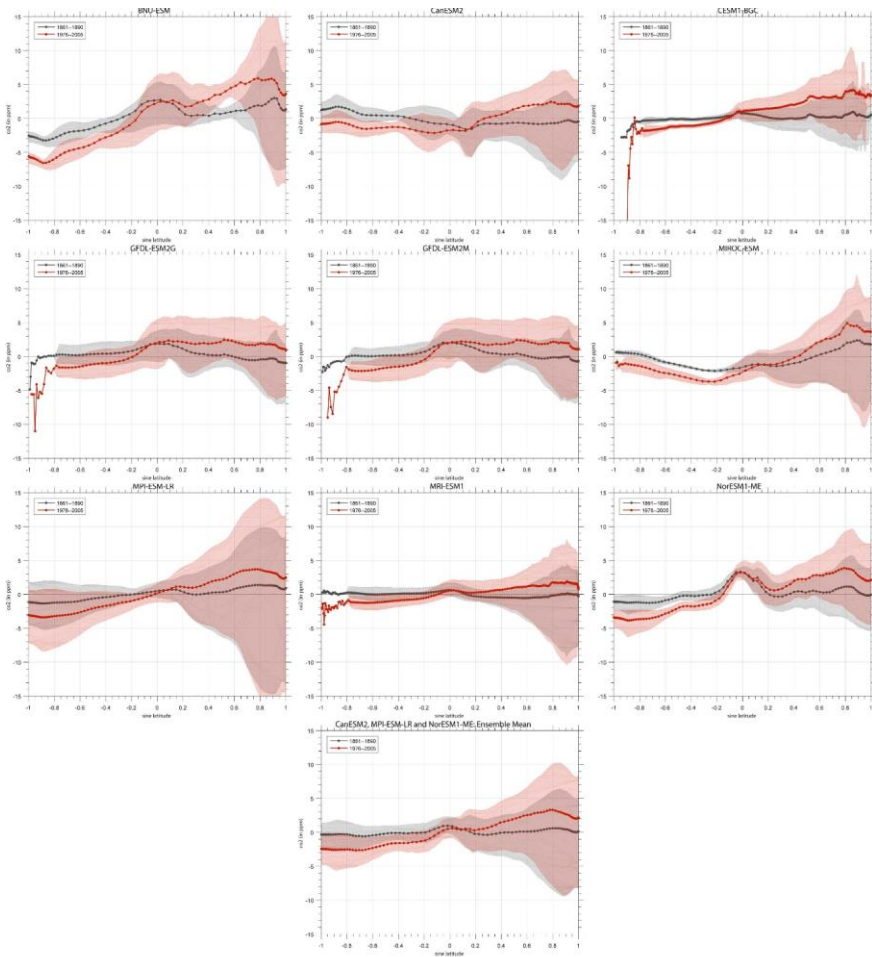


Figure Fig. 62 – Climatological seasonal cycle of CO₂ concentrations in 9 CMIP5 ESM models for the historical experiment's 30-year period 1861-1890.

5 Fig. 63 – Climatological seasonal cycle of CO₂ concentrations in 9 CMIP5 ESM models for the historical experiment's 30-year period 1976-2005.

Fig. 64 - Latitudinal gradient of surface atmospheric CO₂ mixing ratios/concentrations exhibited in 9 considered CMIP5 ESM models for both the preindustrial period (grey lines) and recent period 1976-2005 (red lines). The bold dotted lines indicate the annual means. The 12 finer lines represent the individual monthly averages over the respective 30 year periods. Shaded areas show the min-max of those monthly averages. The lowest panel shows an ensemble mean for three CMIP5 ESMs, namely CanESM2, MPI-ESM-LR and NorESM1-ME.

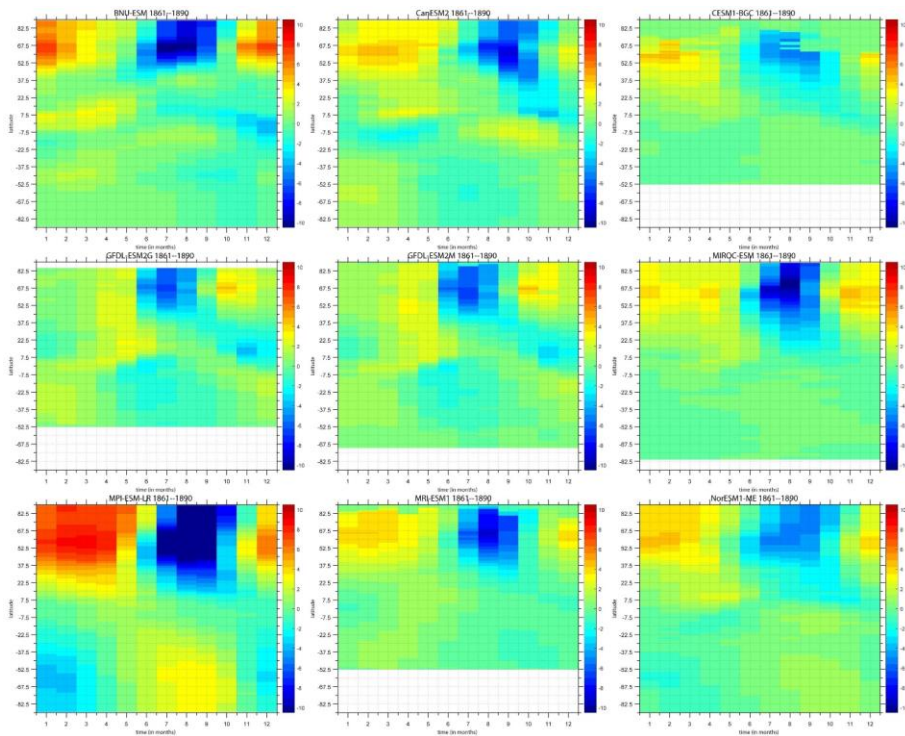


Figure Fig. 65 – Climatological seasonal cycle of CO₂ mixing ratios in 9 CMIP5 ESM models for the historical experiment's 30-year period 1861-1890.

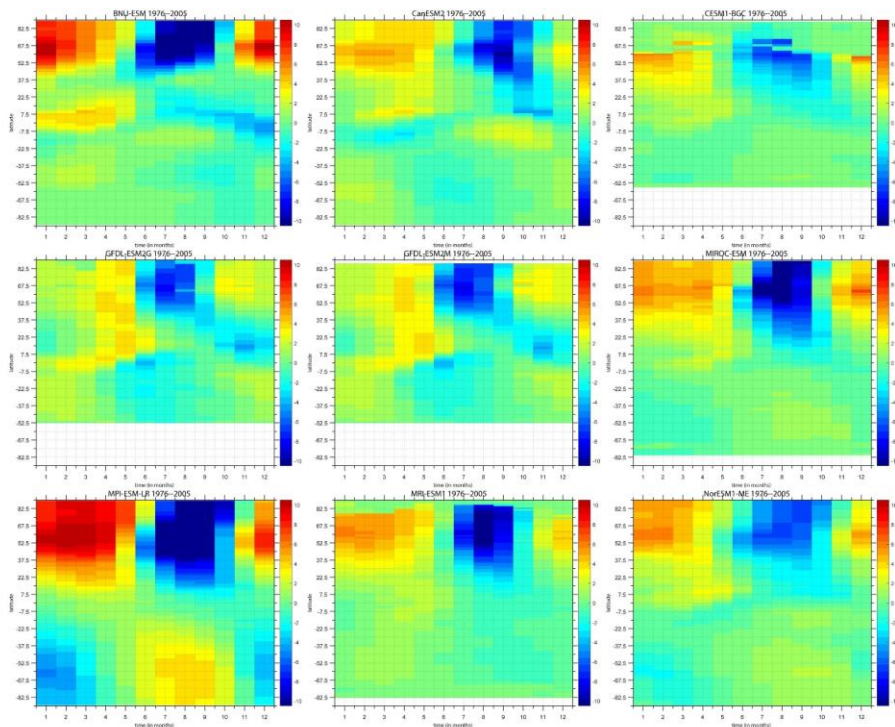


Figure 14 — Climatological seasonal cycle of CO₂ mixing ratios in 9 CMIP5-ESM models for the historical experiment's 30-year period 1976-2005.

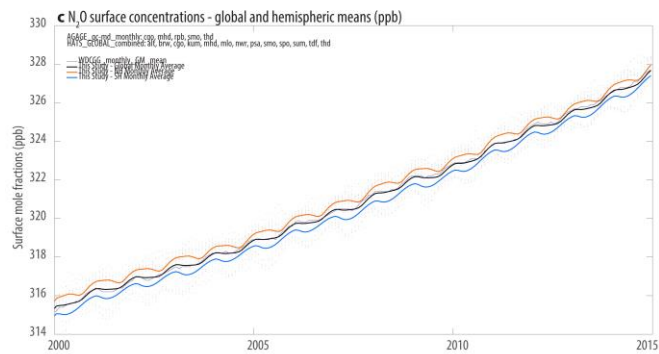
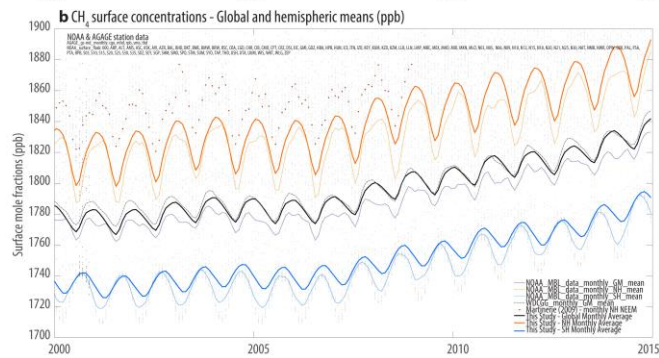
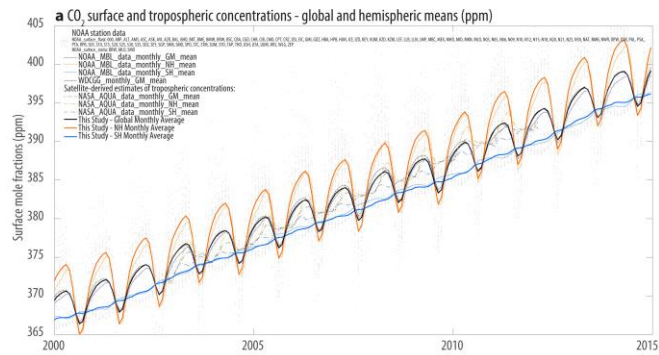


Figure 15—Comparison of global-mean, and hemispheric-monthly average mixing ratios of CO₂ (panel a), CH₄ (panel b) and N₂O (panel c) between the CMIP6 surface mole fractions (this study), the NOAA Marine Layer Boundary products, the World Data Centre of Greenhouse gases (WDCGG) products and the NASA AQUA satellite data of tropospheric CO₂ mixing ratios. For comparison, individual (monthly average) NOAA and AGAGE station data across all latitudes is shown in the background (grey dots).

5

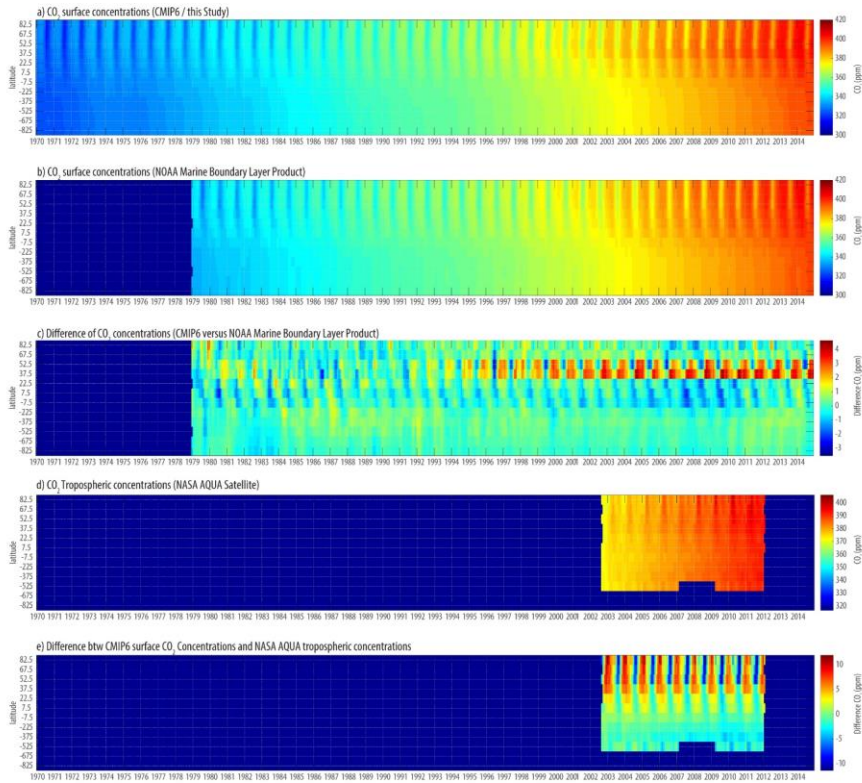


Figure 16—Comparison of the CMIP6 historical CO₂ emissions (panel a) with the NOAA Marine Boundary Layer MBL product from 1979 to 2014 (panel b). Differences indicate that a seasonal higher CO₂ mixing ratio is implied by the CMIP6 data of up to 5 ppmv in mid-latitude northern bands, whereas some monthly tropical CO₂ mixing ratios tend to be slightly lower in the CMIP6 product compared to NOAA MBL (panel c).

10

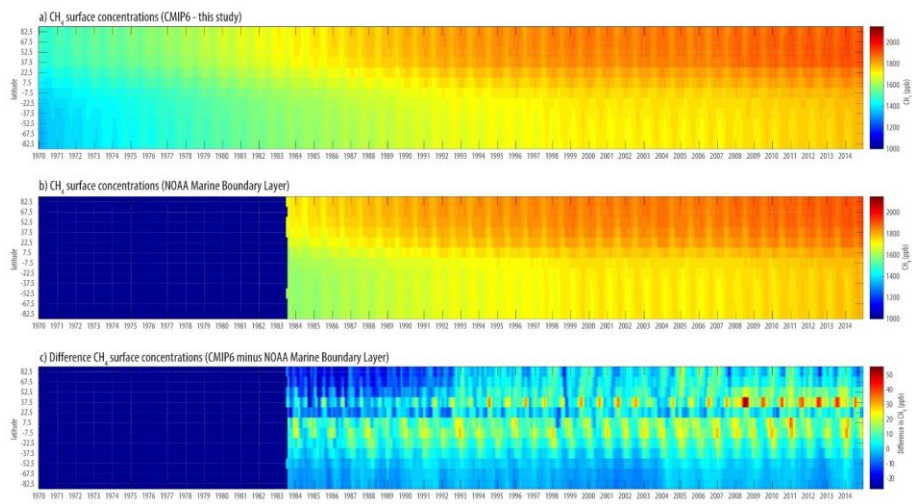


Figure 17— Comparison of the surface CH₄ monthly mean mixing ratios between CMIP6 (panel a), the NOAA Marine Boundary Layer product (panel b) and the difference (panel c). Since around 1992, there are seasonal differences in the mid northern latitudes with the CMIP6 data being up to 50ppb higher than the NOAA MBL product. Similarly, higher mixing ratios are apparent in the areas of tropical southern and lower latitude southern areas, presumably due to differences of data over land areas.

5

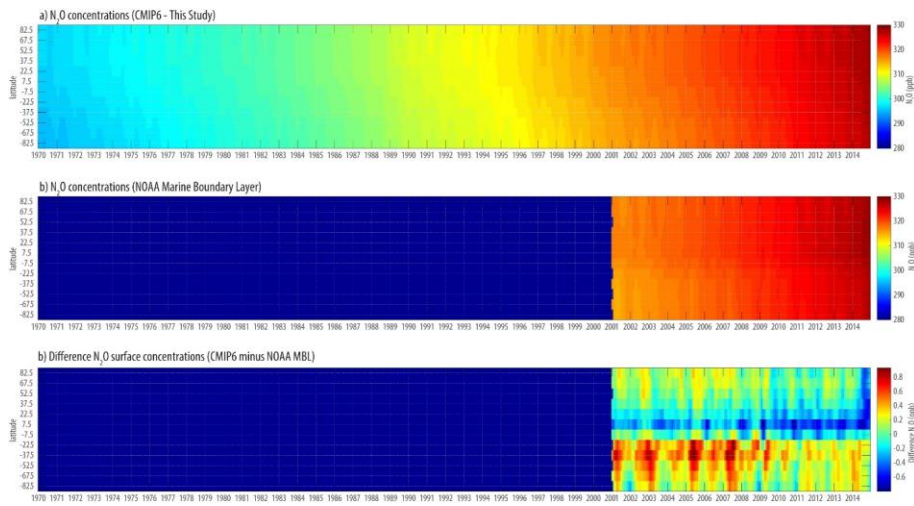


Figure 18 – The comparison between latitudinal and monthly N₂O mixing ratios to the NOAA Marine Boundary Layer product (panel b). The differences (panel c) show that the CIMP6 historical GHG mixing ratios are slightly higher in the southern hemisphere (+0.5ppb) and slightly lower in the tropics (-0.5ppb), as the stronger latitudinal gradient from tropics to southern latitudes is not reproduced in CIMP6 data. **Note: Data submitted by Pieter Tans, pers. Communication.**

5

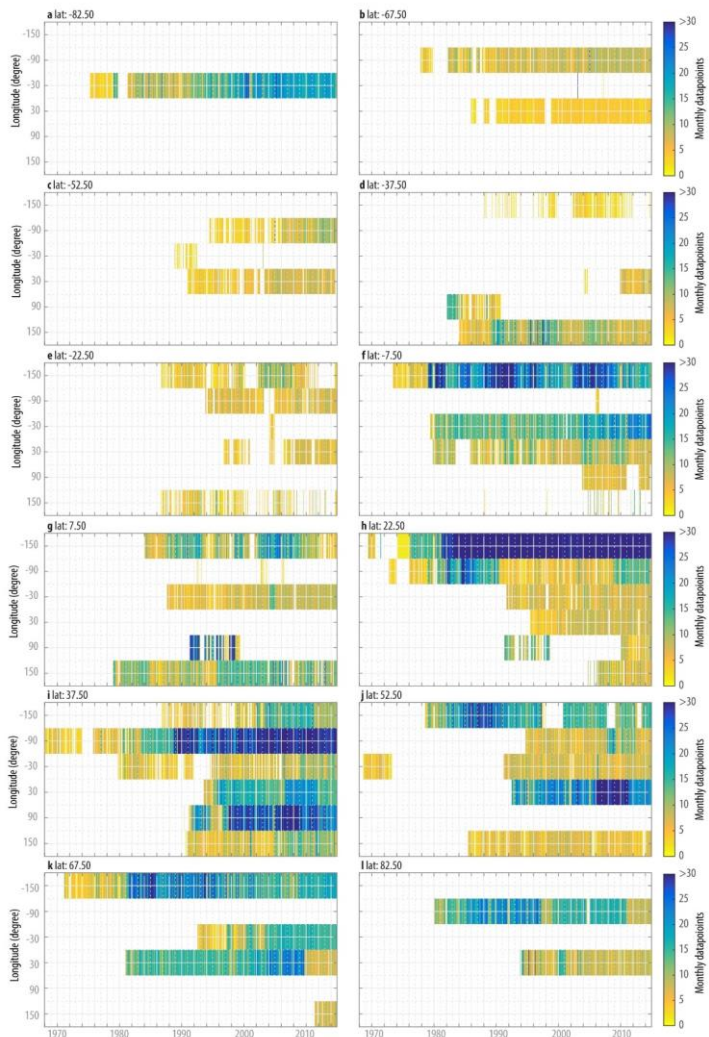


Figure 19— Availability of instrumental carbon dioxide data from 1968 to 2015 from the NOAA-ESRL network, shown as data samples per month, per latitudinal band (panels a to f) and per longitudinal bin within each latitudinal band.

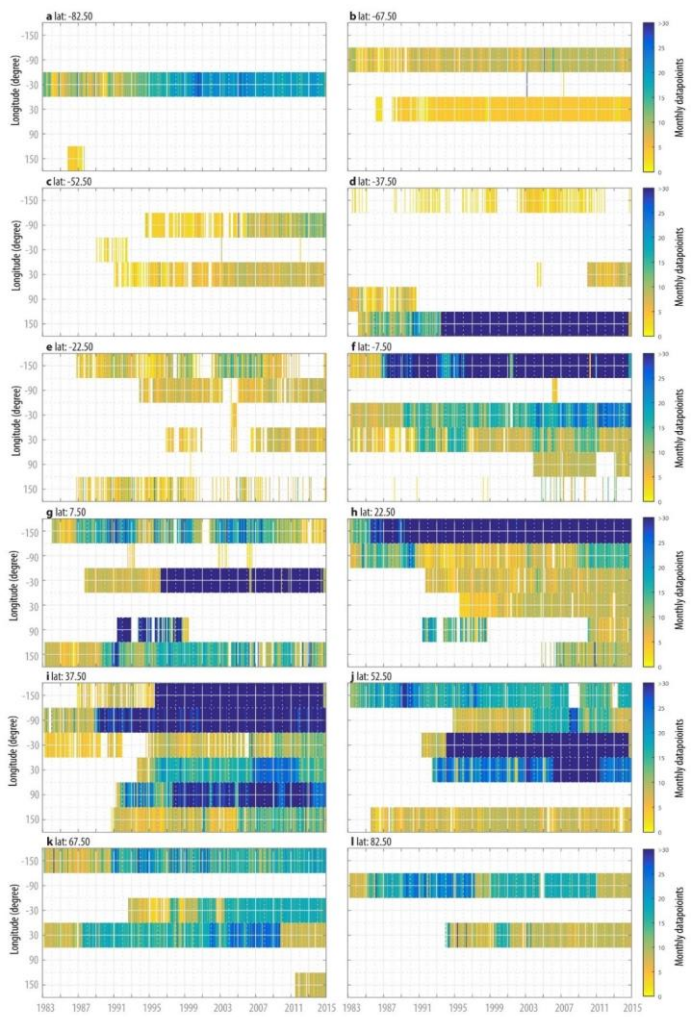


Figure 20—Availability of instrumental CH₄ data from 1983 to 2015 from the AGAGE and NOAA ESRL networks, shown as data samples per month, per latitudinal band (panels a to l) and per longitudinal bin within each latitudinal band.

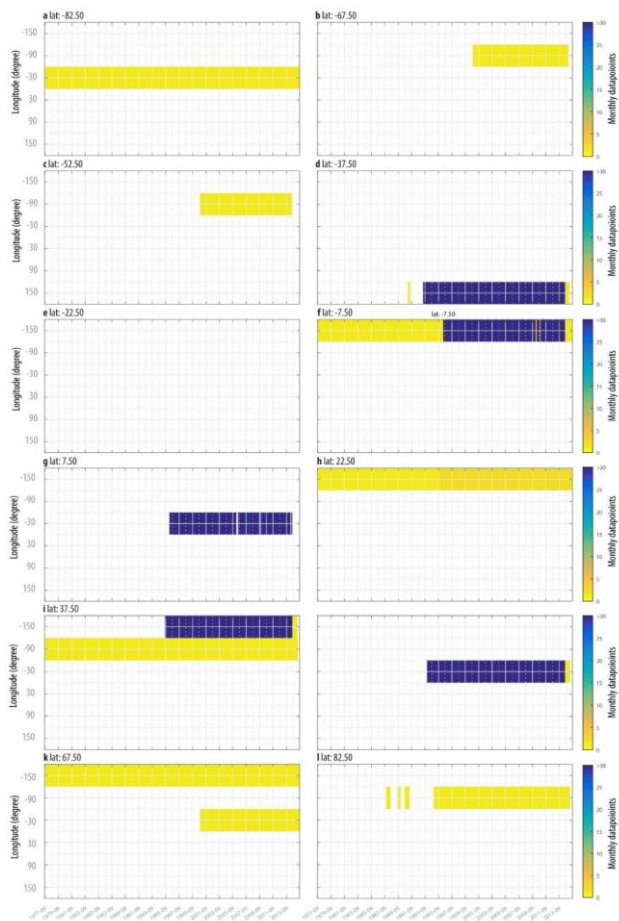


Figure 21—Availability of instrumental N_2O data from 1983 to 2015 from the AGAGE and NOAA ESRL networks, shown as data samples per month, per-latitudinal band (panels a to l) and per-longitudinal bin within each latitudinal band.

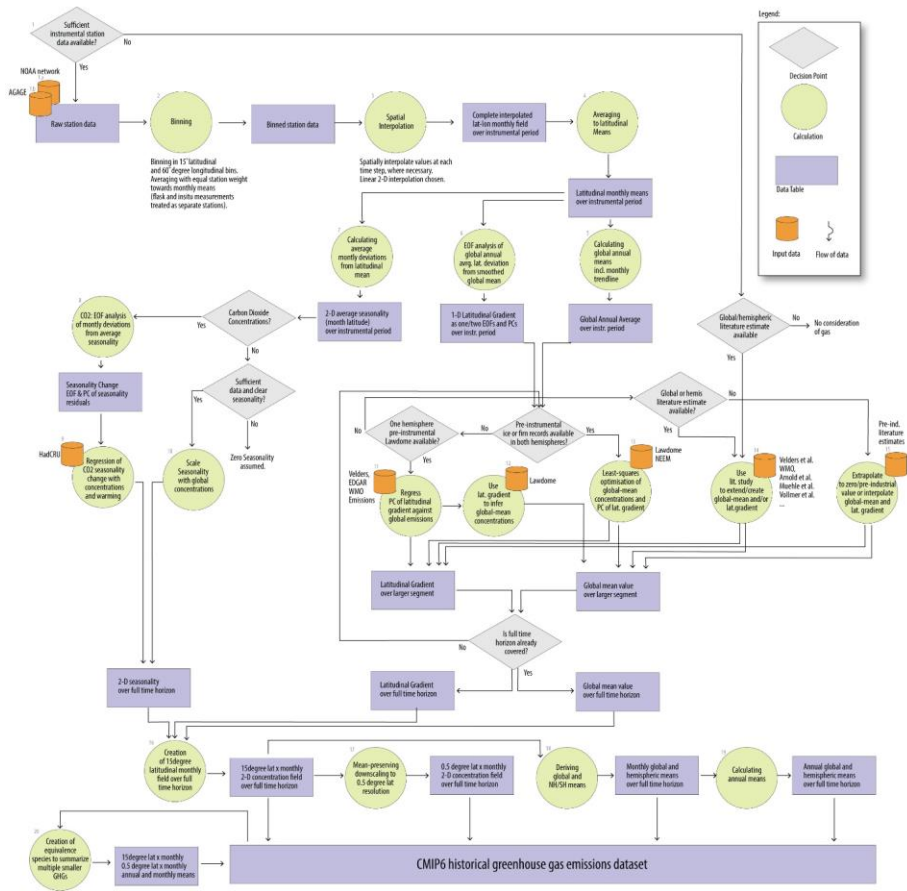


Figure 22 – Data flow diagram of how historical GHG mixing ratios are derived in this study. See text.

13—Appendix A: Individual GHGs other than CO₂, CH₄ and N₂O

CCl4

Carbon tetrachloride (CCl4): Lifetime: 26yrs ; Radiative Efficiency : 0.17 Wm2/ppb

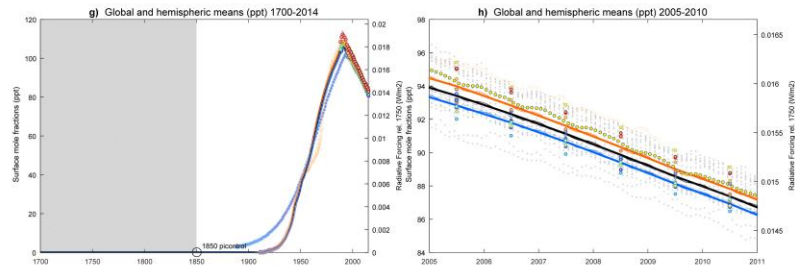
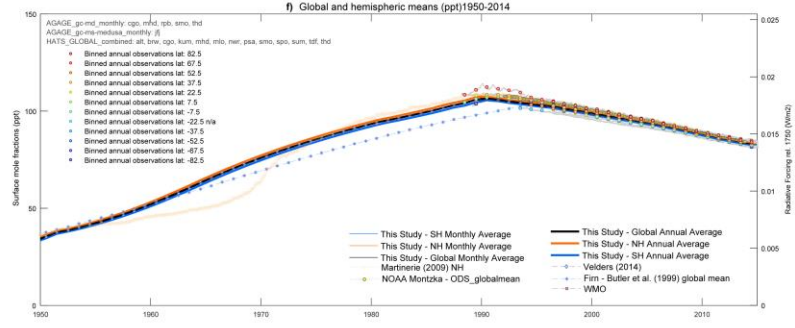
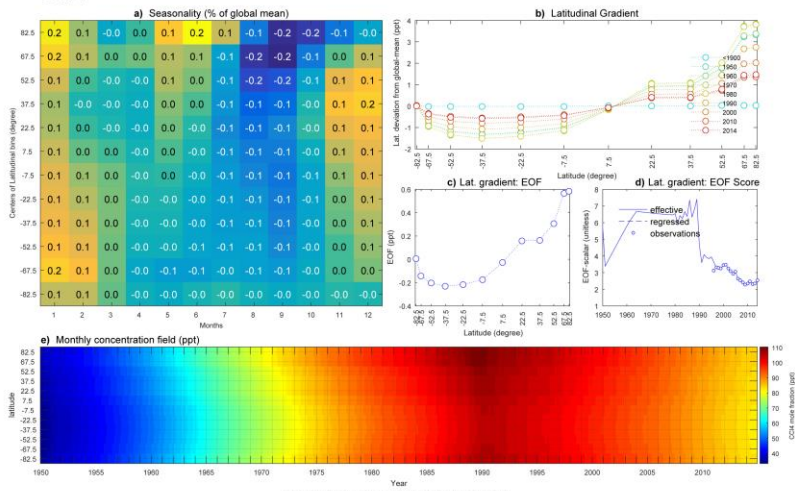
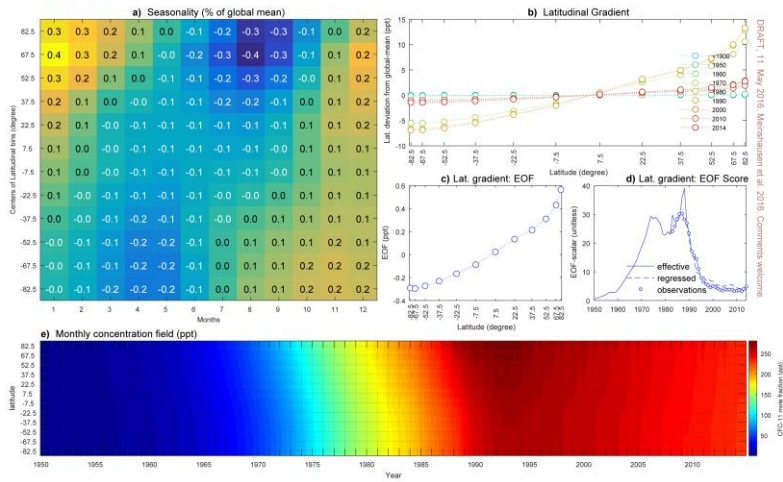


Figure 23 – CCl4 Factsheet

CFC-11

CFC-11 (CCSF) Lifetime: 45yrs ; Radiative Efficiency : 0.28 Wm²/ppb



PBLAFT_11_May_2016_Manchandani et al. 2016_Comments_welcome

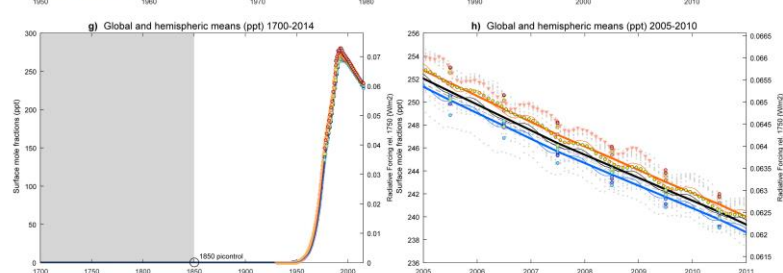
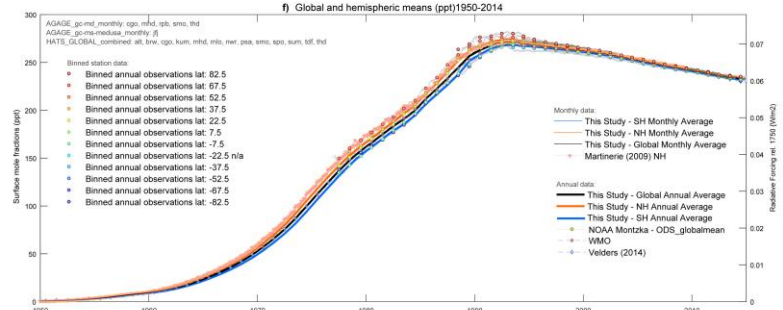


Figure 24—CFC-11 Factsheet

CFC-12

CFC-12 (C02F2) Lifetime: 100yrs Radiative Efficiency: 0.32 W/m2ppb

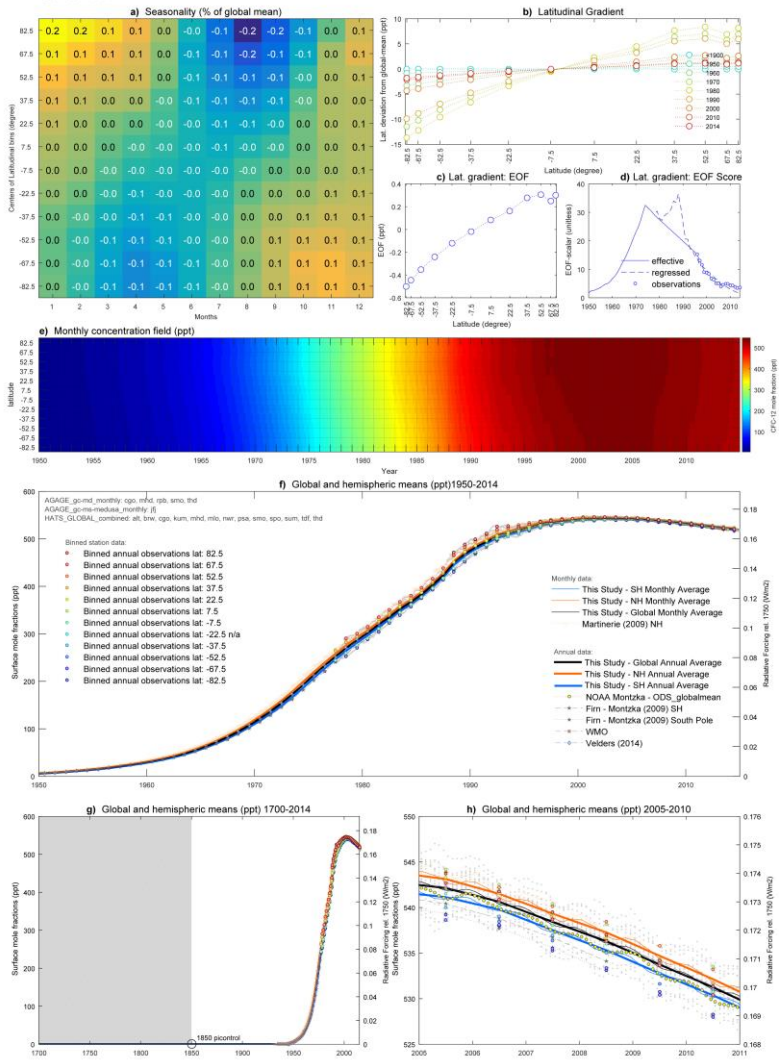


Figure 25—CFC-12 Factsheet

CFC-113

CFC-113 (CC2FCF2) Lifetime: 85yrs ; Radiative Efficiency: 0.3 W/m2/ppb

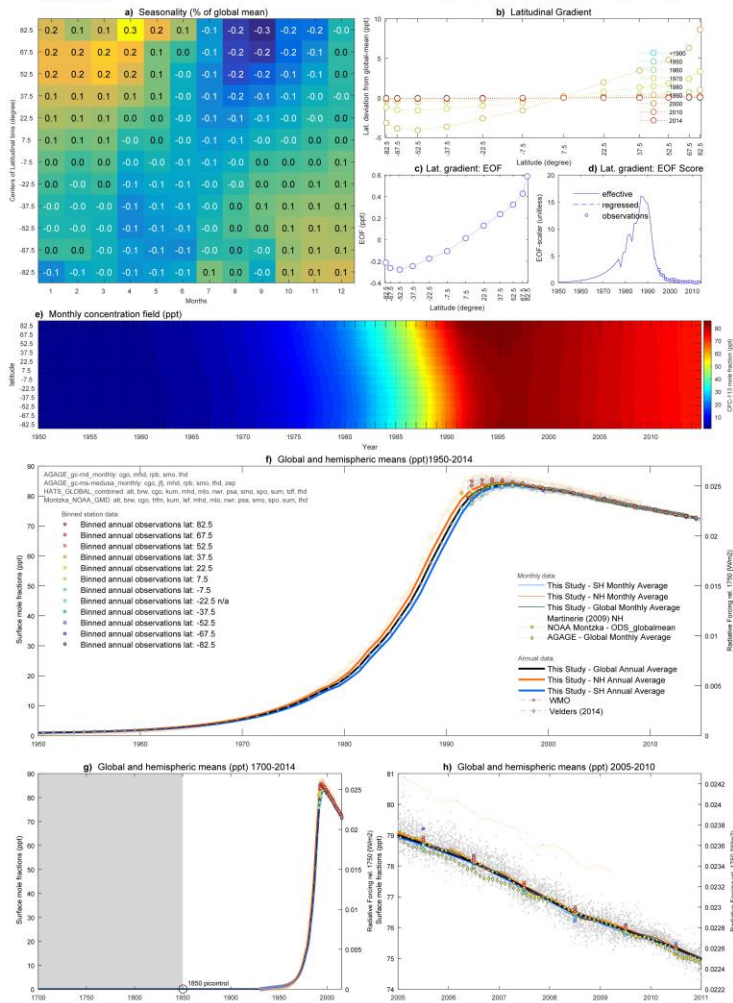


Figure 26 – CFC-113 Factsheet

CFC-114

CFC-114 (CCF2CCF2) Lifetime: 190yrs - Radiative Efficiency: 0.31 W/m2/ppb

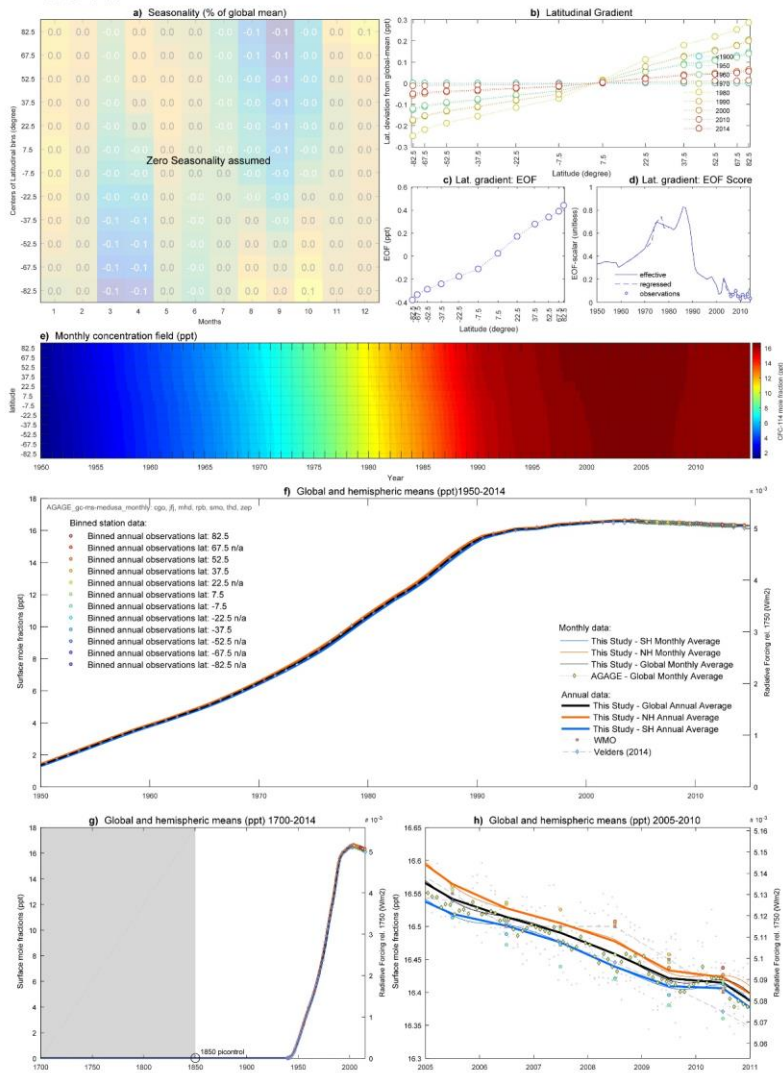


Figure 27—CFC-114 Factsheet

Figure 28 – CFC-115 Factsheet

CH2Cl2

Methylene chloride (CH₂Cl₂): Lifetime: 0.4yrs ; Radiative Efficiency : 0.03 Wm²/ppb

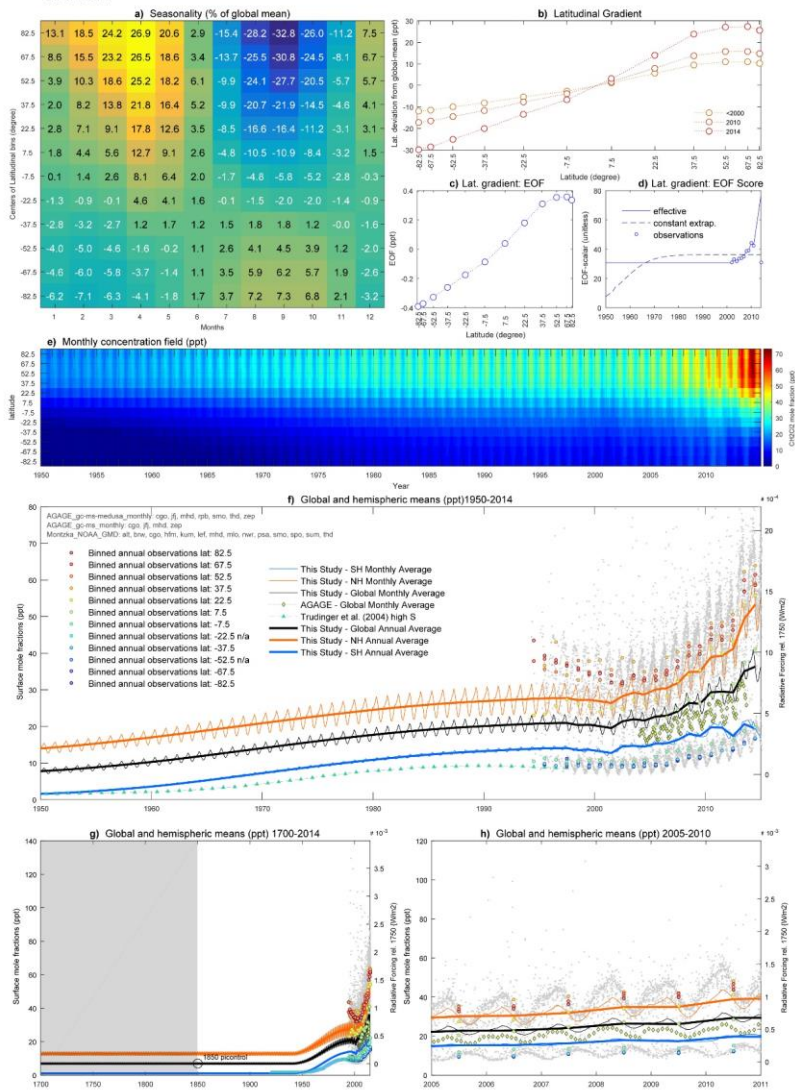


Figure 29—CH2Cl2 Factsheet

CH3Br

Methyl bromide (CH3Br): Lifetime: 0.8yrs; Radiative Efficiency: -0.004 Wm2ppb

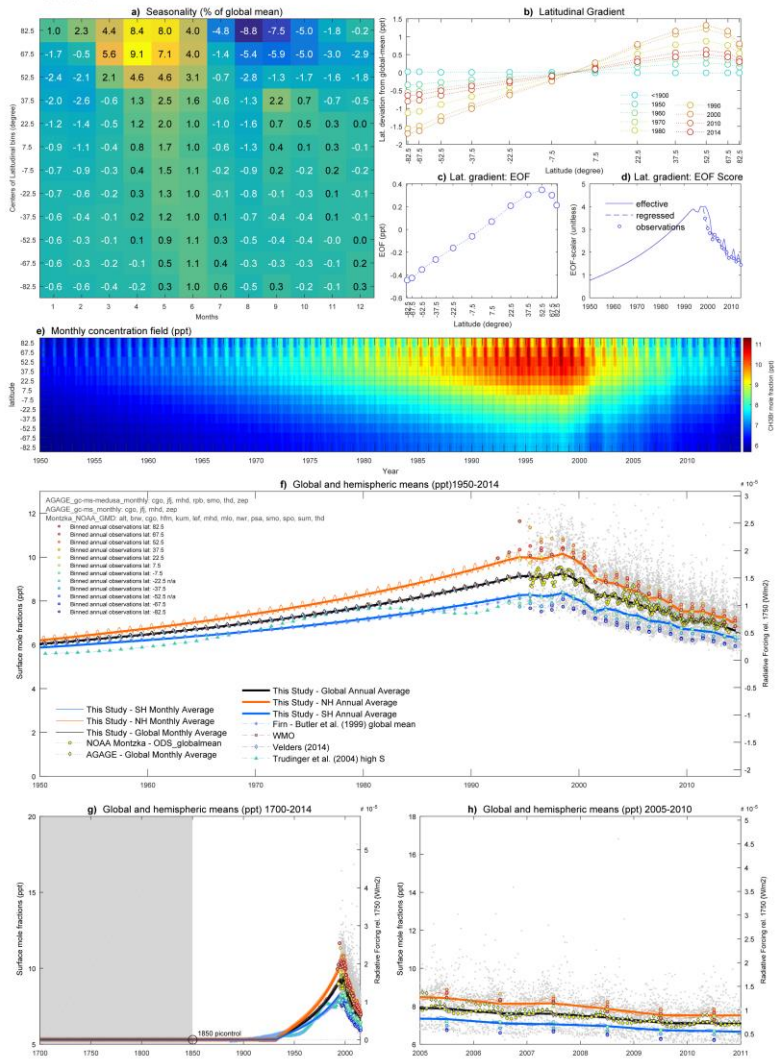


Figure 30—CH3Br Factsheet

CH3CCl3

Methyl chloroform (CH3CCl3): Lifetime: 5yrs ; Radiative Efficiency: 0.07 Wm2ppb

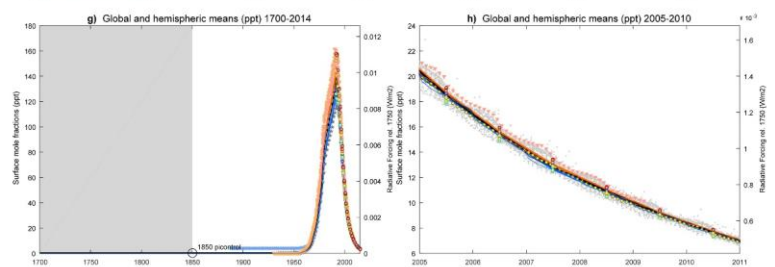
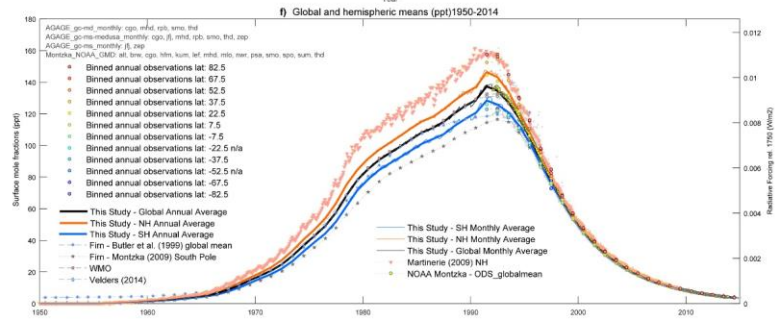
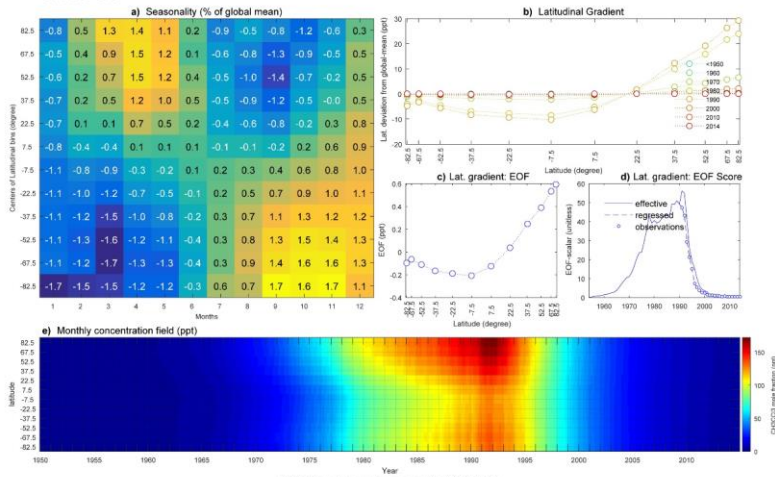


Figure 31—CH3CCl3 Factsheet

CH3CI

Methyl chloride (CH3Cl): Lifetime: 1yrs ; Radiative Efficiency: 0.01 Wm2/ppb

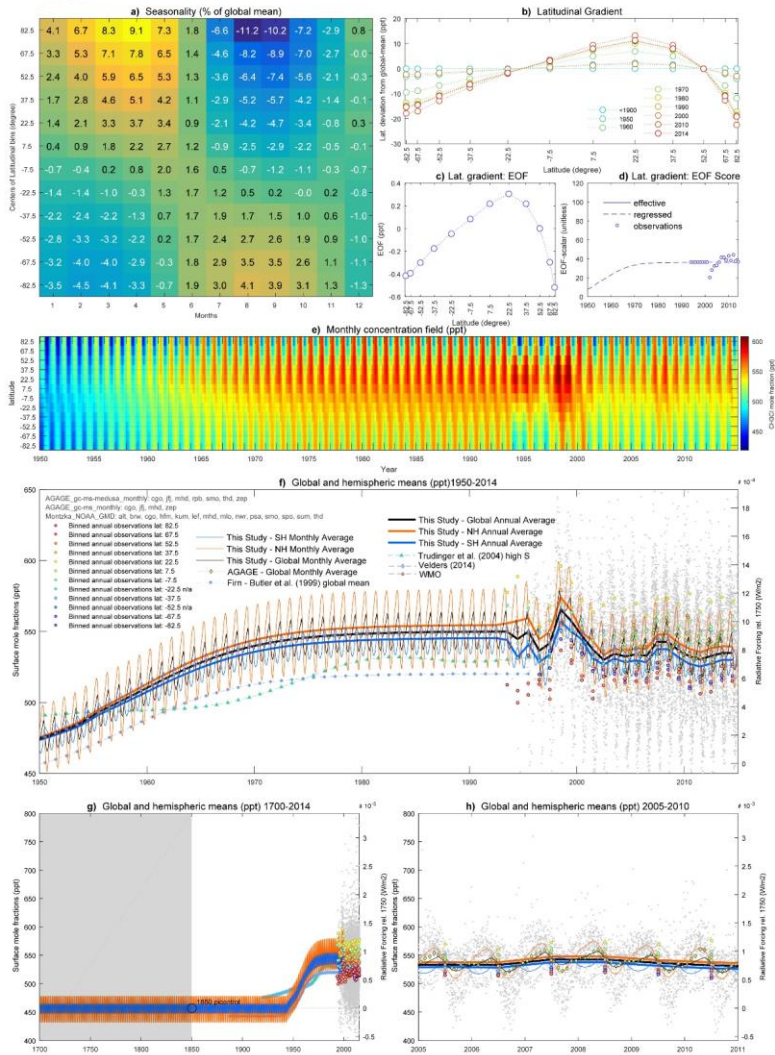


Figure 32—CH₃Cl Factsheet

CHCl3

Chloroform (CHCl₃) Lifetime: 0.4yrs ; Radiative Efficiency: 0.08 W/m²/ppb

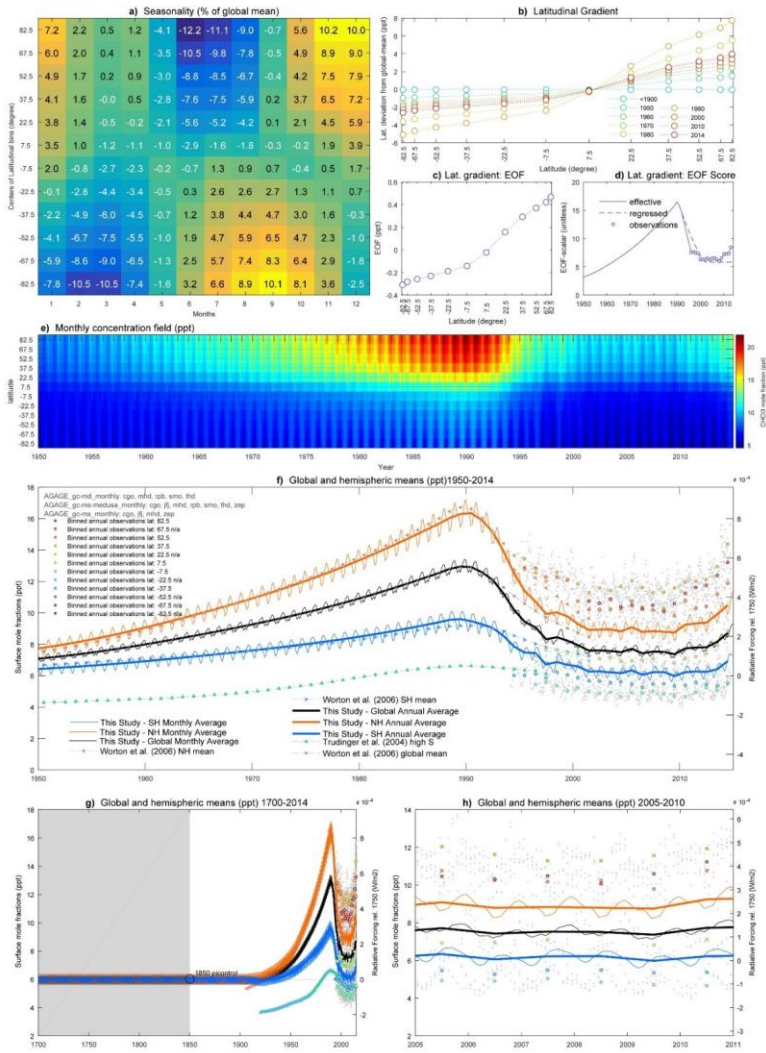


Figure 33—CHCl3 Factsheet

Halón-1211

Halón-1211 (CB-CF2) Lifetime: 16yrs ; Radiative Efficiency : 0.29 Wm2/ppb

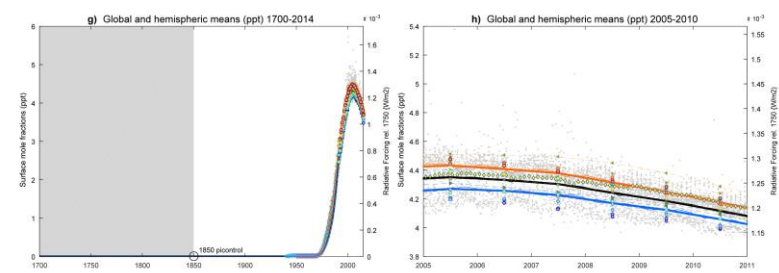
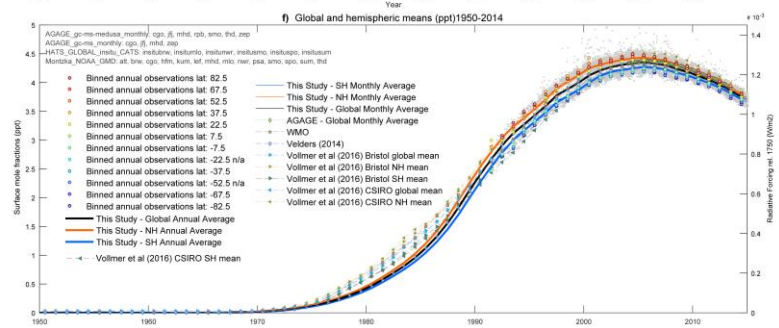
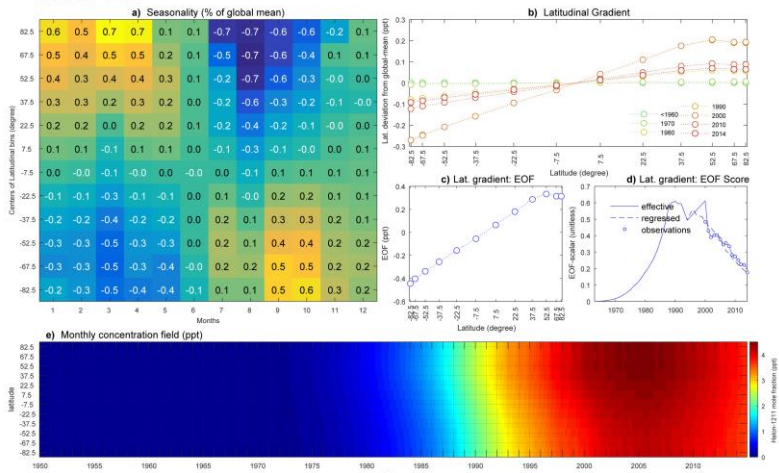


Figure 34—Halon-1211 Factsheet

Halon-1301

Halon-1301 (CBF3) Lifetime: 65yrs : Radiative Efficiency: 0.3 Wm2/ppb

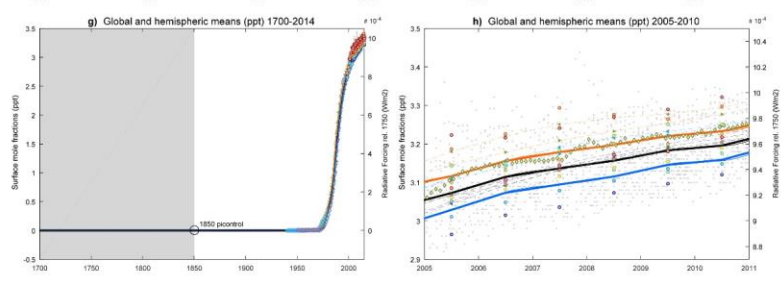
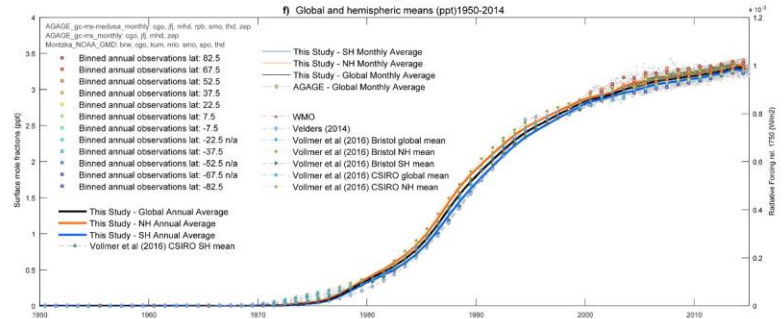
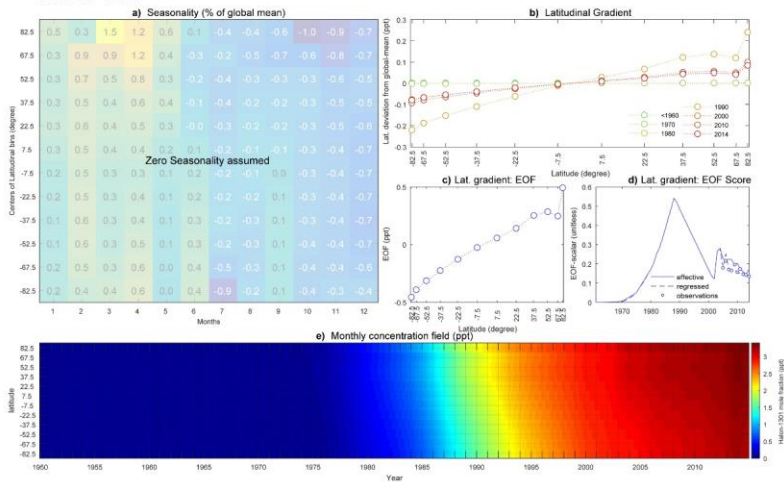


Figure 35—Halon-1301 Factsheet

Halon-2402

Halon-2402 (CBrF₂CBrF₂): Lifetime: 20yrs ; Radiative Efficiency: 0.31 Wm²ppb

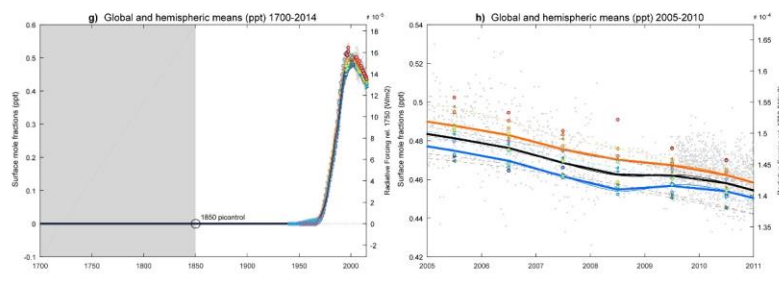
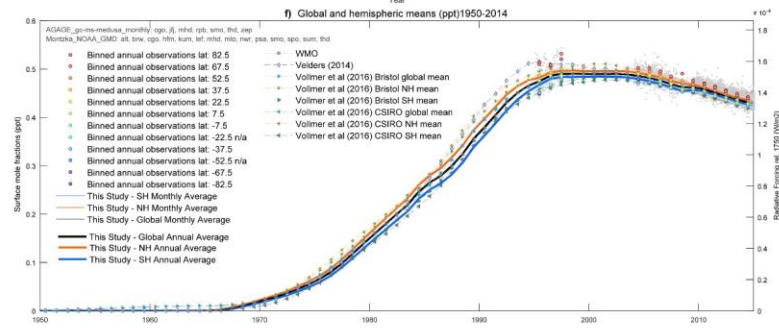
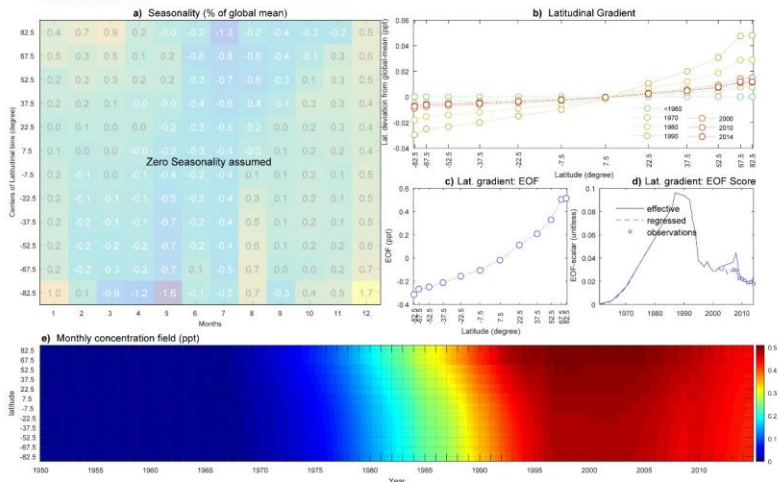


Figure 36—Halon-2402 Factsheet

HCFC-22

HCFC-22 (CHClF₂) Lifetime: 11.9yrs Radiative Efficiency: 0.21 W/m²/ppb

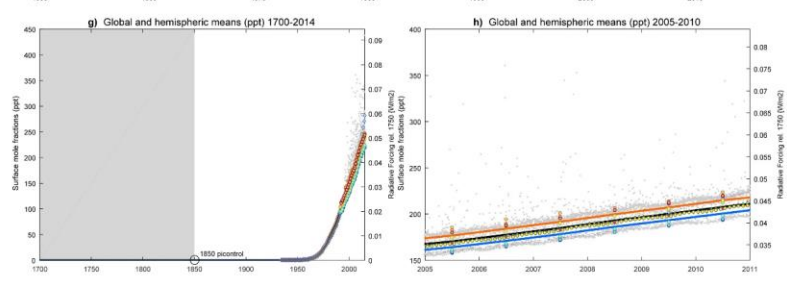
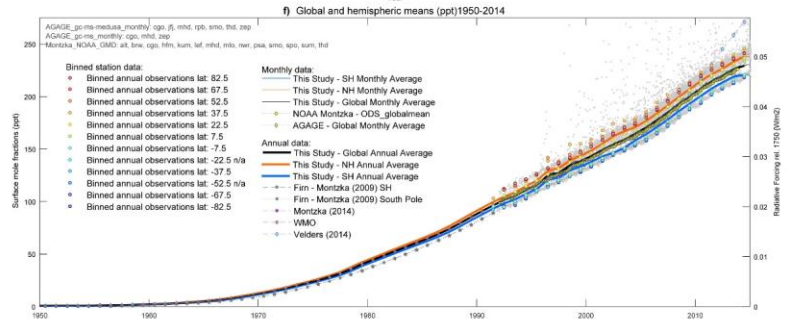
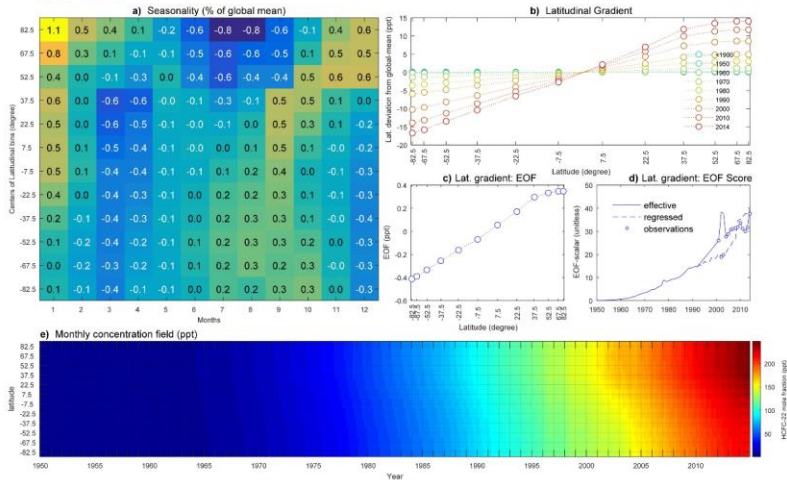


Figure 37—HCFC-22 Factsheet

HCFC-141b

HCFC-141b (CH3CCl2F): Lifetime: 9.2yrs ; Radiative Efficiency : 0.16 Wm2/ppb

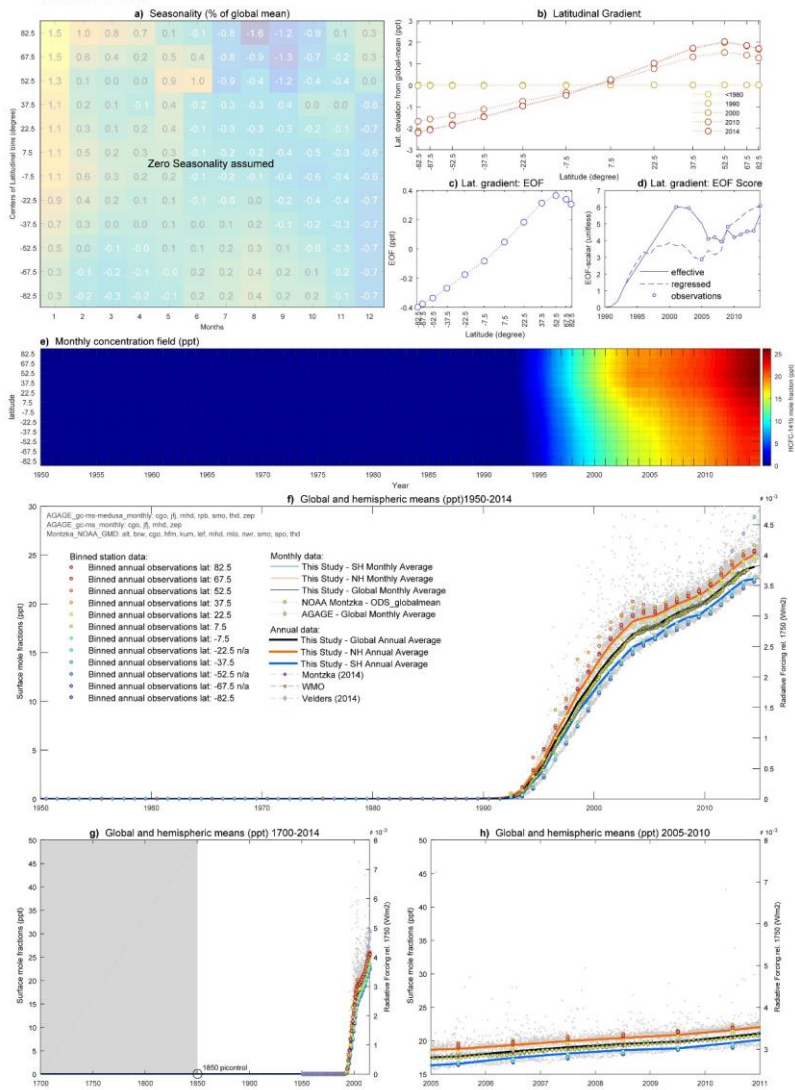


Figure 38—HCFC-141b Factsheet

HCFC-142b

HCFC-142b (CH₂ClCF₂): Lifetime: 17.2yrs ; Radiative Efficiency: 0.19 W/m²/ppb

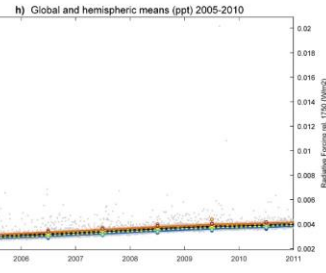
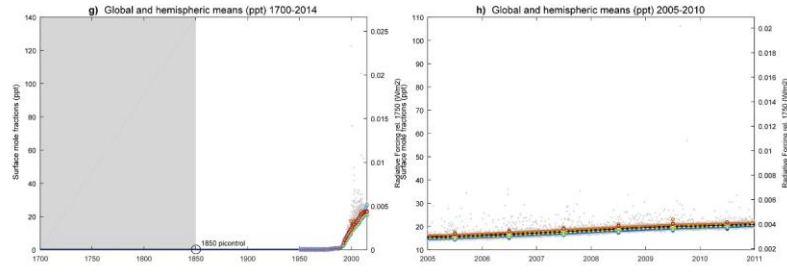
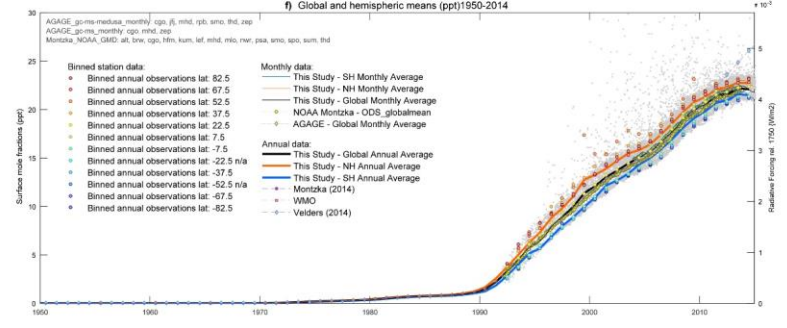
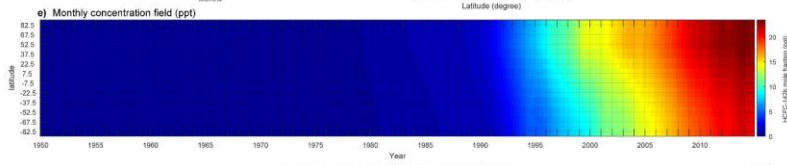
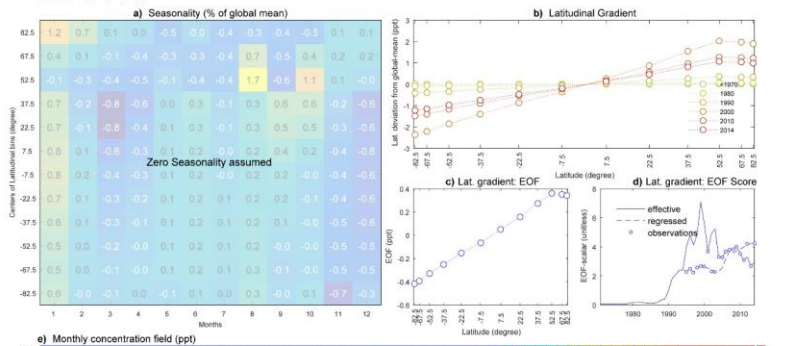


Figure 39—HCFC-142b Factsheet

C2F6

PFC-116 (C2F6): Lifetime: 10000yrs; Radiative Efficiency: 0.25 W/m2/ppb

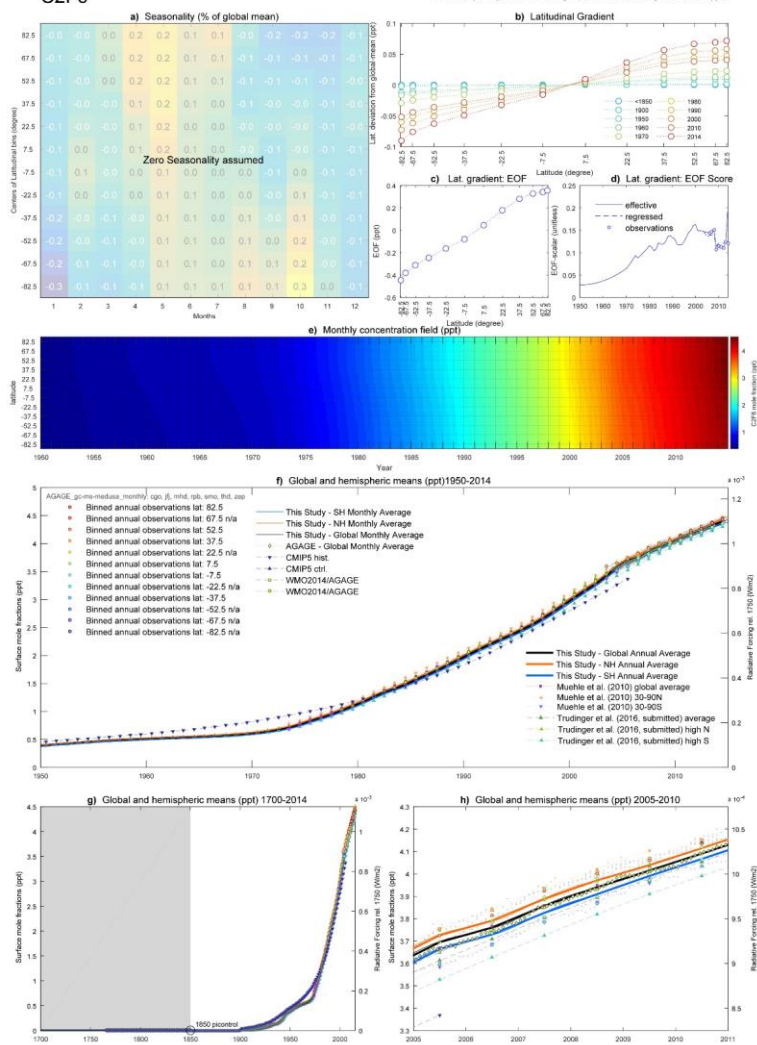


Figure 40—C2F6 Factsheet

C3F8

PFC-218 (C3F8): Lifetime: 2600yrs ; Radiative Efficiency: 0.28 W/m²/ppb

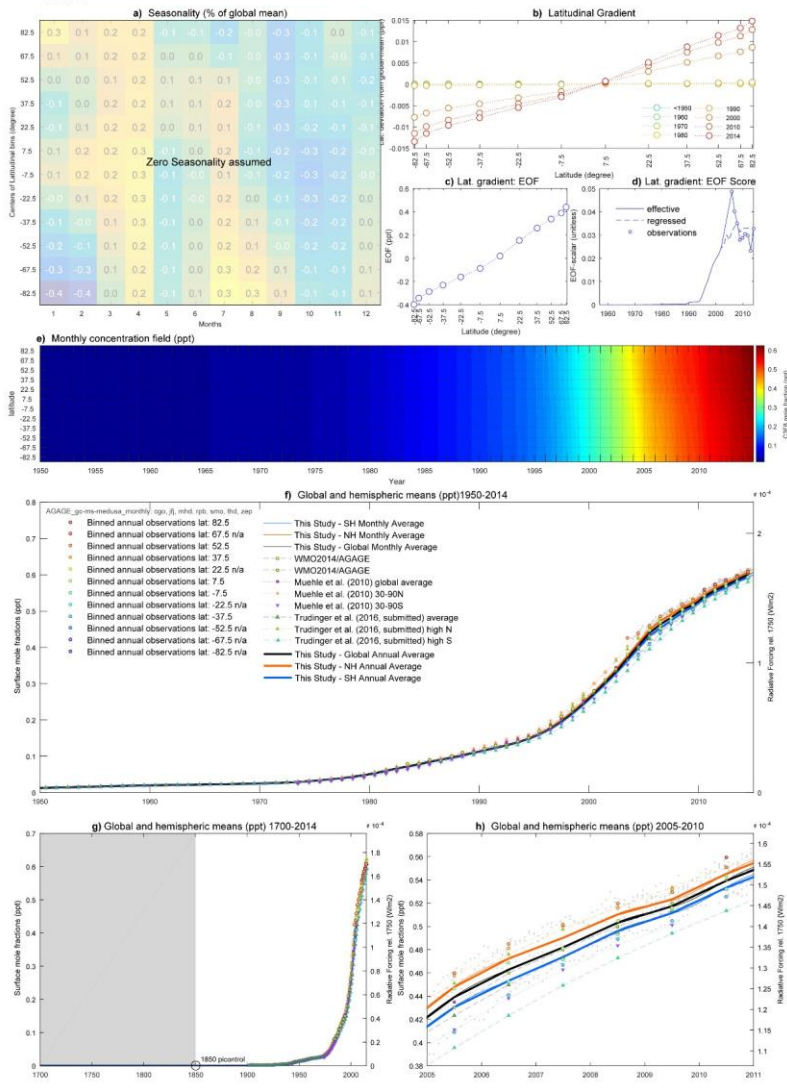


Figure 41—C3F8 Factsheet

C4F10

PFC-31-10 (C4F10): Lifetime: 2000yrs - Radiative Efficiency: 0.36 Wm²/ppb

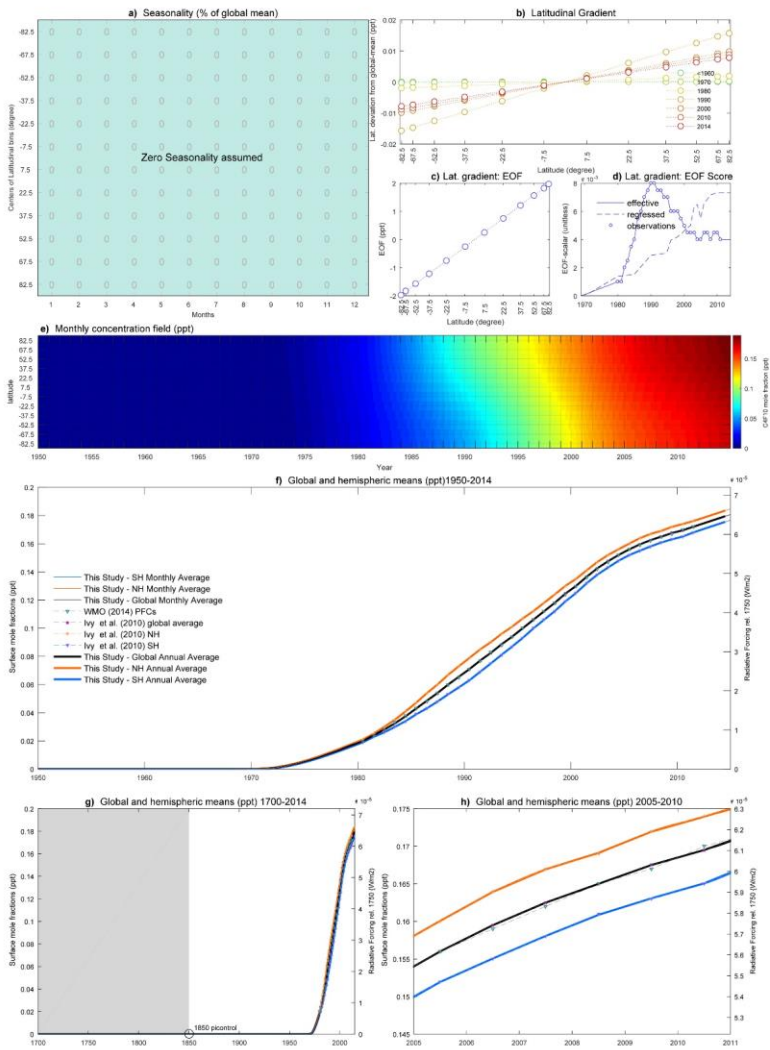


Figure 42—C4E10 Factsheet

C5F12

PFC-41-12 (n-C5F12): Lifetime: 4100yrs ; Radiative Efficiency: 0.41 Wm2/ppb

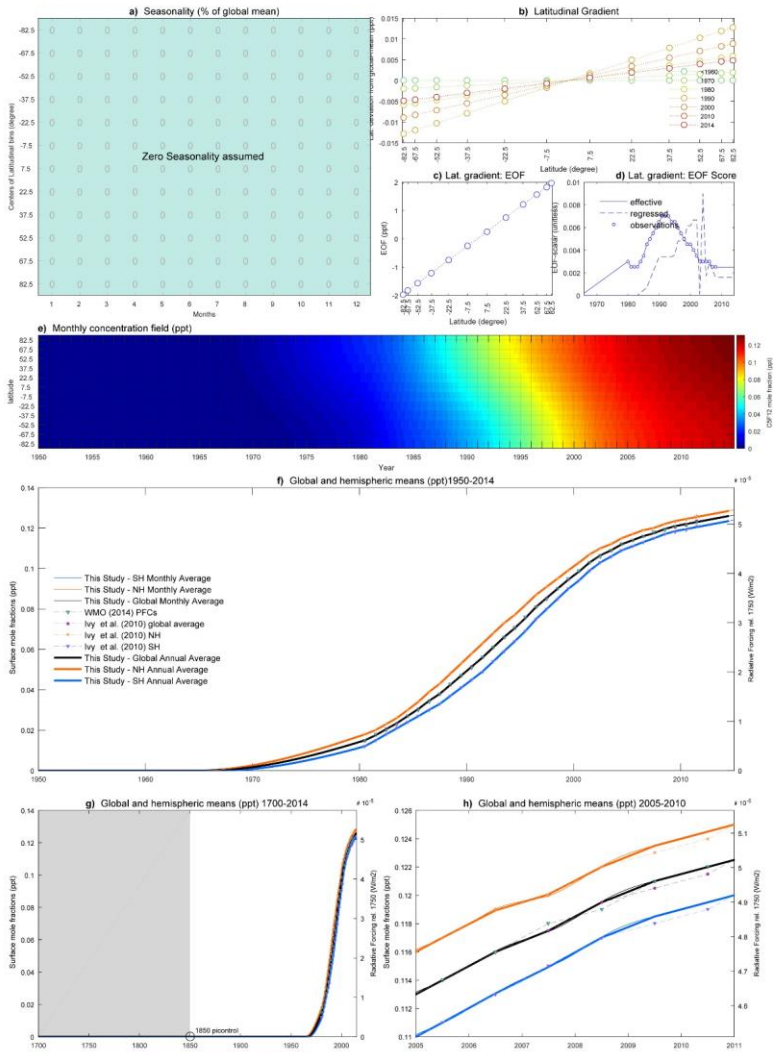


Figure 43—C5F12 Factsheet

C6F14

PFC-51-14 (n-C6F14): Lifetime: 3100yrs ; Radiative Efficiency : 0.44 W/m2/ppb

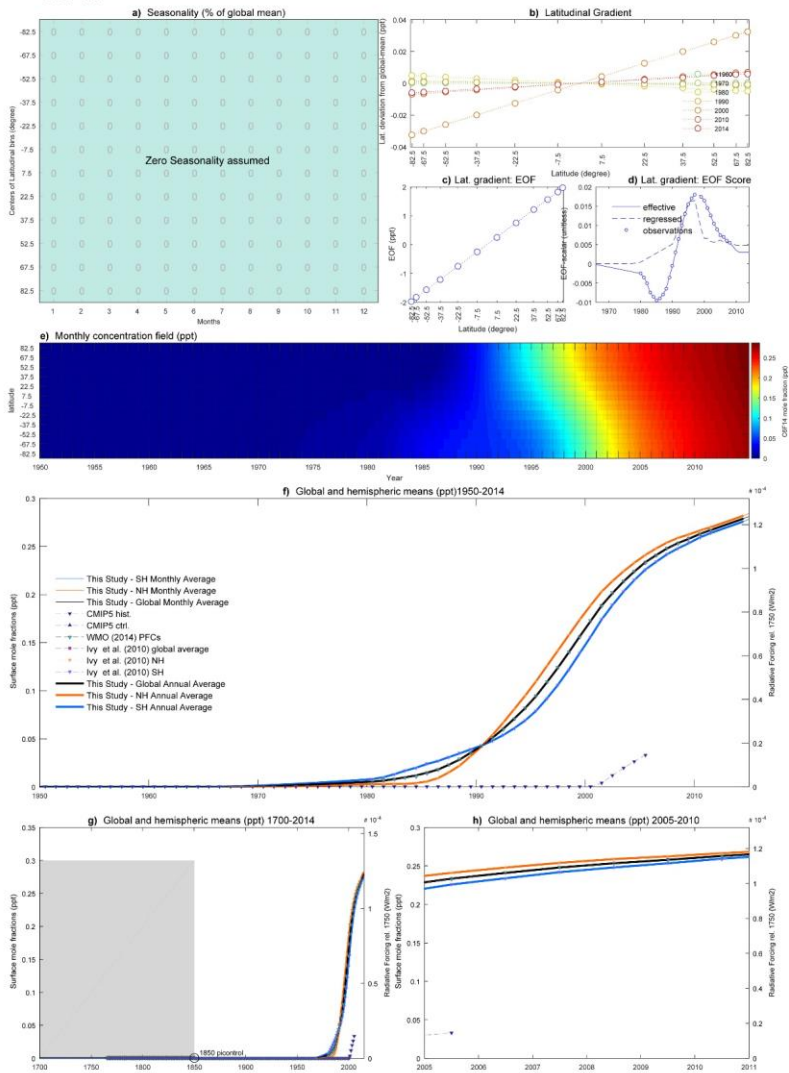


Figure 44—C6F14 Factsheet

C7F16

PFC-61-16 (n-C7F16) Lifetime: 3000yrs ; Radiative Efficiency : 0.5 Wm²/ppb

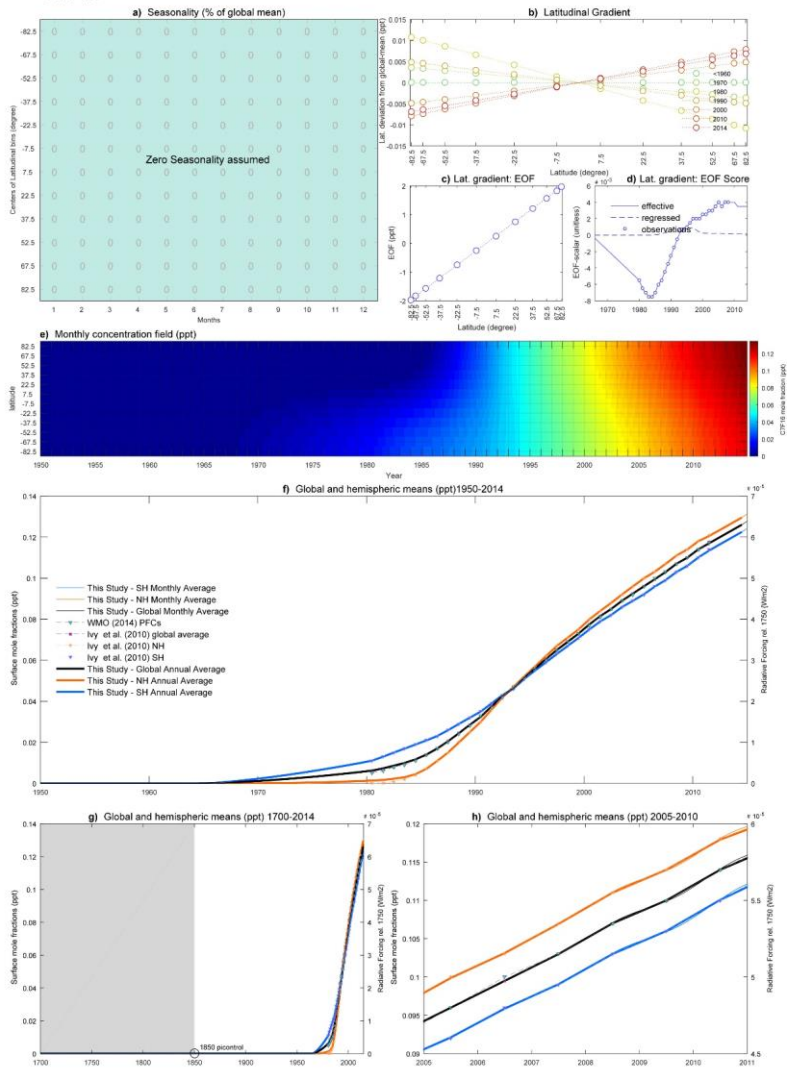


Figure 45 – C7E16 Factsheet

C8F18

PF-C71-18 (C8F18): Lifetime: 3000yrs ; Radiative Efficiency: 0.55 W/m2/ppb

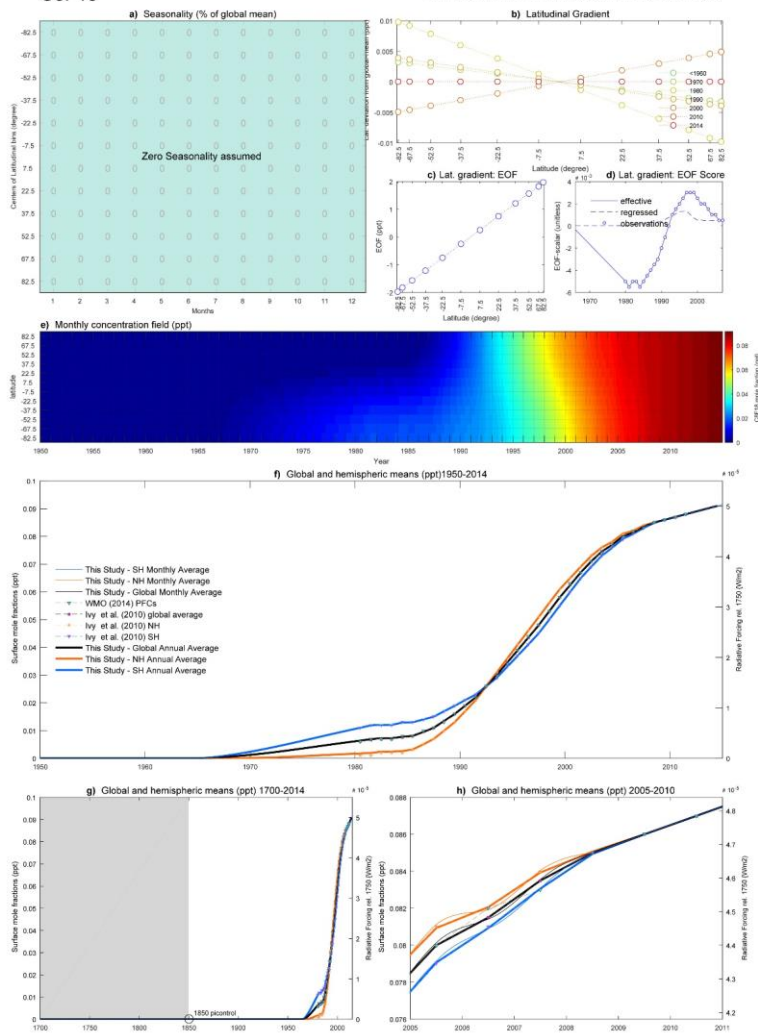


Figure 46 – C8E18 Factsheet

c-C4F8

PFC-318 (c-C4F8): Lifetime: 3200yrs; Radiative Efficiency: 0.32 W/m²/ppb

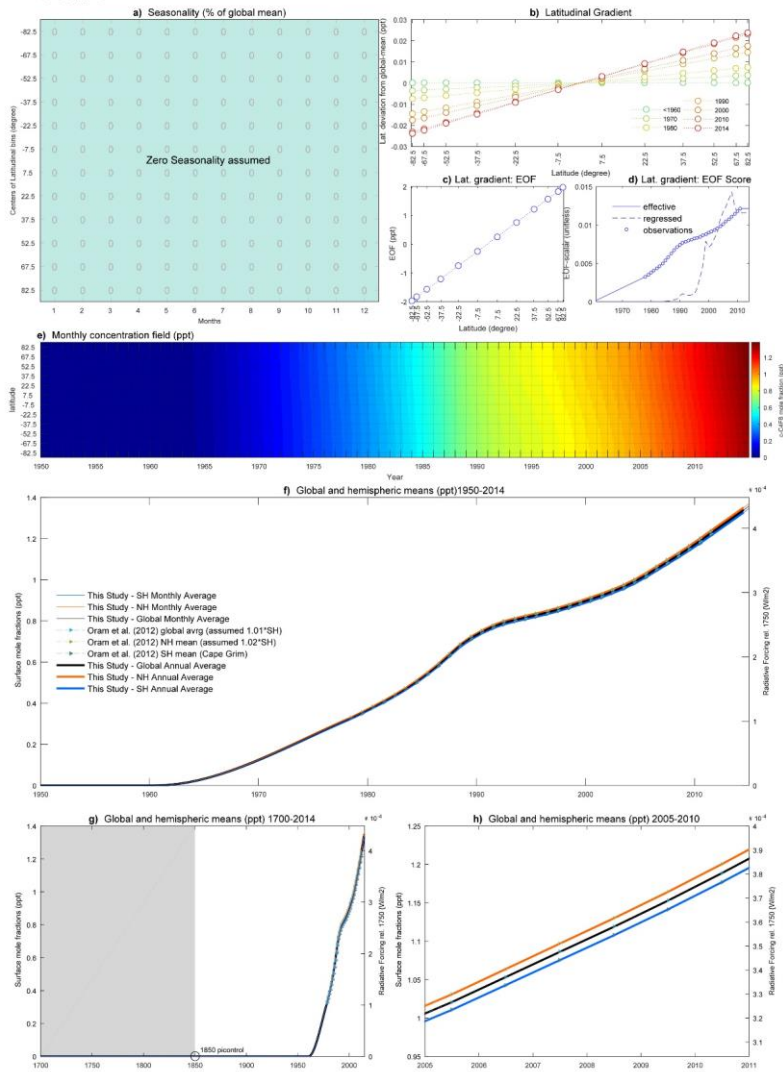


Figure 47—c-C4F8 Factsheet

CF4

PFC-14 (CF4): Lifetime: 50000yrs - Radiative Efficiency: 0.09 W/m2/ppb

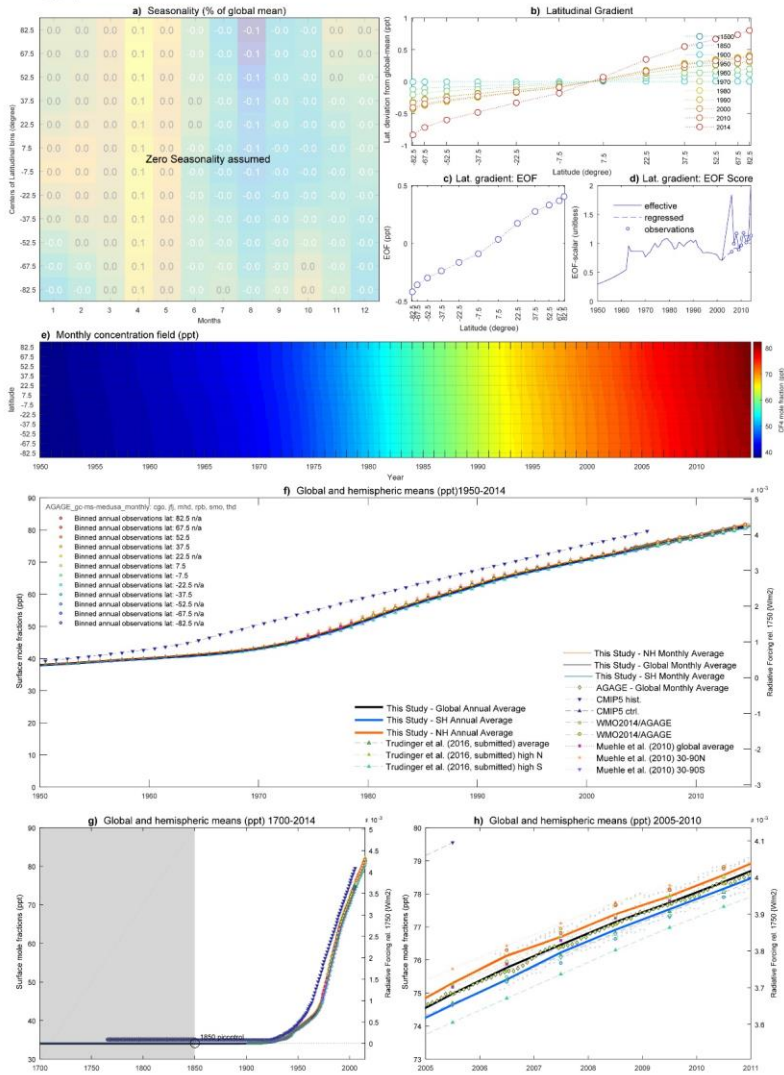


Figure 48 – CF4 Factsheet

HFC-23

HFC-23 (CHF₃) Lifetime: 222yrs Radiative Efficiency: 0.18 Wm²/ppb

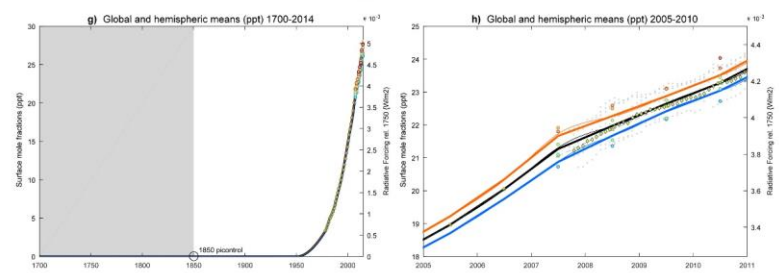
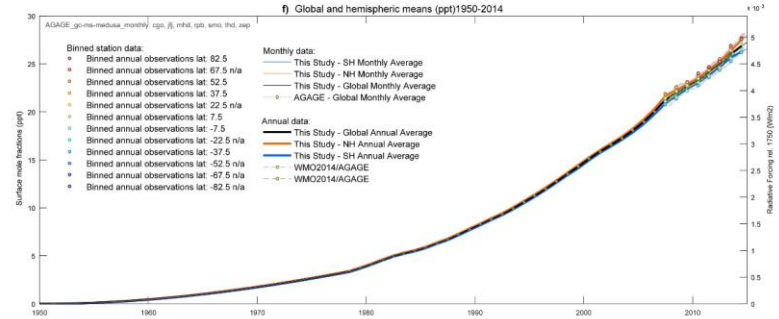
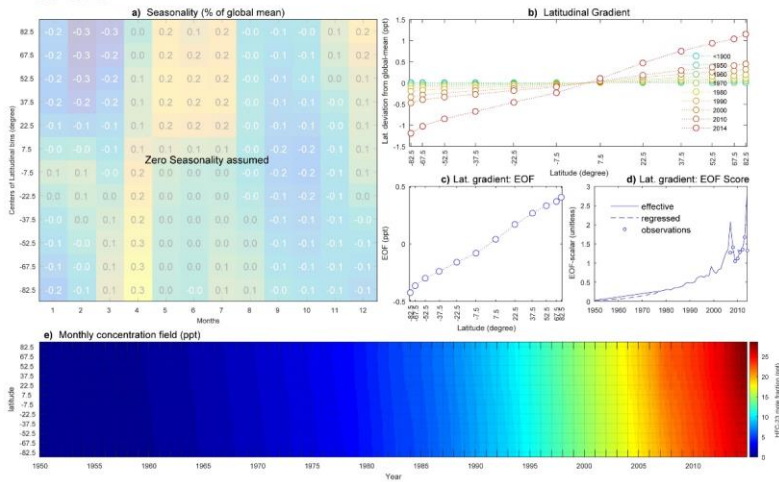


Figure 49—HFC-23 Factsheet

HFC-32

HFC-32 (CH2F2): Lifetime: 5.2yrs ; Radiative Efficiency : 0.11 Wm2/ppb

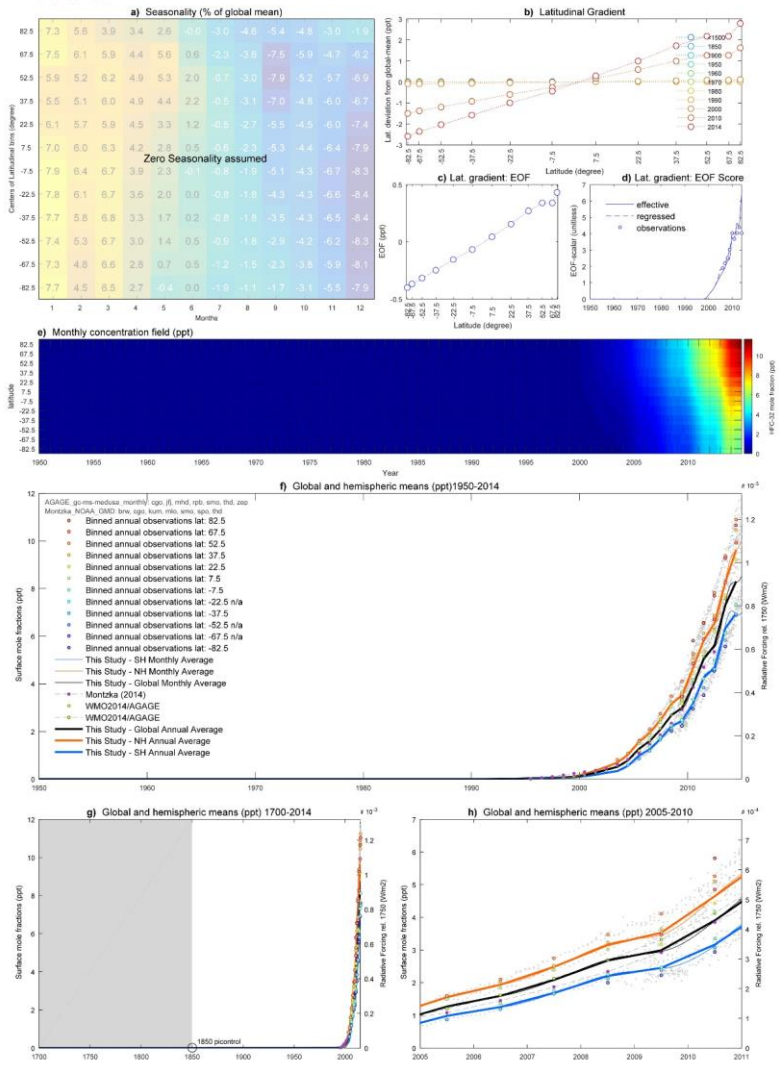


Figure 50—HFC-32 Factsheet

HFC-43-10mee

HFC-43-10mee (CF3CHFCHF2CF3) Lifetime: 16 yrs ; Radiative Efficiency: 0.42 W/m2ppb

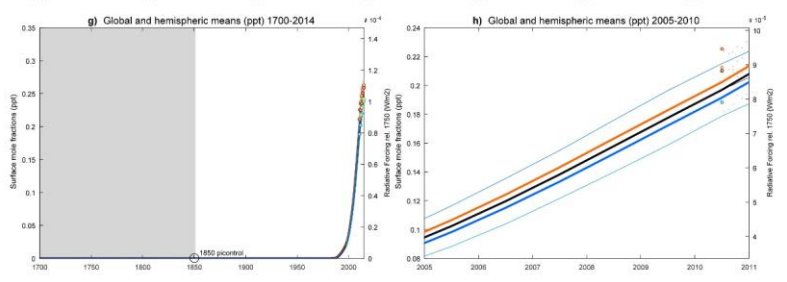
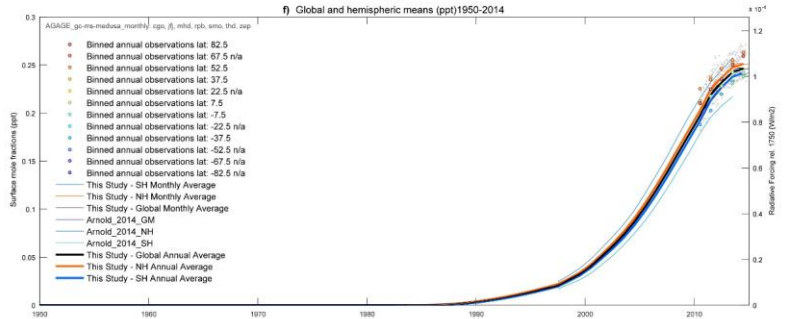
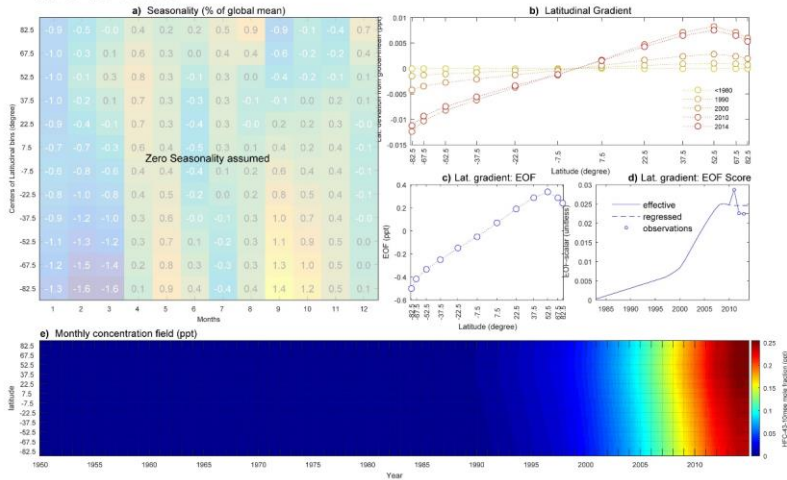


Figure 51—HFC-43-10-mee Factsheet

HFC-125

HFC-125 (CHF₂CF₃): Lifetime: 28.2yrs ; Radiative Efficiency : 0.23 Wm²/ppb

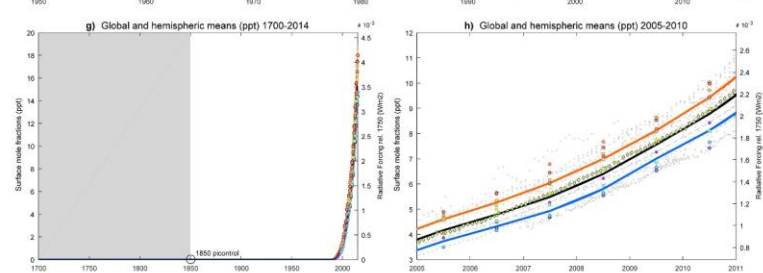
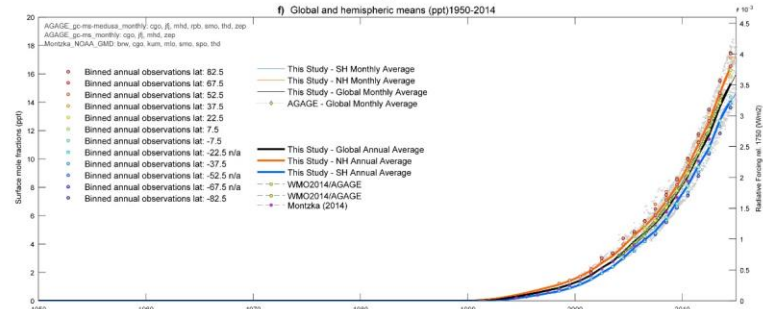
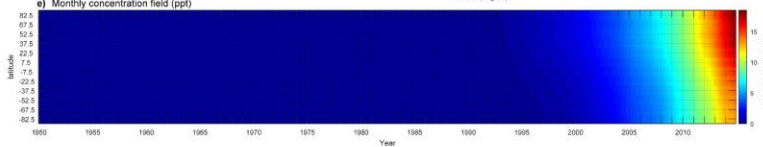
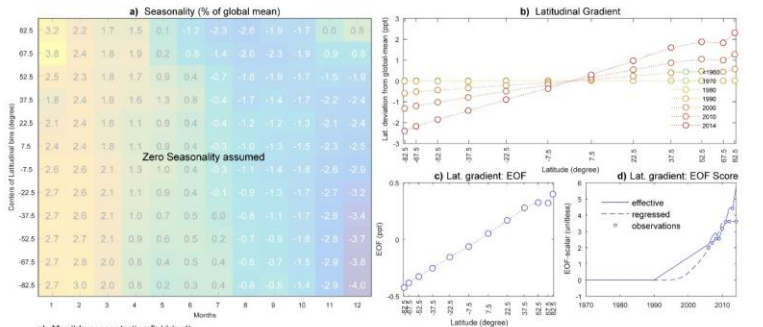


Figure 52—HFC-125 Factsheet

HFC-134a

HFC-134a (CH₂FCF₃): Lifetime: 13.4yrs ; Radiative Efficiency : 0.16 Wm²ppb

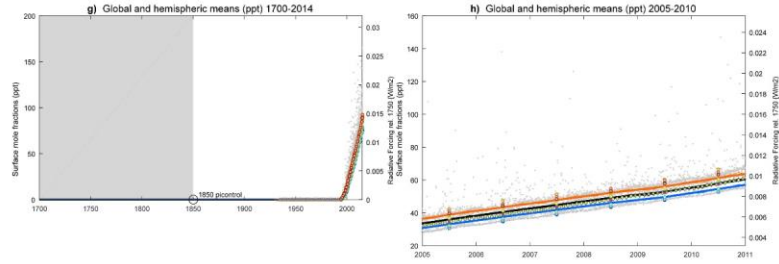
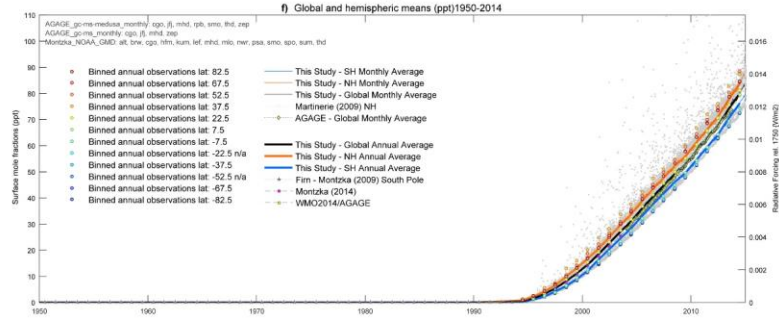
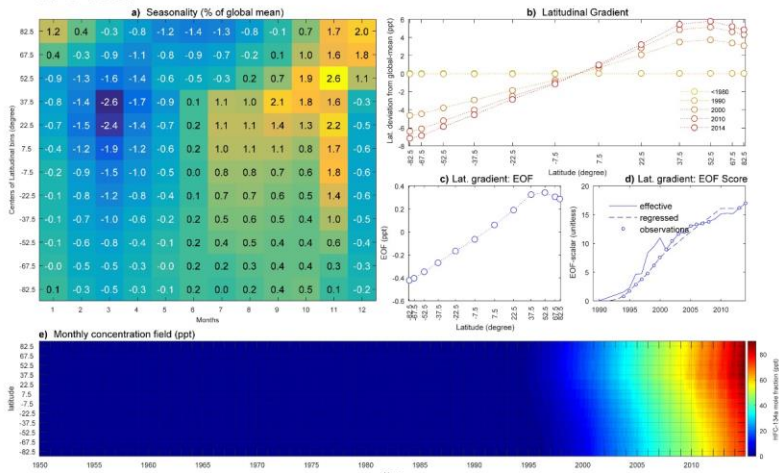


Figure 53—HFC-134a Factsheet

HFC-143a

HFC-143a (CH3CF3) Lifetime: 47.1yrs ; Radiative Efficiency : 0.16 Wm2/ppb

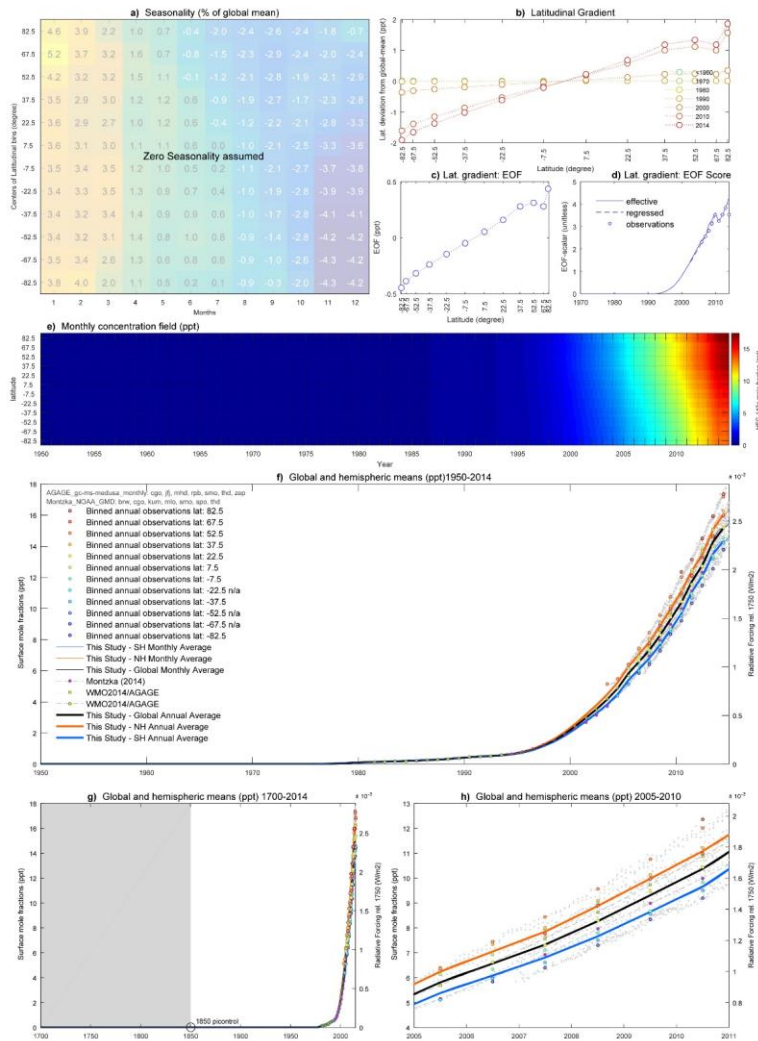


Figure 54—HFC-143a Factsheet

HFC-152a

HFC-152a (CH₃CHF₂): Lifetime: 1.5yrs ; Radiative Efficiency: 0.1 Wm²/ppb

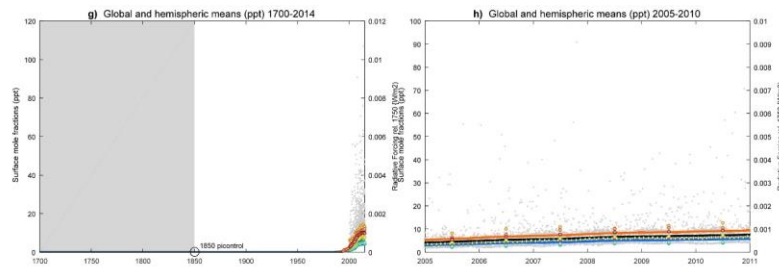
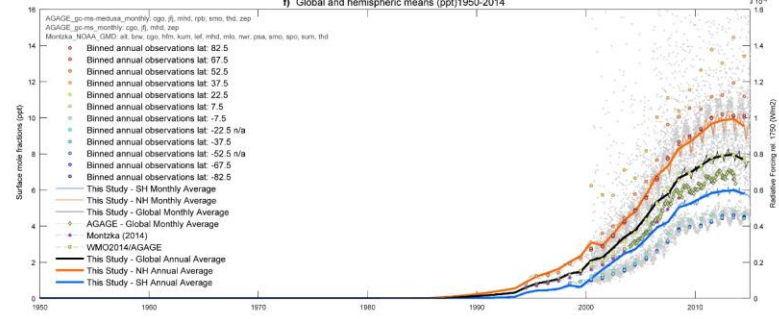
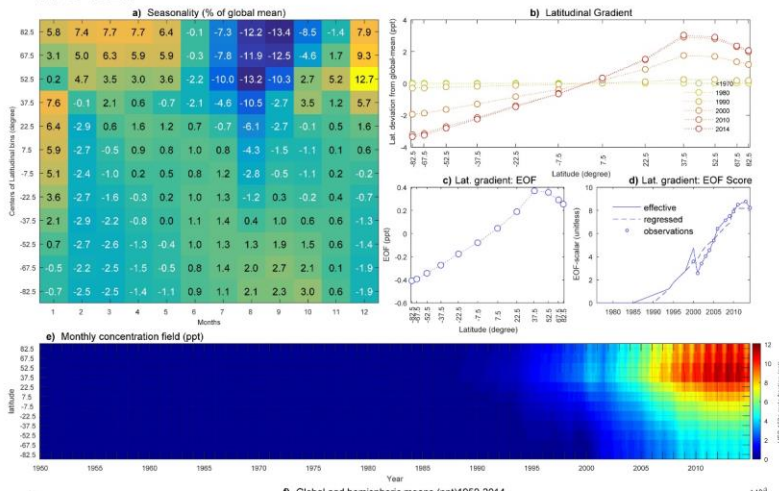


Figure 55—HFC-152a Factsheet

HFC-227ea

HFC-227ea (CF₃CHF₂F₃): Lifetime: 38.9yrs ; Radiative Efficiency : 0.26 Wm²/ppb

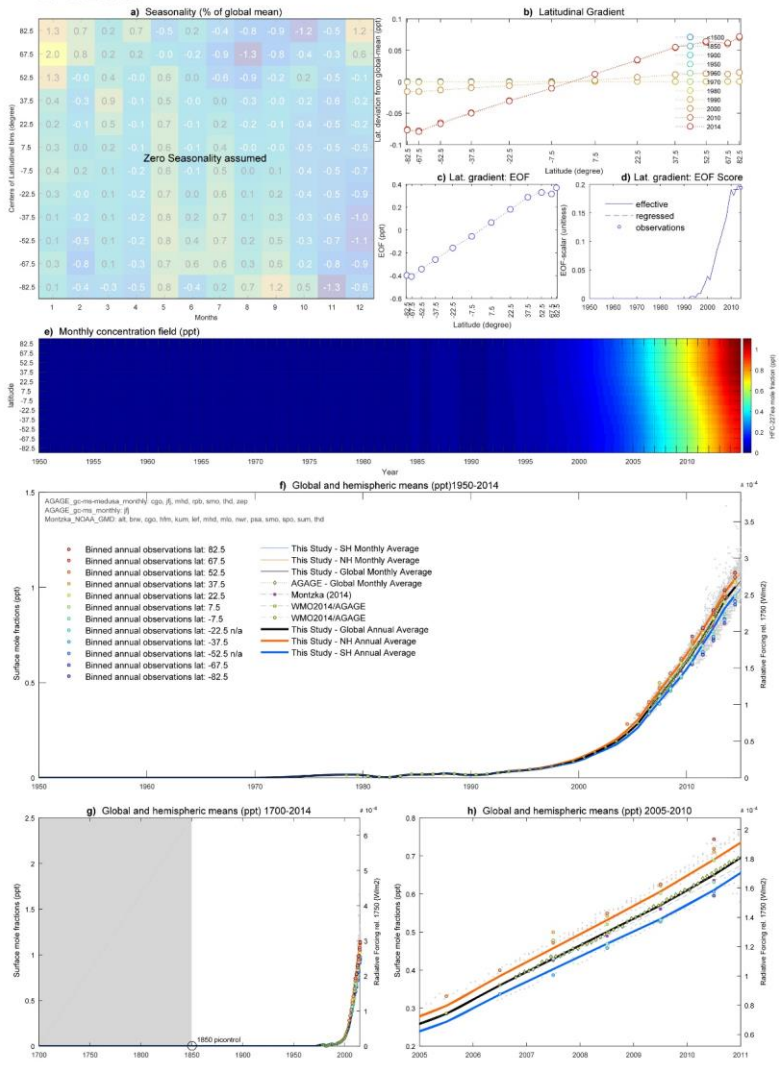


Figure 56 – HFC-227ea Factsheet

HFC-236fa

HFC-236fa (CF3CH2CF3): Lifetime :242yrs ; Radiative Efficiency : 0.24 Wm2/ppb

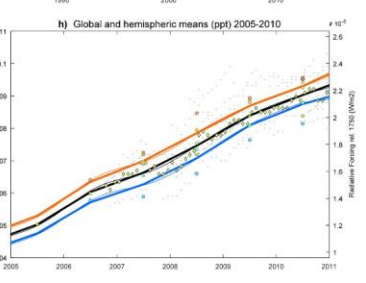
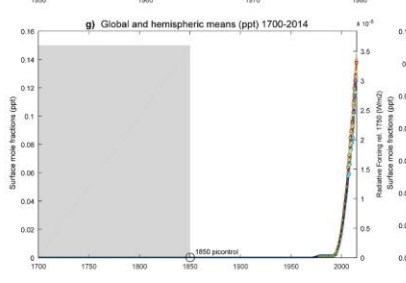
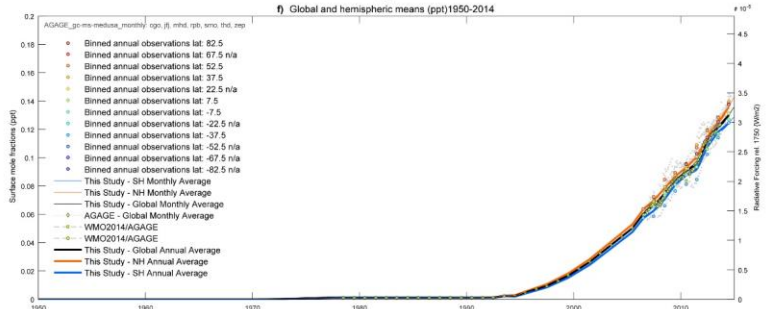
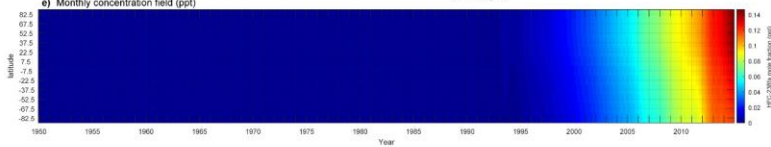
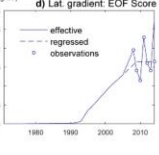
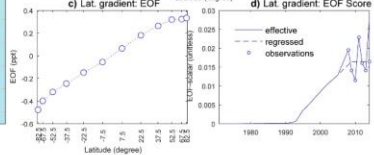
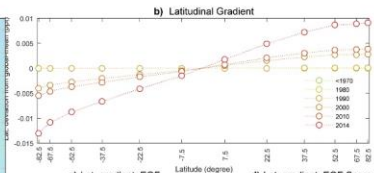
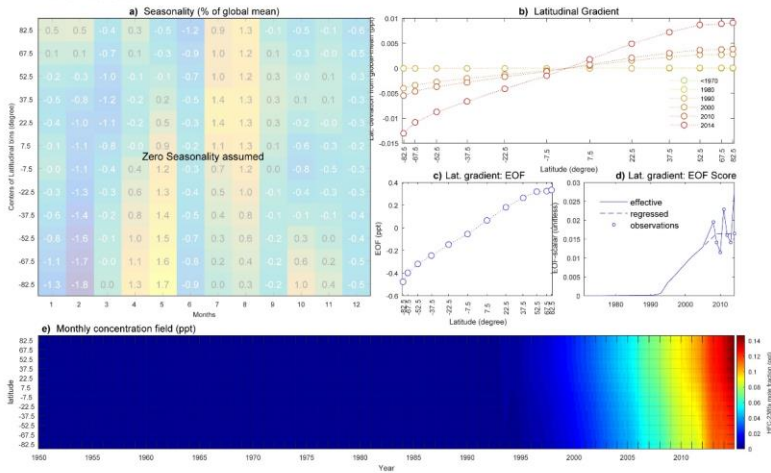
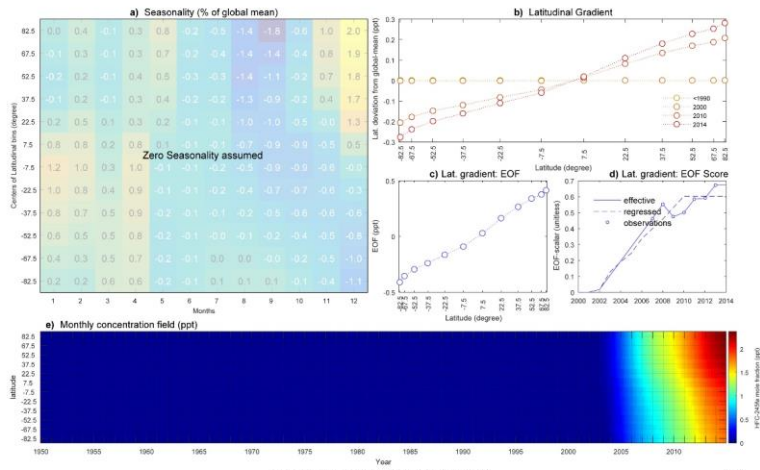


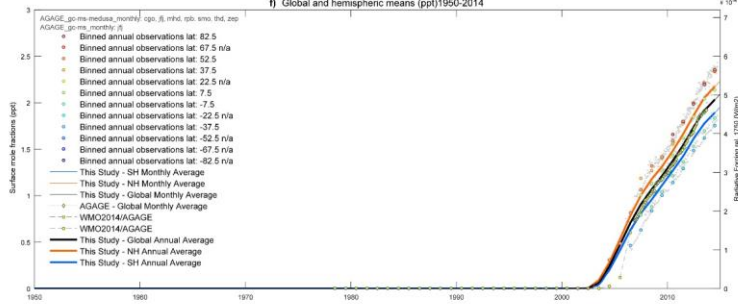
Figure 57—HFC-236fa Factsheet

HFC-245fa

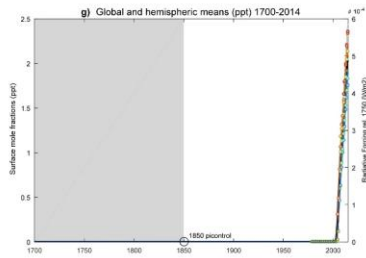
HFC-245fa (CHF2CH2CF3) Lifetime: 7.7yrs ; Radiative Efficiency : 0.24 Wm²/ppb



f) Global and hemispheric means (ppt)1950-2014



g) Global and hemispheric means (ppt) 1700-2014



h) Global and hemispheric means (ppt) 2005-2010

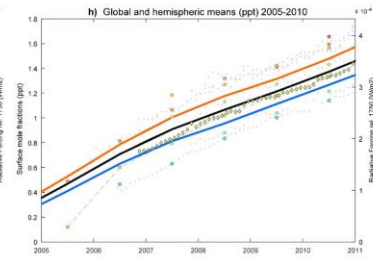


Figure 58—HFC-245fa Factsheet

Figure 59—HFC-365mfe Factsheet

NF3

Nitrogen trifluoride (NF3): Lifetime: 500yrs; Radiative Efficiency: 0.2 Wm²/ppb

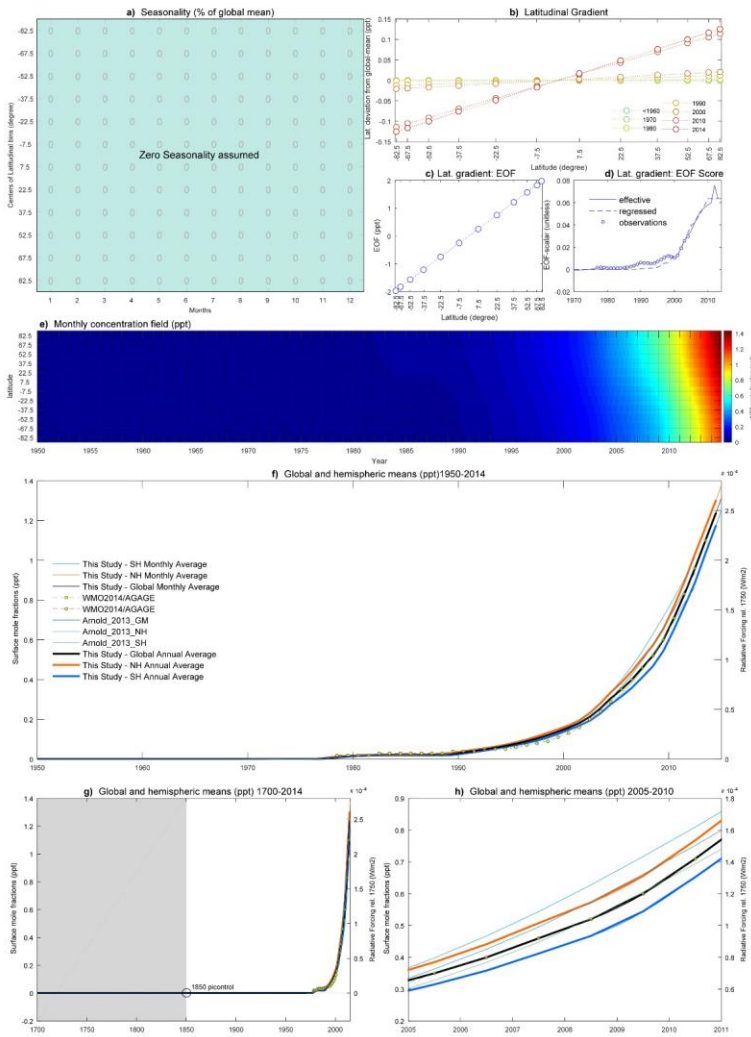


Figure 60—NF₃ Factsheet

Figure 61—SF₆ Factsheet

SO2F2

Sulphuryl fluoride (SO2F2) Lifetime: 36yrs ; Radiative Efficiency: 0.2 Wm2/ppb

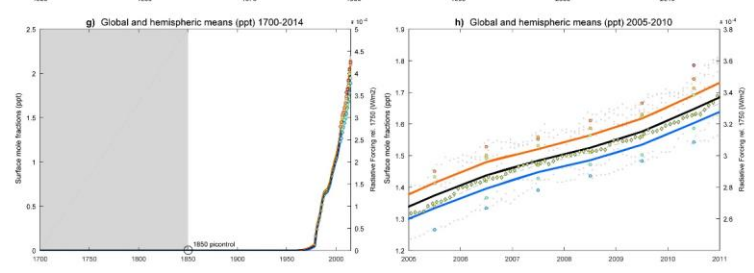
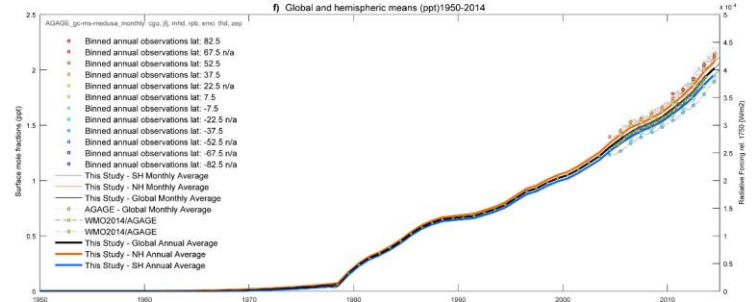
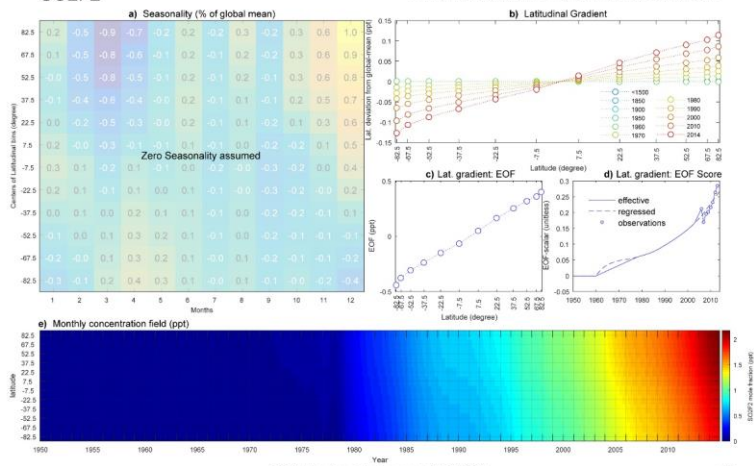


Figure 62—SO₂F₂ Factsheet

5

14—Appendix B: CMIP5 Analysis of CO₂ mixing ratio fields

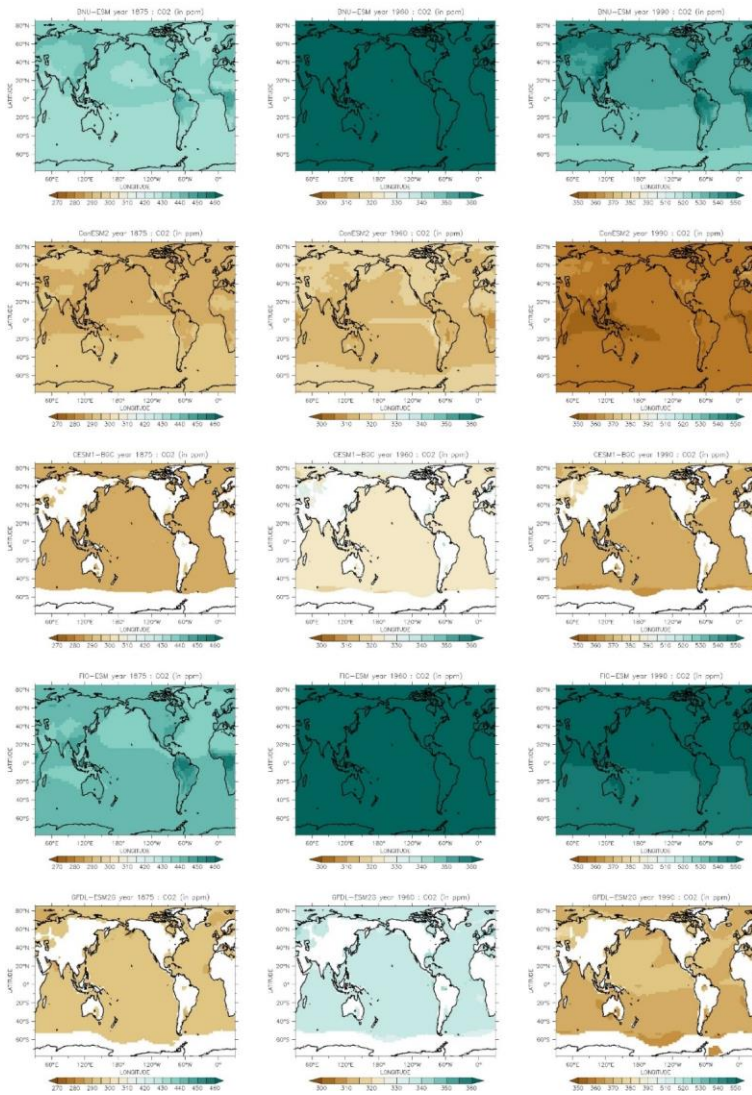


Figure 63— Annual average CO₂ mixing-ratioconcentration fields diagnosed from CMIP5 ESM models for the years 1875 (left column), 1960 (middle column), and 1990 (right column). All models are on the same colorcolour scale, with coloringcolouring steps at 5 ppmvppm. 1990 annual average CO₂ mixing-ratioconcentrations are estimated in this study to be 354.07 ppmvppm and had been specified for CMIP5 with 353.855 ppmvppm.

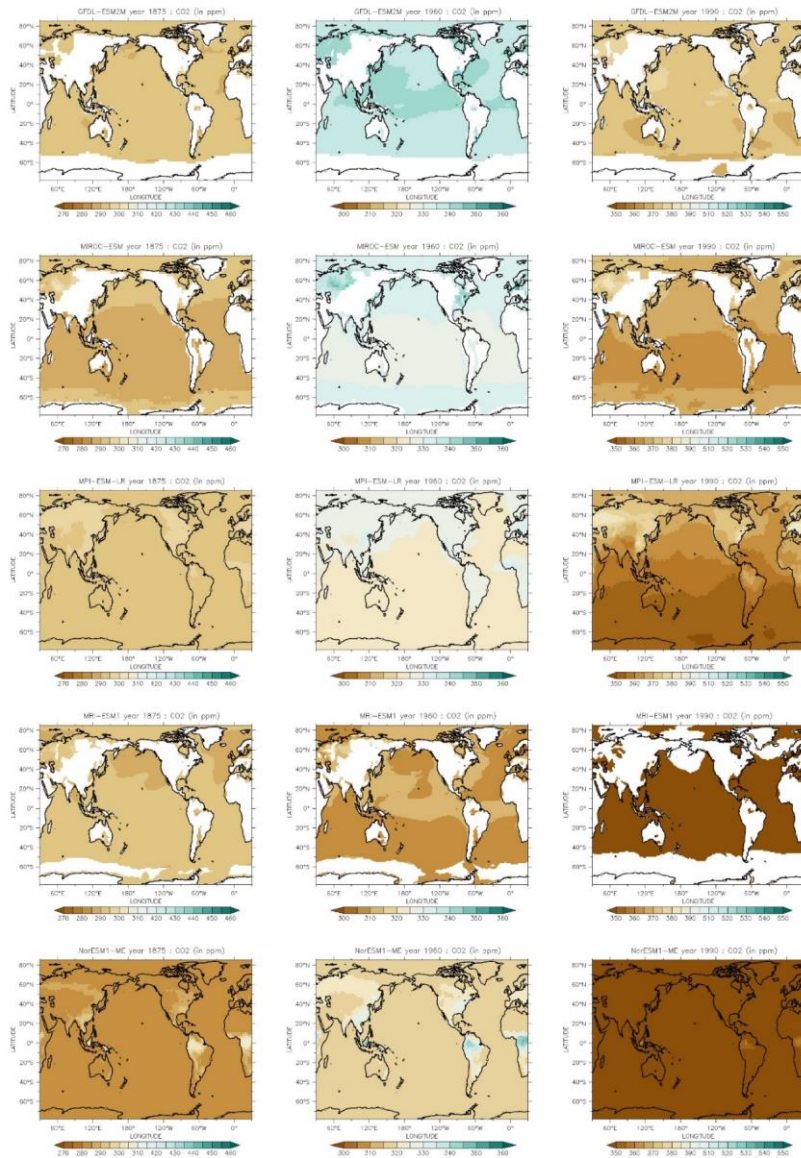


Figure 66 – As Figure 65, but for a different set of five CMIP5 ESM models.

15 References

- Ahn, J., E. J., and Brook, E. J.: [Siple Dome ice reveals two modes of millennial CO2 change during the last ice age](#), *Nature communications*, 5, 2014.
- 5 [Ahn, J., Brook, E. J., Mitchell, J. L., Rosen, J. R., McConnell, K. J. R., Taylor, D. K., Etheridge, D., and M. Rubino \(2012\)](#): Atmospheric CO2 over the last 1000 years: A high-resolution record from the West Antarctic Ice Sheet (WAIS) Divide ice core. *Global Biogeochemical Cycles*, 26(4), 2012.
- Anklin, M., J. Barnola, J. Schwander, B. J., Stauffer, B., and D. Raynaud (1995): Processes affecting the CO2 concentrations measured in Greenland ice. *Tellus B*, 47(4), 461-470, 1995.
- 10 [Arnold, T., C. M. Harth, J. C. M., Mühle, A. J., Manning, P. K. A. J., Salameh, J. P. K., Kim, D. J., Ivy, L. P. D. J., Steele, V. L. P., Petrenko, V. V., and J. P. Severinghaus \(2013\)](#): Nitrogen trifluoride global emissions estimated from updated atmospheric measurements. *Proceedings of the National Academy of Sciences*, 110(6), 2029-2034, 2013.
- 15 [Arnold, T., D. J. Ivy, C. M. D. J., Harth, C. M. K., Vollmer, J. M. K., Mühle, P. K. J., Salameh, L. P. K., Paul Steele, P. B. L., Krummel, R. H. P. B., Wang, R. H., and D. Young \(2014\)](#): HFC-43-10mee atmospheric abundances and global emission estimates. *Geophysical Research Letters*, 41(6), 2228-2235, 2014.
- [Aucott, M., A. McCulloch, F. A., Graedel, G. T., Kleiman, P. G., Midgley, P., and Li, Y. F. \(1999\)](#): Anthropogenic emissions of trichloromethane (chloroform, CHCl3) and chlorodifluoromethane (HCFC-22): Reactive chlorine emissions inventory. *Journal of Geophysical Research: Atmospheres*, 104(D7), 8405-8415, 1999.
- 20 [Aydin, M., Montzka, S., Battle, M., Williams, M., De Bruyn, W. J., Butler, J., Verhulst, K., Tatum, C., Gun, B., and Plotkin, D.](#): Post-core entrainment of modern air in some shallow ice cores collected near the firn-ice transition: evidence from CFC-12 measurements in Antarctic firn air and ice cores, *Atmospheric Chemistry and Physics*, 10, 5135-5144, 2010.
- 25 [Bacastow, R.](#): Modulation of atmospheric carbon dioxide by the Southern Oscillation, *Nature*, 261, 116-118, 1976.
- [Baker, D., R. Law, K. R., Gurney, P. K., Rayner, P., Peylin, A. P., Denning, P. A., Bousquet, L. P., Bruhwiler, V. H. L., Chen, Y. H., and P. Ciais \(2006\)](#): TransCom 3 inversion intercomparison: Impact of transport model errors on the interannual variability of regional CO2 fluxes, 1988-2003. *Global Biogeochemical Cycles*, 20(4), 2006.
- 30 [Barbante, C., J. M. Barnola, S. J. M., Becagli, J. S., Beer, M. J., Bigler, C. M., Boutron, F. C., Blunier, E. T., Castellano, E., Cattani, O., and J. Chappellaz \(2006\)](#): One-to-one coupling of glacial climate variability in Greenland and Antarctica. *Nature*, 444(7116), 195-198, 2006a.
- [Barnola, J., M. Anklin, J. Porcheron, D. Raynaud, J. Schwander and B. Stauffer \(1995\)](#): "CO2 evolution during the last millennium as recorded by Antarctic and Greenland ice." *Tellus B* 47(1-2): 264-272.
- 35 [Barbante, C., Barnola, J. M., Becagli, S., Beer, J., Bigler, M., Boutron, C., Blunier, T., Castellano, E., Cattani, O., Chappellaz, J., Dahl-Jensen, D., Debret, M., Delmonte, B., Dick, D., Falourd, S., Faria, S., Federer, U., Fischer, H., Freitag, J., Frenzel, A., Fritzsche, D., Fundel, F., Gabrielli, P., Gaspari, V., Gersonde, R., Graf, W., Grigoriev, D., Hamann, I., Hansson, M., Hoffmann, G., Hutterli, M. A., Huybrechts, P., Isaksson, E., Johnsen, S., Jouzel, J., Kaczmarek, M., Karlin, T., Kaufmann, P., Kipfstuhl, S., Kohno, M., Lambert, F., Lambrecht, A., Lambrecht, A., Landais, A., Lawer, G., Leuenberger, M., Littot, G., Loulergue, L., Luthi, D., Maggi, V., Marino, F., Masson-Delmotte, V., Meyer, H., Miller, H., Mulvaney, R., Narcisi, B., Oerlemans, J., Oerter, H., Parrenin, F., Petit, J. R., Raisbeck, G., Raynaud, D., Rothlisberger, R., Ruth, U., Rybak, O., Severi,](#)
- 40

- 5 [M., Schmitt, J., Schwander, J., Siegenthaler, U., Siggaard-Andersen, M. L., Spahni, R., Steffensen, J. P., Stenni, B., Stocker, T. F., Tison, J. L., Traversi, R., Udisti, R., Valero-Delgado, F., van den Broeke, M. R., van de Wal, R. S. W., Wagenbach, D., Wegner, A., Weiler, K., Wilhelms, F., Winther, J. G., Wolff, E., and Members, E. C.: One-to-one coupling of glacial climate variability in Greenland and Antarctica, *Nature*, **444**, 195-198, 2006b.](#)
- [Barnola, J., Anklin, M., Porcheron, J., Raynaud, D., Schwander, J., and Stauffer, B.: CO2 evolution during the last millennium as recorded by Antarctic and Greenland ice, *Tellus B*, **47**, 264-272, 1995.](#)
- [Bastos, A., Ciais, P., Barichivich, J., Bopp, L., Brovkin, V., Gasser, T., Peng, S., Pongratz, J., Viovy, N., and Trudinger, C. M.: Re-evaluating the 1940s CO2 plateau, *Biogeosciences*, **13**, 4877-4897, 2016.](#)
- 10 [Battle, M., Bender, M., Sowerst, T., Tansi, P., Butleri, J., Elkins, J., Ellis, J., Conway, T., Zhangt, N., and Langt, P.: Atmospheric gas concentrations over the past century measured in air from firn at, *Nature*, **383**, 19, 1996.](#)
- [Bauska, T. K., Joos, A. G. F., Mix, R. A. C., Roth, J. R., Ahn, J., and Brook, E. J.: Links between atmospheric carbon dioxide, the land carbon reservoir and climate over the past millennium, *Nature Geoscience*, **8**\(5\), 383-387, 2015.](#)
- 15 [Bereiter, B., Eggleston, S., Schmitt, J., Nehrass-Ahles, F. C., Stocker, H. T. F., Fischer, S. H., Kipfstuhl, S., and Chappellaz, J.: Revision of the EPICA Dome C CO2 record from 800 to 600 kyr before present, *Geophysical Research Letters*, **42**\(2\), 542-549, 2015.](#)
- [Bereiter, B., Lüthi, D., Siegrist, M., Schüpbach, S., Stocker, T. F., and Fischer, H.: Mode change of millennial CO2 variability during the last glacial cycle associated with a bipolar marine carbon seesaw, *Proceedings of the National Academy of Sciences*, **109**, 9755-9760, 2012.](#)
- 20 [Boden, T. A., Marland, G., and Andres, R. J.: Global, Regional, and National Fossil-Fuel CO2 Emissions—Oak Ridge, Tenn., USA., Carbon Dioxide Information Analysis Center, Oak Ridge National Laboratory, U.S. Department of Energy, Oak Ridge, Tenn., USA., 2013.](#)
- 25 [Buizert, C., Martinerie, V. V. P., Petrenko, J. P. V., Severinghaus, C. M. J. P., Trudinger, E. C. M., Witrant, J. L. E., Rosen, A. J. L., Orsi, M. A. J., Rubino, D. M., Etheridge, L. P. D. M., Steele, G. L. P., Hogan, J. C., Laube, W. T. J. C., Sturges, V. A. W. T., Levchenko, V. A. M., Smith, L. A. M., Levin, T. J., Conway, T. J., Dlugokencky, P. M. E. J., Lang, K. P. M., Kawamura, T. M. K., Jenk, J. W. C. T. M., White, T. J. W. C., Sowers, J. T., Schwander, J., and Blunier, T.: Gas transport in firn: multiple-tracer characterisation and model intercomparison for NEEM, Northern Greenland, *Atmos. Chem. Phys.*, **12**\(9\), 4259-4277, 2012.](#)
- 30 [Butler, J. H., Battle, M., Bender, S. A. M. L., Montzka, S. A. D., Clarke, E. S. A. D., Saltzman, C. M. E. S., Sucher, J. P. C. M., Severinghaus, J. P., and Elkins, J. W.: A record of atmospheric halocarbons during the twentieth century from polar firn air, *Nature*, **399**\(6738\), 749-755, 1999.](#)
- [Capron, E., Landais, B. A., Lemieux-Dudon, A. B., Schilt, V. A., Masson-Delmotte, D. V., Buiron, J. D., Chappellaz, J., Dahl-Jensen, S. D., Johnsen, S., and Leuenberger, M.: Synchronising EDML and NorthGRIP ice cores using \$\delta\$ 18 O of atmospheric oxygen \(\$\delta\$ 18 O atm\) and CH4 measurements over MIS5 \(80–123 kyr\), *Quaternary Science Reviews*, **29**\(4\), 222-234, 2010.](#)
- 35 [Conway, T. J., Tans, P. P., Waterman, K. W. L. S., Thoning, K. A. W., Masarie, K. A., and Gammon, R. H.: Atmospheric carbon dioxide measurements in the remote global troposphere, 1981–1984, *Tellus B*, **40B**\(2\), 81-115, 1988.](#)
- 40 [Conway, T. J., Tans, P. P., Waterman, K. W. L. S., Thoning, D. R. K. W., Kitzis, K. A. D. R., Masarie, K. A., and Zhang, N.: Evidence for interannual variability of the carbon cycle from the National Oceanic and Atmospheric Administration/Climate Monitoring and Diagnostics Laboratory Global Air Sampling Network, *Journal of Geophysical Research: Atmospheres*, **99**\(D11\), 22831-22855, 1994.](#)

[Cooperative Global Atmospheric Data Integration Project \(2013\). Multi-laboratory compilation of synchronized and gap-filled atmospheric carbon dioxide records for the period 1979–2012 \(obspack_co2_1_GLOBALVIEW-CO2_2013_v1.0.4_2013_12_23\)](#). C. NOAA Global Monitoring Division: Boulder, U.S.A.

- 5 Cox, M., [G. Sturrock](#), [P. G.](#), [Fraser, S. P.](#), [Siems, P. S.](#), [Krummel, P.](#), and [S. O'doherty \(2003\)](#). ["S.": Regional sources of methyl chloride, chloroform and dichloromethane identified from AGAGE observations at Cape Grim, Tasmania, 1998–2000](#). [Journal of atmospheric chemistry](#), 45(1), 79-99, 2003.
- 10 Cunnold, D., [L. Steele](#), [P. L.](#), [Fraser, P.](#), [Simmonds, R. P.](#), [Prinn, R.](#), [Weiss, T. R.](#), [Porter, S. L.](#), [O'Doherty, R. S.](#), [Langenfelds, R.](#), and [P. Krummel \(2002\)](#). ["P.": In situ measurements of atmospheric methane at GAGE/AGAGE sites during 1985–2000 and resulting source inferences](#). [Journal of Geophysical Research: Atmospheres](#), 107(D14), 2002.
- 15 Cunnold, D., [R. Weiss](#), [R. Prinn](#), [D. R.](#), [Hartley, P. D.](#), [Simmonds, P.](#), [Fraser, B. P.](#), [Miller, F. B.](#), [Alyea, F.](#), and [L. Porter \(1997\)](#). ["L.": GAGE/AGAGE measurements indicating reductions in global emissions of CCl3F and CCl2F2 in 1992–1994](#). [Journal of Geophysical Research: Atmospheres](#), 102(D1), 1259-1269, 1997.
- 20 Dahl-Jensen, D., [M. Albert](#), [A. M.](#), [Aldahan, N. A.](#), [Azuma, D. N.](#), [Balslev-Clausen, M. D.](#), [Baumgartner, A. M.](#), [Berggren, A. M.](#), [Bigler, T. M.](#), [Binder, T.](#), and [T. Blunier \(2013\)](#). ["T.": Eemian interglacial reconstructed from a Greenland folded ice core](#). [Nature](#), 493(7433), 489-494, 2013.
- 25 Denning, A. S., [T. Y. Fung](#), [I. Y.](#), and [D. Randall \(1995\)](#). ["D.": Latitudinal gradient of atmospheric CO2 due to seasonal exchange with land biota](#). [Nature](#), 376(6537), 240-243, 1995.
- 30 Denning, A. S., [T. Takahashi, T.](#), and [P. Friedlingstein \(1999\)](#). ["P.": Can a strong atmospheric CO2 rectifier effect be reconciled with a "reasonable" carbon budget?](#) [Tellus B](#), 51(2), 249-253, 1999.
- 35 Dlugokencky, E. J., [L. Bruhwiler, J. W. C. L.](#), [White, T. K. J. W. C.](#), [Emmons, P. C. L. K.](#), [Novelli, S. A. P. C.](#), [Montzka, S. A.](#), [Masarie, P. M. K. A.](#), [Lang, P. M.](#), [Crotwell, J. B. A. M.](#), [Miller, J. B.](#), and [L. V. Gatti \(2009\)](#). ["L. V.": Observational constraints on recent increases in the atmospheric CH4 burden](#). [Geophysical Research Letters](#), 36(18), n/a-n/a, 2009.
- 40 Dlugokencky, E. J., [K. A. Masarie, P. M. K. A.](#), [Lang, P. M.](#), [Tans, L. P. P.](#), [Steele, L. P.](#), and [E. G. Nisbet \(1994a\)](#). ["E. G.": A dramatic decrease in the growth rate of atmospheric methane in the northern hemisphere during 1992](#). [Geophysical Research Letters](#), 21(1), 45-48, 1994a.
- 45 Dlugokencky, E. J., [K. A. Masarie, P. M. K. A.](#), [Lang, P. M.](#), and [P. Tans \(1998\)](#). ["P. P.": Continuing decline in the growth rate of the atmospheric methane burden](#). [Nature](#), 393(6684), 447-450, 1998.
- 50 Dlugokencky, E. J., [R. C. Myers, P. M. R. C.](#), [Lang, K. A. P. M.](#), [Masarie, K. A. M.](#), [Crotwell, K. W. A. M.](#), [Thoning, B. D. K. W.](#), [Hall, J. W. B. D.](#), [Elkins, J. W.](#), and [L. P. Steele \(2005\)](#). ["L. P.": Conversion of NOAA atmospheric dry air CH4 mole fractions to a gravimetrically prepared standard scale](#). [Journal of Geophysical Research: Atmospheres](#), 110(D18), n/a-n/a, 2005.
- 55 Dlugokencky, E. J., [P. M. Lang, A. M. Crotwell, K. A. Masarie, and M. J. Crotwell \(2015a\)](#). ["P. P.": Atmospheric Methane Dry Air Mole Fractions from the NOAA ESRL Carbon Cycle Cooperative Global Air Sampling Network, 1983–2014](#). NOAA (Ed.), 2015a.
- 60 Dlugokencky, E. J., [P. M. Lang, K. A. Masarie, A. M. Crotwell, M. J. Crotwell \(2015b\)](#). ["P. P.": Atmospheric Carbon Dioxide Dry Air Mole Fractions from the NOAA ESRL Carbon Cycle Cooperative Global Air Sampling Network, 1968–2014](#). NOAA (Ed.), 2015b.
- 65 Dlugokencky, E. J., [L. P. Steele, L. P. M.](#), [Lang, P. M.](#), and [K. A. Masarie \(1994b\)](#). ["K. A.": The Growth-Rate and Distribution of Atmospheric Methane](#). [Journal of Geophysical Research: Atmospheres, J. Geophys. Res.-Atmos.](#), 99(D8), 17021-17043, 1994b.

- Dlugokencky, E. J., L. P. Dlugokencky, E. J., Steele, L. P., M., Lang, P. M., and K. A. Masarie (1994c). "K. A.: The growth rate and distribution of atmospheric methane." *Journal of Geophysical Research: Atmospheres*, 99(D8), 17021-17043, 1994c.
- 5 Dlugokencky, E. J., Dlugokencky, E. J., B. P., Walter, K. A. B. P., Masarie, P. M., K. A., Lang, P. M., and E. S. Kasischke (2001). "E. S.: Measurements of an anomalous global methane increase during 1998." *Geophysical Research Letters*, 28(3), 499-502, 2001.
- Elkins, J., Thompson, T., Swanson, T., Butler, J., Hall, B., Cummings, S., Fisher, D., and Raffo, A.: Decrease in the growth rates of atmospheric chlorofluorocarbons 11 and 12, *Nature*, 364, 780-783, 1993.
- 10 Enting, I. and J. Mansbridge (1989). "Seasonal sources and sinks of atmospheric CO₂ direct inversion of filtered data." *Tellus B*, 41(2).
- Enting, I. and J. Mansbridge (1991). "J.: Latitudinal distribution of sources and sinks of CO₂: Results of an inversion study." *Tellus B*, 43(2), 156-170, 1991.
- Enting, I. and Mansbridge, J.: Seasonal sources and sinks of atmospheric CO₂ direct inversion of filtered data, *Tellus B*, 41, 1989.
- 15 Enting, I., C. Trudinger, C., and R. Francey (1995). "R.: A synthesis inversion of the concentration and δ¹³C of atmospheric CO₂." *Tellus B*, 47(1-2), 35-52, 1995.
- Enting, I. G. (1998). "Green's function methods of tracer inversion, Wiley Online Library, 1998.
- Etheridge, D., L. P., M., Steele, R. L. P., Francey, R. J., and R. Langenfelds (1998a). "R. L.: Atmospheric methane between 1000 AD and present: Evidence of anthropogenic emissions and climatic variability." *Journal of Geophysical Research: Atmospheres*, 103(D13), 15979-15993, 1998a.
- 20 Etheridge, D. M., L. P., Steele, L. P., Langenfelds, R. J., Francey, R. J., Barnola, J. M., and R. L. Langenfelds (1998b). "Atmospheric methane between 1000 AD and present: Evidence of anthropogenic emissions and climatic variability." *Journal of Geophysical Research: Atmospheres*, 103(D13), 15979-15993 Morgan, V. I.: ftp://ftp.ncdc.noaa.gov/pub/data/paleo/icecore/antarctica/law/law_co2.txt, last access: May 2007.
- 25 Etheridge, D. M., L. P., Steele, R. L. P., Langenfelds, R. J., Francey, R. J., Barnola, J. M., and V. I. Morgan (1998c). "Historical CO₂ record from the Law Dome DE08, DE08-2, and DSS ice cores." Retrieved May, 2007, from ftp://ftp.ncdc.noaa.gov/pub/data/paleo/icecore/antarctica/law/law_co2.txt.
- Etheridge, D. M., L. P., Steele, R. L., Langenfelds, R. J., Francey, J. M., Barnola, J. M., and V. I. Morgan (1996). "V. I.: Natural and anthropogenic changes in atmospheric CO₂ over the last 1000 years from air in Antarctic ice and firn." *Journal of Geophysical Research: Atmospheres*, 101(D2), 4115-4128, 1996.
- 30 Eyring, V., S. Bony, G. A. S., Meehl, C. G. A., Senior, B. C. A., Stevens, R. J. B., Stouffer, R. J., and K. E. Taylor (2015). "Overview of the Coupled Model Intercomparison Project Phase 6 (CMIP6) experimental design and organization." *Geosci. Model Dev. Discuss.*, 2015:10539-10583.
- 35 Eyring, V., S. Bony, G. A. Meehl, C. A. Senior, B. Stevens, R. J. Stouffer and K. E. Taylor (2016). "K. E.: Overview of the Coupled Model Intercomparison Project Phase 6 (CMIP6) experimental design and organization." *Geosci. Model Dev.*, 9(5), 1937-1958, 2016.
- Fluckiger, J., E. Monnin, B. E., Stauffer, J. B., Schwander, T. F. J., Stocker, T. F., Chappellaz, B. J., Raynaud, D., and J. M. Barnola (2002). "J. M.: High-resolution Holocene N₂O ice core record and its relationship with CH₄ and CO₂." *Global Biogeochemical Cycles*, 16(4), -, 2002.
- 40 Forkel, M., N. Carvalhais, C. N., Rödenbeck, R. C., Keeling, M. R., Heimann, K. M., Thonicke, S. K., Zaehle, S., and M. Reichstein (2016). "M.: Enhanced seasonal CO₂ exchange caused by amplified plant productivity in northern ecosystems." *Science*, 2016. aac4971, 2016.

- Francey, R. J. and ~~J. S.~~ Frederiksen ~~(2016)~~. ~~J. S.~~: The 2009–2010 step in atmospheric CO2 interhemispheric difference. *Biogeosciences*, 13(3), 873-885, [2016](#).
- Francey, R. J., ~~C. M.~~ Trudinger, ~~C. M.~~ van der Schoot, ~~R. M.~~ Law, ~~P. B. R. M.~~, Krummel, ~~R. L. P. B.~~, Langenfelds, ~~R. L.~~, Paul Steele, ~~C. E. L.~~, Allison, ~~A. R. C. E.~~, Stavert, ~~A. R. J.~~, Andres, ~~R. J.~~, and ~~C.~~ Rodenbeck ~~(2013)~~. ~~C.~~: Atmospheric verification of anthropogenic CO2 emission trends. *Nature Clim. Change*, 3(5), 520-524, [2013](#).
- Fraser, P., ~~D.~~ Cunnold, ~~F. D.~~, Aleya, ~~R. F.~~, Weiss, R., Prinn, ~~P. R.~~, Simmonds, ~~B. P.~~, Miller, ~~B.~~, and ~~R.~~ Langenfelds ~~(1996)~~. ~~R.~~: Lifetime and emission estimates of 1, 1, 2-trichlorotrifluoroethane (CFC-113) from daily global background observations June 1982–June 1994. *Journal of Geophysical Research: Atmospheres*, 101(D7), 12585-12599, [1996](#).
- Fung, I., ~~J.~~ John, ~~J.~~ Lerner, ~~E. J.~~, Matthews, ~~M. E.~~, Prather, ~~L. M.~~, Steele, ~~L.~~, and ~~P.~~ Fraser ~~(1991)~~. ~~P.~~: Three-dimensional model synthesis of the global methane cycle. *Journal of Geophysical Research: Atmospheres*, 96(D7), 13033-13065, [1991](#).
- Ghosh, A., ~~P. K.~~ Patra, ~~P. K.~~, Ishijima, ~~T. K.~~, Umezawa, ~~A. T.~~, Ito, ~~D. M. A.~~, Etheridge, ~~S. D. M.~~, Sugawara, ~~K. S.~~, Kawamura, ~~T. B. K.~~, Miller, ~~E. J. B.~~, Dlugokencky, ~~P. B. E. J.~~, Krummel, ~~P. B.~~, Fraser, ~~L. P. J.~~, Steele, ~~R. L. P.~~, Langenfelds, ~~C. M. R. L.~~, Trudinger, ~~J. W. C. M.~~, White, ~~B. J. W. C.~~, Vaughn, ~~T. B.~~, Saeki, ~~S. T.~~, Aoki, ~~S.~~, and ~~T.~~ Nakazawa ~~(2015)~~. ~~T.~~: Variations in global methane sources and sinks during 1910–2010. *Atmos. Chem. Phys.*, 15(5), 2595-2612, [2015](#).
- Graven, H. D., ~~R. F.~~ Keeling, ~~S. C. R. F.~~, Piper, ~~P. K. S. C.~~, Patra, ~~B. B. P. K.~~, Stephens, ~~S. C. B. B.~~, Wofsy, ~~L. R. S. C.~~, Welp, ~~C. L. R.~~, Sweeney, ~~P. P. C.~~, Tans, ~~J. P. P.~~, Kelley, ~~B. C. J. J.~~, Daube, ~~E. A. B. C.~~, Kort, ~~G. W. E. A.~~, Santoni, ~~G. W.~~, and ~~J. D.~~ Bent ~~(2013)~~. ~~J. D.~~: Enhanced Seasonal Exchange of CO2 by Northern Ecosystems Since 1960. *Science*, 341(6150), 1085-1089, [2013](#).
- Gray, J. M., ~~S.~~ Frolking, ~~E. A. S.~~, Kort, ~~D. K. E. A.~~, Ray, ~~C. J. D. K.~~, Kucharik, ~~N. C. J.~~, Ramankutty, ~~N.~~, and ~~M. A.~~ Friedl ~~(2014)~~. ~~M. A.~~: Direct human influence on atmospheric CO2 seasonality from increased cropland productivity. *Nature*, 515(7527), 398-401, [2014](#).
- Gurney, K. R., ~~R. M.~~ Law, ~~A. S. R. M.~~, Denning, ~~P. J. A. S.~~, Rayner, ~~D. P. J.~~, Baker, ~~P. D.~~, Bousquet, ~~L. P.~~, Bruhwiler, ~~Y. H. L.~~, Chen, ~~P. Y. H.~~, Ciais, ~~P.~~, and ~~S.~~ Fan ~~(2002)~~. ~~S.~~: Towards robust regional estimates of CO2 sources and sinks using atmospheric transport models. *Nature*, 415(6872), 626-630, [2002](#).
- Gurney, K. R., ~~R. M.~~ Law, ~~A. S. R. M.~~, Denning, ~~P. J. A. S.~~, Rayner, ~~D. P. J.~~, Baker, ~~P. D.~~, Bousquet, ~~L. P.~~, Bruhwiler, ~~Y. H. L.~~, CHEN, ~~P. Y. H.~~, Ciais, ~~P.~~, and ~~S.~~ Fan ~~(2003)~~. ~~S.~~: TransCom 3 CO2 inversion intercomparison: 1. Annual mean control results and sensitivity to transport and prior flux information. *Tellus B*, 55(2), 555-579, [2003](#).
- Gurney, K. R., ~~R. M.~~ Law, ~~A. S. R. M.~~, Denning, ~~P. J. A. S.~~, Rayner, ~~B. C. P. J.~~, Pak, ~~D. B. C.~~, Baker, ~~P. D.~~, Bousquet, ~~L. P.~~, Bruhwiler, ~~Y. H. L.~~, Chen, ~~Y. H.~~, and ~~P.~~ Ciais ~~(2004)~~. ~~P.~~: Transcom 3 inversion intercomparison: Model mean results for the estimation of seasonal carbon sources and sinks. *Global Biogeochemical Cycles*, 18(1), [2004](#).
- Gütschow, J., ~~M. L.~~ Jeffery, ~~R. M. L.~~, Gieseke, R., Gebel, ~~D. R.~~, Stevens, ~~M. D.~~, Krapp, ~~M.~~, and ~~M.~~ Rocha ~~(2016)~~. ~~M.~~: The PRIMAP-hist national historical emissions time series. *Earth Syst. Sci. Data Discuss.*, [2016](#), 1-44, [2016](#), 1-44.
- [Hall, B. D.](#), [Engel, A.](#), [Mühle, J.](#), [Elkins, J. W.](#), [Artuso, F.](#), [Atlas, E.](#), [Aydin, M.](#), [Blake, D.](#), [Brunke, E. G.](#), [Chiavarini, S.](#), [Fraser, P. J.](#), [Happell, J.](#), [Krummel, P. B.](#), [Levin, I.](#), [Loewenstein, M.](#), [Maione, M.](#), [Montzka, S. A.](#), [O'Doherty, S.](#), [Reimann, S.](#), [Rhoderick, G.](#), [Saltzman, E. S.](#), [Scheel, H. E.](#), [Steele, L. P.](#), [Vollmer, M. K.](#), [Weiss, R. F.](#),

- [Worthy, D., and Yokouchi, Y.: Results from the International Halocarbons in Air Comparison Experiment \(IHALACE\), Atmos. Meas. Tech., 7, 469-490, 2014.](#)
- Hurrell, J. W., ~~M. M. Holland, P. R. M. M., Gent, S. P. R., Ghan, J. E. S., Kay, P. J. E., Kushner, P. J. F., Lamarque, W. G. J. F., Large, D. W. G., Lawrence, K. D., Lindsay, W. H. K., Lipscomb, M. C. W. H., Long, A. M. C., Mahowald, D. R. N., Marsh, D. R. B., Neale, P. R. B., Rasch, S. P., Vavrus, M. S., Vertenstein, D. M., Bader, W. D., Collins, J. J. W. D., Hack, J. J., Kiehl, J., and S. Marshall (2013).~~ [S.: The Community Earth System Model: A Framework for Collaborative Research.](#) *Bulletin of the American Meteorological Society*, 94(9), 1339-1360, 2013.
- Hurttt, G., ~~L. P. Chini, S. L. P., Frolking, R. S., Betts, J. R., Feddema, G. J., Fischer, J. G., Fisk, K. J., Hibbard, R. K., Houghton, R., and A. Janetos (2011).~~ [A.: Harmonization of land-use scenarios for the period 1500–2100: 600 years of global gridded annual land-use transitions, wood harvest, and resulting secondary lands.](#) *Climatic Change*, 109(1-2), 117-161, 2011.
- IPCC (Ed. (2013).): [Climate Change 2013: The Physical Science Basis. Contribution of Working Group I to the Fifth Assessment Report of the Intergovernmental Panel on Climate Change.](#) Cambridge University Press, Cambridge, United Kingdom and New York, NY, USA, Cambridge University Press 2013.
- [Ishijima, K., Sugawara, S., Kawamura, K., Hashida, G., Morimoto, S., Murayama, S., Aoki, S., and Nakazawa, T.: Temporal variations of the atmospheric nitrous oxide concentration and its \$\delta^{15}\text{N}\$ and \$\delta^{18}\text{O}\$ for the latter half of the 20th century reconstructed from firn air analyses, Journal of Geophysical Research: Atmospheres, 112, 2007.](#)
- Ivy, D. J., ~~M. Rigby, M., Baasandorj, J. B. M., Burkholder, J. B., and R. G. Prinn (2012).~~ [R. G.: Global emission estimates and radiative impact of \$\text{C}_{4\text{F}_{10}}\$, \$\text{C}_{5\text{F}_{12}}\$, \$\text{C}_{6\text{F}_{14}}\$, and \$\text{C}_{7\text{F}_{16}}\$ and \$\text{C}_{8\text{F}_{18}}\$, C4F10, C5F12, C6F14, C7F16 and C8F18, Atmos. Chem. Phys., 12\(16\), 7635-7645, 2012.](#)
- Jones, C. D. and ~~P. M. Cox (2001).~~ [P. M.: Modeling the volcanic signal in the atmospheric CO2 record.](#) *Global Biogeochemical Cycles*, 15(2), 453-465, 2001.
- [Jungclaus, J., Bard, E., Baroni, M., Braconnot, P., Cao, J., Chini, L. P., Egorova, T., Evans, M., Gonzalez-Rouco, J. F., Krivova, N., LeGande, A. N., Lorenz, S. J., Luterbacher, J., Man, W., Meinshausen, M., Moberg, A., Nehrbass-Ahles, C., Otterå, O., Otto-Bliesner, B. L., Phipps, S. J., Pongratz, J., Rozanov, E., Schmidt, G. A., Schmitt, H., Schmutz, W., Schurer, A., Shapiro, A. I., Sigl, M., Smerdon, J. E., Solanki, S. K., Toohey, M., Timmreck, C., Usoskin, I., Wagner, S., Wu, C.-J., Yeo, K. L., Zanchettin, D., Zhang, D., and Zorita, E.: The PMIP4 simulations of the last millennium \(PMIP past1000\), in preparation. in preparation.](#)
- [Kageyama, M., Braconnot, P., Harrison, S. P., Haywood, A. M., Jungclaus, J., Otto-Bliesner, B. L., Peterschmitt, J. Y., Abe-Ouchi, A., Albani, S., Bartlein, P. J., Brierley, C., Crucifix, M., Dolan, A., Fernandez-Donado, L., Fischer, H., Hopcroft, P. O., Ivanovic, R. F., Lambert, F., Lunt, D. J., Mahowald, N. M., Peltier, W. R., Phipps, S. J., Roche, D. M., Schmidt, G. A., Tarasov, L., Valdes, P. J., Zhang, Q., and Zhou, T.: PMIP4-CMIP6: the contribution of the Paleoclimate Modelling Intercomparison Project to CMIP6, Geosci. Model Dev. Discuss., 2016, 1-46, 2016.](#)
- Keeling, C. D., ~~R. B. Bacastow, A. E. R. B., Bainbridge, G. A. E., Ekdahl, P. R. C. A., Guenther, L. S. P. R., Waterman, L. S., and J. F. Chin (1976).~~ [J. F.: Atmospheric carbon dioxide variations at Mauna Loa observatory, Hawaii.](#) *Tellus*, 28(6), 538-551, 1976.
- Keeling, C. D., ~~R. B. Bacastow, A. R. B., Carter, S. C. A., Piper, T. P. S. C., Whorf, M. T. P., Heimann, W. G. M., Mook, W. G., and H. Roeloffzen (1989a).~~ [H.: A three-dimensional model of atmospheric CO2 transport based](#)

- on observed winds: 1. Analysis of observational data¹². Aspects of climate variability in the Pacific and the Western Americas, [1989a](#), 165-236, [1989a](#).
- 5 [Keeling, C. D., S. C. Piper and M. Heimann \(1989b\)](#)¹². [Keeling, C. D., Piper, S. C., Bacastow, R. B., Wahlen, M., Whorf, T. P., Heimann, M., and Meijer, H. A.: Exchanges of atmospheric CO₂ and 13CO₂ with the terrestrial biosphere and oceans from 1978 to 2000. I. Global aspects, Scripps Institution of Oceanography, 2001, 2001.](#)
- [Keeling, C. D., Piper, S. C., and Heimann, M.:](#) A three-dimensional model of atmospheric CO₂ transport based on observed winds: 4. Mean annual gradients and interannual variations¹². Aspects of climate variability in the Pacific and the Western Americas, [1989b](#), 305-363, [1989b](#).
- 10 Keeling, C. D., ~~S. C. Piper~~, ~~T. P. S. C.~~, Whorf, T. P., and ~~R. F. Keeling (2011)~~¹², R. F.: Evolution of natural and anthropogenic fluxes of atmospheric CO₂ from 1957 to 2003¹². *Tellus B*, 63(1), 1-22, [2011](#).
- [Kirschke, S., Bousquet, P., Ciais, P., Saunoy, M., Canadell, J. G., Dlugokencky, E. J., Bergamaschi, P., Bergmann, D., Blake, D. R., Bruhwiler, L., Cameron-Smith, P., Castaldi, S., Chevallier, F., Feng, L., Fraser, A., Heimann, M., Hodson, E. L., Houweling, S., Josse, B., Fraser, P. J., Krummel, P. B., Lamarque, J.-F., Langenfelds, R. L., Le Quere, C., Naik, V., O'Doherty, S., Palmer, P. I., Pison, I., Plummer, D., Poulter, B., Prinn, R. G., Rigby, M., Ringeval, B., Santini, M., Schmidt, M., Shindell, D. T., Simpson, I. J., Spahni, R., Steele, L. P., Strode, S. A., Sudo, K., Szopa, S., van der Werf, G. R., Voulgarakis, A., van Weele, M., Weiss, R. F., Williams, J. E., and Zeng, G.: Three decades of global methane sources and sinks, *Nature Geosci*, 6, 813-823, \[2013\]\(#\).](#)
- 15 Kohlmaier, G. H., ~~E. O. Siré~~, ~~A. E. O.~~, Janecek, ~~C. D. A.~~, Keeling, ~~S. C. D.~~, Piper, ~~S. C.~~, and ~~R. Revelle (1989)~~¹², R.: Modelling the seasonal contribution of a CO₂ fertilization effect of the terrestrial vegetation to the amplitude increase in atmospheric CO₂ at Mauna Loa Observatory¹². *Tellus B*, 41(5), 487-510, [1989](#).
- 20 Komhyr, W. D., ~~R. H. Gammon~~, ~~T. B. R. H.~~, Harris, ~~L. S. T. B.~~, Waterman, ~~T. J. L. S.~~, Conway, ~~W. R. T. J.~~, Taylor, ~~W. R.~~, and ~~K. W. Thoning (1985)~~¹², K. W.: Global atmospheric CO₂ distribution and variations from 1968–1982 NOAA/GMCC CO₂ flask sample data¹². *Journal of Geophysical Research: Atmospheres*, 90(13), 5567-5596, [1985](#).
- 25 Komhyr, W. D., ~~L. S.~~ Waterman, ~~L. S.~~, and ~~W. R. Taylor (1983)~~¹², W. R.: Semiautomatic nondispersive infrared analyzer apparatus for CO₂ air sample analyses¹². *Journal of Geophysical Research: Oceans*, 88(62), 1315-1322, [1983](#).
- 30 Koppmann, R., ~~F. Johnen~~, ~~C. F.~~, Plass-Dülmer, ~~C.~~, and ~~J. Rudolph (1993)~~¹², J.: Distribution of methylchloride, dichloromethane, trichloroethene and tetrachloroethene over the North and South Atlantic¹². *Journal of Geophysical Research: Atmospheres*, 98(14), 20517-20526, [1993](#).
- Lang, P. M., L.P. Steele, and R.C. Martin ~~(1990a)~~¹²: Atmospheric methane data for the period 1986-1988 from the NOAA/CMDL global cooperative flask sampling network¹². NOAA Technical Memorandum ERL CMDL-2, [1990a](#). [1990a](#).
- 35 Lang, P. M., L.P. Steele, L.S. Waterman, R.C. Martin, K.A. Masarie, and E.J. Dlugokencky ~~(1992)~~¹²: NOAA/CMDL Atmospheric methane data for the period 1983-1990 from shipboard flask sampling¹². NOAA Technical Memorandum ERL CMDL-4, [1992](#). [1992](#).
- Lang, P. M., L.P. Steele, R.C. Martin, and K.A. Masarie ~~(1990b)~~¹²: Atmospheric methane data for the period 1983-1985 from the NOAA/GMCC global cooperative flask sampling network¹². NOAA Technical Memorandum ERL CMDL-1, [1990b](#). [1990b](#).
- 40 Lewis, D. ~~(2016)~~¹²: Australian climate job cuts leave hole in Southern Hemisphere research¹². *Nature*, [doi: 10.1038/nature.2016.19944](#), [2016](#). [2016](#).
- [Liang, Q., Newman, P., and Reimann, S.: SPARC Report on the Mystery of Carbon Tetrachloride, 2016. 2016.](#)

- Loulergue, L., A-Schilt, R.A., Spahni, V.R., Masson-Delmotte, F.V., Blunier, B.T., Lemieux, J.-M.B., Barnola, D.-J.-M., Raynaud, F.-F.D., Stocker, T. F., and J-Chappellaz (2008). "J.: Orbital and millennial-scale features of atmospheric CH4 over the past 800,000 years." *Nature*, 453(7193), 383-386, 2008.
- 5 Lüthi, D., M-Le Floch, B.M., Bereiter, T.B., Blunier, J.-M.T., Barnola, U.-J.-M., Siegenthaler, D.-U., Raynaud, J.D., Jouzel, H.-J., Fischer, H., and K-Kawamura (2008). "K.: High-resolution carbon dioxide concentration record 650,000–800,000 years before present." *Nature*, 453(7193), 379-382, 2008.
- MacFarling Meure, C., D-Etheridge, E.D., Trudinger, P.C., Steele, R.P., Langenfelds, T.R., Van Ommen, A.T., Smith, A., and J-Elkins (2006). "J.: Law Dome CO2, CH4 and N2O ice core records extended to 2000 years BP." *Geophysical Research Letters*, 33(14), 2006.
- 10 [Machida, T., Nakazawa, T., Fujii, Y., Aoki, S., and Watanabe, O.: Increase in the Atmospheric Nitrous-Oxide Concentration during the Last 250 Years, *Geophysical Research Letters*, 22, 2921-2924, 1995.](#)
[Marcott, S. A., Bauska, T. K., Buizert, C., Steig, E. J., Rosen, J. L., Cuffey, K. M., Fudge, T., Severinghaus, J. P., Ahn, J., and Kalk, M. L.: Centennial-scale changes in the global carbon cycle during the last deglaciation, *Nature*, 514, 616-619, 2014.](#)
- 15 Martinerie, P., E-Nourtier-Mazaauric, J.-M.E., Barnola, W.-T.J.M., Sturges, D.-R.W.T., Worton, E.-D.R., Atlas, L.-K.E., Gohar, L.-K.-P., Shine, K. P., and G.-P. Brasseur (2009). "G. P.: Long-lived halocarbon trends and budgets from atmospheric chemistry modelling constrained with measurements in polar firn." *Atmos. Chem. Phys.*, 9(12), 3911-3934, 2009.
- 20 Masarie, K. A. and P.-P. Tans (1995). "P. P.: Extension and integration of atmospheric carbon dioxide data into a globally consistent measurement record." *Journal of Geophysical Research: Atmospheres*, 100(06), 11593-11610, 1995.
- Matthes, K., B-Funke, M.-E.B., Anderson, T.-M.E., Barnard, J.-L., Beer, P.-J., Charbonneau, M.-A.P., Clilverd, T.-M.A., Dudok de Wit, M.-T., Haberleiter, A.-M., Hendry, G.-H.A., Jackman, M.-C.H., Kretschmar, T.-M., Kruschke, M.-T., Kunze, U.-M., Langematz, D.-R.U., Marsh, A.-D.R., Maycock, S.-A., Misios, C.-J.S., Rodger, A.-A.C.J., Scaife, A. A., Seppälä, M.-A., Shangguan, M., Sinnhuber, K.-M., Tourpali, I.-K., Usoskin, M.-I., van de Kamp, P.-T.M., Verronen, P.-T., and S.-Versick (2016). "S.: Solar Forcing for CMIP6 (v3.1)." *Geosci. Model Dev. Discuss.*, 2016, 1-82, 2016-1-82.
- 25 Meehl, G. A., E-Covey, B.-C., McAvaney, M.-B., Latif, M., and R.-J. Stouffer (2005). "R. J.: Overview of coupled model intercomparison project." *Bulletin of the American Meteorological Society (BAMS)*, 86(09), 2005.
- 30 [Meinshausen, M., S-Smith, K.-S., Calvin, J.-K., Daniel, M.-J., Kainuma, J.-F.M., Lamarque, K.-J.F., Matsumoto, S.-K., Montzka, S., Raper, K.-S., Riahi, A.-K., Thomson, G.-A., Velders, G., and D.-P. van Vuuren \(2011a\). "D. P.: The RCP greenhouse gas concentrations and their extensions from 1765 to 2300." *Climatic Change*, 109\(1-2\), 213-241, 2011.](#)
[Meinshausen, M., S.-J. Smith, K. Calvin, J. S. Daniel, M. Kainuma, J. Lamarque, K. Matsumoto, S. Montzka, S. Raper and K. Riahi \(2011b\). "The RCP greenhouse gas concentrations and their extensions from 1765 to 2300." *Climatic Change* 109\(1-2\): 213-241.](#)
- 35 Miller, B., J-Huang, R.-J., Weiss, R., Prinn, R., and P-Fraser (1998). "P.: Atmospheric trend and lifetime of chlorodifluoromethane (HCFC-22) and the global tropospheric OH concentration." *Journal of Geophysical Research: Atmospheres*, 103(011), 13237-13248, 1998.
- 40 Mitchell, L., E-Brook, J.-E., Lee, C.-J.E., Buizert, C., and T-Sowers (2013). "T.: Constraints on the Late Holocene anthropogenic contribution to the atmospheric methane budget." *Science*, 342(6161), 964-966, 2013.
- [Monnin, E., Steig, E. J., Siegenthaler, U., Kawamura, K., Schwander, J., Stauffer, B., Stocker, T. F., Morse, D. L., Barnola, J. M., Bellier, B., Raynaud, D., and Fischer, H.: Evidence for substantial accumulation rate](#)

- [variability in Antarctica during the Holocene, through synchronization of CO2 in the Taylor Dome, Dome C and DML ice cores, Earth and Planetary Science Letters, 224, 45-54, 2004.](#)
- Montzka, S., ~~J.~~ Butler, ~~B.~~ J., Hall, ~~D.~~ B., Mondeel, ~~D.~~, and ~~J.~~ Elkins ~~(2002)~~, ~~J.~~: A decline in tropospheric organic bromine. [Geophysical Research Letters, 30\(15\), 2003.](#)
- 5 Montzka, S., ~~L.~~ Kuijpers, ~~M.~~ L., Battle, M., Aydin, ~~K.~~ M., Verhulst, ~~E.~~ K., Saltzman, ~~E.~~, and ~~D.~~ Fahey ~~(2010)~~, ~~D.~~: Recent increases in global HFC-23 emissions. [Geophysical Research Letters, 37\(2\), 2010.](#)
- Montzka, S., ~~M.~~ McFarland, ~~S.~~ M., Andersen, ~~B.~~ S., Miller, ~~B.~~ B., Fahey, ~~B.~~ D., Hall, ~~L.~~ B., Hu, ~~C.~~ L., Siso, ~~C.~~, and ~~J.~~ Elkins ~~(2014)~~, ~~J.~~: Recent trends in global emissions of hydrochlorofluorocarbons and hydrofluorocarbons: Reflecting on the 2007 adjustments to the Montreal Protocol. [The Journal of Physical Chemistry A, 119\(19\), 4439-4449, 2015.](#)
- 10 [Montzka, S., Myers, R., Butler, J., Elkins, J., and Cummings, S.: Global tropospheric distribution and calibration scale of HCFC-22, Geophysical research letters, 20, 703-706, 1993.](#)
- Montzka, S. A., ~~Butler, J. H.~~ ~~Butler, J. H.~~ Elkins, J. W. ~~Elkins, T. M.~~, Thompson, ~~A. D. T. M.~~, Clarke, ~~A. D.~~, and ~~L. T.~~ Lock ~~(1999)~~, ~~L. T.~~: Present and future trends in the atmospheric burden of ozone-depleting halogens. [Nature, 398\(6729\), 690-694, 1999.](#)
- 15 Montzka, S. A., ~~E. J.~~ Dlugokencky, ~~E. J.~~, and ~~Butler, J. H.~~ ~~Butler (2011)~~: Non-CO2 greenhouse gases and climate change. [Nature, 476\(7358\), 43-50, 2011.](#)
- [Montzka, S. A., Myers, R. C., Butler, J. H., Elkins, J. W., Lock, L. T., Clarke, A. D., and Goldstein, A. H.: Observations of HFC-134a in the remote troposphere, Geophysical Research Letters, 23, 169-172, 1996.](#)
- 20 [Montzka, S. A., Spivakovsky, C. M., Butler, J. H., Elkins, J. W., Lock, L. T., and Mondeel, D. J.: New observational constraints for atmospheric hydroxyl on global and hemispheric scales, Science, 288, 500-503, 2000.](#)
- [Morice, C. P., Kennedy, J. J., Rayner, N. A., and Jones, P. D.: Quantifying uncertainties in global and regional temperature change using an ensemble of observational estimates: The HadCRUT4 data set, Journal of Geophysical Research: Atmospheres, 117, 2012.](#)
- 25 Mühle, J., ~~A.~~ Ganesan, ~~B. A. L.~~, Miller, ~~P. B. R.~~, Salameh, ~~C. P. K.~~, Harth, ~~B. C. M.~~, Grealley, ~~M. B. R.~~, Rigby, ~~L. M.~~, Porter, ~~L. W.~~, Steele ~~and C. L. P.~~, Trudinger ~~(2010a)~~, ~~C. M.~~, Krummel, ~~P. B.~~, O'Doherty, ~~S.~~, Fraser, ~~P. J.~~, Simmonds, ~~P. G.~~, Prinn, ~~R. G.~~, and Weiss, ~~R. F.~~: Perfluorocarbons in the global atmosphere: tetrafluoromethane, hexafluoroethane, and octafluoropropane. [Atmospheric Chemistry and Physics, Atmos. Chem. Phys., 10\(11\), 5145-5164, 2010.](#)
- 30 Mühle, J., ~~A. L.~~ Ganesan, ~~B. R.~~ Huang, ~~J.~~, Weiss, ~~R.~~, Prinn, ~~R.~~, Miller, ~~P. K. B.~~, Salameh, ~~C. M. P.~~, Harth, ~~B. R.~~ Grealley, ~~M.~~ Rigby, ~~L. W. C.~~, Fraser, ~~P.~~, Porter, ~~L. P.~~ Steele, ~~C. M.~~ Trudinger, ~~P. B.~~ Krummel, ~~S.~~ O'Doherty, ~~P. J.~~ Fraser, ~~P. G.~~ Simmonds, ~~R. G.~~ Prinn, ~~and R. F. Weiss (2010b)~~. "Perfluorocarbons in the global atmosphere: tetrafluoromethane, hexafluoroethane, and octafluoropropane." [Atmos. Chem. Phys.](#) **10**(11): 5145-5164.
- Mühle, J., J. Huang, R. Weiss, R. Prinn, B. Miller, P. Salameh, C. Harth, P. Fraser, L. Porter and B. Grealley (2009). ["Grealley, B.: Sulfuryl fluoride in the global atmosphere", Journal of Geophysical Research: Atmospheres, 114\(D5\), 2009.](#)
- 35 [Newland, M., Reeves, C., Oram, D., Laube, J., Sturges, W., Hogan, C., Begley, P., and Fraser, P.: Southern hemispheric halon trends and global halon emissions, 1978–2011, Atmospheric Chemistry and Physics, 13, 5551-5565, 2013.](#)
- 40 [Nisbet, E., Dlugokencky, E., Manning, M., Lowry, D., Fisher, R., France, J., Michel, S., Miller, J., White, J., and Vaughn, B.: Rising atmospheric methane: 2007–2014 growth and isotopic shift, Global Biogeochemical Cycles, 30, 1356-1370, 2016.](#)
- [Nisbet, E. G., Dlugokencky, E. J., and Bousquet, P.: Methane on the rise—again, Science, 343, 493-495, 2014.](#)

- NOAA ~~(2013)~~: Cooperative Global Atmospheric Data Integration Project: Multi-laboratory compilation of synchronized and gap-filled atmospheric carbon dioxide records for the period 1979-2012 (obspack_co2_1_GLOBALVIEW-CO2_2013_v1.0.4_2013-12-23). ~~C~~—NOAA Global Monitoring Division: Boulder, ~~C~~, U.S.A. ~~(Ed.)~~, 2013.
- 5 NOAA ESRL GMD ~~(2014a)~~: Atmospheric Carbon Dioxide Dry Air Mole Fractions from quasi-continuous measurements at American Samoa. ~~D. R. K. K.W. Thoning, and A. Crotwell~~ K.W. Thoning, D. R. K., and A. Crotwell (Ed.), National Oceanic and Atmospheric Administration (NOAA), Earth System Research Laboratory (ESRL), Global Monitoring Division (GMD): Boulder, Colorado, USA, 2014a.
NOAA ESRL GMD: Atmospheric Carbon Dioxide Dry Air Mole Fractions from quasi-continuous measurements at
- 10 Barrow, Alaska. K.W. Thoning, D. R. K., and A. Crotwell (Ed.), National Oceanic and Atmospheric Administration (NOAA), Earth System Research Laboratory (ESRL), Global Monitoring Division (GMD): Boulder, Colorado, USA, 2014b.
- NOAA ESRL GMD ~~(2014b)~~: Atmospheric Carbon Dioxide Dry Air Mole Fractions from quasi-continuous measurements at ~~Barrow, Alaska~~ Mauna Loa, Hawaii. K.W. Thoning, D. R. K., and A. Crotwell. ~~(Ed.)~~, National Oceanic and Atmospheric Administration (NOAA), Earth System Research Laboratory (ESRL), Global Monitoring Division (GMD): Boulder, Colorado, USA, 2014c.
- 15 NOAA ESRL GMD ~~(2014c)~~: Atmospheric Carbon Dioxide Dry Air Mole Fractions from quasi-continuous measurements at Mauna Loa, Hawaii. ~~D. R. K.~~ South Pole. K.W. Thoning, D. R. K., and A. Crotwell. ~~(Ed.)~~, National Oceanic and Atmospheric Administration (NOAA), Earth System Research Laboratory (ESRL), Global Monitoring Division (GMD): Boulder, Colorado, USA, 2014d.
- 20 O'Doherty, S., ~~D.~~ Cunnold, A. D., Manning, ~~B. A.~~ Miller, R. B., Wang, ~~P. R.~~ Krummel, P., Fraser, ~~P.~~ Simmonds, A. P., McCulloch, A., and ~~R.~~ Weiss (2004). ~~R.~~ R.: Rapid growth of hydrofluorocarbon 134a and hydrochlorofluorocarbons 141b, 142b, and 22 from advanced global atmospheric gases experiment (AGAGE) observations at Cape Grim, Tasmania, and Mace Head, Ireland. J. Journal of Geophysical Research: Atmospheres, 109(D6), 2004.
- 25 O'Doherty, S., ~~P.~~ Simmonds, D. P., Cunnold, ~~H. D.~~ Wang, G. H., Sturrock, ~~P. G.~~ Fraser, D. P., Ryall, ~~R. D.~~ Derwent, R., Weiss, R., and ~~P.~~ Salameh (2001). ~~P.~~ P.: In situ chloroform measurements at Advanced Global Atmospheric Gases Experiment atmospheric research stations from 1994 to 1998. J. Journal of Geophysical Research: Atmospheres, 106(D17), 20429-20444, 2001.
- 30 O'Neill, B. C., ~~G.~~ Tebaldi, D. C., van Vuuren, ~~V. D.~~ Eyring, P. V., Friedlingstein, ~~G. P.~~ Hurt, R. G., Knutti, ~~E. R.~~ Kriegler, J. F. E., Lamarque, J. ~~F.~~ Lowe, J., Meehl, ~~R. J.~~ Moss, K. R., Riahi, ~~K.~~ and B. M. Sanderson (2016). ~~B. M.~~ B. M.: The Scenario Model Intercomparison Project (ScenarioMIP) for CMIP6. J. Geosci. Model Dev. Discuss, 2016, 1-35, 2016.
- Olsen, S. C. and ~~J. T.~~ Randerson (2004). ~~J. T.~~ J. T.: Differences between surface and column atmospheric CO2 and implications for carbon cycle research. J. Journal of Geophysical Research: Atmospheres, 109(D2), 2004.
- 35 Oram, D., ~~F. S.~~ Mani, F. S., Laube, ~~M. J.~~ Newland, G. M., Reeves, ~~W. C.~~ Sturges, S. W., Penkett, ~~G. S.~~ Brenninkmeijer, T. C., Röckmann, T., and ~~P.~~ Fraser (2012). ~~P.~~ P.: Long-term tropospheric trend of octafluorocyclobutane (CFC 4 F 8 or PFC-318). J. Atmospheric chemistry and physics, 12(1), 261-269, 2012.
- 40 Park, S., Croteau, P., Boering, K., Etheridge, D., Ferretti, D., Fraser, P., Kim, K.-R., Krummel, P., Langenfelds, R., and Van Ommen, T.: Trends and seasonal cycles in the isotopic composition of nitrous oxide since 1940. Nature Geoscience, 5, 261-265, 2012.

- Petit, J.-R., Jouzel, J., Raynaud, D., Barkov, N. I., Barnola, J.-M., Basile, I., Bender, M., Chappellaz, J., Davis, M., and Delaygue, G.: Climate and atmospheric history of the past 420,000 years from the Vostok ice core, Antarctica, *Nature*, 399, 429-436, 1999.
- 5 Peylin, P., P-Bousquet, C-P., Le Quéré, S-C., Sitch, P-S., Friedlingstein, G-P., McKinley, N-G., Gruber, P-N., Rayner, P., and P-Ciais (2005)-" P.: Multiple constraints on regional CO2 flux variations over land and oceans." Global Biogeochemical Cycles, 19(4), n/a-n/a, 2005.
- Peylin, P., R-M-Law, K-R. M., Gurney, F-K. R., Chevallier, A-R-F., Jacobson, F-A. R., Maki, Y-T., Niwa, P-K-Y., Patra, W-P. K., Peters, P-J-W., Rayner, G-P. J., Rödenbeck, H-T-C., van der Laan-Luijckx, I. T., and X-Zhang (2013)-" X.: Global atmospheric carbon budget: results from an ensemble of atmospheric CO₂ inversions." Biogeosciences, 10(40), 6699-6720, 2013.
- 10 Prinn, R., D-Cunnold, R-D., Rasmussen, P-R., Simmonds, F-P., Alyea, A-F., Crawford, P-A., Fraser, P., and R-Rosen (1990)-" R.: Atmospheric emissions and trends of nitrous oxide deduced from 10 years of ALE-GAGE data." Journal of Geophysical Research: Atmospheres, 95(D11), 18369-18385, 1990.
- 15 Prinn, R., J-Huang, R-J., Weiss, D-R., Cunnold, P-D., Fraser, P., Simmonds, A-P., McCulloch, C-A., Harth, S-C., Reimann, S., and P-Salameh (2005)-" P.: Evidence for variability of atmospheric hydroxyl radicals over the past quarter century." Geophysical Research Letters, 32(7), 2005.
- Prinn, R., J-Huang, R-J., Weiss, D-R., Cunnold, P-D., Fraser, P., Simmonds, A-P., McCulloch, C-A., Harth, P-C., Salameh, P., and S-O'Doherty (2001)-" S.: Evidence for substantial variations of atmospheric hydroxyl radicals in the past two decades." Science, 292(5523), 1882-1888, 2001.
- 20 Prinn, R., R-Weiss, P-R., Fraser, P., Simmonds, D-P., Cunnold, F-D., Alyea, S-F., O'Doherty, P-S., Salameh, B-P., Miller, B., and J-Huang (2000a)-" J.: A history of chemically and radiatively important gases in air deduced from ALE/GAGE/AGAGE." Journal of Geophysical Research: Atmospheres, 105(D14), 17751-17792, 2000a.
- 25 Prinn, R. G., R-F-Weiss, P-J-R. F., Fraser, P. G-J., Simmonds, D-M-P. G., Cunnold, F-N-D. M., Alyea, S-F. N., O'Doherty, P-S., Salameh, B-R-P., Miller, J-B. R., Huang, R-H-J., Wang, D-E-R. H. J., Hartley, C-D. E., Harth, L-P. C., Steele, G-L. P., Sturrock, P-M. G., Midgley, P. M., and A-McCulloch (2000b)-" A.: A history of chemically and radiatively important gases in air deduced from ALE/GAGE/AGAGE." Journal of Geophysical Research: Atmospheres, 105(D14), 17751-17792, 2000b.
- 30 Rayner, P., H-Enting, R-L., Francey, R., and R-Langenfelds (1999)-" R.: Reconstructing the recent carbon cycle from atmospheric CO2, δ13C and O2/N2 observations." Tellus B, 51(2), 213-232, 1999.
- Reimann, S., A-J-Manning, P-G-A. J., Simmonds, D-M-P. G., Cunnold, R-H-D. M., Wang, J-R. H., Li, A-J., McCulloch, R-G-A., Prinn, J-R. G., Huang, J., and R-F-Weiss (2005)-" R. F.: Low European methyl chloroform emissions inferred from long-term atmospheric measurements." Nature, 433(7025), 506-508, 2005.
- 35 Rhoderick, G. C., Hall, B. D., Harth, C. M., Kim, J. S., Lee, J., Montzka, S. A., Mühle, J., Reimann, S., Vollmer, M. K., and Weiss, R. F.: Comparison of halocarbon measurements in an atmospheric dry whole air sample, *Elementa (Washington, DC)*, 3, 2015.
- Rhodes, R. H., X-Fain, C-X., Stowasser, T-C., Blunier, H-T., Chappellaz, J-R., McConnell, D-J. R., Romanini, L-E-D., Mitchell, L. E., and E-J-Brook (2013)-" E. J.: Continuous methane measurements from a late Holocene Greenland ice core: Atmospheric and in-situ signals." Earth and Planetary Science Letters, 368, 9-19, 2013.
- 40 Rigby, M., A-L-Ganesan, A. L., and R-G-Prinn (2011)-" R. G.: Deriving emissions time series from sparse atmospheric mole fractions." Journal of Geophysical Research: Atmospheres, 116(D8), n/a-n/a, 2011.

- Rigby, M., [R.G. Prinn](#), [S.R.G.](#), O'Doherty, [B.R.S.](#), Miller, [D.B.R.](#), Ivy, [J.D.](#), Mühle, [C.M.J.](#), Harth, [P.K.C.M.](#), Salameh, [T.P.K.](#), Arnold, [R.F.T.](#), Weiss, [P.B.R.F.](#), Krummel, [L.P.](#), Steele, [L.P.J.](#), Fraser, [D.P.J.](#), Young, [D.](#), and [P.G. Simmonds \(2014\)](#). [P.G.](#): Recent and future trends in synthetic greenhouse gas radiative forcing. *Geophysical Research Letters*, **41**(7), 2623-2630, [2014](#).
- 5 Rigby, M., [R.G. Prinn](#), [S.R.G.](#), O'Doherty, [S.A.](#), Montzka, [S.A.](#), McCulloch, [C.M.A.](#), Harth, [J.C.M.](#), Mühle, [P.K.J.](#), Salameh, [R.F.P.K.](#), Weiss, [D.R.F.](#), Young, [P.G.D.](#), Simmonds, [B.D.P.G.](#), Hall, [G.S.B.D.](#), Dutton, [D.G.S.](#), Nance, [D.J.](#), Mondeel, [D.J.W.](#), Elkins, [P.B.J.W.](#), Krummel, [L.P.](#), Steele, [L.P.](#), and [P.J. Fraser \(2013\)](#). [P.J.](#): Re-evaluation of the lifetimes of the major CFCs and CH₃Cl using atmospheric trends. *Atmos. Chem. Phys.*, **13**(5), 2691-2702, [2013](#).
- 10 Rubino, M., [D. Etheridge](#), [C.D.](#), Trudinger, [C.](#), Allison, [M.C.](#), Battle, [R.M.](#), Langenfelds, [L.R.](#), Steele, [M.L.](#), Curran, [M.](#), Bender, [M.](#), and [J. White \(2013\)](#). [J.](#): A revised 1000 year atmospheric δ¹³C-CO₂ record from Law Dome and South Pole, Antarctica. *Journal of Geophysical Research: Atmospheres*, **118**(15), 8482-8499, [2013](#).
- [Rubino, M., Etheridge, D. M., Trudinger, C. M., Allison, C. E., Rayner, P. J., Enting, I., Mulvaney, R., Steele, L. P., Langenfelds, R. L., Sturges, W. T., Curran, M. A. J., and Smith, A. M.: Low atmospheric CO₂ levels during the Little Ice Age due to cooling-induced terrestrial uptake, *Nature Geosci*, **9**, 691-694, \[2016\]\(#\).](#)
- 15 Schilt, A., [M. Baumgartner](#), [T.M.](#), Blunier, [T.J.](#), Schwander, [R.J.](#), Spahni, [H.R.](#), Fischer, [H.](#), and [T.F. Stocker \(2010a\)](#). [T.F.](#): Glacial-interglacial and millennial-scale variations in the atmospheric nitrous oxide concentration during the last 800,000 years. *Quaternary Science Reviews*, **29**(1), 182-192, [2010a](#).
- 20 Schilt, A., [M. Baumgartner](#), [T.M.](#), Schwander, [D.J.](#), Buiron, [E.D.](#), Capron, [J.E.](#), Chappellaz, [L.J.](#), Loulergue, [S.L.](#), Schüpbach, [R.S.](#), Spahni, [H.R.](#), Fischer, [H.](#), and [T.F. Stocker \(2010b\)](#). [T.F.](#): Atmospheric nitrous oxide during the last 140,000 years. *Earth and Planetary Science Letters*, **300**(1-2), 33-43, [2010b](#).
- [Schneider, R., Schmitt, J., Köhler, P., Joos, F., and Fischer, H.: A reconstruction of atmospheric carbon dioxide and its stable carbon isotopic composition from the penultimate glacial maximum to the last glacial inception, *Climate of the Past*, **9**, 2507-2523, \[2013\]\(#\).](#)
- 25 Shindell, D., [G. Faluvegi](#), [L.G.](#), Nazarenko, [K.L.](#), Bowman, [J.F.K.](#), Lamarque, [A.J.F.](#), Voulgarakis, [G.A.](#), Schmidt, [G.A.](#), Pechony, [O.](#), and [R. Ruedy \(2013\)](#). [R.](#): Attribution of historical ozone forcing to anthropogenic emissions. *Nature Climate Change*, **3**(6), 567-570, [2013](#).
- [Siegenthaler, U., Stocker, T. F., Monnin, E., Lüthi, D., Schwander, J., Stauffer, B., Raynaud, D., Barnola, J.-M., Fischer, H., and Masson-Delmotte, V.: Stable carbon cycle-climate relationship during the late Pleistocene, *Science*, **310**, 1313-1317, \[2005\]\(#\).](#)
- 30 Simmonds, P., [D. Cunnold](#), [R.D.](#), Weiss, [R.](#), Prinn, [P.R.](#), Fraser, [A.P.](#), McCulloch, [F.A.](#), Alyea, [F.](#), and [S. O'Doherty \(1998\)](#). [S.](#): Global trends and emission estimates of CCl₄ from in situ background observations from July 1978 to June 1996. *Journal of Geophysical Research: Atmospheres*, **103**(D13), 16017-16027, [1998](#).
- 35 Simmonds, P., [R. Derwent](#), [A.R.](#), Manning, [P.A.](#), Fraser, [P.](#), Krummel, [S.P.](#), O'doherty, [R.S.](#), Prinn, [D.R.](#), Cunnold, [B.D.](#), Miller, [B.](#), and [H. Wang \(2004\)](#). [H.](#): AGAGE observations of methyl bromide and methyl chloride at Mace Head, Ireland, and Cape Grim, Tasmania, 1998–2001. *Journal of atmospheric chemistry*, **47**(3), 243-269, [2004](#).
- Sowers, T., [R.B. Alley](#), [R.B.](#), and [J. Jubenville \(2003\)](#). [J.](#): Ice core records of atmospheric N₂O covering the last 106,000 years. *Science*, **301**(5635), 945-948, [2003](#).
- 40 Spahni, R., [J. Chappellaz](#), [T.F.J.](#), Stocker, [T.F.](#), Loulergue, [G.L.](#), Hausammann, [K.G.](#), Kawamura, [J.K.](#), Flückiger, [J.](#), Schwander, [D.J.](#), Raynaud, [D.](#), and [V. Masson-Delmotte \(2005\)](#). [V.](#): Atmospheric methane and nitrous oxide of the late Pleistocene from Antarctic ice cores. *Science*, **310**(5752), 1317-1321, [2005](#).

- Steele, L. P., E. J. Dlugokencky, P. M. E. J., Lang, P. P. M., Tans, R. C. P. P., Martin, R. C., and K. A. Masarie (1992). "K. A.: Slowing down of the global accumulation of atmospheric methane during the 1980s." *Nature*, 358(6384), 313-316, 1992.
- Steele, L. P., P. J. Fraser, R. A. P. J., Rasmussen, R. A. K., Khalil, T. J. M. A. K., Conway, A. T. J., Crawford, R. H. A. J., Gammon, K. A. R. H., Masarie, K. A., and K. W. Thoning (1987). "K. W.: The global distribution of methane in the troposphere." *Journal of Atmospheric Chemistry*, 5(2), 125-171, 1987.
- Steele, L. P. a. P. M. L. (1991). "Atmospheric methane concentrations - the NOAA/CMDL global cooperative flask sampling network, 1983-1988." 1991.
- Sturrock, G. A., D. M. Etheridge, C. D. M., Trudinger, P. J. C. M., Fraser, P. J., and A. M. Smith (2002). "A. M.: Atmospheric histories of halocarbons from analysis of Antarctic firn air: Major Montreal Protocol species." *Journal of Geophysical Research: Atmospheres*, 107(D24), ACH 12-11-ACH 12-14, 2002.
- Tans, P. P., T. J. Conway, T. J., and T. Nakazawa (1989). "T.: Latitudinal distribution of the sources and sinks of atmospheric carbon dioxide derived from surface observations and an atmospheric transport model." *Journal of Geophysical Research: Atmospheres*, 94(D4), 5151-5172, 1989.
- Tans, P. P., I. Y. Fung, I. Y., and T. Takahashi (1990a). "T.: Observational constraints on the global atmospheric CO2 budget." *Science*, 247(4949), 1431-1438, 1990a.
- Tans, P. P., K. W. Thoning, K. W. P., Elliott, W. P., and T. J. Conway (1990b). "T. J.: Error estimates of background atmospheric CO2 patterns from weekly flask samples." *Journal of Geophysical Research: Atmospheres*, 95(D9), 14063-14070, 1990b.
- Thoning, K. W., T. J. Conway, N. T. J., Zhang, N., and D. Kitzis (1995). "D.: Analysis System for Measurement of CO2 Mixing Ratios in Flask Air Samples." *Journal of Atmospheric and Oceanic Technology*, 12(6), 1349-1356, 1995.
- Thoning, K. W., P. Tans, T. J. Conway, and L. S. Waterman (1987). "NOAA/GMCC calibrations of CO2-in-air reference gases: 1979-1985." NOAA Tech. Memo. ERL ARL-150, NOAA Environmental Research Laboratories, Boulder, CO., 1987, 1987.
- Thoning, K. W., P. P. Tans, P. P., and W. D. Komhyr (1989). "W. D.: Atmospheric carbon dioxide at Mauna Loa Observatory: 2. Analysis of the NOAA GMCC data, 1974-1985." *Journal of Geophysical Research: Atmospheres*, 94(D6), 8549-8565, 1989.
- Trolier, M., J. W. C. White, P. P. J. W. C., Tans, K. A. P. P., Masarie, K. A., and P. A. Gemery (1996). "P. A.: Monitoring the isotopic composition of atmospheric CO2: Measurements from the NOAA Global Air Sampling Network." *Journal of Geophysical Research: Atmospheres*, 101(D20), 25897-25916, 1996.
- Trudinger, C., D. Enting, I., Rayner, P., and Francey, R.: Kalman filter analysis of ice core data 2. Double deconvolution of CO2 and δ13C measurements, *Journal of Geophysical Research: Atmospheres*, 107, 2002a.
- Trudinger, C., Etheridge, G. D., Sturrock, P. G., Fraser, P., Krummel, P., and A. McCulloch (2004). "A.: Atmospheric histories of halocarbons from analysis of Antarctic firn air: Methyl bromide, methyl chloride, chloroform, and dichloromethane." *Journal of Geophysical Research: Atmospheres*, 109(D22), 2004.
- Trudinger, C. M., D. M. Etheridge, P. J. D. M., Rayner, I. G. P. J., Enting, I. G. A., Sturrock, G. A., and R. L. Langenfelds (2002). "R. L.: Reconstructing atmospheric histories from measurements of air composition in firn." *Journal of Geophysical Research: Atmospheres*, 107(D24), ACH 15-11-ACH 15-13, 2002b.

Worton, D. R., ~~W. T.~~ Sturges, ~~J. W. T.~~, Gohar, L. K., Shine, K. P., Martinerie, P., Oram, D. E., Humphrey, S. P., Begley, P., Gunn, L., Barnola, J. M., Schwander, ~~R. J.~~, and Mulvaney, ~~J. M.~~ ~~Barnola~~R.: Atmospheric trends and radiative forcings of CF4 and C2F6 inferred from firn air, *Environ Sci Technol*, **41**, 2184-2189, 2007.

5 ~~Worton, D. R., Sturges, W. T., Schwander, J., Mulvaney, R., Barnola, J. M., and Chappellaz (2006).~~ J.: 20th century trends and budget implications of chloroform and related tri-and dihalomethanes inferred from firn air. *Atmos. Chem. Phys.*, **6**(10), 2847-2863, 2006.

Xiang, B., ~~P. K.~~ Patra, ~~S. A. P. K.~~, Montzka, S. ~~M. A.~~, Miller, ~~J. W. S. M.~~, Elkins, ~~F. L. J. W.~~, Moore, ~~F. L.~~, Atlas, ~~B. R. E. L.~~, Miller, ~~B. R. F.~~, Weiss, R. ~~G. F.~~, Prinn, ~~R. G.~~, and ~~S. C.~~ Wofsy ~~(2014).~~ S. C.: Global emissions of refrigerants HCFC-22 and HFC-134a: Unforeseen seasonal contributions. *Proceedings of the National Academy of Sciences*, **111**(49), 17379-17384, 2014.

10 Zhao, C. L. and ~~P. P.~~ Tans ~~(2006).~~ P. P.: Estimating uncertainty of the WMO mole fraction scale for carbon dioxide in air. *Journal of Geophysical Research: Atmospheres*, **111**(D8): n/a-n/a, 2006.